

# Effect of quantum well states on the magnetic anisotropy of ferromagnetic films

DISSERTATION

zur Erlangung des akademischen Grades  
doctor rerum naturalium (Dr. rer. nat.)

vorgelegt der  
Naturwissenschaftlichen Fakultät II - Chemie und Physik  
der Martin-Luther-Universität Halle-Wittenberg

von Herrn **Maciej Krzysztof Dąbrowski**  
geboren am 8.3.1984 in Białystok, Polen

angefertigt am  
Max-Planck-Institut für Mikrostrukturphysik  
in Halle an der Saale

Gutachter:

1. Prof. Dr. J. Kirschner
2. Prof. Dr. G. Schmidt
3. Prof. Dr. J. Fassbender

Verteidigungsdatum: 07. 04. 2014



<b>1</b>	<b>Introduction</b>	<b>5</b>
<b>2</b>	<b>Theoretical background</b>	<b>8</b>
2.1	Magnetic anisotropy . . . . .	8
2.1.1	Magnetocrystalline anisotropy . . . . .	8
2.1.2	Shape anisotropy . . . . .	9
2.1.3	Magnetic anisotropy of ferromagnetic films on vicinal surfaces . . . . .	10
2.2	Quantum well states . . . . .	11
2.3	Effect of quantum well states on magnetic anisotropy . . . . .	12
<b>3</b>	<b>Film growth, structure and morphology</b>	<b>15</b>
3.1	Sample preparation . . . . .	15
3.2	Sample characterization by LEED and STM . . . . .	18
<b>4</b>	<b>Experimental methods for magnetic analysis</b>	<b>23</b>
4.1	Magneto-Optical Kerr Effect (MOKE) . . . . .	23
4.1.1	Principle of MOKE . . . . .	23
4.1.2	Experimental setup . . . . .	24
4.1.3	Magnetization reversal on vicinal surfaces . . . . .	25
4.2	X-ray Magnetic Circular Dichroism (XMCD) . . . . .	29
4.2.1	Principle of XMCD . . . . .	29
4.2.2	XMCD experimental setup . . . . .	31
4.2.3	Analysis of absorption spectra . . . . .	32
4.3	Spin Polarized Low Energy Electron Microscopy (SPLEEM) . . . . .	34
4.3.1	Origin of magnetic contrast . . . . .	34
4.3.2	Experimental setup . . . . .	34
4.3.3	Image acquisition . . . . .	35
<b>5</b>	<b>Results</b>	<b>37</b>
5.1	Magnetization orientations and anisotropy fields from MOKE . . . . .	37
5.1.1	Effects of varying thickness of ferromagnetic films . . . . .	37
5.1.2	Effects of covering with nonmagnetic overlayers . . . . .	52
5.2	Spin and orbital magnetic moments in Fe films on Ag(116) surface using XMCD . . . . .	56
5.2.1	Spin and orbital magnetic moment values . . . . .	56
5.2.2	Magnetization orientation in remanence . . . . .	59
5.3	Domain structure of ferromagnetic films on vicinal surfaces from SPLEEM . . . . .	62
5.3.1	Fe films on Ag(116) surface . . . . .	62
5.3.2	Co films on Cu(1 1 13) surface . . . . .	67

<b>6 Discussion</b>	<b>69</b>
6.1 Necessary conditions for the observation of magnetic anisotropy oscillations . . . . .	69
6.2 Spin reorientation transition in films grown on vicinal surfaces . . . . .	80
6.3 Oscillatory magnetic anisotropy . . . . .	85
6.3.1 Magnetic anisotropy oscillations due to <i>d</i> -QWS in Co films . . . . .	85
6.3.2 Magnetic anisotropy oscillations due to <i>d</i> -QWS in Fe films . . . . .	89
6.3.3 Magnetic anisotropy oscillations due to <i>sp</i> -resonant states in Cu films . . . . .	96
<b>7 Conclusion</b>	<b>99</b>
<b>Bibliography</b>	<b>103</b>
<b>Publications</b>	<b>117</b>
<b>Acknowledgments</b>	<b>119</b>
<b>Erklärung</b>	<b>121</b>

## Introduction

Over the past decades, the study of magnetic thin films has brought significant contributions to the fundamental understanding of the physics of magnetism along with the advent of spintronics and important applications in magnetic storage media [1–6]. In this context, magnetic anisotropy is a key property of ferromagnetic films. Indeed magnetic anisotropy determines the easy magnetization direction of a ferromagnet and is thus decisive for the magnetization reversal in external fields or by means of spin-polarized currents. Understanding why the magnetization favors a given direction in a particular system is therefore crucial to engineering specific desired properties in magnetic structures. Magnetic anisotropy is directly related to the electronic structure and it is determined by the  $d$ -electrons at the Fermi level. Thus, any changes in the  $d$ -electron band structure are expected to result in changes of the magnetic anisotropy. Several possibilities allow to manipulate the electronic structure in order to achieve a desired configuration of the magnetic anisotropy. Since the electronic structure is sensitive to the crystallographic symmetry and chemical surrounding, it can be modified for instance by tetragonal distortion [7, 8] or a change in the number of valence electrons per unit cell [9, 10].

Specific periodic changes to the electronic structure can be introduced by quantum well states (QWS). QWS are realized in thin films through electronic confinement by potential barriers at the interfaces. In a more general context, the presence of QWS in metallic nanostructures has been shown to be at the origin of many intriguing phenomena, such as interlayer exchange coupling [1, 11], oscillations of the superconducting transition temperature [12], oscillatory magneto-optical Kerr effect [13, 14], thermal stability on the atomic level [15], oscillatory tunneling conductance [16], surface reactivity [17], and the modulation of the Kondo resonance [18]. These observations indicate that as the film thickness is increased, the electronic band structure can be periodically modified by the presence of QWS. Hence one can anticipate that in the presence of QWS originating from  $d$ -band electrons in ferromagnetic thin films, periodic changes in the magnetic anisotropy should occur due to the evolution of the QWS with increasing film thickness.

The results presented in this work contribute to the general understanding of QWS from  $d$ -bands, which in contrast to QWS involving  $sp$  electrons, are still poorly explored. Oscillations of the magnetic anisotropy due to QWS in ferromagnetic films have been theoretically predicted in Co/Cu(001) system [19–21]. Here we provide the first experimental confirmation of those predictions. We also present the results concerning the magnetic anisotropy oscillations in  $bcc$  Fe films, the only system for which such oscillations have been observed experimentally up to now [22]. The systematic Magneto-Optical Kerr Effect (MOKE) studies on several film/substrate combinations lead to an understanding of the fundamental mechanisms responsible for changes in magnetic anisotropy due to the presence of QWS. In particular, the period of the anisotropy oscillations determined in our experiments allows to associate the origin of the anisotropy oscillations to specific electronic bands. We demonstrate that the oscillations of the magnetic anisotropy in our ferromagnetic films are a direct consequence of the quantization of the  $d_{xz}$ ,

$d_{yz}$  electron orbitals. In addition, we show that the measured oscillation amplitude of magnetic anisotropy strongly depends on temperature and we discuss this effect in view of second order perturbation theory.

The magnetic anisotropy can be changed not only through QWS formed in the ferromagnetic films, but also through QWS in the nonmagnetic overlayers grown on the underlying ferromagnetic films [23, 24]. The results of such nonmagnetic/ferromagnetic bilayer systems are also presented in this work. In particular it is shown that the mechanism governing the magnetic anisotropy oscillations is substantially different in nonmagnetic/ferromagnetic bilayers as compared to ferromagnetic layers. By combining the experimental results with recent theoretical calculations [25] we show that the hybridization of the electronic states plays a decisive role in the case of oscillatory magnetic anisotropy in nonmagnetic/ferromagnetic bilayer systems.

As proposed by Bruno [26], a direct connection between the orbital moment anisotropy and magnetocrystalline anisotropy can exist. In this respect, the orbital magnetic moment provides a link between electronic orbitals and magnetic anisotropy, determining the preferred spin orientation direction. It is therefore essential to verify whether the formation of QWS influences the orbital magnetic moment. For this purpose, X-ray Magnetic Circular Dichroism (XMCD) measurements have been performed. In particular we show here the first experimental observations of the quantization of the orbital magnetic moment due to QWS.

Quantitatively, the effect of QWS on magnetic anisotropy is expected to be rather small. Thus, the measurements presented in this thesis require a large sensitivity to small changes in the magnetic anisotropy. To this effect, the ferromagnetic films were grown on vicinal surfaces which causes the lowest-index crystallographic directions to be non-equivalent. In this way, MOKE measurements on vicinal surfaces allow to determine both the period and the amplitude of magnetic anisotropy oscillations [22, 27]. In addition, we demonstrate that QWS affect not only the magnitude of the magnetic anisotropy energy but also the orientation of the easy magnetization axis. Indeed, the presence of steps on the vicinal surfaces leads to a complex behavior of the magnetic anisotropy. We show that the magnetization direction can alternate into/out-of the sample plane with film thickness and moreover, that oscillatory switching of the easy magnetization axis between two orthogonal in-plane directions can also occur. The orientations of the magnetization derived from MOKE are interpreted using the assumption of a single domain state. A better understanding of the magnetic anisotropy of ferromagnetic films grown on vicinal surfaces is achieved through studies of the domain structure by using Spin-Polarized Low Energy Electron Microscopy (SPLEEM) [28]. With SPLEEM, we show how the orientation of the easy magnetization axis is related to the domain structure.

This thesis is organized as follows. **Chapter 2** describes the main theoretical aspects of magnetic anisotropy, quantum well states and the expected relation between these two phenomena. **Chapter 3** is dedicated to sample preparation and characterization of the growth mode and morphology, investigated by Low Energy Electron Diffraction (LEED) and Scanning Tunneling Microscopy (STM). The experimental methods used to study the magnetic properties of the investigated thin films are described in **chapter 4**. In **chapter 5**, section 5.1, the results of MOKE measurements are presented. We demonstrate the oscillatory magnetic anisotropy as a function of film thickness for *fcc* and *bcc* Co, *bcc* Fe and *fcc* FeCo alloys. It is also shown how the magnetic anisotropy of the ferromagnetic films changes upon covering with nonmagnetic Cu and Au overlayers. In section 5.2, XMCD results on Fe/Ag(116) are presented. We show how the spin and orbital magnetic moment values as well as the magnetization orientations change upon increasing Fe film thickness. The last section of the experimental results present studies on the domain structure in Fe/Ag(116) and Co/Cu(1 1 13). The results in this section show how the domain structure evolves upon increasing the film thickness and corresponding changes of the orientation of the easy magnetization axis between two in-plane directions and between the out-of-plane and the in-plane directions. In particular, we discuss the specific changes caused by covering the ferromagnetic films with Au. The most important experimental findings reported in this thesis are discussed in

**chapter 6.** The experimental conditions, which have to be met to observe the anisotropy oscillations as well as the influence of film morphology on the magnetic anisotropy are discussed in section 6.1. Indeed, the formation of QWS and the resulting oscillations in magnetic anisotropy depend on the quality of the interfaces and require appropriate sample preparation conditions. In this section we also explain how hysteresis loops measured by MOKE can be affected by the complex magnetic anisotropy present in ferromagnetic films grown on vicinal surfaces. In section 6.2, a phenomenological model describing the spin reorientation transition in ferromagnetic films on vicinal surfaces is compared with our experimental results. Finally, the results pertaining to oscillatory magnetic anisotropy are discussed in section 6.3. We demonstrate that the magnetic anisotropy oscillations observed in our experiments as a function of ferromagnetic film thickness are indeed caused by the quantization of  $d$ -electron bands. We discuss how the oscillation period depends on electronic structure and how the oscillation amplitude changes with varying temperature. The discussion part closes with the interpretation of the oscillatory magnetic anisotropy in nonmagnetic/ferromagnetic bilayer systems.

## Theoretical background

### 2.1 Magnetic anisotropy

It is known that the magnetization  $\mathbf{M}$  of a ferromagnet tends to lie along one or several preferred axes, called the easy axes. The magnetic anisotropy (MA) is defined as the energy that it takes to rotate the magnetization from the easy into the hard direction. In the following, we distinguish only two types of the magnetic anisotropy:

- The magnetocrystalline anisotropy, which originates from the non spherical charge distribution in conjunction with spin-orbit interaction.
- The shape anisotropy, which originates from the dipolar interaction and depends entirely on the sample shape.

In common phenomenology other types of MA can be distinguished like magneto-elastic anisotropy or surface anisotropy. On a microscopic level, however, they arise from the same mechanism as the magnetocrystalline anisotropy.

#### 2.1.1 Magnetocrystalline anisotropy

Van Vleck was the first to propose that magnetocrystalline anisotropy (MCA) in transition metals arises from the spin-orbit (SO) interaction which couples the isotropic spin moment to an anisotropic lattice [29]. In order to quantitatively link bonding anisotropy with MCA,  $d$ -orbitals are used for the description of the bonding. Their energetic positions and splitting is described by the independent electron ligand field (LF) theory or the electronic band structure. The electronic states created by the crystal potential alone possess no orbital moment, since all  $d$ -orbitals have a perfect balance of substates with magnetic quantum numbers  $+m_l$  and  $-m_l$ . This balance is broken when two or more of the orbitals are mixed by the SO interaction and the new orbitals can then have a finite angular momentum.

#### Spin-Orbit Interaction

The spin-orbit (SO) interaction is a relativistic phenomenon which describes the coupling between the spin moment and the orbital moment. The SO term naturally arises when the Dirac equation is evaluated up to order  $(v/c)^2$  in the nonrelativistic limit [30, 31].

$$\mathcal{H}_{SO} = \xi(r)\mathbf{S} \cdot \mathbf{L} = -\frac{e\hbar^2}{2m_e^2} \frac{1}{r} \frac{d\Phi(r)}{dr} \mathbf{L} \cdot \mathbf{S} \quad (2.1.1)$$

where  $\Phi(r) = Ze/4\pi\epsilon_0 r$  is the electrostatic potential of the nuclear charges  $+Ze$  and  $\mathbf{S}$  and  $\mathbf{L}$  are the vector operators of the spin moment and the orbital moment, respectively. The expectation value

$$\xi = \langle \xi(r) \rangle = \int_0^\infty R_{3d}(r)\xi_{nl}(r)R_{3d}^*(r)r^2 dr \quad (2.1.2)$$



is called the *spin-orbit coupling constant*. The value of the SO interaction energy for the ferromagnetic  $3d$  transition metals is of the order of 10 - 100 meV, i.e., significantly weaker than the exchange interaction ( $\sim 1$  eV) and the ligand field interaction (a few eV). A total magnetic moment has two contributions arising from the spin and the orbital moment  $m_{tot} = m_{spin} + m_{orb}$ . In ferromagnetic metals, the spin moment is about ten times larger than the orbital moment. The spin moment is intrinsically isotropic since the exchange interaction is isotropic. Through SO coupling, the small orbital moment which is "locked" into a favorite direction by the anisotropic bonding of the lattice, directs the spin moment along a favored lattice direction. The SO coupling for the ferromagnetic metals keeps the orbital and spin moments parallel to each other according to Hund's rules.

### Magnetocrystalline anisotropy in view of perturbation theory

The MCA energy is defined as the difference in energy, including the SO Hamiltonian  $\mathcal{H}_{SO}$ , with the magnetization pointing in two different crystallographic directions. Since the SO interaction in  $3d$  transition metals is over an order of magnitude smaller than the exchange interaction and the ligand field interaction, it can be treated to a good approximation by perturbation theory [26, 32]. The correction to the energy of a thin film to the lowest order (i.e., second order for the energy correction since the first order correction vanishes due to time reversal symmetry [26, 33]) is given by:

$$\delta E(\theta, \psi) = \frac{1}{2} \sum_{\mathbf{k}} \sum_{n\sigma} \sum_{n'\sigma' \neq n\sigma} \frac{f(\varepsilon_{n\sigma}(\mathbf{k})) - f(\varepsilon_{n'\sigma'}(\mathbf{k}))}{\varepsilon_{n\sigma}(\mathbf{k}) - \varepsilon_{n'\sigma'}(\mathbf{k})} |\langle n\sigma\mathbf{k} | \mathcal{H}_{SO}(\theta, \psi) | n'\sigma'\mathbf{k} \rangle|^2 \quad (2.1.3)$$

where  $f(\varepsilon, T) = 1 / \{1 + \exp[(\varepsilon - \varepsilon_f) / k_B T]\}$  is the Fermi-Dirac occupation factor,  $|n\sigma\mathbf{k}\rangle$  and  $|n'\sigma'\mathbf{k}\rangle$  denote the occupied and unoccupied electron eigenstates, respectively, while  $\varepsilon_{n\sigma}(\mathbf{k})$  and  $\varepsilon_{n'\sigma'}(\mathbf{k})$  are their corresponding energies. The coupling between pairs of occupied (or unoccupied) states does not need to be considered since the spin-orbit terms cancel each other for any such pair [26]. As can be seen from expression 2.1.3, MCA energy is inversely proportional to the energy difference between the occupied and unoccupied states. Therefore, a significantly enhanced MCA can be expected for an electron configuration where one of the states is just below and another just above the Fermi energy.

One way to visualize the origin of the MCA is its relation to the anisotropy of the orbital moment as proposed first by Bruno [26]. By considering the second order correction to energy, the MCA can be related to the orbital moment through the expression:

$$\delta E \approx -\frac{1}{4} \xi(r) \hat{\mathbf{S}} \cdot [\langle \mathbf{L}^\downarrow \rangle - \langle \mathbf{L}^\uparrow \rangle] \quad (2.1.4)$$

where  $\hat{\mathbf{S}}$  is the magnetization direction along the unit vector of the spin magnetic moment and  $\mathbf{L}^{\downarrow(\uparrow)}$  is the orbital moment vector of the spin down (up) band.

Following the approximation made by Bruno [26], in which the majority spin band is completely filled, its orbital moment vanishes and  $\delta E$  is directly proportional to  $\langle \mathbf{L} \rangle$ . Although for metals with a nearly filled band this often accounts for the main contribution to the MCA energy, in a detailed analysis the orbital moments of the spin up and spin down bands have to be taken separately into account [34]. Furthermore, in proper analysis, additional term which accounts for the spin-flip excitations between the exchange split majority and minority spin bands has to be included, as shown by Laan [34].

#### 2.1.2 Shape anisotropy

The shape effects of the dipolar interaction in ferromagnetic samples can be described via an anisotropic demagnetizing field,  $H_d$ , given by  $H_d = -\mathcal{N}M$ . Here  $\mathbf{M}$  is the magnetization vector and  $\mathcal{N}$  is a shape-dependent demagnetizing tensor. For a thin film, all tensor elements are zero except for the diagonal

element corresponding to the direction perpendicular to the film plane, which is equal to unity. The magnetostatic energy per unit volume  $V$  of a film can be expressed as

$$E_d = -\frac{1}{2}\mu_0\mathbf{M}^2\cos^2\theta \quad (2.1.5)$$

where  $\mu_0$  is the permeability of the vacuum and  $\theta$  is the angle of the magnetization  $M$  with respect to the film normal. According to this expression, the shape anisotropy for a thin film favors an in-plane orientation of the magnetization. Since the film thickness does not enter into the expression, the shape anisotropy is a bulk quantity and is proportional to the number of atoms [35].

### 2.1.3 Magnetic anisotropy of ferromagnetic films on vicinal surfaces

Since magnetocrystalline anisotropy is a result of the coupling between spin of the electrons and anisotropic charge distribution (Sec. 2.1.1), it reflects the symmetry of the lattice. The lowest symmetry of MCA is symmetry of the lattice. At the film surface it is known that no uniaxial anisotropy can exist if the surface normal is an  $n$ -fold rotation axis with  $n > 2$  [36, 37]. However, the symmetry can be reduced by growing a ferromagnetic (FM) film on a vicinal/stepped surface. Atomic, regular steps, break the four-fold rotational symmetry of the film surface, inducing in-plane uniaxial anisotropy (usually called step-induced uniaxial anisotropy) [38–40]. Essentially, the step-induced uniaxial anisotropy has two sources: i) different atomic configuration at the step edges, which modifies the anisotropic bonding and ii) distortion of the film structure in the direction perpendicular to the terraces plane, which cause the additional strain inside the film volume [27, 41–43].

When a FM film is deposited on a flat surface, the in-plane four-fold symmetry of the system results in square hysteresis loop when the magnetic field is applied along one of the easy axes ([100] or [010] for a *bcc* structure). By growing the film on a stepped surface, an additional uniaxial anisotropy is introduced and the two easy axes, [100] and [010], are not equivalent anymore. In case the steps are oriented along one of the easy axes of the four-fold anisotropy of a FM film, one of them becomes an easy magnetization axis and the other an intermediate/harder magnetization axis [39, 40]. By applying the magnetic field along the intermediate axis, so-called split hysteresis loops can be measured (Fig. 2.1). Split hysteresis loops are characterized by a shift field  $H_s$ , which is defined as the field difference between zero field and the center of the single shifted loop. The more the magnetization prefers an orientation along the easy axis, the larger the anisotropy and the larger  $H_s$ .  $H_s$  is therefore a measure of the change in magnetic anisotropy introduced by the substrate steps.

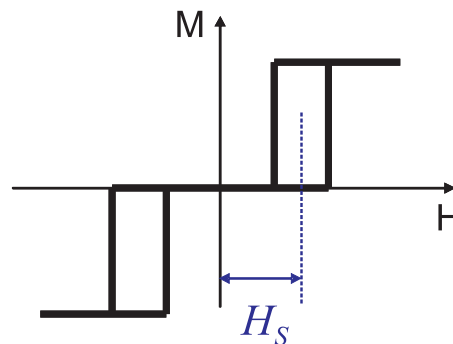


**Figure 2.1:** Schematic split hysteresis loop which can be measured by applying the magnetic field  $\mathbf{H}$  along the intermediate axis (i.e., perpendicular to the easy magnetization axis).  $H_s$  denotes shift field, defined as half of the distance between two constituent loops.

Several attempts have been undertaken to describe the magnetization reversal of FM films grown on a vicinal surface and to describe the measured shift field  $H_s$  with appropriate anisotropy constants [37, 40, 44–47]. In a first approximation it seems that  $H_s = K_u/M_s$ , where  $K_u$  is the in-plane uniaxial anisotropy constant and  $M_s$  the saturation magnetization [44]. More detailed studies have shown however that the magnetization reversal in such systems proceeds via domain nucleation and domain wall motion, and not via a coherent rotation [46]. This makes the theoretical description of the magnetization reversal on vicinal surfaces more complicated and includes anisotropy constants of the higher order [45, 46].

Another consequence of the stepped surface arises from the competition between magnetocrystalline anisotropy, preferring an orientation of the magnetization along the principal crystallographic directions and the shape anisotropy, preferring an orientation of the magnetization in the film plane (which, for vicinal surfaces, is not equivalent to the principal crystallographic planes) [47]. As a result, if the magnetization is oriented perpendicular to the step edges, it can be tilted away from the film plane toward the terraces plane. The measurement of the tilting angle of the magnetization allows to follow changes in the perpendicular magnetic anisotropy [47, 48].

For many years, FM films deposited on the stepped surfaces have been successfully used to tackle many open questions in magnetic anisotropy [40, 49–55]. In particular, in the case of oscillatory magnetic anisotropy, split hysteresis loops have proven to be an invaluable tool [22–24, 27, 39, 44, 56, 57]. Detailed evaluation of the split hysteresis loops makes it possible to determine both the oscillation period and the oscillation amplitude of the magnetic anisotropy oscillations.

## 2.2 Quantum well states

As the physical size of a system approaches atomic dimensions, quantum effects start to play a significant role. One of the most beautiful examples is the confinement of electron motion in metallic ultrathin films. Such confined electronic states, owing to a close analogy to the elementary quantum mechanics model of a particle in a box, are often called quantum well states (QWS).

The quantization condition for the existence of QWS can be described by considering a free electron traveling in a thin film of thickness  $t$  experiencing multiple-reflection due to potential barriers at the interfaces [11, 58]. The multiple interferences that take place in the film induce a change in the density of states. The bound states occur when the interferences are constructive, i.e., when

$$2k_{\perp}t + \phi_1 + \phi_2 = 2\pi n \quad (2.2.1)$$

where  $n$  is the number of the confined electron half-wavelengths,  $\phi_{1,2}$  are the phase shifts of the reflected electron wave functions at the interfaces and  $k_{\perp}$  describes the electron wavevector component perpendicular to the film plane.

However, the film thickness is an integer multiple ( $N$ ) of the atomic spacing  $a/2$  (where  $a$  is the lattice constant) i.e.,  $t = N \cdot a/2$ . Equation (2.2.1) can then be rewritten in terms of a new index  $\nu$ :

$$2(k_{BZ} - k_{\perp})t - \phi_1 - \phi_2 = 2\pi\nu \quad (2.2.2)$$

with the Brillouin zone (BZ) vector  $k_{BZ} = 2\pi/a$  and  $\nu = N - n$ . It is worth to note that the  $k_{BZ} - k_{\perp}$  and  $\nu$  turn out to be the wavevector and the number of nodes of an envelope function that modulates the QW wavefunction [59, 60]. From now, the wavevector of the QW wavefunction will be defined as  $k_{env} = k_{BZ} - k_{\perp}$ . Equations (2.2.1) and (2.2.2) are identical for integral number of layers, however only the latter one adequately describes the experimental results. At non-integer thickness, the film should consist of atomic steps due to the presence of both thicknesses  $t = N \cdot a/2$  and  $t = (N + 1) \cdot a/2$ . Since the number of terraces is usually quite large, the QWS will evolve continuously from that of  $N \cdot a/2$  to that of  $(N + 1)a/2$ . Upon increasing the thickness from  $N \cdot a/2$  to  $(N + 1)a/2$ , the new QW state with  $n+1$  half-wavelengths in the layer is close in energy to the old state with  $n$  half-wavelengths. Owing to blurring, which is due to imperfect thickness, the states with constant  $N - n$  (rather than constant  $n$ ) will merge [60].

Based on Eq. 2.2.2, the period of oscillations  $L$  can be correlated with the corresponding wave vector  $k_{env}$  of the confined electronic state as follows:

$$L = \frac{2\pi}{a} \cdot (k_{env})^{-1} \quad (2.2.3)$$

This equation holds that at a chosen energy, the period of oscillations corresponds to the inverse of the distance between the wave vector  $k_{\perp}$  and the Brillouin zone boundary  $k_{BZ}$ . In particular, in case of the QWS crossing the Fermi level  $E_F$ ,  $k_{\perp}$  equals the Fermi wave vector  $k_F$ . Since the period of oscillations  $L$  can be experimentally determined, Eq. 2.2.3 allows to determine the wavevector  $k_{env}$  of the corresponding confined electronic state.

In general QWS can be formed in both occupied and unoccupied bands. The most direct observation of the QWS below the Fermi level provides photoemission spectroscopy (PES). PES is an ideal tool for QWS study because the photoemission intensity is proportional to the number of electrons at a given energy (the density of states). The QWS appear as thickness dependent peaks in the photoelectron energy spectrum [60–65]. The unoccupied QWS can be probed for instance by inverse photoemission spectroscopy [66], multi-photon photoemission [67] or low energy electron microscopy (LEEM) [68]. A spectacular view of QWS (both occupied and unoccupied) can be obtained by scanning tunneling microscopy (STM), in particular in case of nanostructures [69, 70]. Nowadays, all of those techniques are spin-resolved and thus, capable of measuring spin-polarized QWS.

### 2.3 Effect of quantum well states on magnetic anisotropy

As described in Sec. 2.1.1, the MCA energy originates from the spin-orbit interaction between adjacent occupied and unoccupied states. In general, any modification of the electronic states close to  $E_F$  can result in a change of the MCA energy. A particular case of such a modification of the electronic states in the vicinity of  $E_F$  takes place when QWS are present. With increasing film thickness the energy of the QWS changes and in consequence, QWS cross the Fermi energy, changing the occupancy of the states. The resulting electron configuration modifies the MCA energy (Eq. 2.1.3).

There are two ways of considering the contribution to MCA energy of the ferromagnetic (FM) film due to QWS: i) the effect of QWS formed in the FM film itself, and ii) the effect of QWS formed in a nonmagnetic (NM) overlayer/underlayer on adjacent FM film.

The MCA energy of a ferromagnetic film can be modified when QWS are formed by  $d$ -electrons. As discussed in Sec. 2.2, the formation of QWS in thin films is associated with the quantization of the perpendicular to the film plane direction component,  $k_{\perp}$ , of the three-dimensional electron wavevector  $\mathbf{k} = (k_{\parallel}, k_{\perp})$ , where  $k_{\parallel}$  is the two-dimensional wavevector in the sample plane. With increasing film thickness, the QWS energies periodically cross  $E_F$ , i.e., the occupancy of electron states changes from occupied  $|n\sigma\mathbf{k}_{\parallel}\rangle$  to unoccupied  $|n'\sigma'\mathbf{k}_{\parallel}\rangle$  or vice versa. As a consequence, the QWS couple to a different set of states (e.g., occupied instead unoccupied), thereby changing the contribution to MCA energy. This contribution can be significant only when the energies of such a pair of coupled states are very close to each other (since MCA energy is inversely proportional to the energy difference between occupied and unoccupied states, see Eq. 2.1.3). In particular such an effect can take place, when the QWS arise from  $d$ -bands with  $\Delta_5$  symmetry. The electronic states with  $\Delta_5$  symmetry are intrinsically degenerate and can result in large contributions\* to MCA energy due to the lifting of degeneracies at  $E_F$  by the SO interaction [71]. A schematic representation of QWS originating from a  $\Delta_5$  band in the vicinity of the  $\bar{\Gamma}$  point (i.e.,  $k_{\parallel} = 0$ ) is shown in Fig. 2.2. Such QWS form pairs which have energies very close to each other and can contribute strongly to MCA energy when  $E_F$  lies in between the energies of the pair states. In case of  $E_F$  situated below or above the two subbands, no contribution to MCA energy is observed. Therefore, a contribution to MCA energy can only occur due to such QWS, at specific thicknesses. In this way, QWS lead to an oscillatory MA on the film thickness. The oscillation period  $L$  is determined by the wavevector  $k_{env}$  of the corresponding QWS crossing  $E_F$  (see Eq. 2.2.3). The phases of the MCA oscillations depend on the precise positions of the energies of the corresponding QWS with respect to the  $E_F$ . These position in turn, depend on the phase shifts  $\phi_{1,2}$  of the reflected electrons at the interfaces

---

\*The contributions of those states to MCA energy scale with the square of the SO coupling constant  $\xi$

(see Eq. 2.2.1). As can be seen from Eq. 2.1.3, the amplitude of the MCA oscillations depends on the SO coupling constant  $\xi$ , the energy separation between the pair of states contributing to the MCA energy and the temperature. Since the energy separation between such states is of the order of a few  $k_B T$  over a significant region of the Brillouin zone around the  $\bar{\Gamma}$  point, the MCA oscillation amplitude strongly decreases with increasing temperature [19].

This particular mechanism of MCA oscillations due to QWS formed in a FM film has been theoretically identified to be responsible for oscillatory MCA in *fcc* Co films on Cu(001) [19, 21]. By using a tight-binding (TB) model it was shown that the oscillations of MCA energy with a period of  $\sim 2$  ML come mostly from QWS formed by the minority-spin  $\Delta_5$  band degenerate at the  $\bar{\Gamma}$  point [19]. Later, the calculations were extended to Co films on vicinal surfaces of Cu(001), where the in-plane uniaxial MCA was found to oscillate with the same period as in Co films on a Cu(001) flat surface [21].

The oscillatory MCA can be also caused by QWS formed in a nonmagnetic overlayer/underlayer. This effect was theoretically predicted for the Pd/Co system, where the oscillatory MCA is governed by QWS existing in the nonmagnetic Pd layers of varying thickness [33, 72, 73]. Although the basic principle of the MCA oscillations in Pd/Co is similar to MCA oscillations due to QWS in FM film (the oscillations arise from the changes of *d*-bands around the  $E_F$ ), the mechanism leading to MCA oscillations is different in both cases. In case of Pd/Co, the electrons confined inside the Pd film are subject to different boundary conditions at the Pd/Co interface depending on spin (because in Co film, the majority and minority *d*-bands differ in energy). As a consequence, while majority-spin electrons are completely confined inside the Pd layer, minority-spin electrons can penetrate into the Co film and are only partially confined (forming so called resonances) [73]. In this way, the QWS in the NM Pd overlayer, which has no, or very small, magnetic moment, can influence the MCA energy of the Co/Pd system. Moreover, due to the

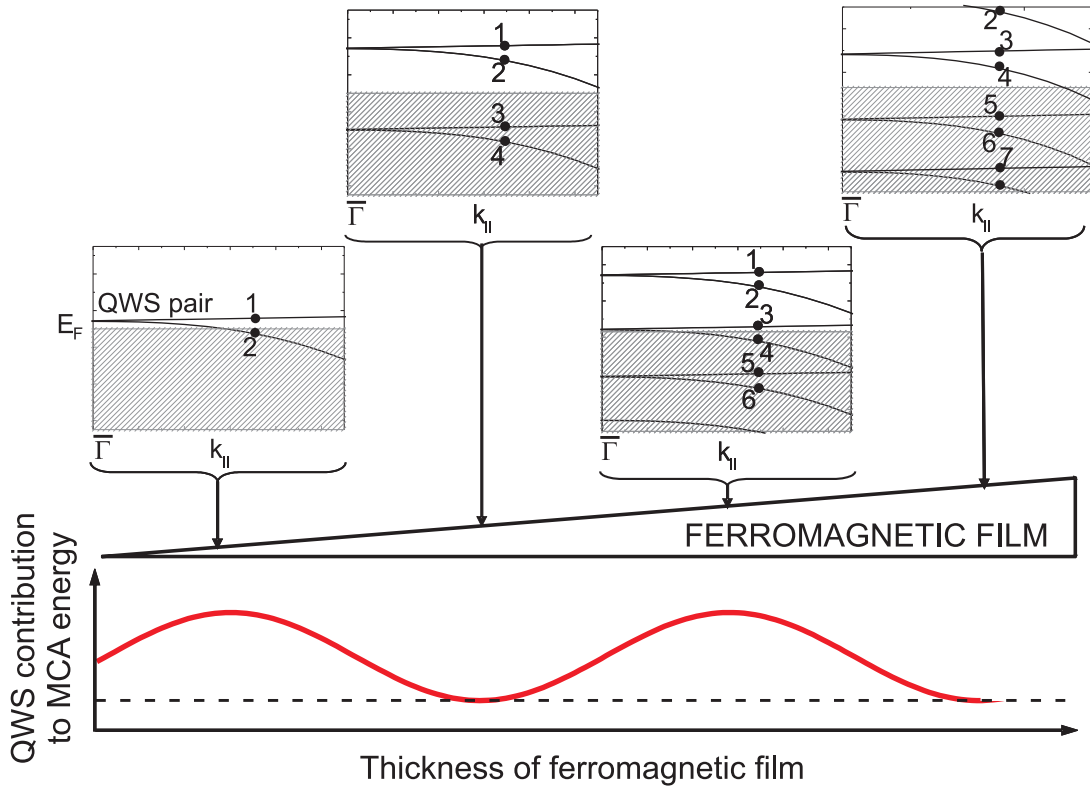


**Figure 2.2:** Schematic representation of QWS energies with respect to  $E_F$  and of their contribution to MCA energy with increasing film thickness. The QWS contribution to MCA energy (red solid line) is plotted with respect to the MCA energy without QWS (dashed line).

large SO coupling in Pd, the MCA oscillation amplitude is predicted to be comparable to that observed due to QWS formed directly in the FM film [19].

Experimentally, the effect of QWS in a NM overlayer on MCA of FM/NM bilayer has so far been only observed for one system, Cu films grown on Co/Cu(001) vicinal surface [23, 56]. The observed oscillations of shift field  $H_s$  as a function of Cu thickness consist of two periods, 2.4 ML and 5.4 ML [23]. The oscillations were attributed to QWS from  $\Delta_1$  *sp* bands. Such QWS, with nearly exactly identical periods of 2.6 ML (originating from the *neck* of the Cu Fermi surface) and 5.9 ML (originating from the *belly* of the Cu Fermi surface), have been observed by PES experiments [74–76]. The mechanism governing the MCA oscillations in Cu/Co due to QWS in Cu layers has not been fully explained up to now.

## Film growth, structure and morphology

In this chapter, thin films preparation and growth mode is described. In general, the growth of FM films on vicinal surfaces is similar to their growth on flat surfaces. However, the quality of the vicinal surfaces is also determined by width of the terraces  $w$ . The quality of the vicinal surfaces was verified: i) globally by probing the crystallographic structure and morphology using Low Energy Electron Diffraction (LEED) which yields the average properties of the surface. Depending on the electron beam size, the measurements cover around  $1\text{ mm}^2$  of the sample surface and ii) locally by probing the surface topography using Scanning Tunneling Microscopy (STM), which allows to characterize regions of up to  $100\text{ nm}^2$ .

### 3.1 Sample preparation

Several substrates were used in this work: Ag(001), Ag(116), Cu(1113) and Au(1113). Miller indexes (116) and (1113) refer to vicinal surfaces with miscut angles  $\omega = 13.3^\circ$  and  $\omega = 6.2^\circ$ , respectively. Such vicinal surfaces are characterized by regular (001) terraces separated by monoatomic steps. The width of the terraces  $w$  of the (11 $n$ ) surface on average equals  $w = n/2 \cdot a/\sqrt{2}$ , where  $a$  is the lattice constant. The atomic steps at the surfaces of the crystals used in our experiment are oriented parallel to  $[1\bar{1}0]$  direction.

The crystals have been cleaned by cycles of ion bombardment ( $\text{Ar}^+$ ,  $2 \times 10^{-7}$  mbar, 1 keV) and subsequent annealing at 775 K [for Ag(001), Ag(116)] and 900 K [for Cu(1113) and Au(1113)]. The chemical cleanness and surface roughness of the substrates were verified by Auger electron spectroscopy (AES), low energy electron diffraction (LEED) (Sec. 3.2) and scanning tunneling microscopy (STM) (Sec. 3.2). Thin films were deposited by using Knudsen effusion cells and electron beam evaporators. Prior to deposition, thickness calibration was performed by using reflection high-energy electron diffraction (RHEED)\* and a quartz monitor. In case of electron beam evaporation additional thickness control was performed by a flux monitor, which allows to control the evaporation rate during deposition [77].

Several systems were investigated in this work and different sample preparation conditions were used in order to optimize the film quality. Constant-thickness or wedge-shaped samples were grown depending on demands of the particular experiments. A short description of the investigated samples and their growth is listed below.

---

\*Since it is difficult to observe RHEED intensity oscillations during film growth on vicinal surface, the thickness calibrations were performed on flat crystals.

### i) Ferromagnetic (FM) films:

#### Fe and Co/Fe films on Ag(001) and Ag(116) surfaces

The mismatch for the epitaxial growth of *bcc* Fe film on *fcc* Ag(001) is of only 0.8%, obtained upon rotation of the Fe(001) plane by  $45^\circ$  with respect to the Ag(001) plane [78, 79]. Following previous reports [80–82], Fe films were grown at RT and annealed for 30 min at 425 K in order to improve the surface morphology. It is known that Ag atoms migrate to the top of Fe layer during growth at RT (or during annealing) reducing the surface energy of the Fe film [81, 82]. By growing Fe films at temperatures of 200 K or lower, the migration of Ag atoms can be prevented [82]. Nevertheless, in order to obtain smooth surfaces, the films have to be post-annealed at elevated temperatures. It was found that both preparation conditions (i.e., growing at 300 K or 200 K and post-annealed at 425 K) result in nearly identical magnetic properties, as verified by Magneto-Optical Kerr Effect (MOKE) measurements (i.e., the spin reorientation transition (SRT) thickness and the amplitude/period of the magnetic anisotropy oscillations are the same in both cases).

In one set of experiments, Co layers were deposited at RT on top of Fe/Ag(116) films grown as described above. The Co films evaporated on *bcc* Fe(001) grow pseudomorphically up to  $\sim 10$  ML and are claimed to have a *bct* structure with the interlayer distance contracted by  $\sim 8\%$  [83–85]. Thicker Co films (above  $\sim 10$  ML) contain defects and crystallographic disorder with the regions having a strained *hcp* ( $\overline{1120}$ ) structure [84].

#### Fe films on Au(1113) surface

Similar to Fe films grown on Ag(001), Fe films grown on Au(001) are only weakly strained due to the nearly perfect lattice match between the *bcc* Fe(001) rotated by  $45^\circ$  and the *fcc* Au(001) substrate (mismatch: 0.6%) [86, 87]. The growth of Fe on Au(001) proceeds via a layer-by-layer mode with Au acting as a surfactant [88, 89].

Although Fe films on Au(001) are usually grown at RT (or below), in this work it was found that samples grown at elevated temperatures were of better quality. Although Fe films grown at 300 K and 425 K are of nearly identical quality, the MA and QWS formation, are very sensitive to any change of morphology, intermixing etc. Hence, only the films grown at 425 K display oscillatory behavior of the MA. Detailed discussion of the influence of the morphology on MA is described in Sec. 6.1. In the present experiments, the optimum growth conditions for Fe/Au(1113) were found for Fe deposition at 425 K and post-annealing at 475 K for 30 min.

#### Co films on Cu(1113) surface

Co/Cu(001) is one of the most often studied systems due to its a nearly ideal layer-by-layer growth mode [90]. The Co film adopts the lateral Cu spacing with an in-plane lattice expansion of  $\sim 2^\circ$  and a contraction of the vertical interlayer distances. The Co films grow in a *fcc* structure with nearly constant strain up to 15 - 16 ML. Above this thickness the strain is released via formation of dislocations [56, 90].

The optimum growth condition was found for Co films deposited at 200 K and then warmed up to 300 K in order to improve the surface morphology.

#### Co films on Au(1113) surface

By growing Co films on Au(001) the *bcc* structure of Co can be stabilized at least up to 15 ML [91–95]. The growth of Co layers at RT results in a relatively flat surface with the epitaxial relationship of *fcc* Au(110)  $\parallel$  *bcc* Co(100) [95].

The deposition of Co films at 375 K and post-annealing at 425 K for 30 min was found to be optimum growth condition. It is known from STM studies [95] that post-annealing activates several diffusion



## SECTION 3.2

mechanisms, including surface segregation of Au and phase separation between Au and Co. As a consequence, regular nanostructures aligned in the Co(001) direction and consisting of buried Co islands are formed with characteristic reconstruction of the Au(001) surface [92, 94, 95].

### $Fe_xCo_{1-x}$ films on Cu(1113) surface

The structure, morphology, electronic properties and magnetism of epitaxial  $Fe_xCo_{1-x}$  alloys grown on Cu(001) have been intensively studied, over the whole composition range [96–100]. It was found that for concentrations up to  $x \sim 0.6$  of Fe, films grow in the *fcc* structure in layer-by-layer mode with random chemical order.

Four compositions of  $Fe_xCo_{1-x}$  were grown on a Cu(1113) crystal with  $x = 0.07, 0.13, 0.23$  and  $0.43$  of Fe. The films were grown at 200 K and warmed up to 300 K in order to improve the surface morphology.

### $Fe_{1-x}Co_x$ films on Ag(116) surface

Since Fe on Ag(001) grows in a well stabilized *bcc* structure one can expect that Ag(001) is a good candidate for growing *bcc*  $Fe_{1-x}Co_x$  alloys (at least for low concentrations of Co). The  $Fe_{1-x}Co_x$  films grown on Ag(001) surface were studied experimentally [101, 102], however, with no information about morphology and growth mode. By using photoelectron diffraction (PED) Schellenberg *et al.* [101, 102] concluded that  $Fe_{1-x}Co_x$  grown at RT maintains the *bcc* structure in a wide composition range, at least up to  $x = 0.7$ .

Four compositions of  $Fe_{1-x}Co_x$  were grown with  $x = 0.05, 0.13, 0.18$  and  $0.3$  of Co. The films were deposited at RT and post-annealed at 425 K for 30 min in order to improve surface morphology.

## ii) Nonmagnetic (NM) films

### Fe and Co films covered with Cu

The growth of Cu on *bcc* Fe(001) is complex and depends strongly on the preparation conditions. It has been shown that Cu on Fe/Ag(001) grows layer-by-layer up to  $\sim 11$  ML before undergoing a structural transition from *bcc* to *fcc*, when deposited by MBE at 300 K [103]. Further studies, however, for sputter deposition of Cu on Fe/Mg(001), revealed that although the initially deposited Cu is strained such that it resembles a *bcc* structure, it is actually a tetragonally distorted *fcc* structure (*ft*) [104]. Subsequent deposition results in continuous strain relaxation (occurring largely at thicknesses below 11 ML).

The Cu films grown on *fcc* Co(001), both flat and vicinal, have been widely investigated and the growth of this system is well characterized [23, 24, 39, 76, 105, 106]. Although smooth *fcc* Cu films can be grown at RT, STM and PES studies show that deposition at lower temperatures and subsequent annealing improve the morphology and sharpness of the Cu/Co interface due to suppressed intermixing during film growth [23, 106].

Therefore, our Cu films were grown on Fe/Ag(116) at RT and on Co/Cu(1113) at 170 K (and then slowly warmed up to RT). Fe and Co films underneath the Cu overlayers were deposited as described above.

### Fe and Co films covered with Au

Au capping layers were grown at RT on Fe/Ag(116) and Co/Cu(1113).

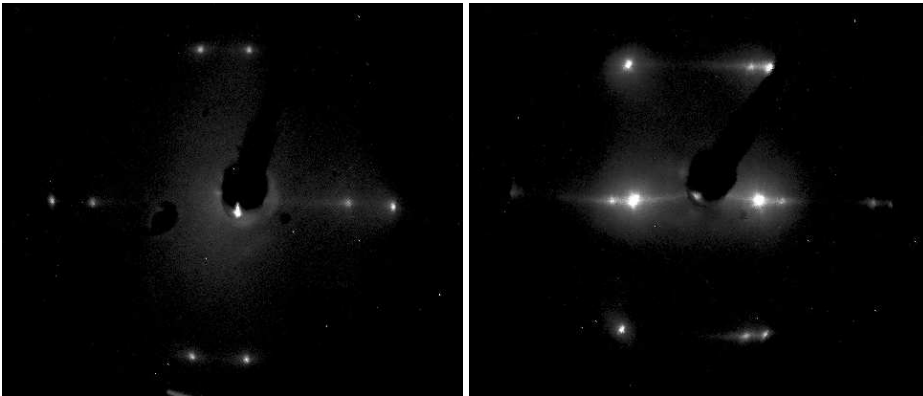


**Figure 3.1:** LEED patterns of Ag(116) surface (on the left) and Cu(113) surface (on the right). The images were obtained at 73 eV and 130 eV, respectively.

## 3.2 Sample characterization by LEED and STM

### Low Energy Electron Diffraction (LEED)

In a low energy electron diffraction (LEED) experiment, electrons with energies in the range between 20 to 500 eV are elastically backscattered from a crystal surface and form a diffraction pattern that is an image of the reciprocal unit cell. From the spot positions, the reciprocal unit cell can be directly determined, and hence the size and shape of the unit cell in real space. A sharp spot pattern implies the existence of a well ordered surface and provides direct information about the symmetry. Besides the existence and intensity of a spot, a lot of additional information can be derived from the spot profile (profile in  $k$ -space) [107–109]. Such spot profiles can provide valuable information about steps, dislocations, domains, faceting, etc. In particular, it is known that stepped (vicinal) surfaces change the LEED pattern in a characteristic manner, splitting spots into doublets or even multiplets [107]. The direction of the multiplet is the direction in the surface plane perpendicular to the steps. The width of each step in the step array can be derived from the separation of the adjacent spots. The energy dependence of the resulting pattern can be derived from the Ewald construction applied to the macroscopic stepped surface diffraction pattern modulated by the terrace width structure factor [108]. If the terrace widths are not too big, each diffraction beam may alternately take the form of a sharp single spot and split pair of beams, as a function of incident beam energy.

In this work LEED was used to inspect the crystallographic order and quality of the surface prior to and after film growth. As an example of LEED pattern for vicinal surfaces, diffraction patterns from Ag(116) and Cu(113) substrates are shown in Fig. 3.1. Sharp, equivalently split spots, confirm the formation of regular mono-atomic steps on the surface. The terrace width  $w$  can be estimated from the distance of the split spots. For Ag(116) and Cu(113) surfaces presented in Fig. 3.1 the width of the terraces  $w$  is estimated to be  $\sim 0.86$  nm and  $\sim 1.65$  nm, respectively. It is in a good agreement with expected values: 0.87 nm for Ag(116) and 1.66 nm for Cu(113), calculated from  $w = n/2 \cdot a/\sqrt{2}$ , where  $a = 0.409$  nm for the lattice constant of Ag and  $a = 0.361$  nm for the lattice constant of Cu. Recorded LEED patterns after deposition of FM films on top of vicinal surfaces remain qualitatively the same (i.e., split spots are visible and the distance between them does not change significantly). However, the sharpness of the spots decreases upon deposition of FM films.

### Scanning Tunneling Microscopy (STM)

Unlike diffraction techniques where the surface in a reciprocal space is observed, scanning tunneling microscopy (STM) directly provides real-space images of the sample surface [110]. STM is based on the tunneling effect. Owing to their wave nature, the electrons (in particularly in metals) are not strictly

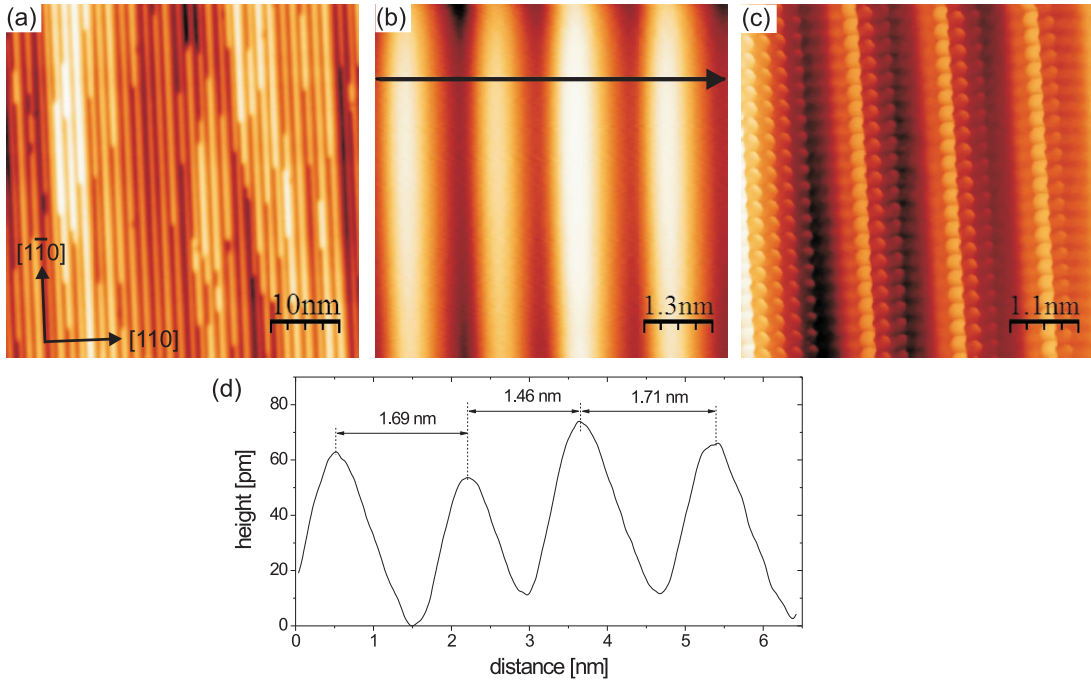


**Figure 3.2:** STM topographic images of the Cu(1113) vicinal surface. Imaging conditions: (a)  $V_{Gap} = 1$  V,  $I_T = 2$  nA ( $50$  nm  $\times$   $50$  nm); (b)  $V_{Gap} = 31$  mV,  $I_T = 3$  nA ( $6.5$  nm  $\times$   $6.5$  nm). Atomically resolved image (c) was obtained at  $V_{Gap} = 21$  mV,  $I_T = 50$  nA ( $5.5$  nm  $\times$   $5.5$  nm). (d) Line scan along the arrow in (b)

confined to the surface of the metal as their wavefunction decays into the vacuum. If two metals are approached to within a few Å, the overlap of their surrounding electron clouds becomes substantial, and a tunneling current  $I_T$  can be induced by applying a small voltage, which causes the Fermi level to shift. The tunneling current is therefore a measure of the wave-function overlap and depends strongly on the distance between the metal tip and the scanned surface. In a *constant current mode* of operation, the tip is scanned laterally across the surface while the tip-sample distance is adjusted to keep  $I_T$  constant. This is realized using an electronic feedback loop, driving a piezo, which is moving the tip perpendicular to the surface. In this way, the displacement of the metal tip given by the voltages applied to the piezodrivers yields a topographic picture of the surface.

A commercial available Low Temperature Omicron STM with a base pressure around  $5 \times 10^{-11}$  was used. The STM stage was cooled down to 4.8 K by using two separate concentric bath cryostats: the outer one, filled with liquid nitrogen and the inner one, filled with liquid helium [111]. The topographic images were recorded using tungsten tips in the constant current mode.

The topography of Cu(1113) crystal is shown in Fig. 3.2. Uniformly distributed steps, oriented along the  $[1\bar{1}0]$  direction can be observed. The width of terraces estimated from a line profile (Fig. 3.2(d))  $w = 1.62 \pm 0.16$  nm is very close to the expected value for this surface and agrees very well with the LEED measurements. Note that the height of the steps observed in the line profile is on average of  $60 \pm 5$  pm, i.e., smaller than interatomic distance of Cu(001) surface (which equals to 1 ML = 185 pm). This is due to the fact that the plane of the crystal is not parallel to the plane of the terraces. The tip of STM is thus not oriented perpendicular to the plane of the terraces. As a consequence, the tip is sliding over the step edges of the terraces (pronounced maxima in Fig. 3.2(d)) but not fully descending to the position at which one terraces ends and another one starts (a step-corner site). Tiny changes in height can be considered as a confirmation that the steps are monoatomic.

As mentioned in Sec. 3.1 Co films on Cu(1113) were grown at 200 K and warmed up to RT in order to improve surface morphology. In fact, no significant difference in the morphology was observed for Co films grown in this way in comparison to the films grown at RT. However, growing Co at lower

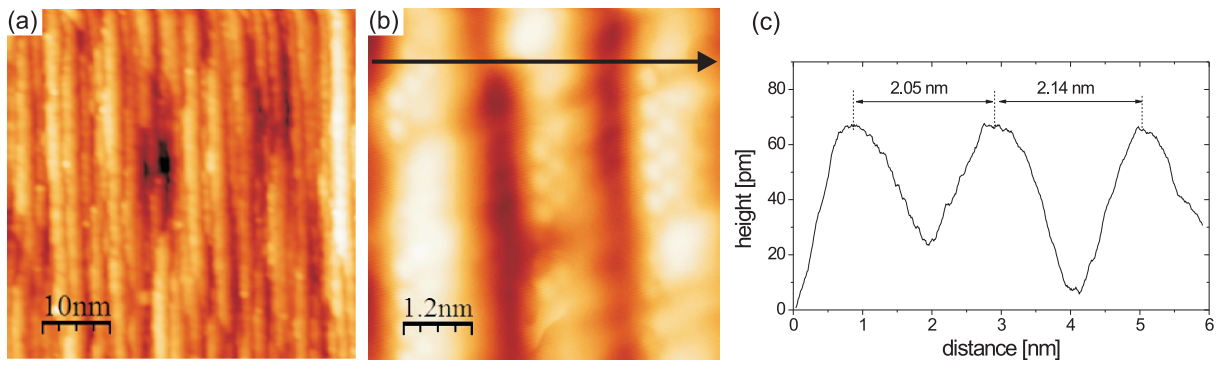


**Figure 3.3:** STM topographic images of 10 ML of Co grown on Cu(1113) vicinal surface. Imaging conditions: (a)  $V_{Gap} = 0.4$  V,  $I_T = 1$  nA ( $50$  nm  $\times$   $50$  nm); (b)  $V_{Gap} = 80$  mV,  $I_T = 2$  nA ( $6$  nm  $\times$   $6$  nm). (c) Line scan along the arrow in (b)

temperature is meaningful for magnetic measurements, as will be described later (Sec. 5.1.1). The topographic image for 10 ML thick Co film on Cu(1113) is shown in Fig. 3.3. Although the terraces tend to be slightly broader in comparison to the substrate terraces, the steps are still clearly visible. Previous STM studies on Co films grown on vicinal surfaces of Cu(001) [112–114] have shown that at lower coverages of Co, (up to  $\sim 5$  ML) the surface is rugged and there is no clear preferential orientation of islands. Upon increasing the Co thickness, the islands coalesce and form straight steps elongated parallel to the step edges of the substrate. It was proposed that initial roughening of the step structure is caused by the minimization of the strain energy [112]. The results presented in this work concern the thickness regime of Co above 5 ML, i.e., for Co films which follow the pattern of the Cu substrate steps, as shown in Fig. 3.3.

The topography of the Ag(116) crystal is shown in Fig. 3.4. Uniformly distributed steps, oriented along the  $[1\bar{1}0]$  direction can be observed. By taking the line profile, the width of the terraces can be estimated (Fig. 3.4(c)). Note that in the case of  $(11n)$  fcc vicinal surface, where  $n$  is an even number, the terraces can consist of  $(n-1)/2$  or  $(n+1)/2$  interatomic distances (nevertheless on average, the width of terraces contains  $n/2$  interatomic distances). Therefore, for Ag(116) the width of terraces should alternate between 0.72 nm and 1.01 nm, which corresponds to the 2.5 and 3.5 interatomic distances along  $[110]$ , respectively. The measured terrace width indeed alternates between 0.72 nm and 1.02 nm (Fig. 3.4(c)).

Both, Fe and  $Fe_{1-x}Co_x$  films were grown on Ag(116) surface. The morphology of Fe films deposited on Ag(116) changes with increasing film thickness in a similar way to Co films grown on vicinal surfaces of Cu(001). At lower coverages of Fe, the islands are not elongated along any preferential direction and

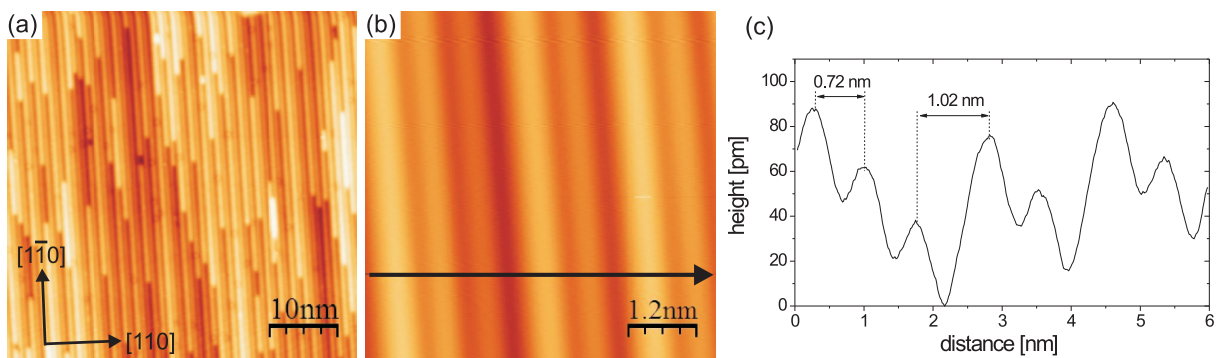


**Figure 3.4:** STM topographic images of Ag(116) vicinal surface. Imaging conditions: (a)  $V_{Gap} = 491$  mV,  $I_T = 0.1$  nA ( $50$  nm  $\times$   $50$  nm); (b)  $V_{Gap} = 94$  mV,  $I_T = 0.15$  nA ( $6$  nm  $\times$   $6$  nm). (c) Line scan along the arrow in (b)

SECTION 3.2

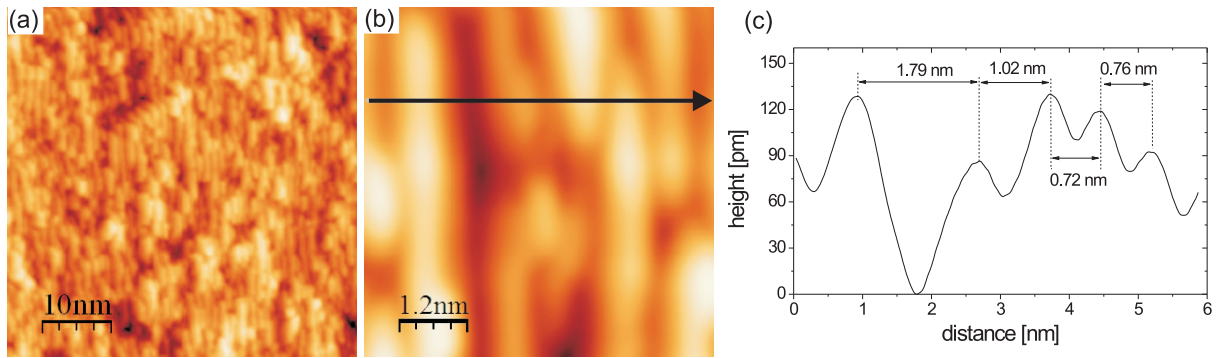


**Figure 3.5:** STM topographic images of 8 ML of Fe grown on Ag(116) vicinal surface. Imaging conditions: (a)  $V_{Gap} = 206$  mV,  $I_T = 1.98$  nA ( $50$  nm  $\times$   $50$  nm); (b)  $V_{Gap} = -313$  mV,  $I_T = 1.48$  nA ( $6$  nm  $\times$   $6$  nm). (c) Line scan along the arrow in (b)

the surface is rough. Upon increasing the Fe thickness, the islands coalesce and form straight structures elongated parallel to the step edges of the substrate. Also in this case, the improvement of the surface morphology with increasing film thickness is most likely due to the strain. Although the mismatch for a *bcc* Fe film grown on a *fcc* Ag(001) in the sample plane is only 0.8% [78, 79], there is a significant difference in the lattice constant in the film normal direction between *bcc* Fe(001) and *fcc* Ag(001). Such a large lattice mismatch (of the order of 29%) is usually not considered in Fe film grown on flat Ag(001), but obviously cannot be neglected for Fe films grown on the stepped surface of Ag(001). The lattice distortion at the step edges induces a significant strain in the Fe film influencing the growth. As can be seen in Fig. 3.5 for an 8 ML thick Fe film grown on Ag(116), the substrate steps are well reproduced by the Fe layers. By drawing the line profile, the width of the terraces can be estimated (Fig. 3.4(c)). It is observed that even after deposition of 8 ML of Fe, the width of the terraces is similar to the step width of the Ag(116) substrate.

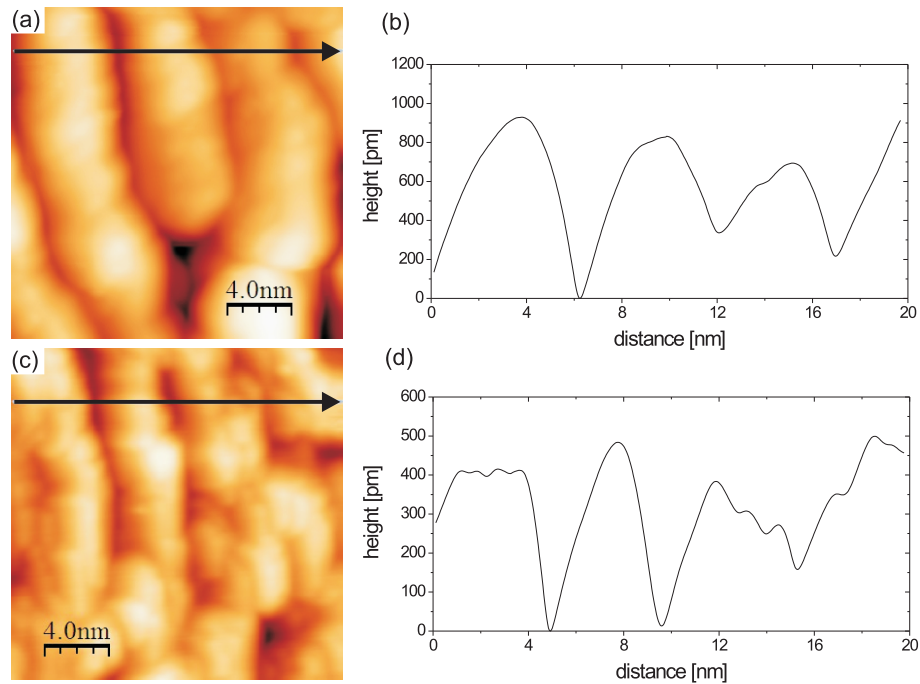


**Figure 3.6:** STM topographic images of 4 ML (a) and 8 ML (c) of  $Fe_{0.7}Co_{0.3}$  alloys grown on Ag(116) vicinal surface. Imaging conditions: (a)  $V_{Gap} = 100$  mV,  $I_T = 1$  nA ( $20$  nm  $\times$   $20$  nm); (c)  $V_{Gap} = 200$  mV,  $I_T = 0.98$  nA ( $20$  nm  $\times$   $20$  nm). (b) and (d) correspond to the line scans in (a) and (c), respectively

The morphology changes dramatically when Co is added to Fe film. The topographic images of  $Fe_{0.7}Co_{0.3}$  alloys for two different thicknesses: 4 ML and 8 ML are shown in Fig. 3.6. In this case, elongated clusters are formed along the step edges of the substrate. These clusters are nearly ten times wider than the terraces width ( $\sim 5$  to  $6$  nm). There is also a significant difference in height as compared to the previous STM line profiles shown in this section. Indeed, in the case of  $Fe_{0.7}Co_{0.3}$ , due to island growth, the changes in height are substantial. In the case of 4 ML thick  $Fe_{0.7}Co_{0.3}$  film the height of the islands is on average  $850$  pm which corresponds to  $\sim 6$  ML of *bcc* Fe(001). For 8 ML thick  $Fe_{0.7}Co_{0.3}$  film, the height of the islands is reduced almost by half of this value with respect to the islands height for 4 ML of  $Fe_{0.7}Co_{0.3}$ . Furthermore, in case of thicker  $Fe_{0.7}Co_{0.3}$  films, a corrugation at surfaces of the islands can be observed, which indicates that the steps of the substrate are at least locally reproduced. Similarly to the case of Co/Cu(1113) and Fe/Ag(116), it can be concluded that the morphology of the  $Fe_{0.7}Co_{0.3}$  films improves upon increasing its thickness.

## Experimental methods for magnetic analysis

### 4.1 Magneto-Optical Kerr Effect (MOKE)

The magneto-optical Kerr effect has been utilized as a premier surface magnetism technique [115–119]. This is due to its sensitivity, experimental simplicity and local probing nature. In the following sections, a short introduction to the basic concepts of MOKE and description of the experimental setup is given. Eventually, the magnetization reversal for FM on vicinal surfaces is explained.

#### 4.1.1 Principle of MOKE

The magneto-optical Kerr effect as applied to ferromagnetic films involves the change in polarization of light reflected from a magnetized medium. Linearly polarized incident light acquires a Kerr rotation and a Kerr ellipticity upon reflection. The part of the induced response that is in-phase with the incident light gives rise to the rotation, while the out-of-phase part accounts for the ellipticity. If an external magnetic field is manipulated to reverse the magnetization direction of the sample, the magneto-optic rotation and ellipticity reverse sign [120]. The magneto-optical Kerr effect is presently described in the context of either macroscopic dielectric theory or microscopic quantum mechanical theory.

Microscopically, the coupling between the electrical field of the light and the electron spin within a magnetic medium occurs through the spin-orbit (SO) interaction [121]. The symmetry between left- and right-hand circularly polarized light is broken due to the SO coupling in a magnetic solid. This leads to different refractive indices for the two kinds of circularly polarized light, so that incident linearly polarized light is reflected with elliptical polarization, and the major elliptical axis is rotated by the so called Kerr angle from the original axis of linear polarization. For nonmagnetic materials, this effect is not strong, although the spin-orbit interaction is present, because the equal number of spin-up and spin-down electrons cancels the net effect. To calculate magneto-optical properties one therefore has to account for magnetism and SO coupling at the same time when dealing with the electronic structure of the material considered. Performing corresponding band structure calculations it is normally sufficient to treat SO coupling as a perturbation [122].

Macroscopically the magneto-optical Kerr effect can be described by off-diagonal terms in the dielectric tensor. In order to characterize MOKE signal, a description of a polarization state of the light is necessary. When a light wave is treated as a time-harmonic electromagnetic wave, the electric field component can be considered as a polarization vector (since the electric field component is dominating in the interaction of light with a matter). It is known that a polarized light is in general elliptically polarized, which means that the electric field vector traces an ellipse in a plane perpendicular to the wavevector at a given point. The ellipse of polarization is determined by four parameters:

- the azimuth (or simply rotation)  $\vartheta$  is an angle of rotation of a major axis (a) of the ellipse;

- the ellipticity  $e$  is a ratio of the length of the minor axis ( $b$ ) of the ellipse to the length of the major axis ( $a$ ):  $e = \pm \frac{b}{a} = \tan \phi$ , where  $\phi$  is the ellipticity angle;
- the amplitude ( $A = \sqrt{a^2 + b^2}$ ) measures the total wave amplitude;
- the absolute phase which is an angle between initial position of the electric field vector and the major axis of the ellipse.

To characterize polarization state itself only the rotation and ellipticity are needed. The Kerr rotation  $\vartheta$  and ellipticity  $\phi$  can be expressed by the Fresnel coefficients  $r_{ij}$  linking the electric field amplitudes of the reflected wave with the incident wave

$$\phi_s + i\vartheta_s = \frac{r_{ps}}{r_{ss}} \quad \text{and} \quad \phi_p + i\vartheta_p = \frac{r_{sp}}{r_{pp}} \quad (4.1.1)$$

where **s** and **p** correspond to the s-polarized and p-polarized light (perpendicular and along the light scattering plane, respectively), while **i** is imaginary unit. It can be shown that when the angles  $\vartheta$  and  $\phi$  are small, then  $\frac{E_s}{E_p} \approx \vartheta + i\phi$ , where  $E_s$  and  $E_p$  denote the electric field components of s- and p-polarized light, respectively [123].

#### 4.1.2 Experimental setup

The principal optical elements of the MOKE setup are shown in Fig. 4.1. A laser diode of wavelength 670 nm and beam diameter  $< 0.2$  mm was used at fixed incidence angle  $\varphi = 30^\circ$  with respect to the sample normal. Since the optical axis of the polarizer is set perpendicularly to the light scattering plane, s-polarized component of the electric field  $E_s$  is transmitted only. Reflected light passes through quarter-wave plate (which is adjusted to compensate phase shifts in the reflected beam) and then through an analyzer that converts the polarization rotation into a change in detected intensity.  $\beta$  is the angle between the orientation of the optical axis of the analyzer at full extinction of the light intensity ( $\pi/2$ ) and the orientation of the optical axis of the analyzer during measurement. The small misalignment  $\beta$  from the full extinction position enhances the contrast of the measured Kerr signal significantly and was found to be an optimum position at  $\sim 1.5^\circ$  [124]. The intensity of the outgoing light measured by photodiode is

$$I = |E_p \sin \beta + E_s \cos \beta|^2 \approx |E_p \beta + E_s| \quad (4.1.2)$$

Recalling that expression  $\frac{E_s}{E_p} \approx \vartheta + i\phi$  gives the Kerr rotation  $\vartheta$  and ellipticity  $\phi$ . It has to be noted that quarter-wave plate (see Fig. 4.1) placed before analyzer not only compensates phase shifts (which for

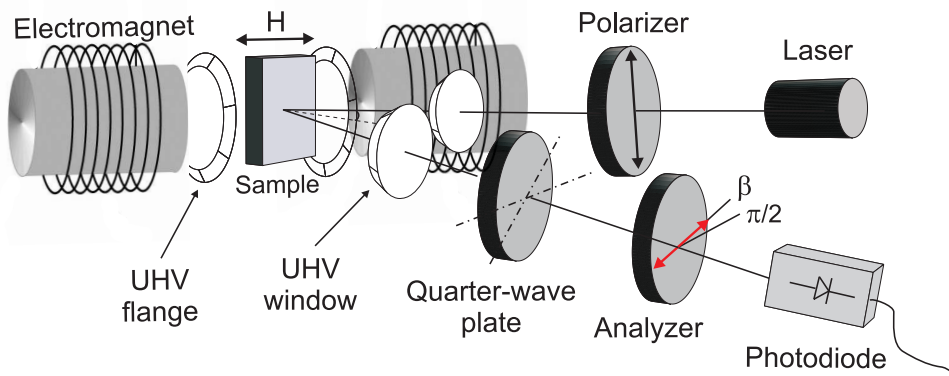


**Figure 4.1:** Schematic drawing of a MOKE experimental setup in longitudinal configuration (magnetic field **H** applied in the sample plane along optical plane). A s-polarized light is reflected from the sample at the angle  $\varphi$  and goes successively through quarter-wave plate and analyzer and eventually is detected by photodiode.



instance can exist due to the window birefringence, if the light is transmitted into the vacuum, through UHV windows) but also produce a  $\pi/2$  phase difference between the  $E_s$  and  $E_p$  components. Therefore, the analyzer will detect  $i(\vartheta + i\phi) = -\phi + i\vartheta$ , i.e., the rotation and ellipticity are interchanged. Then equation (4.1.2) becomes

$$I = |E_p|^2 |\beta - \phi + i\vartheta|^2 \approx |E_p|^2 (\beta^2 + 2\beta\phi) = I_0 \left(1 + \frac{2\phi}{\beta}\right) \quad (4.1.3)$$

with  $I_0 = |E_p|^2 \beta^2$  representing the classical *law of Malus*. As can be seen from (4.1.3) the relative Kerr intensity determines the Kerr ellipticity  $\phi$  rather than rotation  $\vartheta$ .<sup>\*</sup> Since both  $\phi$  and  $\vartheta$  are linearly proportional to the magnetization, the measured intensity (4.1.3) as a function of  $\mathbf{H}$  yields the hysteresis loop. The relative change of the light intensity  $\Delta I/I_0$  upon reversing the magnetization  $\mathbf{M}$  can be described as the Kerr ellipticity  $\phi^H$

$$\phi^H = \frac{\beta}{4} \frac{\Delta I}{I_0} \quad (4.1.4)$$

The Kerr ellipticity  $\phi^H$  of the measured hysteresis loop is defined here as the Kerr ellipticity at certain magnetic field  $\mathbf{H}$  and not always corresponds to the Kerr ellipticity at the saturation magnetization. Note that MOKE signal depends also on the refractive index of the material. In particular, for thin films, two refractive indexes contribute to the MOKE signal: from deposited magnetic film and from the substrate.

The MOKE experimental setup shown in Fig. 4.1 can be used in three main geometries, classified with respect to the orientation of the magnetization  $\mathbf{M}$  to the light scattering plane, mainly: polar, longitudinal and transverse Kerr effect. In this case the measurements were limited only to the longitudinal MOKE configuration (LMOKE), i.e., with magnetic field  $\mathbf{H}$  applied in the sample plane, along the light scattering plane (Fig. 4.1). MOKE measurements were performed *in situ* with pressure below  $1 \times 10^{-10}$  mbar by introducing the light through UHV windows into the MOKE chamber. The sample was placed in slots of the manipulator, which can be rotated and moved in the film plane, with respect to the magnetic field and the plane of incoming and outgoing laser beam. A manipulator has a possibility of the continuous rotation to  $\pm 360^\circ$  and linear movement to  $\pm 10$  mm with the accuracy of  $\pm 0.2^\circ$  and  $\pm 0.05$  mm, respectively. The measurements can be performed in the temperature range from  $T = 5$  K up to  $T = 400$  K by cooling with liquid helium or resistive heating of the sample holder, respectively. The maximum available magnetic field of  $\sim 6000$  Oe is achieved by electromagnet attached to the UHV MOKE chamber.

### 4.1.3 Magnetization reversal on vicinal surfaces

For magnetic thin films grown on vicinal surfaces, regular mono-atomic steps, break the four-fold rotational symmetry of the film surface and induce uniaxial anisotropy within the film plane [38–40]. In case the steps are oriented along one of the easy axes of the four-fold anisotropy of the film, one of them becomes the easy magnetization axis and the other the intermediate magnetization axis. In general, the easy magnetization axis can be oriented either parallel or perpendicular to the step edges. When the magnetization is probed along the steps ( $\alpha^{\parallel}$  geometry in Fig. 4.2), two types of the hysteresis loops can be measured: i) a square loop, for the easy magnetization axis parallel to the steps and ii) a split hysteresis loop, for the easy magnetization axis perpendicular to the steps. Split hysteresis loops are characterized by a shift field  $H_s$ , which is defined as half of the distance between two constituent loops. The Kerr ellipticity of the measured hysteresis loops in  $\alpha^{\parallel}$  geometry  $\phi_{\alpha^{\parallel}}^H$  consists solely of the in-plane magnetization component, i.e., only longitudinal Kerr ellipticity  $\phi_L$  is detected.

<sup>\*</sup>Since it is just a matter of choice what is measured (to measure the rotation  $\vartheta$ , a half-wave plate could be used to replace the quarter-wave plate), terms: Kerr ellipticity and Kerr signal will be used alternatively in the text.

Analogically, when the magnetization is probed perpendicular to the steps, split hysteresis loop and square hysteresis loop is measured for the easy magnetization axis oriented parallel to the steps and perpendicular to the steps, respectively ( $\alpha^+$  geometry in Fig. 4.2). The Kerr ellipticity of the measured hysteresis loop in  $\alpha^+$  geometry,  $\phi_{\alpha^+}^H$ , consists of not only the longitudinal Kerr ellipticity  $\phi_L$ , but also the polar Kerr ellipticity  $\phi_P$ . This is because for FM films on vicinal surface, the magnetization is tilted out of the sample plane when is oriented perpendicular to the steps due to competition between the magnetocrystalline and shape anisotropy. As a consequence, when the hysteresis loop is measured with the magnetic field applied perpendicular to the steps, polar Kerr signal  $\phi_P$  contributes to the total Kerr signal due to a component of the magnetization normal to the film plane. Since the polar Kerr effect is much stronger than the longitudinal Kerr effect [125], even tiny changes of the tilting angle  $\delta$  (of the order of  $\sim 1^\circ$ ) are detectable by MOKE in longitudinal configuration with the magnetic field applied perpendicular to the steps\*.

In order to obtain quantitative information about the Kerr signal  $\phi^H$  from the measured hysteresis loop perpendicular to the steps, deconvolution of the mixed longitudinal  $\phi_L$  and polar  $\phi_P$  components has to be performed. The idea of the separation of longitudinal and polar component is based on basic symmetry properties of such system [126] and is illustrated schematically in Fig. 4.2. The magnetization  $\mathbf{M}$  can be probed perpendicular to the steps at two geometries:  $\alpha^+$  and  $\alpha^-$  (after rotation of the sample by  $180^\circ$  with respect to the light scattering plane). When magnetization is probed at  $\alpha^+$ , at positive  $\mathbf{H}$  (blue vector) the polar component  $\phi_P$  adds to the positive longitudinal component  $\phi_L$ , while at negative  $\mathbf{H}$  (green vector), the negative polar component  $\phi_P$  adds to the negative longitudinal component  $\phi_L$ . Therefore, total Kerr ellipticity measured in this geometry  $\phi_{\alpha^+}^H = \phi_L + \phi_P$ . On the contrary, when the magnetization is probed at  $\alpha^-$ , at positive  $\mathbf{H}$  the negative  $\phi_P$  adds to the positive  $\phi_L$  and after reversing the  $\mathbf{H}$ , the positive  $\phi_P$  adds to the negative  $\phi_L$ . Thus, total Kerr ellipticity measured at  $\alpha^-$  can be expressed by  $\phi_{\alpha^-}^H = \phi_L - \phi_P$ . Note that  $\phi_{\alpha^-}^H$  and  $\phi_{\alpha^+}^H$  are defined as the Kerr ellipticities at which the magnetization is oriented along the probed direction, i.e., perpendicular to the steps (Fig. 4.2). Therefore, in case of the easy magnetization axis oriented along the steps,  $\phi_{\alpha^-}^H$  and  $\phi_{\alpha^+}^H$  correspond to the Kerr ellipticity at  $H_s$ , i.e., as soon as the magnetization is switched to perpendicular to the steps direction. In case of the easy magnetization axis oriented perpendicular to the steps, a square loop is measured and therefore,  $\phi_{\alpha^-}^H$  and  $\phi_{\alpha^+}^H$  correspond to the Kerr ellipticity at remanence (i.e.,  $H_s = 0$ ). Kerr ellipticity extracted from those two types of hysteresis loops (square and split loop) can be practically defined as Kerr ellipticity  $\phi^H$  at  $H_s$ . The choice of  $\mathbf{H}$  at which  $\phi^H$  is evaluated from the hysteresis loops measured perpendicular to the steps is important because  $\phi^H$  depends on  $\mathbf{H}$  due to tilting angle of the magnetization. After applying sufficiently large magnetic field to saturate the sample,  $\phi_{\alpha^-}^H$  and  $\phi_{\alpha^+}^H$  will correspond to the saturation values and become equal to  $\phi_{\parallel}^H$ .

Eventually, by measuring  $\phi_{\alpha^+}^H$  and  $\phi_{\alpha^-}^H$ , the longitudinal  $\phi_L$  and polar  $\phi_P$  Kerr ellipticities can be obtained from

$$\phi_L = (\phi_{\alpha^+}^H + \phi_{\alpha^-}^H) / 2 \quad (4.1.5)$$

$$\phi_P = (\phi_{\alpha^+}^H - \phi_{\alpha^-}^H) / 2 \quad (4.1.6)$$

Since the mixture of  $\phi_L$  and  $\phi_P$  components is a consequence of tilted magnetization  $\delta$  (Fig. 4.2) it is natural to use those values to quantitative estimation of  $\delta$ . Thus, according to (4.1.5) and (4.1.6), the tilting angle  $\delta$  can be extracted from

$$\tan \delta = \frac{M_z}{M_y} = \frac{\phi_P \phi_L^S}{\phi_L \phi_P^S} \quad (4.1.7)$$

---

\*Since presented afterward measurements were performed in longitudinal geometry, only longitudinal component and projection of polar component onto longitudinal geometry will be considered from now.

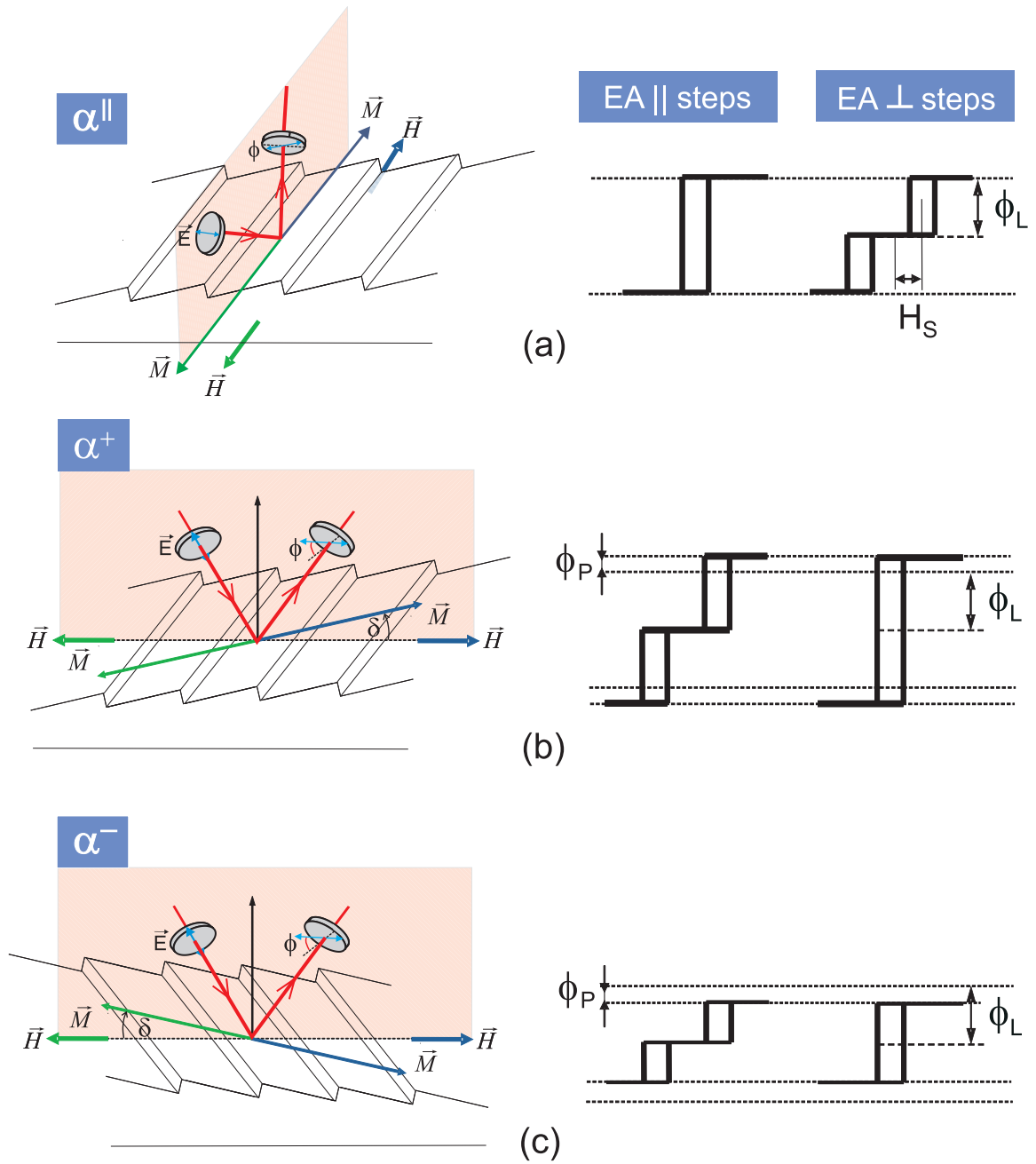


**Figure 4.2:** Schematics of LMOKE measurements on FM film grown on a vicinal surface with the magnetic field and the light scattering plane: (a) along the steps  $\alpha^{\parallel}$ ; (b) perpendicular to the steps  $\alpha^{+}$ ; (c) perpendicular to the steps  $\alpha^{-}$  (after  $180^{\circ}$  rotation of the sample with respect to  $\alpha^{+}$  geometry). The corresponding schematic hysteresis loops are shown for the orientation of the easy magnetization axis (EA) parallel and perpendicular to the steps. The magnetization vectors  $\vec{M}$  represent the easy magnetization axis oriented parallel (a) and perpendicular (b),(c) to the step edges.

where  $\phi_L^s$  and  $\phi_p^s$  are the saturation Kerr signals in longitudinal and polar geometries, respectively. The saturation longitudinal Kerr signal  $\phi_L^s$  can be obtained from the Kerr signal measured in  $\alpha^{\parallel}$  geometry\*, but usually we cannot measure the saturation polar Kerr signal due to the limitation of the magnetic field which can be applied. Fortunately, since the theory of MOKE in ultrathin FM films has been

\*However, only in case of  $\delta$  smaller than  $\sim 10^{\circ}$ . For larger  $\delta$ , the available magnetic field is usually not sufficient to saturate magnetization along the steps ( $\alpha^{\parallel}$ ).

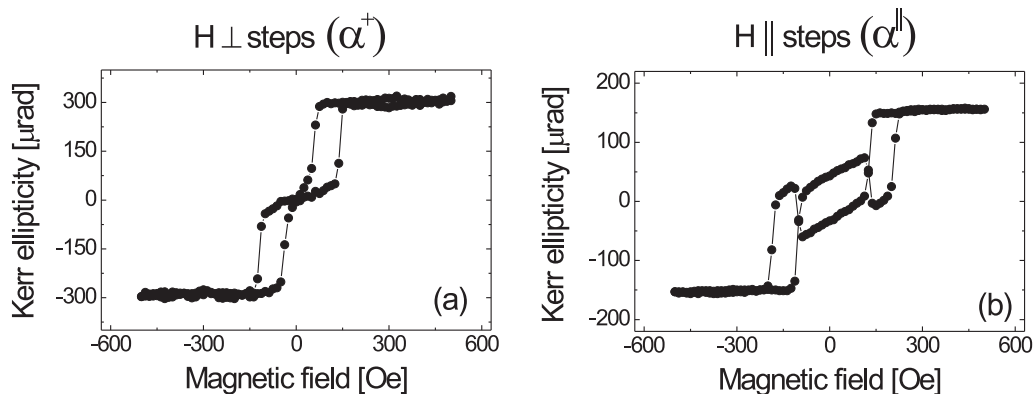


**Figure 4.3:** Split hysteresis loops for two different orientations of the easy magnetization axis: (a) parallel to the steps and (b) perpendicular to the steps. The hysteresis loops were obtained by LMOKE measurements on 9 ML thick Fe film grown on Ag(116) and 15 ML thick Fe film grown on Au(113), respectively

well developed [47, 48, 127, 128], the ratio between the longitudinal and polar saturation signals can be calculated theoretically, by utilizing values of the refractive indices derived from the literature [119, 129–133].

The orientation of the easy axis of magnetization with respect to the step edges of the substrate depends on the magnetic anisotropy of the particular film/substrate configuration. Essentially, except the aforementioned polar Kerr signal contribution  $\phi_P$ , there should be no difference between the split hysteresis loops measured along the steps and perpendicular to the steps (as shown schematically in Fig. 4.2). However, the measured split loops are not equivalent. Assuming that the magnetization is aligned in the sample plane and oriented along the easy magnetization axis, the split hysteresis loops measured along the intermediate magnetization direction (i.e., perpendicular to the easy axis) should show zero signal in remanence. Indeed, this is observed for instance in the case of Fe/Ag(116) (see representative hysteresis loop in Fig. 4.3(a)) and other systems studied up to now [24, 40, 56], where the easy magnetization axis is oriented along the steps.

In case the easy axis is oriented perpendicular to the steps however (i.e., in order to measure the split hysteresis loop the magnetic field has to be applied along the steps), the split hysteresis loops show additional features. At zero magnetic field, the Kerr signal does not vanish and gives remarkable contribution (or even a low field hysteresis loop) to the total Kerr hysteresis loop. An exemplary split hysteresis loop measured along the steps is shown in Fig. 4.3(b). Note the peculiar shape of the low field hysteresis loop. The Kerr signal at low fields switches to positive values at negative magnetic field and switches back to negative values only once a certain positive field is reached. This is typical for so-called reversed hysteresis loops. The complex shape of the hysteresis loops can be explained as the superposition of the split hysteresis loop with the reversed hysteresis loop, as shown schematically in Fig. 4.4. The presence of the reversed hysteresis loop is a consequence of the the polar Kerr signal contribution  $\phi_P$  and is explained in detail in Sec. 6.1.

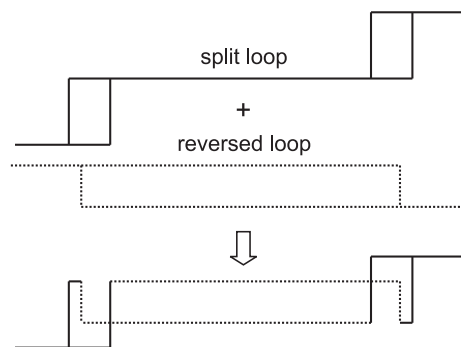


**Figure 4.4:** Schematic representation of a complex hysteresis loop which can be measured at  $\alpha^{\parallel}$  geometry. The shape of such hysteresis loop is explained as a superposition of a split hysteresis loop and reversed rectangular loop

## 4.2 X-ray Magnetic Circular Dichroism (XMCD)

X-ray magnetic circular dichroism (XMCD), pioneered by Schütz et al. [134], is the difference in the absorption between left and right circularly polarized x-rays depending on the magnetic properties of the absorber. XMCD spectroscopy has several capabilities not afforded by traditional magnetic techniques. Its foremost strengths are the element-specific and quantitative determination of spin and orbital magnetic moments. The purpose of the following sections is to elucidate the basic concepts of XMCD and shortly describe the XMCD experimental setup.

### 4.2.1 Principle of XMCD

The basic principle of XMCD can be explained with a simple two-step model as illustrated in Fig. 4.5 for  $3d$  transition metals. In the first step, right or left circularly polarized photons transfer their angular momentum to the excited photoelectrons. Since the initial states  $L_3 : 2p_{3/2}$  and  $L_2 : 2p_{1/2}$  are split by spin-orbit interaction, the photon angular momentum is transferred to both the orbital and spin degrees of freedom of the excited photoelectron. In the second step, the spin-polarization of the photoelectrons is revealed in case of an imbalance for the spin-up and spin-down electrons (equivalently holes) in the  $3d$  valence band. Setting the magnetization  $\mathbf{M}$  of the  $d$  band parallel to the direction of the wave vector  $\mathbf{k}$ , the occupation of the spin-down states is larger than the one of the spin-up states. The photoelectrons excited from  $2p_{3/2}$  ( $2p_{1/2}$ ) by  $\sigma^+$  photons probe mostly the spin-up (spin-down) states above the Fermi level  $E_F$ . Therefore, the absorption of left-circularly polarized x-rays will be enhanced at the  $L_3$  edge and reduced at the  $L_2$  edge with respect to the exchanged-split  $3d$  states. The opposite effect is expected for right circularly polarized x-ray. Hence, the absorption of right and left circularly polarized x-rays will be different. This difference in the x-ray absorption is XMCD. In the above discussion we have assumed that  $\mathbf{M}$  is fixed. Instead of changing the helicity  $\sigma$  of the x-rays one may change the direction of magnetization with respect to  $\mathbf{k}$  in order to obtain XMCD. Both approaches are equivalent [32].

In general, therefore, the XMCD intensity  $\Delta\mu(E)$  is defined as the intensity difference in the absorption spectra obtained for parallel  $\mu^+(E)$  and antiparallel  $\mu^-(E)$  orientations between the sample magnetization and the photon helicity

$$\Delta\mu(E) = \mu^+(E) - \mu^-(E) \quad (4.2.1)$$

The sum rules link the measured polarization dependent resonance intensities with valence band properties, in particular the number of empty states (or holes)  $n_h$  per atom, the spin magnetic moment  $m_{spin}$  per atom and the orbital magnetic moment  $m_{orb}$  per atom. Thole *et al.* [135] and Carra *et al.* [136] have derived the sum rules concerning  $m_{orb}$  and  $m_{spin}$  magnetic moments as

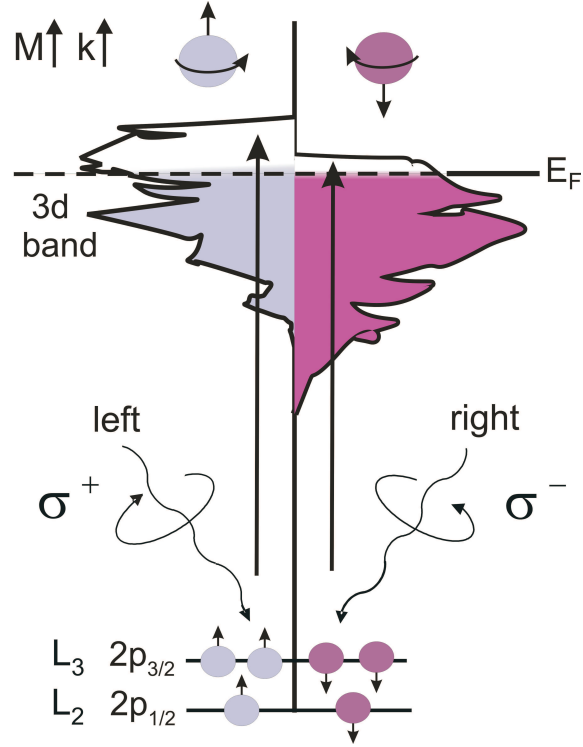
$$m_{orb} = \frac{2n_h\mu_B}{3I_{av}} \int_{L_3+L_2} \Delta\mu(E)dE \quad (4.2.2)$$

$$m_{spin}^{eff} = m_{spin} + 7m_T = \frac{n_h\mu_B}{3I_{av}} \left( \int_{L_3} \Delta\mu(E)dE - 2 \int_{L_2} \Delta\mu(E)dE \right) \quad (4.2.3)$$

Here,  $m_{spin}^{eff}$  is the effective spin magnetic moment,  $n_h$  the  $d$ -hole number,  $\mu_B$  the Bohr magneton and  $m_T = -\langle T \rangle \mu_B / \hbar$  is the projected magnetic dipole moment along the magnetization direction where

$$\mathbf{T} = \sum_i \left( \mathbf{S}_i - \frac{3\mathbf{r}_i(\mathbf{r}_i \cdot \mathbf{S}_i)}{r_i^2} \right) \quad (4.2.4)$$

**Figure 4.5:** Schematic representation of the electronic transitions in XMCD from core  $L_{2,3}$  levels to empty  $3d$  states above the Fermi level  $E_F$ . If the photoelectron is excited from a spin-orbit split level, e.g., the  $2p_{3/2}$  ( $L_3$ ), the angular momentum of the photon can be transferred in part to the spin through the spin-orbit coupling and the excited photoelectrons are spin polarized. The spin polarization is opposite for incident x-rays with positive ( $\sigma^+$ ) and negative ( $\sigma^-$ ) photon helicity. Also, since the  $2p_{3/2}$  ( $L_3$ ) and  $2p_{1/2}$  ( $L_2$ ) levels have opposite spin-orbit coupling ( $j = l + s$  and  $j = l - s$ , respectively) the spin polarization will be opposite at the two edges. The photoelectron spin quantization axis is identical to that of the photon spin, i.e., it is parallel or antiparallel to the X-ray propagation direction  $\mathbf{k}$ . In the second step the exchange split  $3d$ -valence band with unequal spin-up and spin-down populations acts as the detector for the spin of the excited photoelectrons. Hence, the absorption cross section for two different helicities differ due to imbalance of the spin-up and spin-down  $3d$  electrons.



is the intra-atomic magnetic dipole operator and reflects a quadrupole term in the anisotropic spin density within the Wigner-Seitz cell [137]. The normalization factor  $I_{av}$  corresponds to the experimentally obtained average  $L_{3,2}$  peak area ( $2p \rightarrow 3d$  transition intensity) and is given as

$$I_{av} = \int_{L_3+L_2} \left( \frac{\mu^+(E) + \mu^-(E)}{2} - \mu^{BG} \right) dE \quad (4.2.5)$$

where  $\mu^{BG}$  is the background absorption spectrum expressed by the two step functions for edge jump removal before the integration. The edge-jump of the absorption spectrum, defined as the difference of the average intensities well above and below the absorption edge, depends linearly on the number of absorbing atoms. By renormalizing the measured absorption spectra of a given atom in different samples to the same edge jump one obtains spectra that correspond to the same number of absorbing atoms [32].

In order to obtain the absolute value of the spin moments  $m_{spin}$ , the magnetic dipole term  $m_T$  has to be subtracted from the effective spin magnetic moment  $m_s^{eff}$  (which can be obtained experimentally). The absolute values of  $m_{orb}$  and  $m_T$  from angular dependent XMCD measurement can be derived from formulas proposed by Stöhr and König [137]:

$$m_{orb}(\theta, \psi) = m_{orb}^x \sin^2 \theta \cos^2 \psi + m_{orb}^y \sin^2 \theta \sin^2 \psi + m_{orb}^z \cos^2 \theta \quad (4.2.6)$$

$$m_T(\theta, \psi) = m_T^x \sin^2 \theta \cos^2 \psi + m_T^y \sin^2 \theta \sin^2 \psi + m_T^z \cos^2 \theta \quad (4.2.7)$$

$$m_T^x + m_T^y + m_T^z = 0 \quad (4.2.8)$$

$$m_{spin}^{eff}(\theta, \psi) = m_{spin} + 7m_T(\theta, \psi) \quad (4.2.9)$$

where the  $z$  axis is the surface normal, and  $\theta$  and  $\psi$  are the polar and azimuthal angles of magnetization  $\mathbf{M}$ . The equations can be solved to yield all the quantities when at least three XMCD spectra at different magnetization angles are measured. When the  $x$  and  $y$  axes are equivalent in the system of interest, two XMCD spectra to solve the polar angle dependence are sufficient. Note that for usage of these equations magnetization has to be saturated for all probed directions. Hence, the determination of the angular dependent moments requires the magnetic field of the order of several tesla and superconducting magnet is strongly desired.

### 4.2.2 XMCD experimental setup

The XMCD measurements in the present work were performed at Beamline 4B [138] of the synchrotron radiation facility UVSOR-II in Institute for Molecular Science, Japan. The beamline 4B is equipped in UHV-compatible XMCD stage with a 7 T superconducting magnet and a liquid He cryostat. The sample cryostat has a built in heater and continuous-flow type liquid helium transfer line. This offers the lowest sample temperatures of  $\sim 4\text{ K}$ . The rotatable sample cryostat with accuracy  $\pm 0.5^\circ$  allows to measure angle-dependent XMCD.

There are several advantages in measurements under a high magnetic field. As already mentioned, the determination of the angular dependent orbital magnetic moment requires a magnetic field high enough to saturate the magnetization even along hard axes. Additionally, low temperature of the sample holder is more easily achieved since the sample is surrounded by the liquid He reservoirs for the superconducting magnets [139, 140]. Moreover, since the XMCD spectra are recorded by the drain sample current, at high magnetic field the electron recoiling to the sample due to the Lorentz force can be neglected to yield a larger drain current than in the low magnetic field. To sum up, the ability of low temperature XMCD measurement in high magnetic field is crucial for the measurements of magnetic anisotropy, in particular in the case of oscillatory magnetic anisotropy, which is expected to occur exclusively at low temperatures.

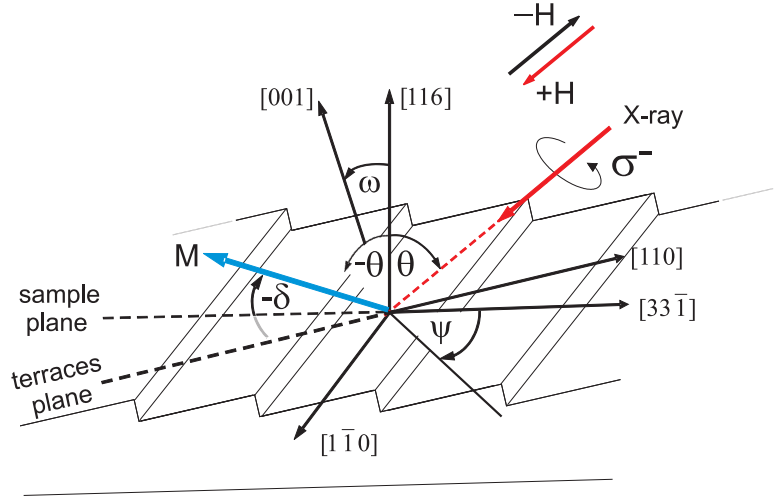
The Beamline 4B is a bending-magnet soft x-ray station equipped with a varied line spacing grating monochromator, which covers the photon energies of 25 - 1000 eV. The circularly polarized x-rays were obtained by adjusting the vertical aperture upstream of the first mirror. The circular polarization factor was estimated to be  $P_c = 0.8 \pm 0.05$  from the storage ring parameters, which was verified by the XMCD measurement of a reference sample.

X-ray absorption spectra were recorded with a total electron yield (TEY) method [141]. It utilizes the photoelectron emission, which is a secondary process. After a photon at given energy is absorbed, the atom, now in its excited state, will eventually relax to a lower energy state. This creates Auger electrons, which are electrons which escape the atom by having absorbed the energy released by the relaxing atom. These Auger electrons typically have high kinetic energy, and often produce secondary Auger electrons by inelastic scattering. The total electron yield is obtained by measuring the electron loss, i.e., the electron current  $I$  from ground to the sample. There are also limitations to the sensitivity of the measurements, due to so called saturation effects [141]. The saturation mechanism in the electron yield signal can be illustrated with the use of two parameters: average x-ray penetration depth  $\lambda_x$ , and the average electron escape depth  $\lambda_e$ . When  $\lambda_x$  is shorter than  $\lambda_e$  all incident photons will be absorbed, and any Auger electrons produced through relaxation will escape through the surface of the sample. In this case the signal has saturated, and is proportional to the incident photon intensity  $I_0$ , but not to the absorption coefficient. The exact expression of the electron yield current with inclusion of the saturation effects for Fe, Co and Ni was derived by Nakajima *et al.* [141]. For all spectra presented in this work saturation effects were taken into account (so called self-absorption correction).

The schematic view of XMCD measurement for film grown on (116) vicinal surface is shown in Fig. 4.6. All the spectra were taken at 5 K by switching the magnetic fields  $\mathbf{H}$ , while leaving the negative photon helicity unchanged. The x-ray propagation direction is always collinear to  $\mathbf{H}$  in the present setup.

The XMCD spectra were basically recorded along three directions:

**Figure 4.6:** Schematics of XMCD measurement for (116) vicinal surface. Left circularly polarized x-ray (helicity  $\sigma^-$ ) is kept collinear with the axis of the applied magnetic field  $\mathbf{H}$ . Note that the geometries of the incident x-ray:  $\theta$  and  $-\theta$  are not equivalent (except the case of the scattering plane along the steps). The vicinal angle  $\omega$  is equal  $13.3^\circ$ . The tilting angle of the magnetization  $\delta$  is defined accordingly as in previous sections.



- $\theta = 0^\circ$  (i.e., along  $[116]$ ),
- $\theta = 55^\circ$  and  $\psi = 0^\circ$  (i.e.,  $55^\circ$  off  $[116]$  toward  $[110]$ ),
- $\theta = 55^\circ$  and  $\psi = 90^\circ$  (i.e.,  $55^\circ$  off  $[116]$  toward  $[1\bar{1}0]$ ).

Such a triplet of XMCD measurement allows to probe the magnetic moment components: perpendicular to the sample plane, in-plane perpendicular to the steps and in-plane along the steps, respectively. Note that sample plane direction (for instance  $[33\bar{1}]$  or  $[1\bar{1}0]$ ) is different than the terraces plane direction, i.e.,  $[110]$ , by vicinal angle  $\omega = 13.3^\circ$ . In fact, it has very important consequences on the symmetry of the measurement. It can be visualized by considering the difference for the incident x-ray with finite  $\theta$ ,  $\psi = 0^\circ$  and  $-\theta$ ,  $\psi = 180^\circ$ , i.e., by probing perpendicular to the steps. Due to broken symmetry of the system the proximity of the  $[001]$  and  $[110]$  directions in both geometries is different. Therefore, the orbital moment anisotropy measured in both cases is expected to be different, even if the thickness of the film and the angles  $\theta$  and  $-\theta$  are exactly of the same value. The influence of vicinal surface symmetry on the anisotropy of the orbital moment is discussed in more detail in Sec. 6.3.2.

### 4.2.3 Analysis of absorption spectra

The basics of the XMCD analysis procedure is presented on the example of 7.6 ML of Fe at normal incidence spectra (Fig. 4.7). The raw x-ray absorption spectroscopy (XAS) spectra  $\mu^+$  and  $\mu^-$  (Fig. 4.7(a)) correspond to the parallel and antiparallel relative orientation of the photon helicity and the magnetization of the sample. Since the offset in the dichroism signal never truly vanishes, it has to be removed before is further analyzed. To remove the offset, a pre-edge and post-edge region is defined. The regions are defined to those where no dichroism signal exists, i.e., the difference of the absorption  $\mu^+$  and  $\mu^-$  are vanishing. The pre-edge is typically defined in the range from  $-40$  to  $-15$  eV, and the post-edge from  $+50$  to  $+100$  eV, with respect to the  $L_3$  peak energy. After the difference  $\Delta\mu = \mu^+ - \mu^-$  is taken, linear curve is fitted to the data points which falls within the two regions. The offset is then removed by subtraction of the linear curve from the XAS spectra.

After the linear background subtraction the non-resonant absorption portion must be removed. The non-resonant absorption function is approximated by a double-step function [142]. The step height of the double-step function is normalized to the height difference between the pre-edge and post-edge region (edge jump). By renormalizing the spectra to the same edge-jump one obtains spectra that correspond to the same number of absorbing atoms (i.e., spectra are comparable on a per-atom basis). Eventually, self-absorption correction is performed. Once the  $\mu^+$  and  $\mu^-$  are properly determined, the XMCD intensity is obtained from (4.2.1). According to the orbital sum rule (4.2.2), the orbital magnetic moment is zero if the integrals of  $L_3$  and  $L_3$  intensities have the same size but opposite signs. By normalizing the dichroism spectra to the  $L_2$  edge intensity, one can therefore conveniently see changes in the orbital moment [143].



SECTION 4.2

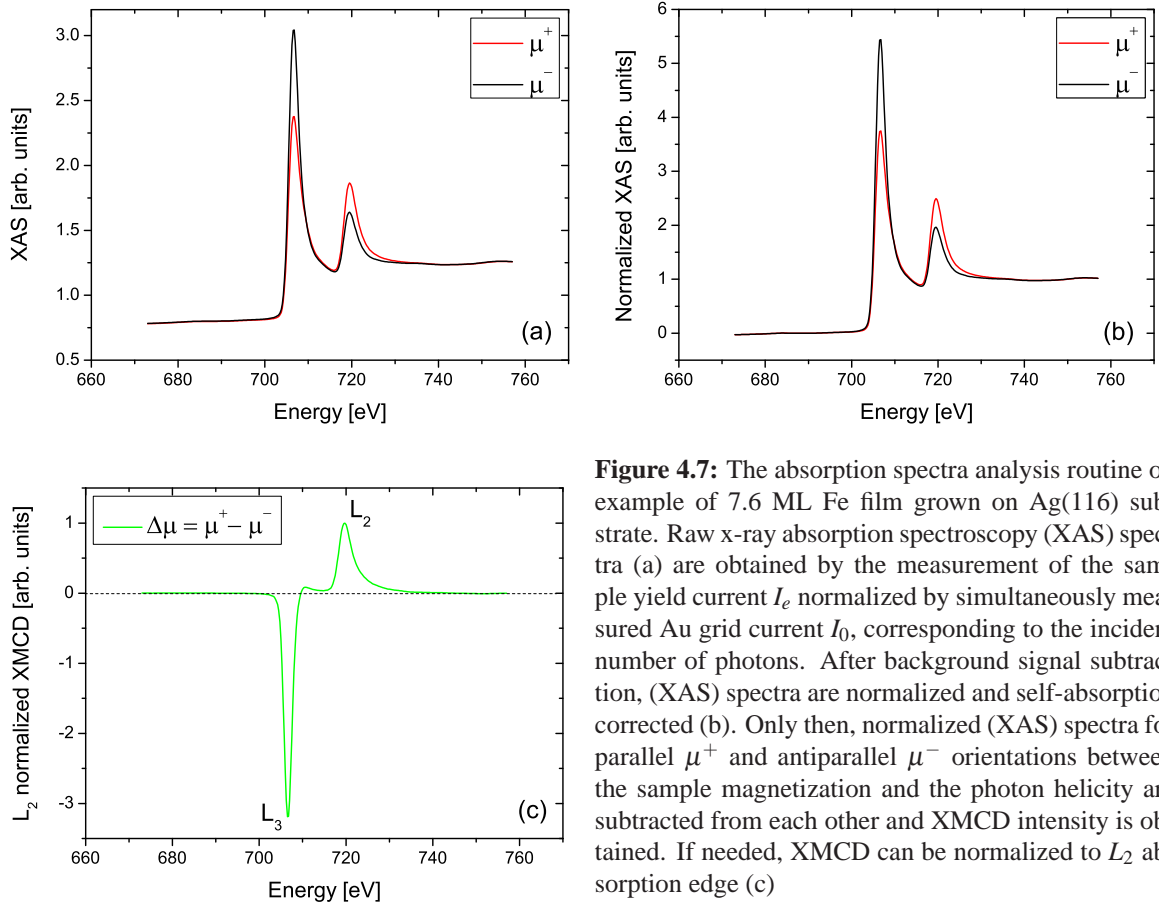


**Figure 4.7:** The absorption spectra analysis routine on example of 7.6 ML Fe film grown on Ag(116) substrate. Raw x-ray absorption spectroscopy (XAS) spectra (a) are obtained by the measurement of the sample yield current  $I_e$  normalized by simultaneously measured Au grid current  $I_0$ , corresponding to the incident number of photons. After background signal subtraction, (XAS) spectra are normalized and self-absorption corrected (b). Only then, normalized (XAS) spectra for parallel  $\mu^+$  and antiparallel  $\mu^-$  orientations between the sample magnetization and the photon helicity are subtracted from each other and XMCD intensity is obtained. If needed, XMCD can be normalized to  $L_2$  absorption edge (c)

XMCD spectrum normalized to the  $L_2$  intensity is shown in Fig. 4.7(c).

In order to obtain quantitative information about spin and orbital magnetic moments, the dichroism intensities must be corrected by the photon polarization  $P_c$ . The photon polarization was verified by the XMCD measurements of the reference sample and was included in the analysis of the spectra. The spin and orbital moments can then be obtained from sum rules according to equations (4.2.3) and (4.2.2). In case of our measurements, the number of holes for Fe is assumed to be constant and equal  $n_h = 3.4$ .

### 4.3 Spin Polarized Low Energy Electron Microscopy (SPLEEM)

A remarkable number of magnetic microscopes for direct, i.e., real-space, imaging have been demonstrated over the past decades. The imaging techniques currently in use may be classified into two groups, according to the physical mechanism of interaction between the probe and sample, that is, stray field mapping and magnetization mapping. Among numerous high-resolution magnetic imaging techniques probing quantities proportional to the local sample magnetization, spin-polarized low energy electron microscopy (SPLEEM) turns out to be one of the most powerful, surface sensitive tool with very good lateral resolution.

SPLEEM is an imaging method that is based on the spin dependence of the elastic back-scattering of slow electrons from ferromagnetic surfaces. SPLEEM differs from LEEM (low energy electron microscopy) [144] in that the incident beam is spin-polarized. The spin-polarized incident electrons are reflected at normal incidence from the surface in a manner that depends upon the relative orientation of the spin polarization  $\mathbf{P}$  of the electron beam and the local magnetization  $\mathbf{M}$  in the surface layers of the sample.

#### 4.3.1 Origin of magnetic contrast

A magnetic contrast in SPLEEM essentially originates from two effects [28]. First of all, the elastic scattering potential between the incident electrons and the electrons in a ferromagnet is spin-dependent. This is due to the fact that electronic bands in a ferromagnet are split by exchange interaction and therefore, can have different energies for two spin directions. In consequence, in the energy range between the onsets of the majority and minority spin bands, the incident electrons with spin parallel to the majority spins can penetrate into the sample, while the incident electrons with spin anti-parallel to the majority spins are reflected [68].

Secondly, the inelastic scattering potential between the incident electrons and the electrons in a ferromagnet is spin-dependent, due to spin-dependent inelastic mean free path (IMFP). Since a density of states of unoccupied states is higher for minority-spin electrons than for majority-spin electrons, minority electrons are more effectively scattered than majority electrons. Therefore, reflectivity of majority electrons is larger than the reflectivity of minority electrons.

These differences in reflectivity can lead to significant magnetic contrasts. Note that the differences in reflectivity arising from both aforementioned effects, decrease with increasing energy of the incident electrons. This is because both, the exchange potential and the spin-dependence of the the IMFP decrease with energy [28, 145]. Thus, the best magnetic contrast in SPLEEM is usually obtained for low energy electrons, with energy of a few eV.

#### 4.3.2 Experimental setup

The experiments presented in this thesis were performed at the National Center for Electron Microscopy of the Lawrence Berkeley National Laboratory in California. In a SPLEEM microscope, spin-polarized electrons are projected toward the sample through the combination of condenser lenses and beam deflectors, magnet A and B (Fig. 4.8). Just before reaching the surface, the electron beam is decelerated in the objective lens and illuminates the surface in normal incidence. After the reflection, backscattered electron beam is reaccelerated again and focused into the back focal plane. The beam separator (magnet B) and beam deflector (magnet C) transfer the SPLEEM image 1:1 in front of the transfer lens. Different combinations of projection lens settings then result in a useful magnification range corresponding to fields of view ranging from  $40 \mu\text{m}$  to  $2 \mu\text{m}$ . In the present design the sample is at ground potential while all lenses are at 3 kV except for the first electrode of the objective lens, which is at 10 kV, resulting in theoretical lateral image resolution of  $\sim 10 \text{ nm}$  at 2 eV electron energy.

One of the most important part of SPLEEM is the spin manipulator, the source of multi-directional spin-polarized electron beam. The spin gun is based on a laser excited GaAs cathode, which excites

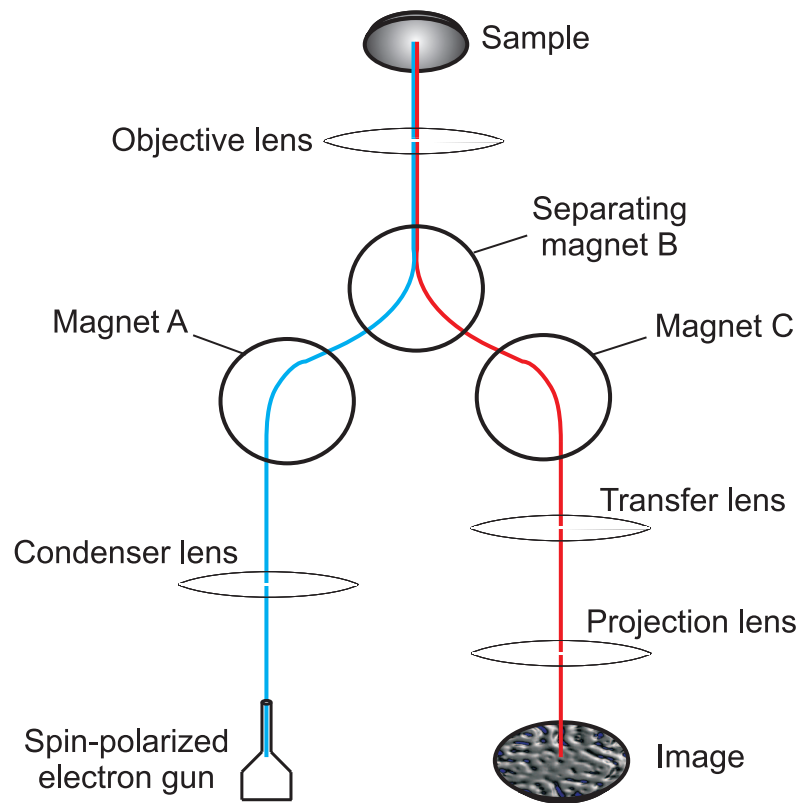


**Figure 4.8:** Schematics of a SPLEEM experimental setup. Spin-polarized electron beam passes through an illumination column (left branch) and is decelerated in the objective lens. Electrons hit the sample with normal incidence. The backscattered electrons are collected in an imaging column (right branch) and focused on a phosphorous screen, where a magnified image of the surface is obtained. The incoming and reflected electron beams are separated in a separating magnet B.

photoemission of spin-polarized electrons with polarization  $\mathbf{P}$  perpendicular to the surface. The direction of  $\mathbf{P}$  is inverted by switching the helicity of the circularly polarized light. Combining electrostatic and magnetic deflection with rotation allows alignment of  $\mathbf{P}$  along any direction in space. Usually two preferred direction in the sample plane and along sample normal are chosen to determine the three components of magnetization  $\mathbf{M}$ . The experimental setup of SPLEEM is described in more detail in references [144, 146, 147].

### 4.3.3 Image acquisition

The magnetic contrast is proportional to  $\mathbf{P} \cdot \mathbf{M}$ . Separation of the magnetic contrast from the structural contrast requires the acquisition of two images with the opposite electron polarizations, corresponding to intensities of the reflected beam ( $I_{\uparrow}$  and  $I_{\downarrow}$ ), and their subtraction from each other (Fig. 4.9). In order to normalize images, the difference image is divided by the sum image. This results in so called asymmetry image

$$A = (I_{\uparrow} - I_{\downarrow}) / (I_{\uparrow} + I_{\downarrow}) \quad (4.3.1)$$

A typical image acquisition time ranges from 1 to 5 sec per image. The procedure for obtaining of the asymmetry image is shown for 3.3 ML thick Fe film grown on Ag(116) (Fig. 4.9). Bright and dark features in the images result from the component of surface magnetization vector along the axis of the spin polarization of the illuminating beam (parallel and anti-parallel, respectively). No magnetic

contrast, i.e. 50% gray color in SPLEEM image is observed if  $|\mathbf{M}| = 0$  (nonmagnetic surface) or if the spin polarization of the incident electron beam is perpendicular to the direction of magnetization at the surface. In general, to follow any orientation of magnetization, images with three orthogonal spin polarizations are recorded.

Since the asymmetry  $A$  changes with energy due to spin-dependent band structure [148], the optimum energy for a maximum magnetic contrast depends on the material and has to be chosen individually. The maximum contrast was found at  $E = 13.5$  eV for Fe/Ag(116) and at  $E = 8.5$  eV for Co/Cu(1113).

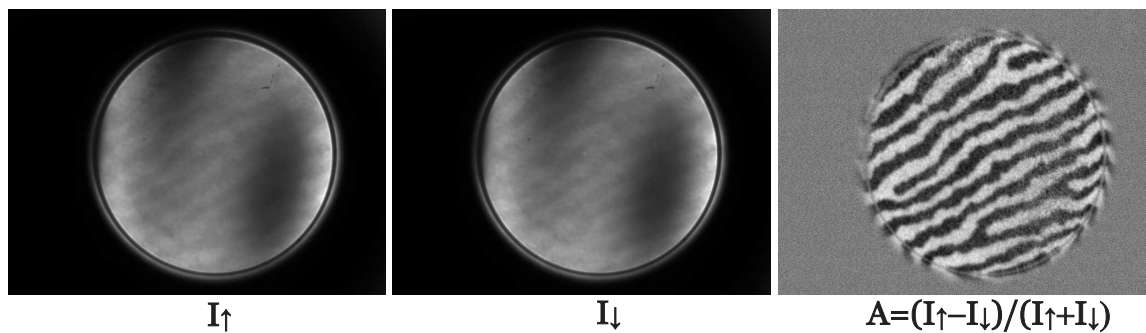


**Figure 4.9:** SPLEEM images of a 3.3 ML thick Fe layer on Ag(116). The images  $I_{\uparrow}$  and  $I_{\downarrow}$  are taken with opposite electron polarization along sample normal (nearly easy axis) at the electron energy 13.5 eV. Contrast-enhanced difference image is obtained by  $A = (I_{\uparrow} - I_{\downarrow}) / (I_{\uparrow} + I_{\downarrow})$ . The field of view is  $12 \mu\text{m}$

It is worth to recall that LEEM can be used either at normal incidence (bright-field) or off-normal incidence (dark-field) mode. The terms bright-field and dark-field imaging originate from optical microscopy and are in common usage in transmission electron microscopy. Dark-field imaging by SPLEEM was successfully employed e.g., to distinguish adjacent terraces and identify the locations of intervening atomic steps [149–151]. In particular, dark-field can be used to distinguish domains of a single structure. This is because in dark-field imaging, the use of diffraction conditions along a fractional-order rod or integer-order rod with non-zero parallel momentum transfer breaks the symmetry between domains [152–154].

The results presented in this thesis were performed in dark-field mode by tilting the macroscopic plane of the sample by  $\sim 2 - 3^\circ$  with respect to the sample normal. The magnetic contrast in dark-field mode was found to be much greater in comparison to the bright-field mode, which is most likely associated with the symmetry of the vicinal surface. Note that in case of Ag(116) and Cu(1113) crystals used in the experiment, the plane of the terraces is tilted by  $\omega = 13.3^\circ$  and  $\omega = 6.2^\circ$ , respectively, with respect to the macroscopic plane of the sample. Therefore, by tilting the macroscopic plane of the sample and imaging in dark-field mode the electrons backscattered from the the terraces plane are collected more effectively .

## 5.1 Magnetization orientations and anisotropy fields from MOKE

In this section, the results of MOKE measurements are presented. The following subsections are classified with respect to different materials and substrates used in the experiment. As described in Sec. 4.1.3, MOKE is the method particularly suitable for estimation of the in-plane uniaxial magnetic anisotropy. By depositing the magnetic film on a stepped surface, broken by atomic steps, symmetry introduces additional uniaxial anisotropy and results in split hysteresis loops, when the magnetic field is applied along the intermediate axis (i.e., in the sample plane, perpendicular to the easy axis). By measurements of the split hysteresis loops and magneto-optical Kerr signal (from which the information about the tilting angle  $\delta$  of magnetization can be obtained), even tiny changes of magnetic anisotropy can be followed.

### 5.1.1 Effects of varying thickness of ferromagnetic films

#### *bcc* Fe films on Ag(001) and Ag(116) surface

Fe/Ag(001) has been studied extensively in the past quarter-century. As almost completely unstrained system, it had attracted much attention of both: theoretical calculations and experiments. Among others, the enhancement of the interface magnetic moments by  $\sim 30\%$  in comparison to the bulk value was predicted [155, 156] and confirmed experimentally [157, 158]. An attention was paid also on magnetic anisotropy of this system [80, 81, 159, 160] due to the easy axis of magnetization oriented perpendicular to the sample plane below  $\sim 5ML$  of Fe. Finally, the Fe/Ag(001) is the first system, where the oscillatory magnetic anisotropy as a function of Fe film thickness was observed experimentally [22, 27, 161]. The results in this subsection are an extension of these previous studies. In particular, the oscillatory magnetic anisotropy in the vicinity of a spin reorientation transition SRT (from in-plane to out-of-plane orientation of the magnetization) is presented.

As already described (sec.2.1.3), by growing the films on stepped surfaces, split hysteresis loops can be measured when the external magnetic field is applied perpendicular to the easy axis (i.e., along the intermediate axis). In case of Fe/Ag(116), split hysteresis loops can be recorded by applying the magnetic field perpendicular to the step edges, along [110] crystallographic axis of the Ag substrate (i.e., along [100] of *bcc* Fe film). Split hysteresis loops for several thicknesses of Fe film are shown in Fig. 5.1.

Split hysteresis loops are characterized by a shift field  $H_s$ , which is a measure of the in-plane step-induced uniaxial anisotropy. The  $H_s$  values evaluated from measured hysteresis loops at 300 K and 5 K as a function of Fe film thickness are plotted in Fig. 5.2a. Positive  $H_s$  means that the easy axis of magnetization is oriented along the steps and in order to measure split loops, the magnetic field was applied perpendicular to the steps. The dependence at 300 K in Fig. 5.2a shows that shift field  $H_s$  increases with increasing Fe thickness and saturates above 25 ML of Fe. In a first approximation,

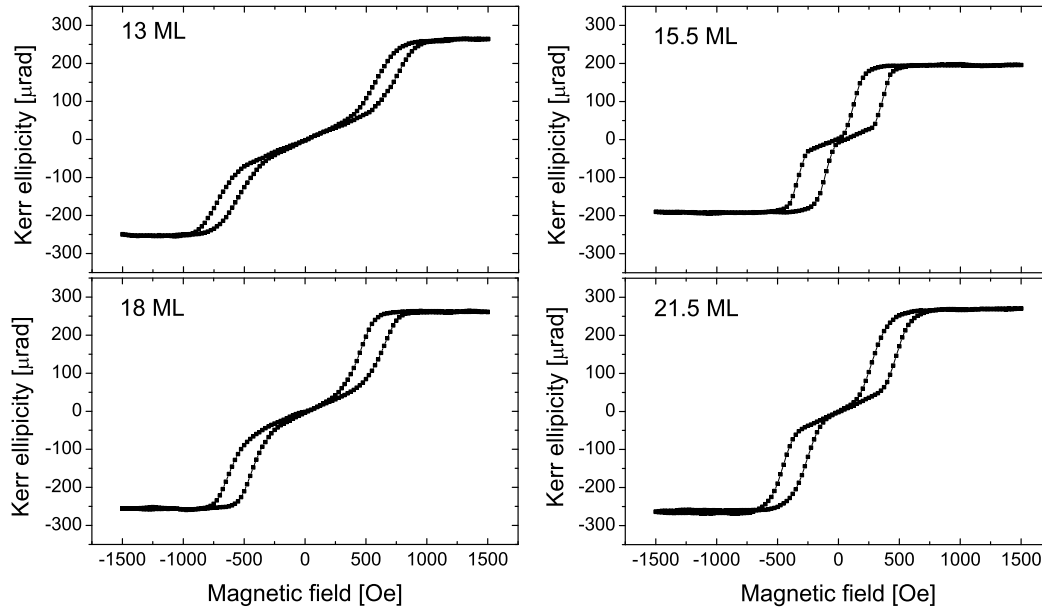


**Figure 5.1:** Split hysteresis loops for Fe/Ag(116) measured perpendicular to the step edges at  $T = 5$  K.

such dependence can be described by  $\mathbf{H}_s = \mathbf{H}_s^{\text{vol}} + \mathbf{H}_s^{\text{surf}}/t$ , where  $H_s^{\text{vol}}$  is the value which  $H_s$  approaches in the limit of large film thickness  $t$  and can be interpreted as the result of the structural distortion in the film volume, while  $H_s^{\text{surf}}$  can be ascribed to the surface contribution to the in-plane uniaxial anisotropy [27,42]. In general, the dependence of  $H_s$  can be more complex (than shown in Fig. 5.2a) and does not scale simply as  $1/t$ . This is due to the fact that the lattice distortion (and therefore  $H_s^{\text{vol}}$ ) can vary with increasing the film thickness.

Although the easy magnetization axis of the Fe film is oriented along the steps direction, the  $H_s$  dependence indicates that  $H_s^{\text{surf}}$  from Fe/Ag and UHV/Fe interfaces prefers to align the magnetic moment perpendicular to the step direction, i.e.,  $H_s^{\text{surf}}$  is negative. Below 8 ML of Fe split hysteresis loops cannot be measured due to approaching SRT\* and thereby strong polar Kerr effect contributing to the total Kerr ellipticity. At 5 K, the shift field  $H_s$  exhibits a large amplitude oscillation as a function of Fe film thickness with a period of  $L_{Fe} = 5.5 \pm 0.3$  ML. Below  $\sim 10$  ML the oscillatory  $H_s$  is perturbed by rapid decrease of  $H_s$  due to approaching SRT. With increasing Fe film thickness the oscillation amplitude decreases gradually from  $\sim 530$  Oe to  $\sim 100$  Oe.

A similar MOKE experiment was performed for Fe films grown on Ag(001) nominally flat surface. In this case, a fourfold magnetic anisotropy with the easy axis parallel to [100] and [010] (i.e., along [110] and  $[\bar{1}10]$  of Ag(001), respectively) supposed to be maintained (since nominally there are no steps). It means that the hysteresis loops measured along [100] and [010] should be square and exactly the same. In a real experiment however, it is not always the case. This is due to the fact that the nominally flat Ag(001) crystal used in experiment is not perfectly flat and consists of wide terraces separated by monoatomic steps. Hence, the Ag(001) nominally flat surface can be treated as a stepped surface with a low step density. Using STM, an averaged terrace width of the monoatomic terraces of Ag(001) was determined for  $\sim 200$  nm. Even such steps modify magnetic anisotropy and split hysteresis loops can be measured by applying magnetic field perpendicular to the step edges. The dependence of the shift field  $H_s$  as a function of Fe thickness is shown in Fig. 5.2b. Similarly as in the case of Fe/Ag(116), due to the strong polar Kerr contribution to the hysteresis loops measured in longitudinal geometry with approaching SRT, the measurement of split hysteresis loops below  $\sim 7$  ML of Fe is not possible. At 300 K,  $H_s$  slightly decreases with increasing Fe thickness. This is most likely due to relaxation of the of the structural

\*The influence of SRT on the dependence of  $H_s$  is discussed in Sec. 6.3.2.

## SECTION 5.1

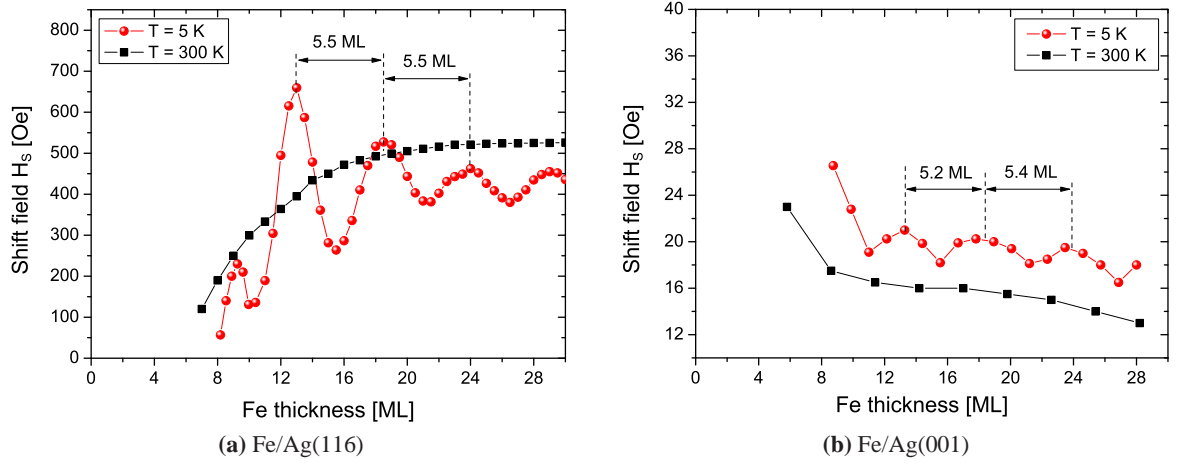


**Figure 5.2:** Shift field  $H_s$  as a function of thickness of Fe film grown on Ag(116) vicinal surface and Ag(001) nominally flat surface.  $H_s$  values were evaluated from split hysteresis loops measured perpendicular to the step edges at 300 K and 5 K.

distortion introduced by the steps. Such decrease of  $H_s$  is not visible in the case of Fe/Ag(116) because for densely packed steps the structural distortion cannot relax along the terraces which are too narrow. In the case of wide terraces (e.g., as for nominally flat Ag(001) surface), the vertical perturbation can relax and eventually disappear with increasing film thickness. Although with a small amplitude ( $\sim 3$  Oe), clearly distinguishable oscillations of  $H_s$  as a function of Fe thickness are observed at 5 K. The oscillation amplitude is different for Fe films grown on Ag(116) and Ag(001) because its scales quadratically with the step density and depends on how much the anisotropy in the film volume is modified by the steps [27]. The period of oscillations  $L_{Fe}$  is the same as for the Fe films grown on Ag(116) surface [22, 27, 161] and on average is equal  $L_{Fe} = 5.3 \pm 0.3$  ML. This experiment shows that even negligible in-plane uniaxial anisotropy, which can be present in Fe film grown on Ag(001) nominally flat surface, is sufficient to detect the magnetic anisotropy oscillations.

As already mentioned in Sec. 2.1.3, due to the competition between magnetocrystalline anisotropy and magnetic shape anisotropy, the magnetization can be tilted from the sample plane when is oriented perpendicular to the step edges. By measuring the Kerr ellipticity  $\phi^H$  at  $H_s$  in longitudinal geometries:  $\alpha^+$  (perpendicular to the steps) and  $\alpha^-$  (perpendicular to the steps after  $180^\circ$  rotation of the sample), the tilting angle  $\delta$  of the magnetization can be evaluated (Sec. 4.1.3). Some representative hysteresis loops measured in these geometries at 5 K are shown in Fig. 5.3. Depending on the thickness of Fe film, the easy magnetization axis can be oriented parallel to the steps or perpendicular to the steps. Thus, by applying the magnetic field perpendicular to the steps, split loops or square loops are observed, respectively (Fig. 5.3). Kerr ellipticity measured at  $\alpha^+$  and  $\alpha^-$  geometries consist of two contributions, longitudinal  $\phi_L$  and polar  $\phi_P$ . In case of the hysteresis loops shown in Fig. 5.3, at  $\alpha^-$  (left column) polar Kerr signal is additive, while at  $\alpha^+$  (right column) polar Kerr signal is subtractive. The hysteresis loops measured at  $\alpha^+$  are reversed (show positive signal at negative magnetic field and negative signal at positive magnetic field) because polar Kerr signal (which is subtractive in this geometry) is larger than the longitudinal signal. With decreasing Fe thickness, in particular below 6 ML of Fe, the coercivity of the hysteresis loop increases. This is associated with SRT from in-plane to out-of-plane orientation of magnetization. Therefore, the magnetic field which is applied in the sample plane, has to be larger in the vicinity of SRT, since the out-of-plane component of the magnetization become dominant. For thicknesses lower than 4 ML, magnetization could not be switched even with the maximum available magnetic field 6000 Oe. However, by using MOKE in polar geometry (i.e. by applying magnetic field perpendicular to the sample plane), square hysteresis loops were detectable down to 2 ML of Fe.

The dependence of Kerr ellipticity  $\phi^H$  at  $H_s$  on Fe thickness for three geometries  $\alpha^+$ ,  $\alpha^-$  and  $\alpha^\parallel$  is

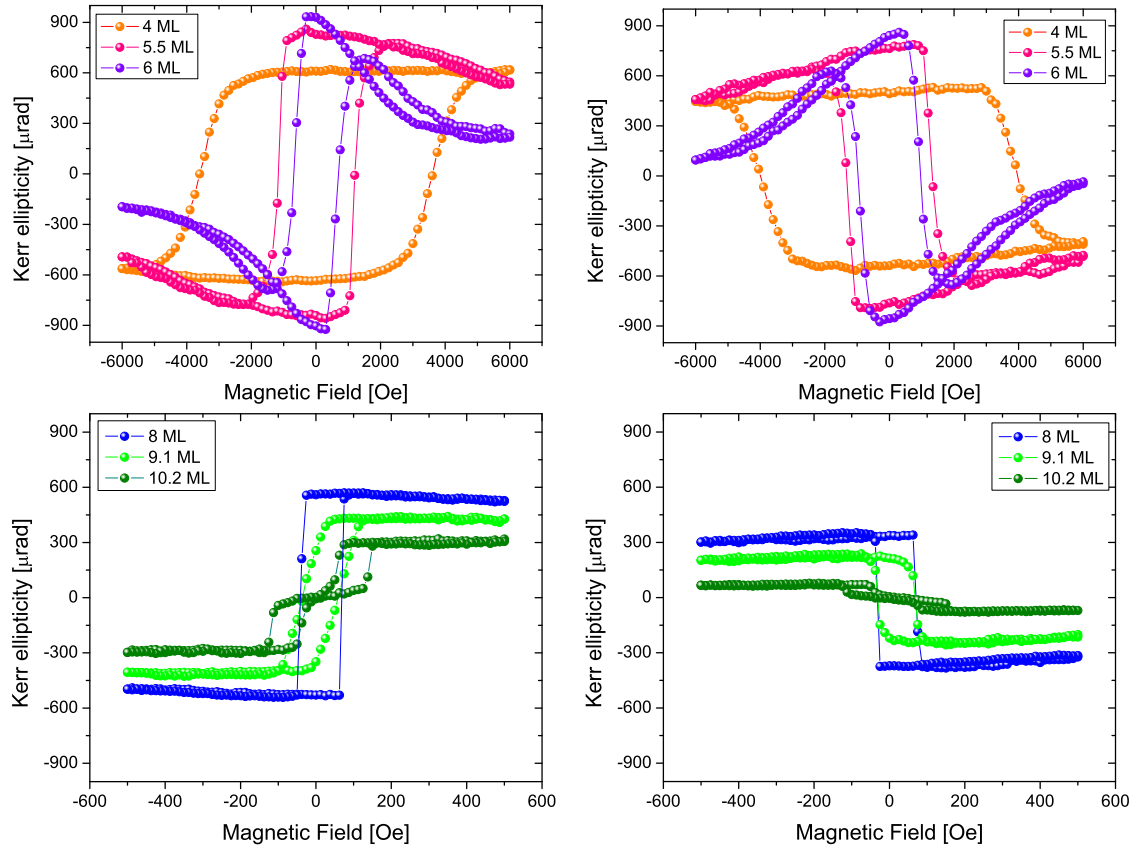


**Figure 5.3:** Hysteresis loops for chosen thicknesses of Fe film on Ag(116) measured at  $T = 5$  K with the magnetic field applied perpendicular to the steps in geometries:  $\alpha^-$  (left column) and  $\alpha^+$  (right column)

shown in Fig. 5.4. It is immediately visible that Kerr ellipticity  $\phi^H$  measured at geometries  $\alpha^+$  and  $\alpha^-$  is significantly different than measured at  $\alpha^\parallel$  and this divergence increases with decreasing Fe film thickness. Negative values of  $\phi^H$  denote that measured hysteresis loops were reversed. Initial increase of the absolute values of  $\phi^H$  at  $\alpha^+$  and  $\alpha^-$  with increasing Fe thickness (up to  $\sim 6$  ML) and subsequently decrease is related to changes of polar Kerr contribution  $\phi_P$ . At 5 K, oscillatory behavior of  $\phi^H$  is observed when probed at  $\alpha^+$  and  $\alpha^-$ . The fact that oscillatory behavior of  $\phi^H$  is observed only at low temperature and only at  $\alpha^+$  and  $\alpha^-$  geometries (no oscillations at  $\alpha^\parallel$ ), clearly indicates that the oscillations of  $\phi^H$  observed in our experiment are not related to the oscillatory magneto-optical effects\*.

The longitudinal  $\phi_L$  and polar  $\phi_P$  contributions to the total Kerr ellipticity were calculated according to equations (4.1.5) and (4.1.6). Consequently, the tilting angle  $\delta$  of magnetization was obtained from the formula (4.1.7). The dependence of  $\delta$  on Fe film thickness is shown in Fig. 5.5. For thicker than 15 ML film, tilting angle  $\delta$  at 300 K is positive, slightly exceeding zero. It means that the magnetization is tilted from the sample plane toward the terraces plane (how  $\delta$  is defined is shown in Fig. 5.5 (a)). With decreasing thickness of the Fe film,  $\delta$  decreases changing the sign at around 13 ML and becomes negative. Below 8 ML, tilting angle changes rapidly due to approaching SRT and reaches the maximum value  $\delta = -76^\circ$  for  $\sim 5$  ML. This angle corresponds roughly to [001] direction, which for bare Ag(116) crystal is oriented  $13.3^\circ$  off the sample normal, i.e., is equivalent to  $\delta = -76.7^\circ$ . At 5 K, the overall changes of  $\delta$  are similar as at 300 K. In addition, the oscillatory behavior of  $\delta$  as a function of Fe thickness is observed at 5 K. Three maxima of  $\delta$  can be distinguished at  $\sim 8$  ML,  $\sim 13$  ML and  $\sim 18.5$  ML, which corresponds to the averaged period of oscillations  $L_{Fe} = 5.3 \pm 0.3$  ML. The oscillations of  $\delta$  are

\*Oscillatory magneto-optical Kerr effect can be observed for instance when QWS from unoccupied  $sp$ -states are formed [13].



SECTION 5.1

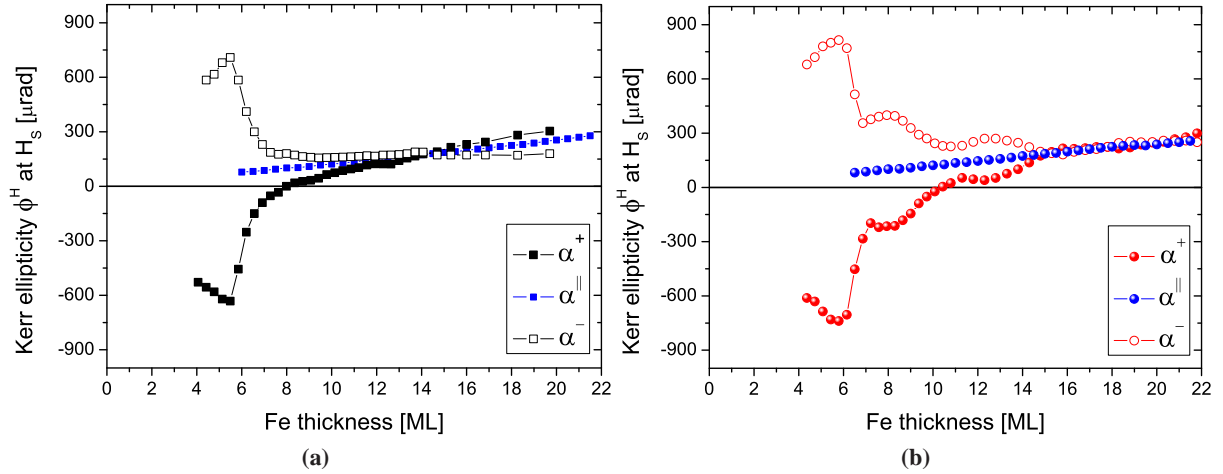


**Figure 5.4:** Kerr ellipticity  $\phi^H$  at  $H_s$  as a function of thickness of Fe film grown on Ag(116) surface obtained from hysteresis loops measured at (a)  $T = 300$  K and (b)  $T = 5$  K

perturbed below  $\sim 7$  ML of Fe due to rapid change of tilting angle related to SRT. As already mentioned, below 4 ML of Fe, the hysteresis loops could not be measured due to large coercivity exceeding the available maximum magnetic field.

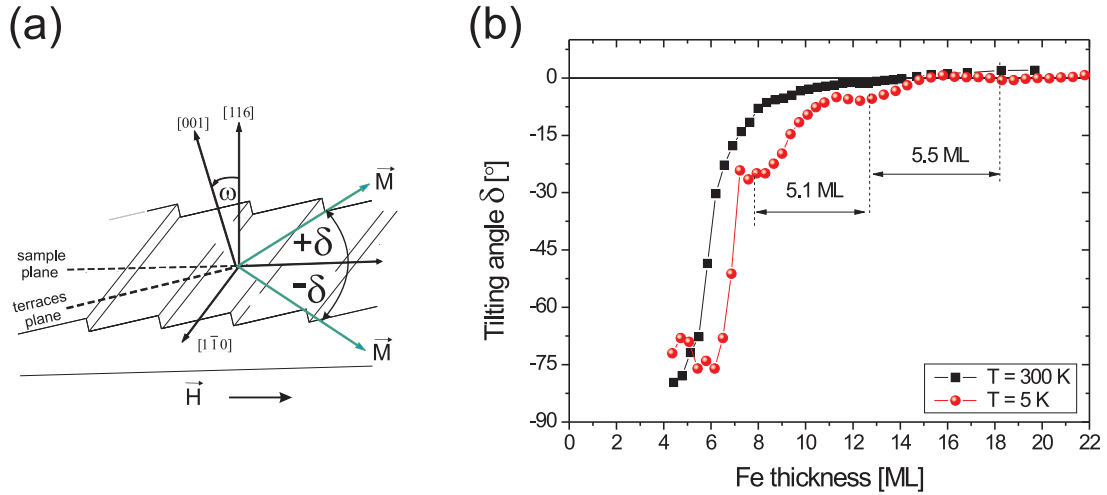


**Figure 5.5:** (a) Schematic representation of (116) vicinal surface with orientations of the magnetization corresponding to positive and negative values of the tilting angle  $\delta$ ; (b) The dependence of the tilting angle as a function of thickness of Fe film on Ag(116) at  $T = 300$  K and  $T = 5$  K

To verify whether the observed oscillatory behavior of  $H_s$  and  $\delta$  as a function of Fe film thickness depends upon covering with nonmagnetic layer, an additional experiment was performed for Fe/Ag(116) covered with constant thickness, 15 ML of Au. The dependence of shift field  $H_s$  as a function of Fe film thickness is shown in Fig. 5.6 (a). It can be observed that covering the Fe films with Au changes the dependence of  $H_s$ . With decreasing thickness of the Fe film,  $H_s$  changes the sign at  $\sim 9$  ML. It means that the easy magnetization axis reorients from parallel to the steps to perpendicular to the steps direction. Thus, the surface contribution  $H_s^{surf}$  from Fe/Au interface prefers the orientation perpendicular to the steps more than in case of the uncovered Fe film.

Similarly as in case of uncovered Fe films,  $H_s$  oscillates as function of Fe thickness at 5 K. Since covering with Au makes  $H_s$  smaller (i.e., less positive and/or more negative), the oscillations result in a

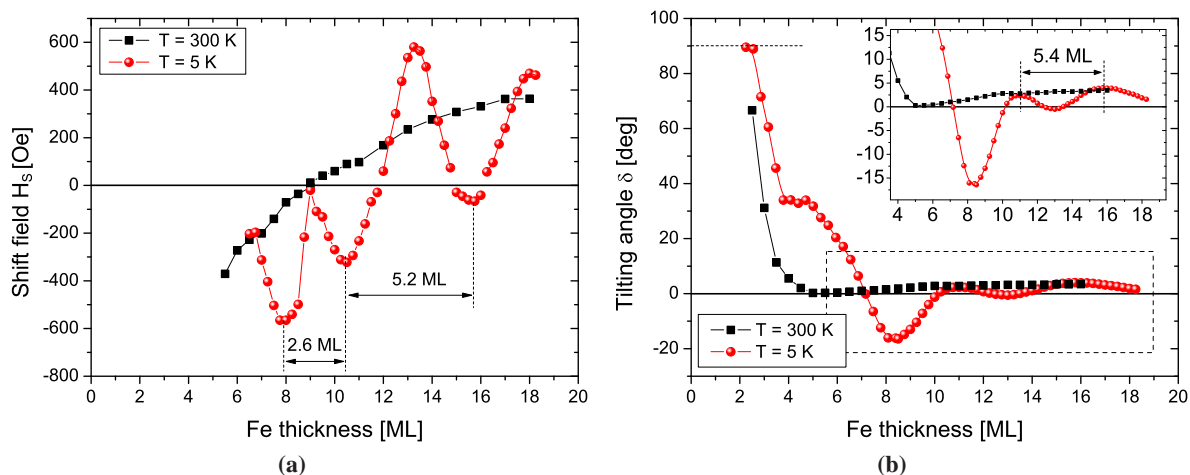


**Figure 5.6:** (a) Shift field  $H_s$  and (b) tilting angle  $\delta$  as a function of thickness of Fe film grown on Ag(116) surface and covered by 15 ML of Au.

oscillations of the easy magnetization axis between parallel and perpendicular to the steps. For thicker Fe films, above 10 ML the oscillation period is the same as in the case of uncovered Fe, i.e., 5.2 ML. However, with decreasing Fe thickness below 10 ML the distance between the minima of  $H_s$  is two times shorter and results in the period of 2.6 ML. Moreover, the oscillation amplitude is also reduced below 10 ML of Fe. The shortening of the oscillation period and amplitude in this thickness regime of Fe film is related to the interplay between in-plane and out-of-plane magnetization components and is discussed in detail in Sec. 6.3.2.

The tilting angle  $\delta$  of the magnetization was evaluated for Au-covered Fe films. The dependence of  $\delta$  on Fe thickness is shown in Fig. 5.6 (b). At 300 K, in the thickness regime of Fe film from 5 ML to 16 ML, the tilting angle is positive, only slightly exceeding zero value (i.e., exactly as in the case of thick uncovered Fe film). With decreasing Fe thickness below  $\sim 4$  ML,  $\delta$  increases rapidly due to SRT. However, differently as in the case of uncovered Fe film, now  $\delta$  is positive. It means that the rotation of the magnetization from in-plane to out-of-plane orientation proceed differently for uncovered and Au-covered. According to the orientation of the Ag(116) surface shown in Fig. 5.5 (a) it corresponds to the clockwise and anticlockwise rotation of the magnetization for uncovered and Au-covered Fe film, respectively. Note that the SRT is shifted down to  $\sim 3$  ML for Au-covered Fe film in comparison to uncovered Fe film, where SRT occurs at  $\sim 6$  ML.

At 5 K the tilting angle oscillates with a period of  $L_{Fe} = 5.4 \pm 0.3$  ML, i.e., the same period as in the case of uncovered Fe film. Differently than in case of the dependence of  $H_s$ , the shortening of the oscillation period is not observed here. Below around 4.5 ML of Fe, rapid increase of  $\delta$  due to SRT affects its oscillatory behavior. The SRT results in increase of the tilting angle value up to  $\delta = +90^\circ$ , which corresponds exactly to the orientation of magnetization perpendicular to the sample plane, i.e., along [116] crystallographic direction.

### ***bcc* Fe films on Au(1113) surface**

Since MA oscillations of *bcc* Fe films grown on Ag(001) surface are ascribed to QWS formed inside the Fe film, their existence should be independent of the substrate material (with the assumption that conditions for the confinement of the electronic band are fulfilled, i.e., appropriate electrons of Fe cannot penetrate into the substrate). Therefore, it is desirable to verify the effect of the oscillatory MA in *bcc* Fe films grown on a different substrate. From the point of view of the epitaxial growth, Au(001) surface seems to be the most appropriate choice. Nearly perfect lattice match of the  $45^\circ$  rotated *bcc* Fe(001) with respect to *fcc* Au(001) (mismatch: 0.6%) results in well stabilized *bcc* Fe films growing in layer-by-layer

## SECTION 5.1

mode [86, 87, 89]. The perpendicular interface anisotropy for Fe/Au(001) is nearly twice smaller than for Fe/Ag(001),  $0.47 \text{ erg/cm}^2$  and  $0.81 \text{ erg/cm}^2$ , respectively [162]. As a result, SRT from in-plane to out-of-plane magnetization orientation is shifted to lower thicknesses (in comparison to Fe film grown on Ag(001)) and occurs at around 3 ML of Fe when grown on Au(001) surface [87, 163, 164].

The MOKE experiment was carried out for Fe films grown on Au(1113) surface. In contrast to Fe/Ag(116), for Fe/Au(1113)  $H_s$  is negative in the whole investigated thickness range (Fig. 5.7(a)). This means that the easy magnetization axis is oriented perpendicular to the steps and thus, in order to measure split hysteresis loops, the magnetic field needs to be applied along the steps. Similarly as in the case of Fe/Ag(116), the  $H_s$  values for Fe/Au(1113) measured at 300 K follow the  $1/t$  dependence. Above 30 ML of Fe, the  $H_s$  dependence saturates, approaching  $H_s \simeq 0$ . This means that both in-plane directions, parallel and perpendicular to the step edges are nearly equivalent for thick Fe film. The dependence of  $H_s$ , both at 300 K and 5 K, indicates a strong negative surface contribution  $H_s^{surf}$ . As a consequence, with decreasing thickness of the Fe film, the absolute value of  $H_s$  increases and thus, more and more magnetic field is necessary to switch the magnetization into the steps direction. Eventually, at  $\sim 8$  ML, split hysteresis loops become hard hysteresis loops and  $H_s$  value cannot be derived. At 5 K, oscillations of  $H_s$  with periodicity of  $L_{Fe} = 6.2 \pm 0.3$  ML are visible. Therefore, the oscillation period  $L_{Fe}$  of  $H_s$  is slightly larger than in case of Fe films grown on Ag(001) and Ag(116) surface. The oscillation amplitude is of the order of 200 Oe.

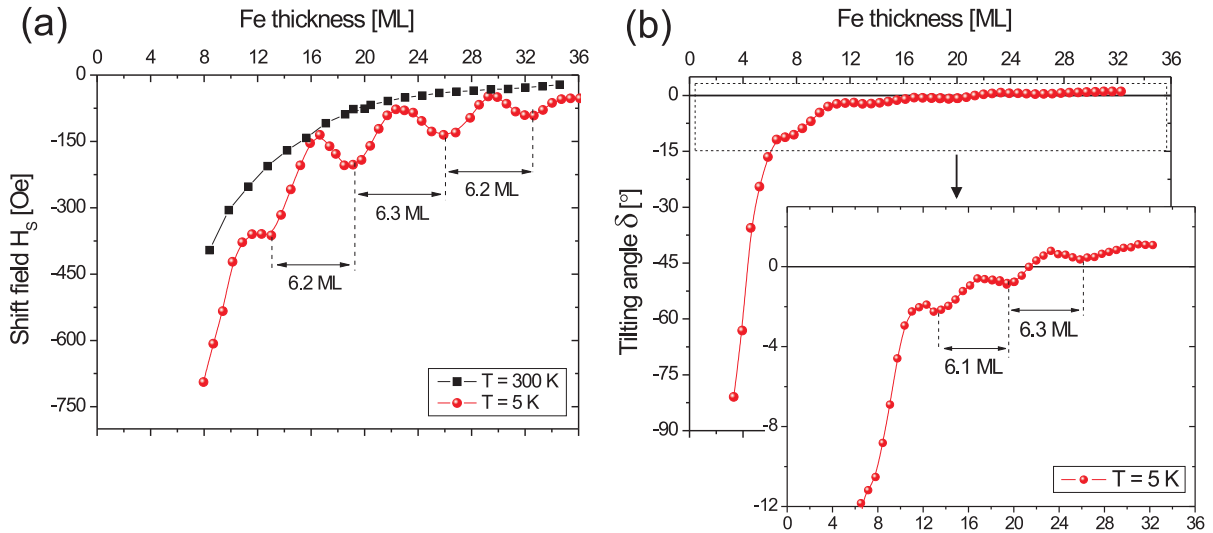


**Figure 5.7:** (a) Shift field  $H_s$  and (b) tilting angle  $\delta$  as a function of thickness of Fe film grown on Au(1113) surface.

The tilting angle  $\delta$ , obtained from the Kerr ellipticity  $\phi^H$  is shown in Fig. 5.7(b). For thick Fe films,  $\delta$  is positive ( $\sim 1^\circ$ ), i.e., the magnetization is tilted from the sample plane toward the terraces plane. With decreasing Fe film thickness,  $\delta$  changes sign at  $\sim 21$  ML and increases its absolute value, eventually reaching  $\delta = -81^\circ$  at 3.3 ML of Fe (the lowest investigated Fe thickness). Thus, the magnetization at 3.3 ML of Fe is oriented almost exactly perpendicular to the terraces plane, which corresponds to the  $\delta = -83.8^\circ$  for Au(1113) surface.

Besides changes related to SRT, the oscillatory behavior of  $\delta$  is observed. The oscillation period of  $\delta$  is equal  $L_{Fe} = 6.2 \pm 0.3$  ML (see inset in Fig. 5.7(b)), i.e., exactly the same as the oscillation period of  $H_s$ . The oscillation amplitude of  $\delta$  is very small in this case ( $1^\circ$ ). The oscillation amplitudes of  $H_s$  and  $\delta$  are different for Fe films grown on Au(1113) and on Ag(116) due to different step density of these surfaces [27].

### *fcc* Co films on Cu(1113) surface

Since the period of the MA oscillations is determined by the wavevector of the corresponding electronic band, different oscillation periods are expected for different FM films. In order to prove the relation of the oscillation period to the electronic structure, MOKE experiments were carried out for *fcc* Co films grown on Cu(1113) surface. *fcc* Co grows on Cu(001) in a nearly ideal layer-by-layer mode [90] and is one of the mostly studied thin FM films. In particular, Co/Cu(001) is the only system for which oscillatory MA due to QWS in FM films has been investigated by theory [19–21]. This allows a direct comparison to experiment. Independent of the film thickness, the remanent magnetization of the Co films is always found to lie within the film plane with in-plane four-fold anisotropy and the easy magnetization axis oriented along [110] direction.

It is known that for uncovered Co films grown on vicinal Cu(001) surface, at 300 K the shift field  $H_s$  initially is positive (i.e., the easy magnetization axis is initially oriented parallel to the steps) and decreases monotonically with increasing Co thickness [56]. At  $\sim 15$  ML of Co, an abrupt decrease of  $H_s$  occurs due to strain relaxation which is accompanied by a switch of the easy magnetization axis to perpendicular to the steps direction (i.e.,  $H_s$  become negative) (see uncovered Co/Cu(1113) in Fig. 5.8a). A large positive value of  $H_s$  in thin regime of Co film indicates that surface contribution  $H_s^{surf}$  to the in-plane uniaxial anisotropy is positive (favors orientation parallel to the steps).

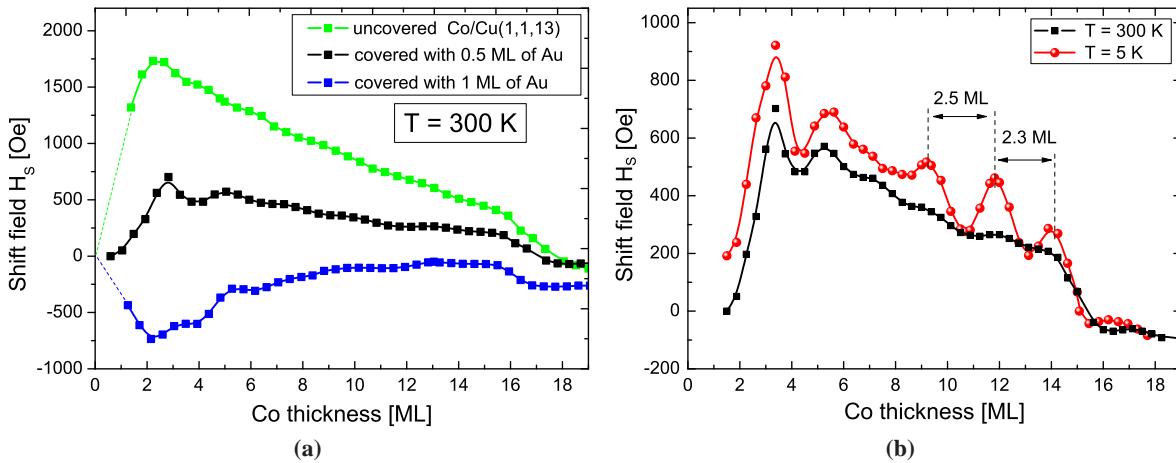


**Figure 5.8:** Shift field  $H_s$  as a function of thickness of Co film grown on Cu(1113) surface: (a) for different thickness of Au coverage and measured at 300 K; (b) for 0.5 ML coverage of Au and measured at 300 K and 5 K.

By covering Co films with a nonmagnetic material such as Au, the local atomic configuration at the Co surface changes and the surface contribution to the step-induced uniaxial anisotropy can be modified [22, 23]. Similarly as for Fe/Ag(116), covering Co films with Au results in negative  $H_s^{surf}$  (i.e., the magnetization is forced to be oriented perpendicular to the steps). How the dependence of  $H_s$  on Co thickness evolves with sub-monolayer Au coverage is shown in Fig. 5.8a. By depositing minute amounts of Au on Co films, the magnitude of  $H_s$  can be significantly reduced and brought close to  $H_s = 0$  over a wide thickness range of Co. This offers a higher sensitivity to small variations of  $H_s$  in the MOKE experiment and allows to change the easy magnetization axis by small variations of  $H_s$ .

At 5 K, the oscillatory behavior of  $H_s$  as a function of Co thickness is observed. Independent of the Au thickness,  $H_s$  oscillates with a period of  $L_{Co} = 2.3 \pm 0.3$  ML. The dependence of  $H_s$  obtained at 300 K and 5 K for Co/Cu(1113) covered by 0.5 ML of Au is shown in Fig. 5.8b. The oscillation amplitude below 15 ML of Co is about 300 Oe. After an abrupt decrease of  $H_s$  related to strain relaxation, the oscillatory behavior of  $H_s$  vanishes.

The oscillatory behavior as a function of Co thickness is also observed in Kerr ellipticity  $\phi^H$  at  $H_s$ . The dependence of  $\phi^H$  at  $H_s$  on Co thickness at 5 K, obtained from the hysteresis loops measured

## SECTION 5.1

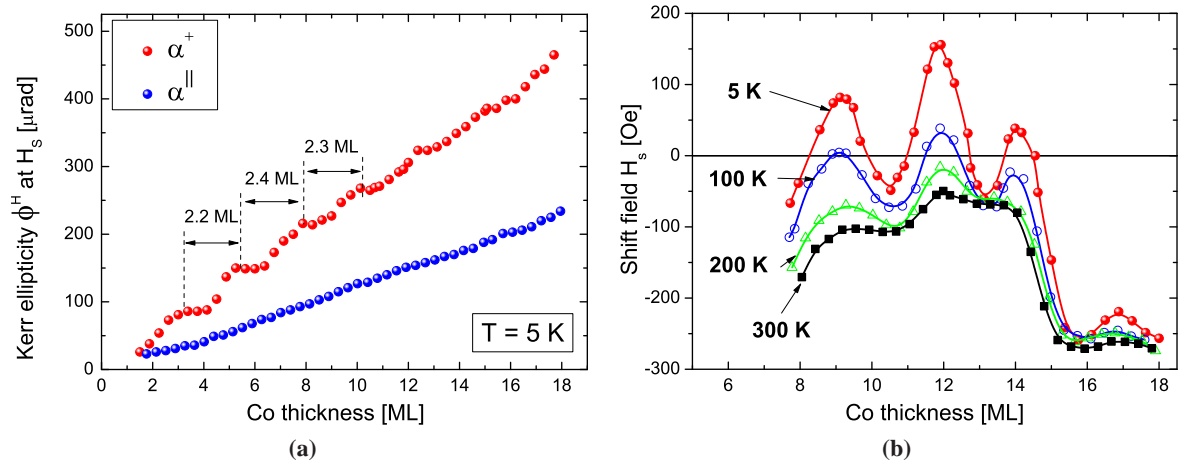


**Figure 5.9:** The dependence of: (a) Kerr ellipticity  $\phi^H$  at  $H_s$  at 5 K and (b) the shift field  $H_s$  at different temperatures as a function of thickness of Co film grown on Cu(1113) surface.

perpendicular to the steps ( $\alpha^+$ ) and parallel to the steps ( $\alpha^{\parallel}$ ), is shown in Fig. 5.9a. The oscillations with a period of  $2.3 \pm 0.3$  ML are only present when measured at  $\alpha^+$  geometry. The Kerr ellipticity at  $\alpha^{\parallel}$  increases linearly with increasing thickness of Co film what confirms that oscillatory behavior of Kerr ellipticity at  $\alpha^+$  is related to change of the tilting angle of the magnetization. The oscillation amplitude of  $\phi^H$  is small and corresponds to changes of the tilting angle  $\delta$  of  $\sim 1^\circ$ .

To investigate the temperature dependence of  $H_s$  as a function of Co thickness, a careful MOKE analysis within the Co thickness range between 8 ML and 18 ML was performed (see Fig. 5.9b). For this experiment the sample was covered with 1 ML of Au, in order to reduce the magnitude of  $H_s$  (compare Fig. 5.8a). The shift field at 9.3, 11.9, 14.0, and 16.6 ML depends strongly on temperature, whereas for 10.6, 13, and 15.6 ML there is almost no dependence on temperature. The oscillation amplitude of  $H_s$  decreases gradually with increasing the temperature and eventually vanishes at 300 K.

### ***bcc* Co films on Au(1113) surface**

Apart from *fcc* Co film, which can be grown on Cu(001), an epitaxial *bcc* Co film can be stabilized by appropriate choice of substrate, e.g. Au(001) [91–95]. The metastable *bcc* phase of Co is particularly interesting due to its novel magnetic properties. For instance, huge magnetoresistance up to 410% at RT for Co(001)/MgO(001)/Co(001) magnetic tunnel junctions with *bcc* Co electrodes was reported [165]. Therefore, *bcc* Co films attract the attention of people interested in fundamental physics of magnetism and in practical applications for spintronic's devices. Since the crystal structure and symmetry play a significant role in determining the electronic band structure, changing the structure symmetry of Co film from *fcc* to *bcc* is also very interesting from the point of view of MA. In particular, one can expect change in the oscillatory behavior of MA.

The *bcc* Co films were grown on vicinal Au(1113) surface. Experimental studies in the low thickness range of Co grown on flat Au(001) show that Co layers grow on the Au(001) surface with the epitaxial relationship of *fcc* Au(110)  $\parallel$  *bcc* Co(100) [95], resulting in fourfold in-plane magnetic anisotropy with the easy axes along [100] of Co [92]. Thus, if indeed *bcc* Co is grown on Au(1113) surface, the easy magnetization axis supposed to be oriented along one of the two crystallographic axes of the substrate: [110] or  $[\bar{1}\bar{1}0]$  axis. This is what is observed in our experiment. The orientation of the easy magnetization in whole investigated thickness range, i.e., from 5 ML up to 30 ML, is oriented along [110] direction of the substrate (i.e., perpendicular to the steps).

The dependence of shift field  $H_s$  as a function of Co thickness is shown in Fig. 5.10a. In contrast to Au/Fe/Ag(116), Au/Co/Cu(1113) and Fe/Au(1113) systems, where the negative interface contribution

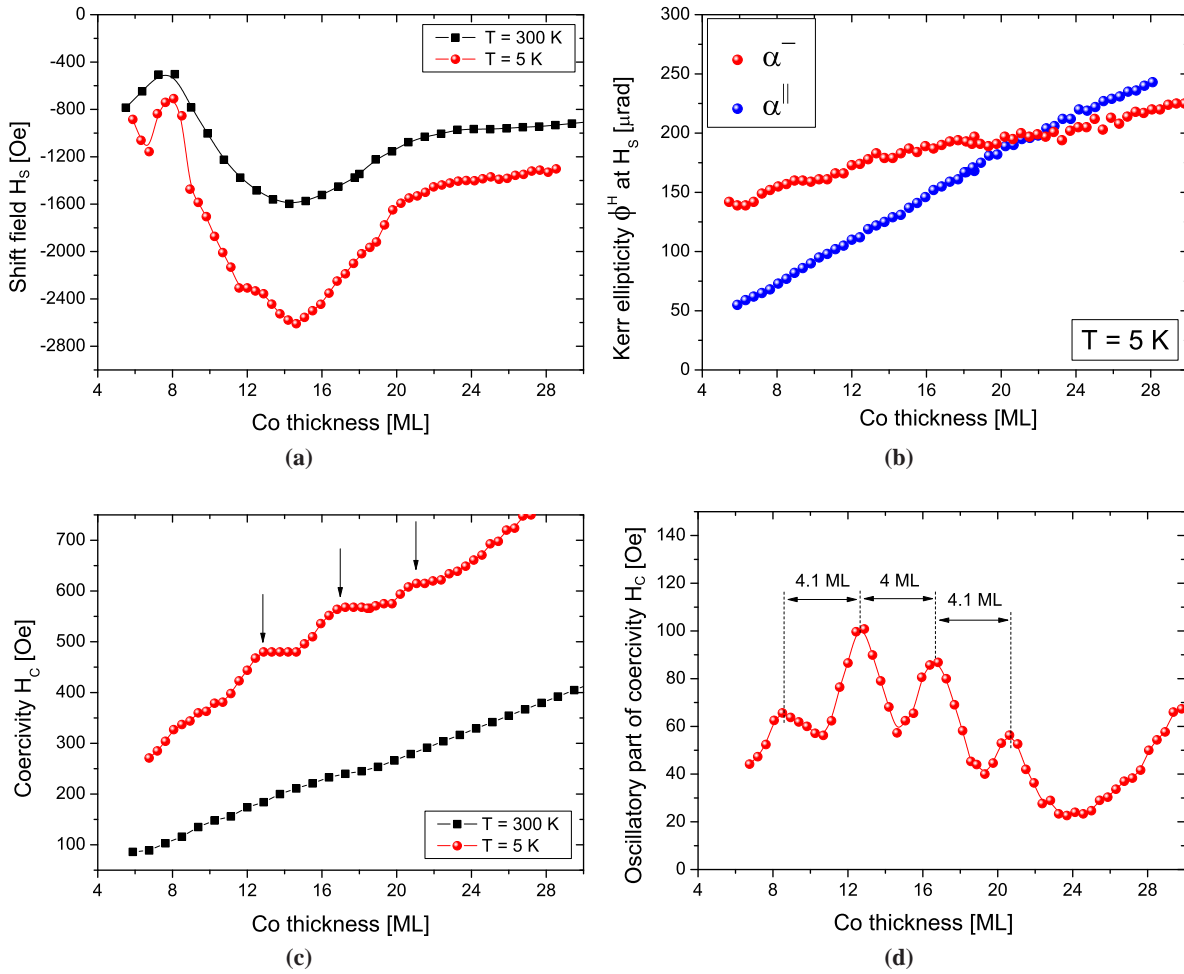


**Figure 5.10:** The dependence of: (a) Shift field  $H_s$ , (b) Kerr ellipticity  $\phi^H$  at  $H_s$ , (c) coercivity  $H_c$  and (d) oscillatory part of  $H_c$  as a function of thickness of Co film grown on Au(1113) surface.

to the in-plane uniaxial anisotropy  $H_s^{surf}$  from Au scales as  $1/N$  (where  $N$  denotes the number of layers), the case of Co/Au(1113) is more complex. First of all, the volume contribution to the in-plane uniaxial anisotropy  $H_s^{vol}$  is strongly negative, approaching  $-800$  Oe and  $-1400$  Oe for thick film at 300 K and 5 K, respectively. At both temperatures, with decreasing Co thickness below 20 ML,  $H_s$  becomes more negative (i.e., the in-plane uniaxial anisotropy increases) approaching the maximum absolute value at 15 ML. With further decreasing Co thickness,  $H_s$  decreases and reaches the minimum at  $\sim 8$  ML. Interestingly, below 8 ML,  $H_s$  increases again. Based on previous reports on Co/Au(001) system, one can expect a non-trivial growth and therefore, significant changes of MA as a function of Co film thickness. STM studies [95] revealed for instance, that post-annealing activates several diffusion mechanisms, including surface segregation of Au with a clear separation between Au and Co. As a consequence, regular nanostructures aligned in the Co(100) direction and consisting of buried Co islands with a characteristic reconstruction of the Au(001) surface can be observed [95].

The height of the mono-atomic layer of *bcc* Co is equal to 0.14 nm [95], i.e., much smaller than the interlayer distance in Au(001) substrate, which is 0.2 nm. Therefore, a strong strain of the Co lattice at the steps of the vicinal surface is expected. With increasing Co thickness, the misfit strain can change, e.g., by structural relaxation. Since  $H_s$  value is very sensitive to changes of the interlayer distance, such structural relaxation can significantly modify the dependence of the  $H_s$ .

As already mentioned, Co layers are embedded with a surfactant Au monolayer [92–95]. There-

fore, the interface contribution to the in-plane uniaxial anisotropy from Au is not only limited to the bottom interface, but also includes the contribution from the upper interface. Note however that with increasing Co thickness, less Au atoms can diffuse on the top of Co film. Therefore, one can expect that the interface contribution to  $H_s$  from the upper interface varies with Co thickness. This, together with possible structural relaxation of Co with increasing thickness can result in a complex dependence of  $H_s$ .

In fact, already at 300 K, the dependence of  $H_s$  could suggest sort of long-period oscillatory behavior (Fig. 5.10a). However, MA oscillations are expected to be the strongest at low temperatures [19, 161] and therefore, any oscillatory MA should be enhanced (and usually only visible) at low temperature. Since it is not the case, such possibility can be excluded. Although in general dependence of  $H_s$  proceed similarly at both temperatures, some features invisible at 300 K, but appearing at 5 K, are observed at  $\sim 8.5$  ML and  $\sim 12.6$  ML. Due to overall high magnitude of  $H_s$  and its non-trivial dependence, it is difficult to extract oscillatory contribution to MA. Furthermore, there is no indication of any oscillatory behavior in the Kerr ellipticity  $\phi^H$  at  $H_s$  (Fig. 5.10b). The Kerr ellipticity derived from the hysteresis loops measured at 5 K either perpendicular to the steps ( $\alpha^-$ ) or parallel to the steps ( $\alpha^\parallel$ ) increases linearly with increasing Co thickness. Crossing of the Kerr ellipticity dependencies  $\alpha^-$  and  $\alpha^\parallel$  at  $\sim 20$  ML reflects a change of the sign of the tilting angle  $\delta$  with increasing Co thickness from negative to positive value, respectively.

Besides the Kerr ellipticity  $\phi^H$  at  $H_s$  derived from square hysteresis loops measured perpendicular to steps, coercivity  $H_c$  as a function of Co thickness was evaluated (as shown in Fig. 5.10c). As can be seen,  $H_c$  at 300 K is not sensitive to the aforementioned changes of the in-plane uniaxial magnetic anisotropy (visible in the  $H_s$  dependence) and increases linearly with increasing film thickness as  $H_{c,300K} = 14.2 \cdot N$  (where N denotes number of Co layers). At 5 K, overall magnitude of  $H_c$  is increased, which is common behavior for most of the ferromagnetic materials due to enhanced MA and thermal activation barrier at low temperature [166–168]. The base value of  $H_c$  dependence can be approximated with the linear fit  $H_{c,5K} = 59 + 24.9 \cdot N$ . Interestingly, additional peaks are superimposed on this linear dependence, as marked by arrows in Fig. 5.10c. In order to get more insight into this peculiar behavior, the linear fit  $H_{c,5K}$  was subtracted from  $H_c$  dependence at 5 K. In this way, purely oscillatory part of  $H_c$  was obtained (Fig. 5.10d). Four distinct maxima in  $H_c$  dependence can be distinguished, separated from each other with nearly equivalent distance of  $4.1 \pm 0.3$  ML. The amplitude of the oscillatory  $H_c$  varies from  $\sim 10$  Oe to  $\sim 50$  Oe. Interestingly, the first two maxima are observed at  $\sim 8.5$  ML and  $\sim 12.6$  ML, i.e., at thicknesses corresponding to the two peaks observed in the dependence of shift field  $H_s$  at 5 K (compare Fig. 5.10a and Fig. 5.10d). This can indicate that oscillatory behavior with the same period is observed also in the case of  $H_s$  dependence on Co thickness. However, due to overall high magnitude of  $H_s$  and its non-trivial dependence on Co thickness, the oscillations of a small amplitude are difficult to recognize and only two first peaks are visible. Moreover, for films with strong in-plane uniaxial anisotropy and the easy axis of magnetization oriented perpendicular to the steps, the split hysteresis loops become more complex. As a consequence, the measurement's precision of  $H_s$  is rather low and not sufficient to detect small changes, of the order of  $\sim 50$  Oe. In contrast, when square loops are measured perpendicular to the steps, less magnetic field is needed to switch the magnetization what allows for precise determination of the coercivity. The mutual dependence of the shift field and the coercivity at the thicknesses at which the characteristic peaks appear, indicate that the oscillatory behavior of the coercivity is due to oscillatory changes of magnetic anisotropy.

### ***bcc* and *fcc* FeCo alloys films on Ag(116) and Cu(1113) surfaces**

The oscillation period of the MA oscillations is determined by the wavevector  $k_{em}$ , corresponding to the QWS that cross  $E_F$ . Thus, any change of the quantized electronic bands with respect to the  $E_F$  should be manifested by change of oscillatory MA. In particular, crossing point of the QWS with  $E_F$  is expected to be modified and therefore, the oscillation period L. One of the way of adjusting  $E_F$  with respect to the electronic bands is to change the number of electrons per unit cell, e.g. by mixing two elements [7]. Such an idea was applied for instance to tetragonally distorted FeCo alloys, where by appropriate choice

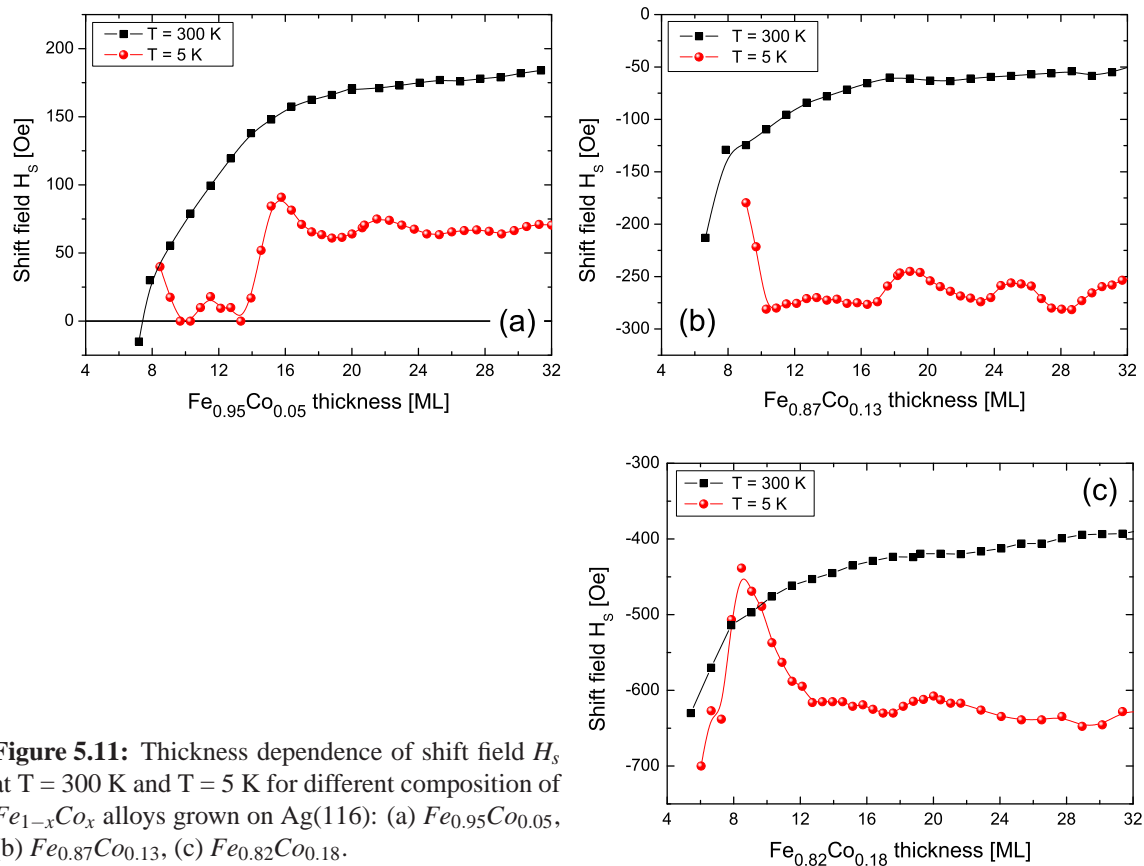


**Figure 5.11:** Thickness dependence of shift field  $H_s$  at  $T = 300$  K and  $T = 5$  K for different composition of  $Fe_{1-x}Co_x$  alloys grown on Ag(116): (a)  $Fe_{0.95}Co_{0.05}$ , (b)  $Fe_{0.87}Co_{0.13}$ , (c)  $Fe_{0.82}Co_{0.18}$ .

of composition, large perpendicular magnetic anisotropy was obtained [8, 10].

In order to study how the oscillatory MA changes as a function of the content of Fe and Co, two kinds of FeCo alloys films were grown: i) *bcc*  $Fe_{1-x}Co_x$  on Ag(116) by adding gradually Co to Fe; and ii) *fcc*  $Fe_xCo_{1-x}$  on Cu(113) by adding gradually Fe to Co.

#### ***bcc* $Fe_{1-x}Co_x$ films on Ag(116) surface**

Three compositions of  $Fe_{1-x}Co_x$  on Ag(116) surface, with  $x = 0.05, 0.13,$  and  $0.18$  of Co have been measured by MOKE. Dependencies of  $H_s$  on  $Fe_{1-x}Co_x$  thickness are shown in Fig. 5.11. It can be observed that with adding Co,  $H_s^{vol}$  (the value of  $H_s$  which approaches in the limit of large film thickness) decreases and already for  $x = 0.13$ ,  $H_s^{vol}$  is negative (i.e., the easy axis of magnetization is oriented perpendicular to the steps). Further increase of Co content causes further change of  $H_s^{vol}$  toward more negative values. Therefore, adding of Co into Fe results in the in-plane uniaxial magnetic anisotropy, forcing the easy magnetization axis to be oriented perpendicularly to the step edges.

Concerning the measurements at 5 K it can be observed that already at the lowest investigated content of Co ( $x = 0.05$ ), the oscillation amplitude of  $H_s$  is significantly reduced in comparison to pure Fe film. While for Fe film, the oscillation amplitude reaches nearly 550 Oe, in the case of  $Fe_{0.95}Co_{0.05}$ , the amplitude is decreased to  $\sim 10$  Oe. Oscillations with similar amplitude are also observed for  $x = 0.13$  of Co. The period of the observed oscillations of  $H_s$  is however not well defined (its value varies between  $\sim 4.5$  ML and  $\sim 6.5$  ML, depending on the thickness of  $Fe_{1-x}Co_x$  film). Moreover, for all three compositions, Kerr ellipticity  $\phi^H$  at  $H_s$  does not show any oscillatory behavior.

#### ***fcc* $Fe_xCo_{1-x}$ films on Cu(113) surface**

Magnetic anisotropy of epitaxial  $Fe_xCo_{1-x}$  alloys grown on Cu(001) was extensively studied in the past, over the whole composition range [96–100]. It was found that for film thicknesses below 4 ML, the



## SECTION 5.1

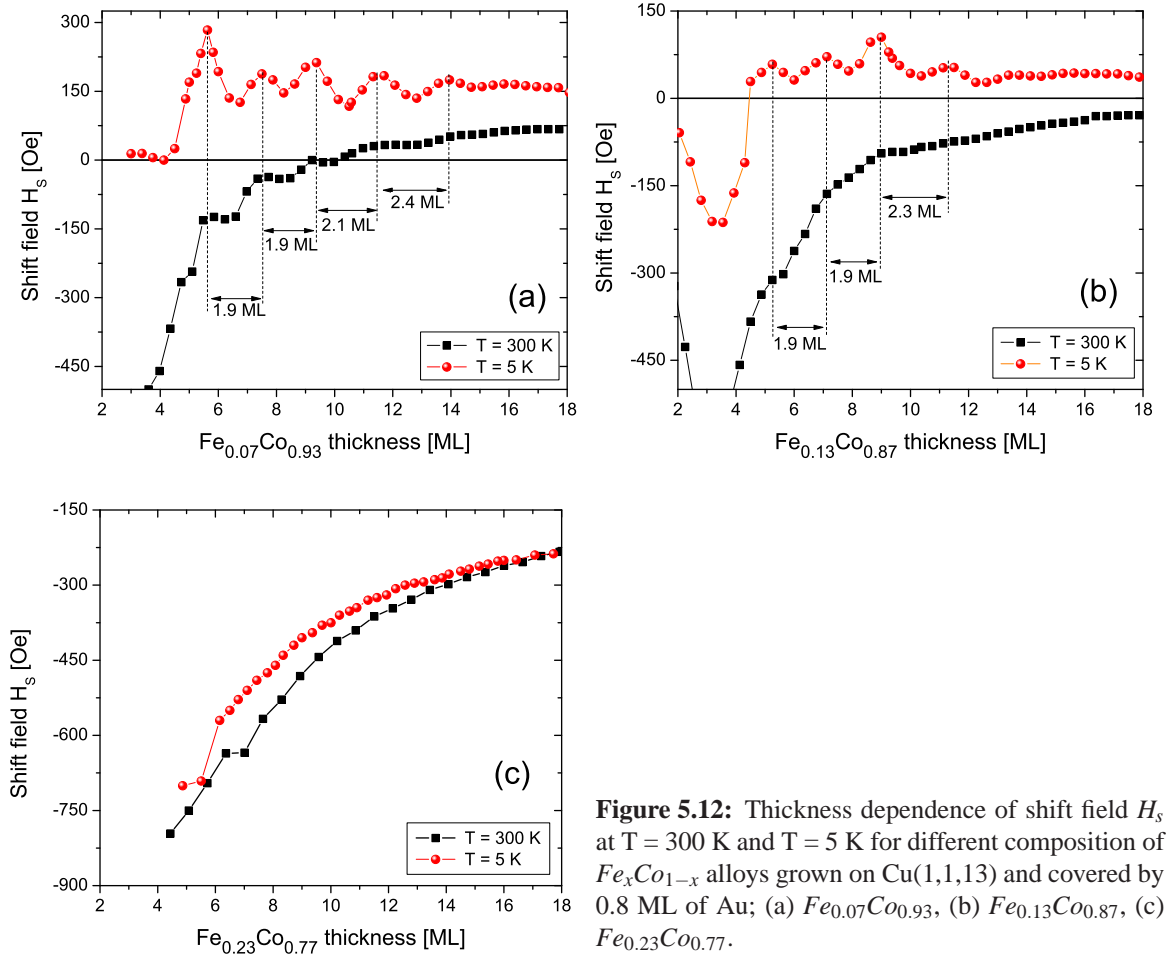


**Figure 5.12:** Thickness dependence of shift field  $H_s$  at  $T = 300$  K and  $T = 5$  K for different composition of  $Fe_xCo_{1-x}$  alloys grown on Cu(1,1,13) and covered by 0.8 ML of Au; (a)  $Fe_{0.07}Co_{0.93}$ , (b)  $Fe_{0.13}Co_{0.87}$ , (c)  $Fe_{0.23}Co_{0.77}$ .

magnetic easy axis changes from in-plane on the Co-rich side to out-of-plane on the Fe-rich side. The four-fold symmetry of the in-plane magnetic anisotropy with easy axes along [110] is maintained until  $x \sim 0.7$  of Fe.

Three compositions of  $Fe_xCo_{1-x}$  were grown on Cu(1113) with  $x = 0.07, 0.13$  and  $0.23$  of Fe. The thickness dependencies of  $H_s$  at  $T = 300$  K and  $T = 5$  K for different compositions of the alloy are shown in Fig. 5.12. Similarly as in case of Co/Cu(1113), sub-monolayer Au coverage was used to fine-tune the interface contribution to the in-plane uniaxial MA and to provide convenient experimental access to MA oscillations. All the samples shown in Fig. 5.12 were covered with 0.8 ML of Au. With adding Co into Fe one can observe changes in  $H_s^{vol}$ . For  $x = 0.07$ ,  $H_s^{vol}$  approaches  $\sim 80$  Oe (at 300 K) and  $\sim 150$  Oe (at 5 K). This is significant change in comparison to pure Co film grown on Cu(1113), where  $H_s^{vol}$  is around  $-100$  Oe, independently of temperature. Further increase of Fe content results in shifting of  $H_s$  down to negative values and in-plane SRT from along the steps (positive  $H_s$ ) toward perpendicular to the steps (negative  $H_s$ ). Thus, adding of Fe in  $Fe_xCo_{1-x}/Cu(1113)$  has similar effect on the in-plane uniaxial MA as adding of Co in  $Fe_{1-x}Co_x/Ag(116)$ . In both alloys, increasing the content  $x$  results in the in-plane uniaxial magnetic anisotropy, forcing the easy magnetization axis to be oriented perpendicularly to the step edges. Interestingly, rapid drop of  $H_s$  at 15 ML for Co/Cu(1113) associated with strain relaxation (Fig. 5.8b) is not observed in the case of  $Fe_xCo_{1-x}/Cu(1113)$ .

At 5 K, oscillations of  $H_s$  as a function of  $Fe_xCo_{1-x}$  film thickness are observed. At  $x = 0.07$  of Fe, the oscillation amplitude is about 100 Oe, i.e., smaller by factor of two in comparison to pure Co film. The period of oscillations seems to slightly increase with increasing thickness and on average is equal  $L_{Fe_xCo_{1-x}} = 2.0 \pm 0.3$  ML, i.e., very similar to  $L_{Co}$  observed for Co/Cu(1113). Further increase of Fe content (up to  $x = 0.13$ ), reduces the oscillation amplitude again by factor of two, i.e., to  $\sim 50$  Oe, while

it does not affect the oscillation period. Eventually, for  $x = 0.23$ , oscillations disappear completely.

### Co/Fe bilayer on Ag(116) surface

So far, effects of varying thickness of FM films have been considered for Fe, Co and FeCo alloys. The question is whether (and how) QWS can affect the magnetic anisotropy in the case of two adjacent FM layers? In order to answer this question, the magnetic anisotropy of Co/Fe bilayers has been studied here.

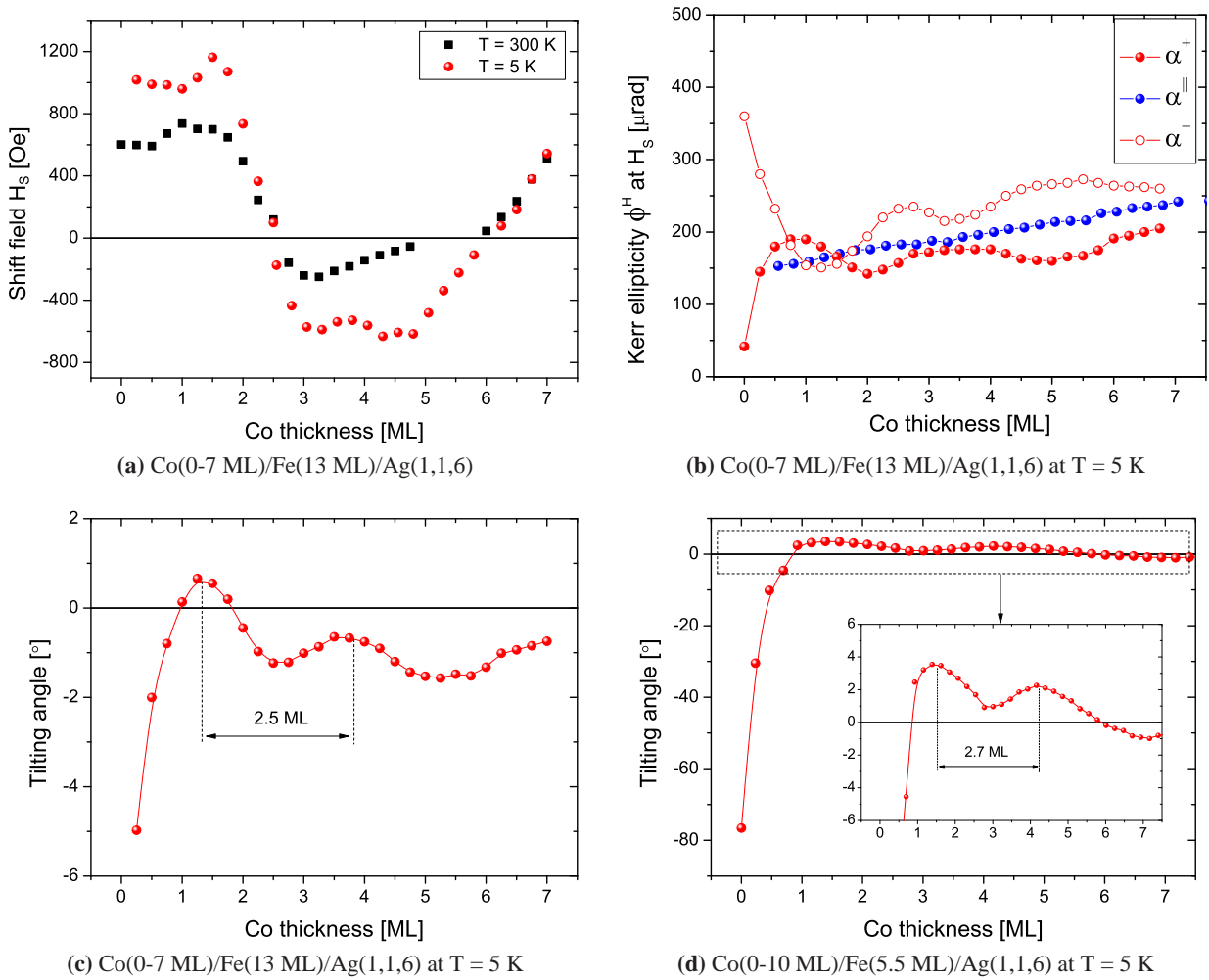


**Figure 5.13:** The dependence of the: (a) Shift field  $H_s$ , (b) Kerr ellipticity  $\phi^H$  at  $H_s$ , (c) tilting angle  $\delta$  as a function of thickness of Co film grown on Fe(13 ML)/Ag(116). (d) The dependence of the tilting angle  $\delta$  on thickness of Co film grown on Fe(5.5 ML)/Ag(116)

Independently of the thickness of Fe film, the effect of Co capping layers on MA is similar. For Co(wedge)/Fe(13 ML)/Ag(116) the measurements of  $H_s$  show that covering with Co cause a SRT from the easy magnetization axis along the steps (positive  $H_s$ ) toward perpendicular to the steps (negative  $H_s$ ) at around 2.5 ML of Co (Fig. 5.13a). Interestingly, with further increase of Co thickness, another SRT occurs and the easy magnetization axis rotates back to along the steps direction at around 6 ML. There are some differences between  $T = 300$  K and  $T = 5$  K dependencies. The value of  $H_s$  for uncovered Fe is much higher at 5 K. This is due to QWS contribution to  $H_s$ , which for 13 ML of Fe corresponds to larger  $H_s$ , in agreement with Fig.5.2a. In addition, at 5 K, sort of periodic modulation of  $H_s$  is visible (Fig. 5.13a). Oscillations have amplitude of  $\sim 100$  Oe and disappear already after two peaks.

The oscillations are also visible in the Kerr ellipticity  $\phi^H$  at  $H_s$ , when measured at 5 K (Fig. 5.13b). Analogously as for other systems presented in this section, having the values of Kerr ellipticities at  $\alpha^+$

## SECTION 5.1

and  $\alpha^-$  geometries, the tilting angle  $\delta$  can be calculated according to Eq. 4.1.7. The oscillations of  $\delta$  are observed with a period of  $L_{Co} = 2.5 \pm 0.3$  ML. Note that the positions of the peaks in  $\delta$ , which appear at  $\sim 1.4$  ML and  $\sim 3.9$  ML of Co, coincide with the peaks observed in  $H_s$  dependence.

In order to see how  $\delta$  changes upon covering with Co for thinner Fe film underneath, an additional experiment was performed for Co(wedge)/Fe(5.5 ML)/Ag(116). As shown in Fig. 5.5, for uncovered 5.5 ML thick Fe film, the easy magnetization axis should be oriented nearly exactly perpendicular to the terraces plane. This is exactly what is observed in Fig. 5.13d, where for uncovered part of Co wedge  $\delta = -76.5^\circ$ . Interestingly, already 1 ML of Co is sufficient to reduce the tilting angle value and cause the magnetization to be oriented in the sample plane. Furthermore, the oscillatory behavior of  $\delta$  with the period of  $L_{Co} = 2.7 \pm 0.3$  ML is observed (see inset of Fig. 5.13d).

Since deposition of Co on Fe/Ag(1,1,6) suppresses SRT and magnetization prefers to be aligned in the sample plane, it is desirable to check, how oscillatory MA due to QWS in Fe behaves in such system. The results for two Fe-wedges with 1 ML and 2 ML thick Co capping layers are presented in Fig. 5.14.

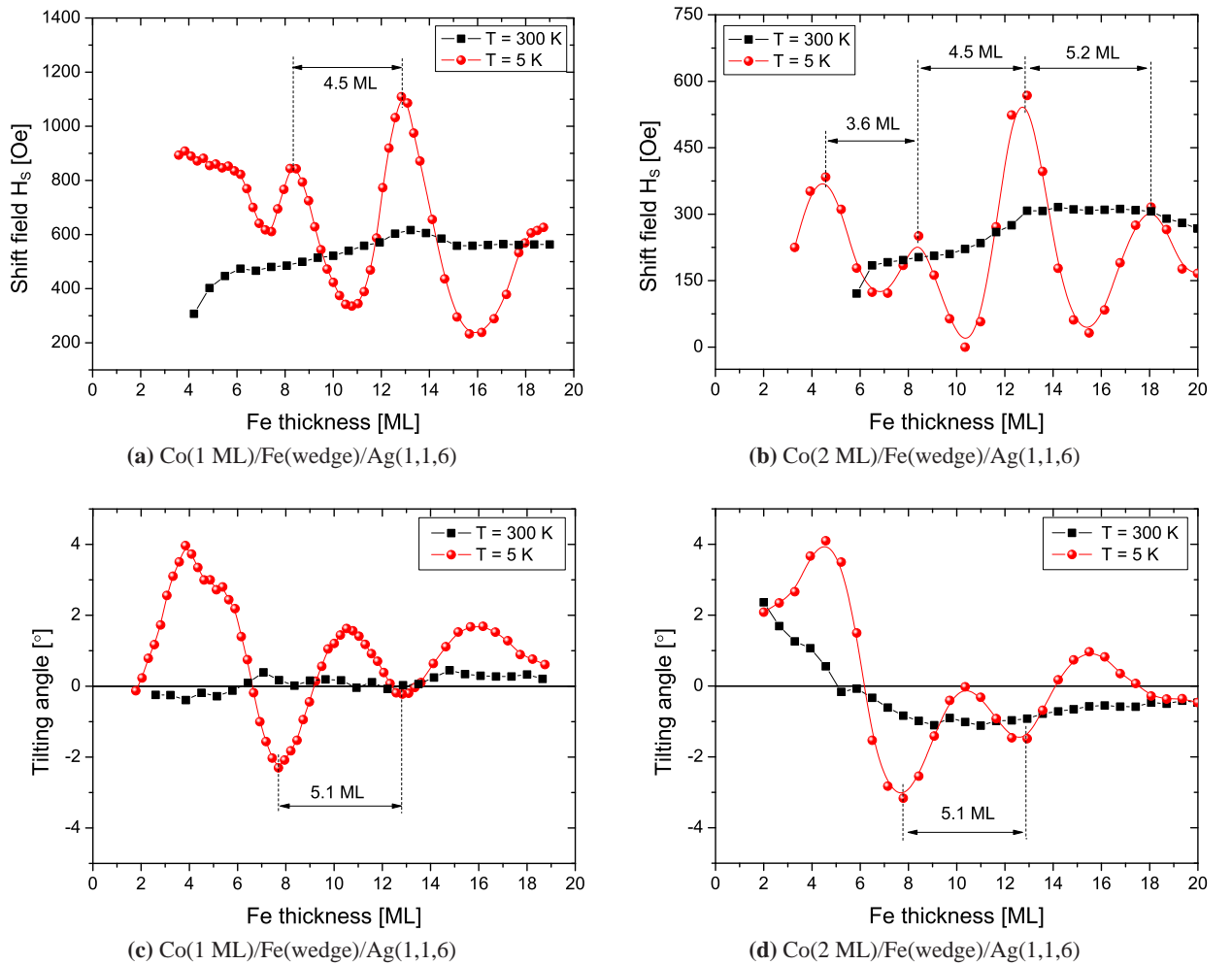


**Figure 5.14:** Dependencies of shift field  $H_s$  and tilting angle  $\delta$  on thickness of Fe film covered by 1 ML and 2 ML thick Co film.

The dependence of the shift field  $H_s$  on Fe thickness is shown in Fig. 5.14a and Fig. 5.14b for different Co thickness, 1 ML and 2 ML, respectively. At 300 K, the shift field does not change significantly with increasing Fe thickness. A change in the volume contribution  $H_s^{vol}$  occurs when the thickness of the Co covering layer is increased, from  $\sim 600$  Oe down to  $\sim 300$  Oe, respectively. At 5 K, oscillatory behavior of  $H_s$  is observed for both coverages of Co. Since maxima of  $H_s$  are observed at  $\sim 12.5$  ML and  $\sim 18$  ML (i.e., at exactly the same thicknesses as for uncovered and Au-covered Fe films) one can

conclude that the oscillatory  $H_s$  due to QWS in Fe film is not affected by covering with Co. Differently than in the case of uncovered and Au-covered Fe films, where  $H_s$  cannot be derived below 10 ML due to SRT, for Co-covered samples  $H_s$  is measurable down to 3 ML of Fe. In particular, in the case of Co(2 ML)/Fe(wedge)/Ag(116) this allows to determine the oscillation period of  $H_s$  even for the thinnest part of Fe film. Interestingly, the oscillation period and amplitude decrease with decreasing Fe thickness below 10 ML (Fig. 5.14b).

Dependencies of  $\delta$  on Fe thickness are shown in Fig. 5.14c and Fig. 5.14d. In agreement with previous results obtained for Co-wedge samples, coverage with 1 ML and 2 ML of Co reduces the value of the tilting angle to nearly zero (the easy magnetization in the sample plane). At 300 K, there are no significant changes of the tilting angle with increasing Fe thickness. At 5 K, clear oscillations of  $\delta$  are observed with the period of  $L_{Fe} = 5.1 \pm 0.3$  ML, which is the same for both coverages of Co. Note that not only the value of the tilting angle change but also the sign.

### 5.1.2 Effects of covering with nonmagnetic overlayers

It is known that QWS can be formed not only in the FM film, but also in NM film. The question is whether QWS formed in NM overlayer can affect periodically the MA of the underlying FM film. In order to study the effects of covering with NM overlayers, Au and Cu overlayers were grown on Fe and Co films.

#### Cu overlayers on Fe and Co films

Obviously, in order to study the effects of QWS in NM overlayers on MA of the FM underlayers, the NM films in which QWS exist have to be chosen. Cu films are one of the most intensively studied system regarding the observation of QWS [60, 63, 169–172], and therefore, there are good candidate for the purpose of our study.

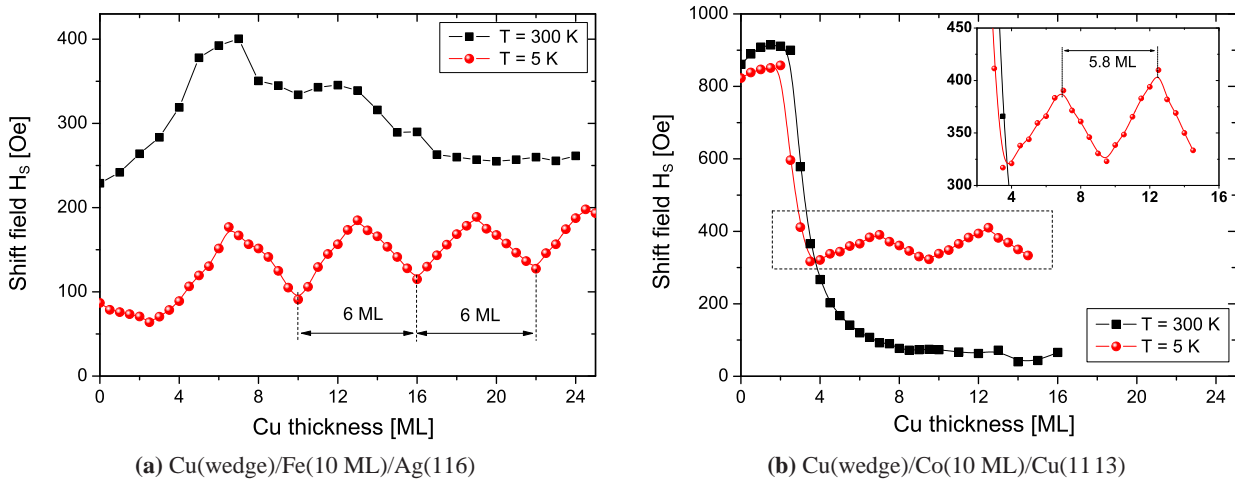


**Figure 5.15:** The dependence of shift field  $H_s$  as a function of thickness of Cu film grown on: (a) Fe(10 ML)/Ag(116) and (b) Co(10 ML)/Cu(1113).

MOKE measurements were performed for Cu films in the thickness range between 0 and 25 ML grown on 10 ML thick Fe films on Ag(116) and on 10 ML thick Co films on Cu(1113). As already shown in the case of Au/Fe/Ag(116) and Au/Co/(1113), covering FM film with NM material can change the interface contribution to the step-induced uniaxial anisotropy. For Cu films grown on Fe(10 ML)/Ag(116), at 300 K  $H_s$  is positive and at 0 ML coverage of Cu is equal  $\sim 240$  Oe, in agreement with Fig. 5.2a. With increasing Cu thickness  $H_s$  initially increases (up to  $\sim 6$  ML) due to a change from the UHV/Fe into the Cu/Fe interface contribution to  $H_s$  (Fig. 5.15a). Afterward,  $H_s$  decreases and saturates above a thickness

of  $\sim 17$  ML. Since the saturated value of  $H_s$  is similar to  $H_s$  for uncovered Fe film of the same thickness, one can conclude that a sufficiently thick Cu overlayer is inert for the in-plane uniaxial magnetic anisotropy of Fe/Ag(116).

The dependence of  $H_s$  at 300 K is different if Cu is grown on top of Co/Cu(1113) (Fig. 5.15b). For uncovered, 10 ML thick Co film,  $H_s$  is  $\sim 860$  Oe, in agreement with Fig. 5.8a. Upon covering with Cu,  $H_s$  decreases due to the interface contribution from Cu to the step-induced magnetic anisotropy. As a consequence,  $H_s$  is much smaller reaching a value of  $\sim 80$  Oe at 16 ML. This value is close to  $H_s$  of thick uncovered and Au-covered Co/Cu(1113) (Fig. 5.8). This confirms that the effect of covering with Cu is purely an interface effect related only to interface contribution to  $H_s$ , which is different for UHV/Co and Cu/Co interfaces [23, 39]. Additionally, this allows to conclude that a large  $H_s$  observed for uncovered Co/Cu(1113) (Fig. 5.8) is more due to the surface of Co than the Co/Cu(1113) interface. The change of  $H_s$  with increasing Cu thickness spreads out to nearly 20 ML, which is a similar Cu thickness range as in the case of change of  $H_s$  upon covering with Cu on Fe/Ag(116). Such changes of  $H_s$  spreading out over several ML of Cu can be surprising for a typical interface effects. This is due to the fact that  $H_s$  value is sensitive to even tiny changes of MA. As a consequence, even very thick Cu layer on top of ferromagnetic material can affect  $H_s$  e.g., via strain. Note that in some cases, changes of MA with increasing Cu thicknesses can last up to 50 ML [173].

The dependence of  $H_s$  changes remarkably at 5 K. For Cu on both: Fe/Ag(116) and Co/Cu(1113)),  $H_s$  oscillate as a function of Cu thickness with similar amplitude ( $\sim 80$  Oe) and almost exactly the same period  $6 \pm 0.3$  ML and  $5.8 \pm 0.3$  ML, respectively. For simplicity, only the measurements at 5 K and 300 K are shown. However, it is worth to note, that the oscillations disappear already above 50 K.

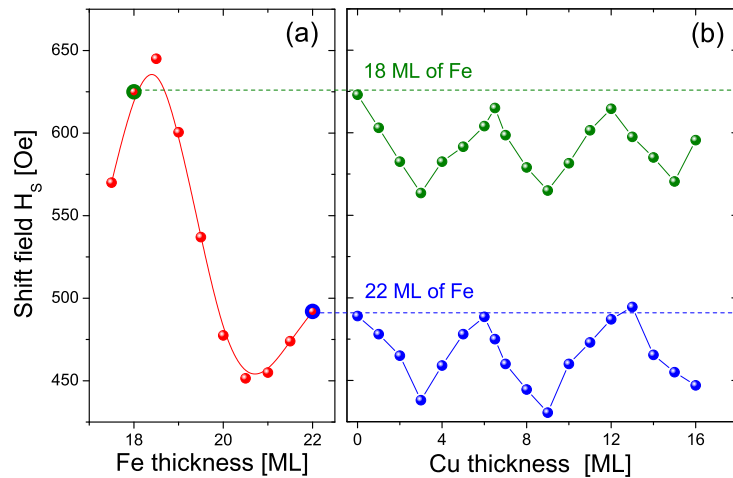


**Figure 5.16:** (a) Shift field  $H_s$  as a function of thickness of Fe film grown on Ag(116) surface; (b) shift field  $H_s$  as a function of thickness of Cu overlayer grown on 18 ML and 22 ML thick Fe film underneath.  $T = 5$  K.

It can be observed, that  $H_s$  for uncovered part of the Fe film (0 ML of Cu) is significantly decreased at 5 K with respect to its value at 300 K (Fig. 5.15a). This effect is related to the oscillatory  $H_s$  due to QWS in Fe film (as shown in Fig. 5.2a). The change of  $H_s$  with decreasing temperature for uncovered part of Co/Cu(1113) is less prominent (Fig. 5.15b) because the oscillation amplitude of  $H_s$  is smaller than in the case of Fe/Ag(116). Therefore, the oscillatory dependence of  $H_s$  with increasing Cu thickness can be shifted either more to positive values or negative values of  $H_s$ , depending whether the thickness of the underlying FM film corresponds to the maximum or minimum of the oscillatory  $H_s$  due to QWS in FM film. The question is whether the period, amplitude or phase of the oscillatory  $H_s$  vs the Cu thickness depends on the thickness of Co and/or Fe film or not. In order to answer this question, an additional sample of two thicknesses of Fe (18 ML and 22 ML thick) was grown. The results of the MOKE experiment are shown in Fig. 5.16. The oscillations are of exactly the same period and the

maxima correspond to the same thicknesses of Cu for both Fe thicknesses. However, as expected for different thicknesses of Fe,  $H_s$  oscillates with respect to different "base" values. This is again because  $H_s$  at 5 K for Fe itself is modified by the QWS formed in Fe. The oscillation amplitude seems to be almost independent of the thickness of Fe at least in the investigated thickness range.

### Au overlayers on Fe films

Thin Au films are another example of NM film, in which QWS can be observed. In particular, oscillatory magneto-optical effects and oscillations of the electron reflectivity due to spin-polarized QWS in Au deposited on Fe(001) and Co(001) surfaces have been reported [13, 174–177]. Since Au is one of the least reactive solid chemical elements, it is commonly used as a capping layer of magnetic thin films. Also within experiments of this thesis, Au was deposited on the top ferromagnetic layers, e.g., in the case of Fe/Ag(116) (Sec. 5.1.1). It is therefore desirable to study, how MA of FM film can change upon covering with Au.

In order to get more insight into influence of Au on MA of the underlying FM film, MOKE measurements were performed as a function of Au coverage on Fe/Ag(116). The dependence of  $H_s$  on Au thickness of 13 ML thick Fe film deposited on Ag(116) is shown in Fig. 5.17a. Since 13 ML thick Fe corresponds nearly to the maximum of the oscillation of  $H_s$  observed for uncovered sample,  $H_s$  at 5 K is larger than at 300 K. Covering with Au reduces the values of  $H_s$  at both temperatures. In particular, a rapid drop of  $H_s$  is observed in the thickness range between 0 ML and 1 ML of Au. Further deposition of Au changes  $H_s$  only a little.

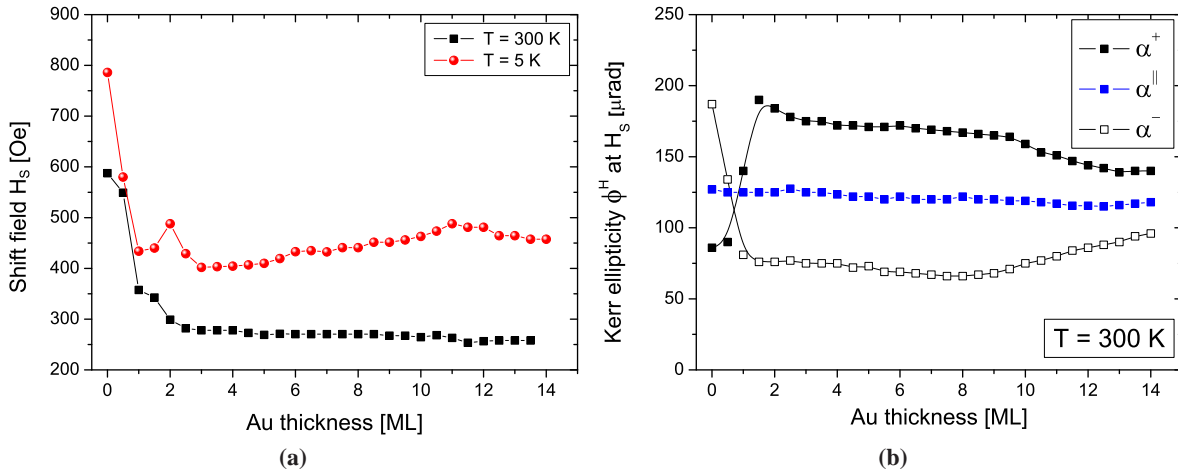


**Figure 5.17:** (a) The dependence of shift field  $H_s$  and (b) Kerr ellipticity  $\phi^H$  at  $H_s$  as a function of thickness of Au overlayer deposited on top of Fe(13 ML)/Ag(116)

Covering with Au also affects the Kerr ellipticity  $\phi^H$  at  $H_s$  (Fig. 5.17b). For uncovered part of Fe(13 ML)/Ag(116),  $\phi^H$  measured at  $\alpha^-$  and  $\alpha^+$  geometry is respectively larger and smaller than  $\phi^H$  at  $\alpha^||$ . This corresponds to the orientation of the magnetization with tilting angle around  $-1^\circ$ , in agreement with the Kerr ellipticity  $\phi^H$  at  $H_s$  and tilting angle dependence for Fe/Ag(116) (Fig. 5.4a and Fig. 5.5, respectively). After deposition of barely 1 ML of Au, the relation of the Kerr ellipticity at  $\alpha^-$  and  $\alpha^+$  with respect to  $\alpha^||$  is just opposite (i.e.,  $\phi^H$  at  $\alpha^+$  is larger than at  $\alpha^||$ , while  $\phi^H$  at  $\alpha^-$  is smaller than at  $\alpha^||$ ). It means that initially tilted magnetization by  $\delta = -1^\circ$ , rotates upon covering with Au and become tilted by about  $\delta = +1^\circ$ . With increasing Au thickness above 8 ML,  $\phi^H$  at  $\alpha^-$  and  $\alpha^+$  slightly converge to  $\phi^H$  measured at  $\alpha^||$ , which is related to tiny decrease of the tilting angle. The fact that Kerr ellipticity at  $\alpha^||$  is independent of Au thickness confirms that the observed change of the Kerr ellipticity at  $\alpha^+$  and  $\alpha^-$  is not related to any magneto-optical effects. Analogous effect of change of the sign of the tilting

## SECTION 5.1

angle upon covering with Au is observed independently of temperature and thickness of Fe. In fact, this effect can be also observed by comparing the tilting angle dependence on Fe thickness for uncovered and Au-covered samples shown in Sec. 5.1.1. No indication of the oscillatory behavior neither of  $H_s$  nor Kerr ellipticity  $\phi^H$  at  $H_s$  is found as a function of Au thickness, even at 5 K.

## 5.2 Spin and orbital magnetic moments in Fe films on Ag(116) surface using XMCD

As shown in Sec. 2.1.1, under certain assumptions the magnetocrystalline anisotropy energy is directly related to the anisotropy of the orbital moment. X-ray magnetic circular dichroism (XMCD) spectroscopy allows to measure an anisotropy of the orbital moment and thus, gives the opportunity of direct observation of the magnetocrystalline anisotropy. In order to explore the oscillatory magnetic anisotropy it is therefore very desirable to study the anisotropy of the orbital magnetic moment. There are no reports concerning XMCD measurements for Fe films on vicinal surfaces and only a very few reports for Fe films on flat Ag(001) [178, 179], however, with no information about the anisotropy of the orbital magnetic moment.

In the following chapter, XMCD results for Fe films grown on Ag(116) surface are presented. Careful thickness dependent measurements in different geometries were performed with particular interest on the evaluation of the anisotropy of the orbital moment. The measurements were carried out at Beamline 4B of the synchrotron radiation facility UVSOR-II in Institute for Molecular Science, Japan.

### 5.2.1 Spin and orbital magnetic moment values

As explained in Sec. 4.2, in order to obtain the spin and orbital magnetic moments from XMCD spectra, the magnetization has to be saturated for all probed directions. This is why all results presented in this chapter were obtained in saturation. Several Fe films were prepared with both: constant and changeable thickness (a wedge type sample), in order to study thickness dependent changes in XMCD signal. All the measurements were performed *in situ* with the pressure below  $1 \times 10^{-10}$  mbar and at  $T = 5$  K. Prior to the measurement of the absorption spectra, the hysteresis loops were detected by recording the electron yield with the photon energy fixed at the maximum of the  $L_3$  absorption edge of Fe ( $\sim 706$  eV). The measurement of the hysteresis loops along different directions and different thicknesses of Fe allowed to estimate saturation field. In most cases the magnetic field  $H = \pm 4$  T was sufficiently high to align all magnetic moments along the direction of the applied magnetic field.

Typically the absorption spectra were recorded in the energy range from 670 eV to 760 eV. This energy range was divided into six blocks with different resolution ranging from 0.25 eV to 4 eV. Each absorption spectrum was averaged at least twice, while one experimental point at given energy was acquired at least for 2 seconds. Analysis procedure of the absorption spectra and evaluation method of the XMCD signal were described in Sec. 4.2.3.

Three geometries of the applied magnetic field were used in order to probe the magnetic moment components: perpendicular to the sample plane ( $\theta = 0^\circ$ ), in-plane perpendicular to the step edges ( $\theta = 55^\circ$ ,  $\psi = 0^\circ$ ) and in-plane parallel to the step edges ( $\theta = 55^\circ$ ,  $\psi = 90^\circ$ ), where the angles are defined according to Fig. 4.6. Representative  $L_2$  normalized XMCD spectra are shown on Fig. 5.18. By looking at the intensity of  $L_3$  resonance peak, changes of the orbital moment are visible. While for thicknesses: 3.6 ML and 7.6 ML, the spectra measured in three directions have similar intensity at  $L_3$ , there is a substantial difference for thicknesses: 4.6 ML and 5 ML, where the spectrum for  $\theta = 55^\circ$ ,  $\psi = 0^\circ$  (red line) has reduced intensity at  $L_3$  peak, in comparison with other directions. This indicates that the orbital moment along  $\theta = 55^\circ$ ,  $\psi = 0^\circ$  direction is reduced at 4.6 ML and 5 ML. In other words, the orbital moment is more anisotropic at 4.6 ML and 5 ML than at 3.6 ML and 7.6 ML.

In order to extract quantitative information about the orbital moment  $m_{orb}$  and effective spin moment  $m_{spin}^{eff}$ , sum rules have to be applied according to equations (4.2.2) and (4.2.3). The values of  $m_{orb}$  and  $m_{spin}^{eff}$  obtained for all measured thicknesses of Fe are summarized in Fig. 5.19. The spin effective moment is nearly isotropic and changes only a little with increasing Fe thickness. For thin Fe films (in the thickness regime 2–7 ML) the averaged over the three probed directions  $m_{spin}^{eff}$  is equal  $2.37 \mu_B/\text{atom}$ , while for thicker films (9–17 ML), the averaged  $m_{spin}^{eff}$  is equal  $2.28 \mu_B/\text{atom}$ . Note that  $m_{spin}^{eff}$  is not the absolute value of the spin moment  $m_{spin}$ . In order to extract the absolute value of  $m_{spin}$ , the projected



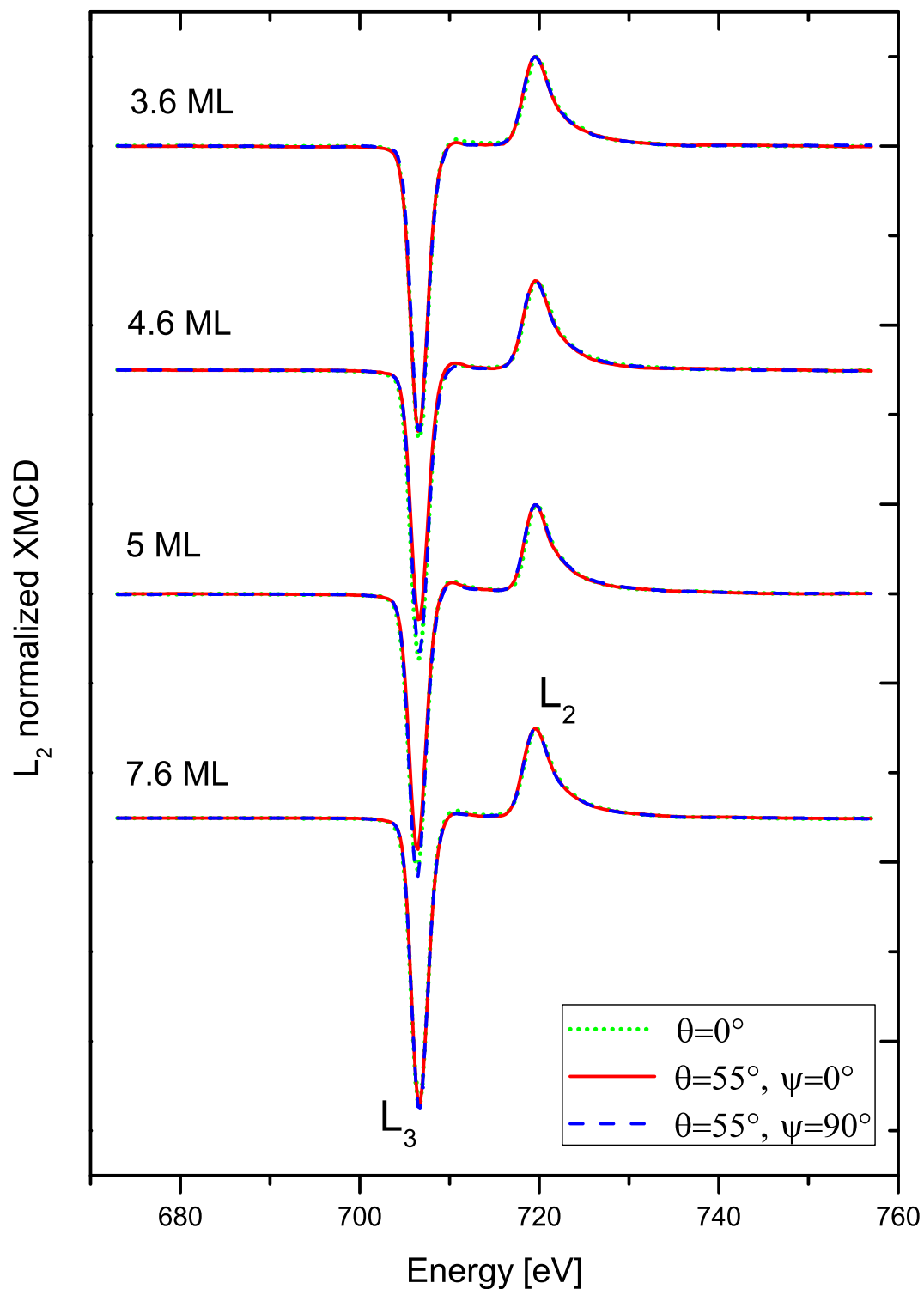


**Figure 5.18:**  $L_2$  normalized XMCD spectra for several thicknesses of Fe film grown on Ag(116) vicinal surface. By looking at intensity of  $L_3$  peak, changes of the orbital moment can be directly distinguished (an increase/decrease of the intensity of  $L_3$  peak correspond to the increase/decrease of the orbital magnetic moment). One can observe that at thicknesses: 4.6 ML and 5 ML, the intensity at the  $L_3$  resonance peak is reduced for the measurement along  $\theta = 55^\circ, \psi = 0^\circ$  (red line) in comparison with other geometries. At thicknesses: 3.6 ML and 7.6 ML the intensity at the  $L_3$  peak is almost the same regardless of the geometry of the measurement. Thus, the orbital moment is nearly isotropic at those thicknesses.

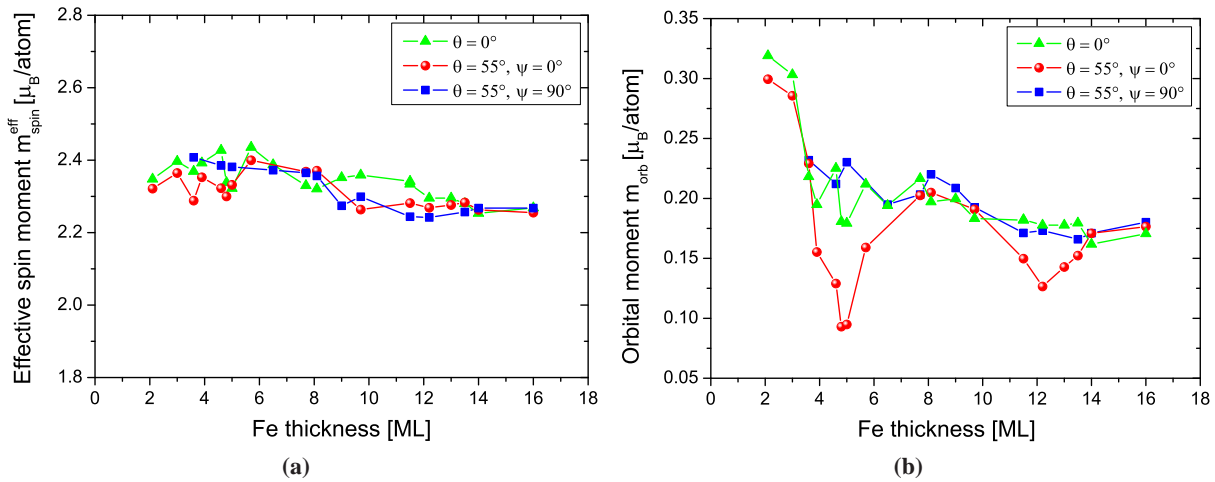


**Figure 5.19:** (a) Effective spin magnetic moment  $m_{spin}^{eff}$  and (b) orbital magnetic moment  $m_{orb}$  as a function of thickness of Fe film grown on Ag(116). The error bars are estimated as follows: thickness ( $\pm 0.2$  ML),  $m_{spin}^{eff}$  ( $\pm 0.05 \mu_B/atom$ ) and  $m_{orb}$  ( $\pm 0.015 \mu_B/atom$ ).

magnetic dipole moment  $m_T$  along the spin quantization axis has to be subtracted according to Eq. 4.2.3. The  $m_T$  reflects a quadrupole term in the anisotropic spin density [137] and thereby, introduces some additional anisotropy to  $m_{spin}^{eff}$  dependence. The orbital moment dependence on Fe film thickness is shown in Fig. 5.19(b). The orbital moment increases with decreasing Fe thickness and for the thinnest measured Fe film (2 ML) is enhanced by around 180% in comparison to the thickest one (16 ML). The enhancement of the orbital moment for thin Fe film can be ascribed to two effects: i) broken symmetry due to the finite size effects [50, 156] and ii) increased magnetic moment at Fe surface-layers and Fe/Ag interface layers [156, 158, 180–182].

Additionally, a strong anisotropy of the  $m_{orb}$  is observed. In particular, differences are evident for the  $m_{orb}$  measured along  $\theta = 55^\circ, \psi = 0^\circ$ , which is substantially reduced in the vicinity of 5 ML and 12.5 ML. The changes of the orbital moment are so large that can be recognized directly from  $L_2$  normalized XMCD spectra, as shown in Fig. 5.18 for the vicinity of the first minimum.

Although dependencies shown on Fig. 5.19 can give already information about the anisotropy of the orbital moment, it is more convenient to operate with the values of  $m_{orb}$  and  $m_{spin}^{eff}$  projected on particular crystallographic directions of the surface (since it allows for comparison with results obtained by other techniques). By using equations (4.2.6) - (4.2.9) all the quantities, i.e.,  $m_{orb}$ ,  $m_{spin}$  and  $m_T$  can be evaluated in case, when the XMCD data set for three independent incidence angles is available.

The magnetic moments were recalculated on following crystallographic directions:  $[11\bar{6}]$  (perpendicular to the sample plane),  $[33\bar{1}]$  (in the sample plane, perpendicular to the step edges) and  $[1\bar{1}0]$  (in the sample plane, parallel to the step edges). The recalculated values of the orbital moments as a function of Fe film thickness are shown in Fig. 5.20a. It is observed that dependencies presented in Fig. 5.19b and their projections on the crystallographic directions (Fig. 5.20a) are qualitatively nearly identical. However there are some quantitative changes in values of the orbital moment. In particular, two characteristic minima for  $m_{orb}$  perpendicular to the step edges direction (red circles) at  $\sim 5$  ML and  $\sim 12.5$  ML are more pronounced after recalculation on crystallographic directions. It is worth to mention that several samples with a uniform thicknesses were performed in the vicinity of those minima in order to confirm the small values of the orbital moments.

This peculiar decrease of the  $m_{orb}$  value at particular thicknesses of Fe can be associated with quantization of the  $d$ -bands in Fe film. As mentioned in Sec. 2.1.1, the value of the  $m_{orb}$  in different directions depends on two ingredients: the  $d$  electron bonding and the size of the SO coupling given by the *spin-orbit coupling constant* (see Eq. 2.1.2). Therefore, in thin FM film in which  $d$  electrons are confined,

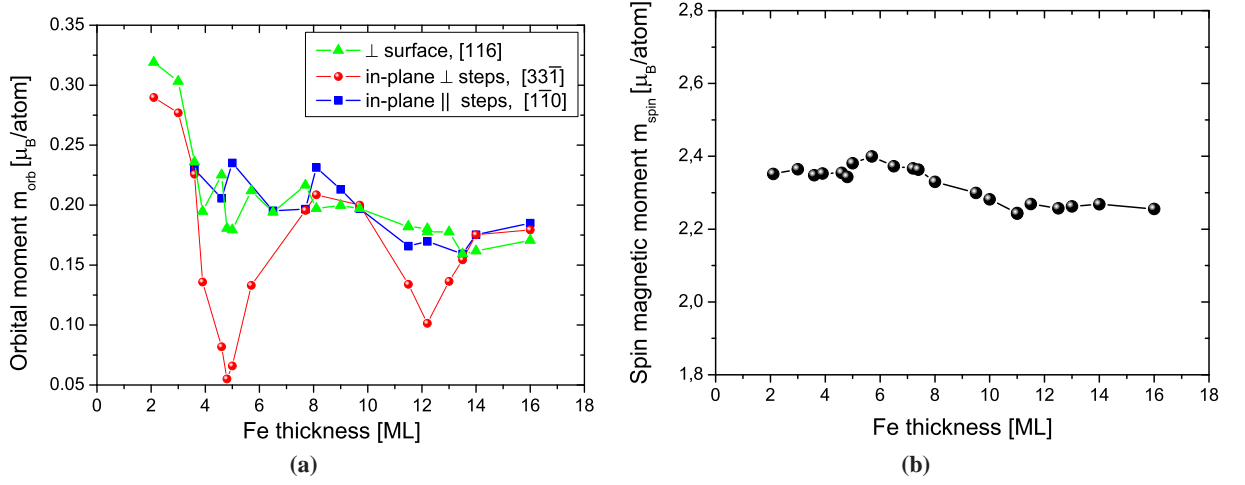


**Figure 5.20:** (a) Orbital magnetic moment  $m_{orb}$  (b) and spin magnetic moment  $m_{spin}$  as a function of thickness of Fe film grown on Ag(116), recalculated on specific crystallographic directions. The error bars are estimated as follows: thickness ( $\pm 0.2$  ML),  $m_{orb}$  ( $\pm 0.015 \mu_B/atom$ ) and  $m_{spin}$  ( $\pm 0.05 \mu_B/atom$ ).

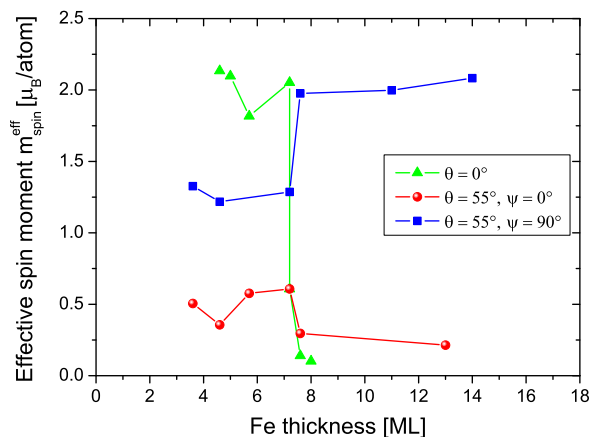
change of the electron bonding should be expected with increasing the thickness (since by changing the film thickness, the orbiting electrons experience alternating stronger/weaker perturbation due to their confinement at the interfaces). Additionally, as shown in Sec. 2.3, the quantization of  $d$  electrons can result in periodic change of the electronic configuration near the Fermi level. Such an effect should change the  $m_{orb}$  value, in particular when QWS cross  $E_F$  and change their occupancy from occupied to unoccupied or vice versa (since the expectation value of  $m_{orb}$  is obtained by summation over coupled pairs of occupied and unoccupied states). A detailed discussion of the orbital moment dependence and its correlation with magnetocrystalline anisotropy is carried out in Sec. 6.3.2.

Having  $m_{orb}$  and  $m_{spin}^{eff}$  values, a spin magnetic moment  $m_{spin}$  can be calculated according to Eq. 4.2.3 and Eq. 4.2.9. The values of  $m_{spin}$  obtained in our experiment (Fig. 5.20b) are in good agreement with previous XMCD reports on *bcc* Fe thin films [178, 179, 183]. In contrast to  $m_{orb}$  dependence, there is no significant increase of  $m_{spin}$  values with decreasing Fe film thickness (only of  $\sim 5\%$ ). This result shows that the effect of reduced dimensionality on value of the magnetic moment and the enhancement of the magnetic moment at the Fe surface/interface layers, are reflected mostly by changes in the orbital magnetic moment value (not the spin moment). In order to compare the obtained enhancement of the magnetic moment with the literature, a total magnetic moment  $m_{tot} = m_{orb} + m_{spin}$  has to be taken. For 3 ML thick Fe film, the total magnetic moment in our experiment equals  $m_{tot} = 2.65 \pm 0.05 \mu_B/atom$ . This value is in a good agreement with the averaged magnetic moment  $m_{tot} = 2.67 \mu_B/atom$  of 2.9 ML thick Fe film measured by SQUID (superconducting quantum interference device) magnetometry [157].

## 5.2.2 Magnetization orientation in remanence

By probing the magnetization along three directions in remanence, three projection components of the remanence can be obtained from XMCD spectra, leading to unique determination of the remanence magnetization vector. As mentioned before, the main interest of the XMCD study here is the anisotropy of the orbital moment, which has to be measured in saturation. The remanence measurements give the information about the magnetic anisotropy only through the orientation of the easy axis of magnetization. In general, it is useful to measure XMCD in both states, remanence and saturation, since it allows for direct correlation of the changes of orbital moment anisotropy with changes of the easy axis orientation. Since the easy axis of magnetization for this system was determined by MOKE and SPLEEM measurements, a full remanence data (i.e., along three directions) from XMCD are derived only for chosen thicknesses

**Figure 5.21:** Effective spin magnetic moments  $m_{spin}^{eff}$  obtained from XMCD measurement in remanence for Fe/Ag(116). The largest value of  $m_{spin}^{eff}$  corresponds to the easy axis of magnetization. Note that probing along  $\theta = 55^\circ, \psi = 0^\circ$  and  $\theta = 55^\circ, \psi = 90^\circ$  is always associated with contribution of the two components of magnetization, in-plane and out-of-plane. Rapid change of the  $m_{spin}^{eff}$  dependence between 7.2 ML and 7.6 ML reflects the SRT from out-of-plane toward in-plane along the steps direction.



of Fe, in the vicinity of SRT. The XMCD measurements in remanence were performed for  $H = \pm 0$  T, i.e., by changing the magnetic field  $\mathbf{H}$  such that  $H = +4$  T  $\rightarrow +0$  T ( $\mu^-$  taken)  $\rightarrow -4$  T  $\rightarrow -0$  T ( $\mu^+$  taken). All conditions and settings for the measurements in remanence were the same as in the case of the measurements in saturation.

The effective spin moment as a function of Fe film thickness is shown in Fig. 5.21. Up to 7.2 ML of Fe, the  $m_{spin}^{eff}$  along  $\theta = 0^\circ$ , (i.e., perpendicular to the sample plane) is the largest among three probed directions, and equal  $\sim 2 \mu_B/\text{atom}$ . This value is slightly different than  $m_{spin}^{eff}$  obtained in the saturation (on average  $2.37 \mu_B/\text{atom}$ ) and indicates that the easy axis of magnetization is oriented in the proximity of  $\theta = 0^\circ$ . Probing along  $\theta = 55^\circ, \psi = 0^\circ$  and  $\theta = 55^\circ, \psi = 90^\circ$  is associated with contribution of the two components of magnetization, in-plane and out-of-plane. However, for  $\theta = 55^\circ, \psi = 0^\circ$ , the effective spin moment is almost zero. This is due to the fact that magnetization is tilted toward perpendicular to steps direction with the angle  $-\delta$  and therefore, oriented nearly perpendicularly to the x-ray wave vector in this geometry (see Fig. 4.6). Above 7.2 ML the SRT occurs and the effective spin moment become the largest along  $\theta = 55^\circ, \psi = 90^\circ$ , i.e., the easy axis of magnetization is oriented in-plane along the step edges.

In order to obtain quantitative information about the easy axis, three components of the magnetization are necessary. Then, the orientation of the magnetization vector can be determined. Representative magnetization vector orientations defined by tilting angle  $\delta$  and azimuthal  $\psi$  angles defined according to Fig. 4.6 are shown in Table 5.1. Additionally, the values of  $m_{spin}^{eff}$  obtained for corresponding magnetization vectors are given. Starting with 4.6 ML thick Fe film, it can be seen that the magnetization is tilted out from the sample plan by  $\delta = -63^\circ$  with the inclination toward perpendicular to step edges direction ( $\psi = 190.5^\circ$ ). With increasing Fe thickness, the absolute value of  $\delta$  increases, i.e., the magnetization rotates toward perpendicular to the sample plane direction, reaching the maximum absolute value  $\delta = -71^\circ$  at 7.2 ML. Therefore, the magnetization for this thickness is oriented almost exactly along [001] direction (which for Ag(116) crystal corresponds to  $\delta = -76.7^\circ$ ). At 7.6 ML rapid change of the magnetization orientation is observed. The easy axis reorients to the sample plane ( $\delta$  close to  $0^\circ$ ) with the azimuthal orientation along the steps ( $\psi$  nearly  $90^\circ$ ). This clearly indicates that SRT from out-of-plane to in-plane is associated with change of the azimuthal angle  $\psi$ .

**Table 5.1:** Orientation of the remanent magnetization vector for chosen thicknesses of Fe film grown on Ag(116). The tilting angle  $\delta$  and the azimuthal angle  $\psi$  are defined according to Fig. 4.6.

Fe thickness [ML]	$m_{spin}^{eff}$ [ $\mu_B/\text{atom}$ ]	$\delta$ [ $^\circ$ ]	$\psi$ [ $^\circ$ ]
$4.6 \pm 0.2$	$2.40 \pm 0.1$	$-63 \pm 5$	$190.5 \pm 5$
$7.2 \pm 0.2$	$2.37 \pm 0.1$	$-71 \pm 5$	$180.5 \pm 5$
$7.6 \pm 0.2$	$2.41 \pm 0.1$	$-3.3 \pm 5$	$96.3 \pm 5$

## SECTION 5.2

The orientation of magnetization derived from XMCD in remanence has limited precision. Since magnetic moments are often not collinear with the wave vector of the incident x-ray, the XMCD signal is weaker and thus the analysis of the XMCD spectra involves larger errors (in comparison with the XMCD spectra obtained in saturation). The estimated errors for angles  $\delta$  and  $\psi$  are  $\sim 5^\circ$  (see Table 5.1). Nevertheless, remanence XMCD data allow for unique determination of the orientation of the easy axis magnetization in 3-dimensional space, which is not easily accessible by conventional techniques like MOKE.

### 5.3 Domain structure of ferromagnetic films on vicinal surfaces from SPLEEM

QWS can affect MA of ultrathin ferromagnetic films. Such changes of the MA can be manifested by the changes of the orientation of the easy axis of magnetization (see Sec. 5.1). In particular, for the films grown on vicinal surfaces, the easy magnetization axis tilting direction can oscillate into/out-of the sample plane and also, oscillatory switching between two orthogonal in-plane directions can occur. The orientation of the easy magnetization axis derived from MOKE is averaged over the area probed by the laser beam ( $\sim 0.2$  mm in our experiment). It would be interesting to examine domain structure, in particular at low temperature, and learn how the domain structure can be affected by QWS. The possibility of LT measurements with good lateral resolution, which is crucial in case our experiment, singled out SPLEEM among other available techniques.

In this chapter, the domain structure studies by SPLEEM are presented for Fe and Co films grown on vicinal Ag(116) and Cu(113) substrates, respectively. Domain structure was investigated as a function of Fe and Co films thickness, at 300 K and 130 K. Additionally, effect of sub-monolayer coverage with Au on the domain structure of Fe/Ag(116) was studied. All SPLEEM experiments were performed on *as grown* samples. The samples were grown as 1 mm wide wedge, with a slope of  $\sim 14$  ML/mm along [110] crystallographic direction of the substrate, according to the description given in Sec. 3.1.

#### 5.3.1 Fe films on Ag(116) surface

In order to evaluate the orientation of magnetization, images with three orthogonal spin polarizations of the incident electrons were recorded: perpendicular to the sample plane ( $\theta = 0^\circ$ ), in-plane perpendicular to the step edges ( $\theta = 90^\circ$ ,  $\psi = 0^\circ$ ), in-plane parallel to the step edges ( $\theta = 90^\circ$ ,  $\psi = 90^\circ$ ). Note that for Ag(116) vicinal crystal, perpendicular to the sample plane direction corresponds to the [116] crystallographic direction (see Fig. 4.6).

The SPLEEM images were acquired by scanning the Fe wedge, i.e., by moving the manipulator with respect to the incident electron beam, keeping the incident angle constant and switching the polarization direction  $\mathbf{P}$  at every step. On average, one SPLEEM image (in one polarization configuration) was obtained at around 5-10 sec. The SPLEEM images recorded for three orthogonal electron polarizations as a function of Fe film thickness are shown in Fig. 5.22. Since the domain structure recorded at 130 K and 300 K are qualitatively similar, the images at 130 K are shown solely. On top of the image columns, the polarization direction of the illuminating beam with respect to the step edges of the vicinal crystal is indicated. The bright and dark features in the SPLEEM images result from the component of surface magnetization vector along the axis defined by the orientation of the spin polarization of the illuminating beam (parallel and anti-parallel, respectively). No magnetic contrast, i.e. 50% gray color in SPLEEM image is observed if  $|\mathbf{M}| = 0$  (nonmagnetic surface) or if the spin polarization of the incident electron beam is perpendicular to the direction of magnetization at the surface. The images are normalized to the background (the area outside the field of view), corresponding to zero magnetic contrast.

The lowest thickness of Fe film at which any domain structure was distinguished is 2.85 ML. Most likely, for Fe films thinner than 2.85 ML, the domains are too small to resolve them and on average they give zero magnetic contrast\*. Since the Curie temperature  $T_C$  for 2.5 ML thick *bcc* Fe film grown on Ag(001) is found to be around 325 K [79, 184], the temperature effect can be excluded as a reason for the absence of the magnetic contrast below 2.85 ML. This is also supported by the fact that the domain structure in the thinnest regime of Fe is nearly identical at 130 K and 300 K.

Note that the measurement was performed on a wedge sample and there is a thickness gradient, which

---

\*Note that the magnetic contrast in SPLEEM is energy and thickness dependent. For very thin Fe films, below  $\sim 5$  ML, the asymmetry intensity decreases with decreasing Fe thickness at  $E = 13.5$  eV. In order to examine the domain structure for very thin Fe films, in particular below 2.85 ML, the energy of the incidence electrons should be optimized in order to see the maximum magnetic contrast in this particular thickness range.

SECTION 5.3

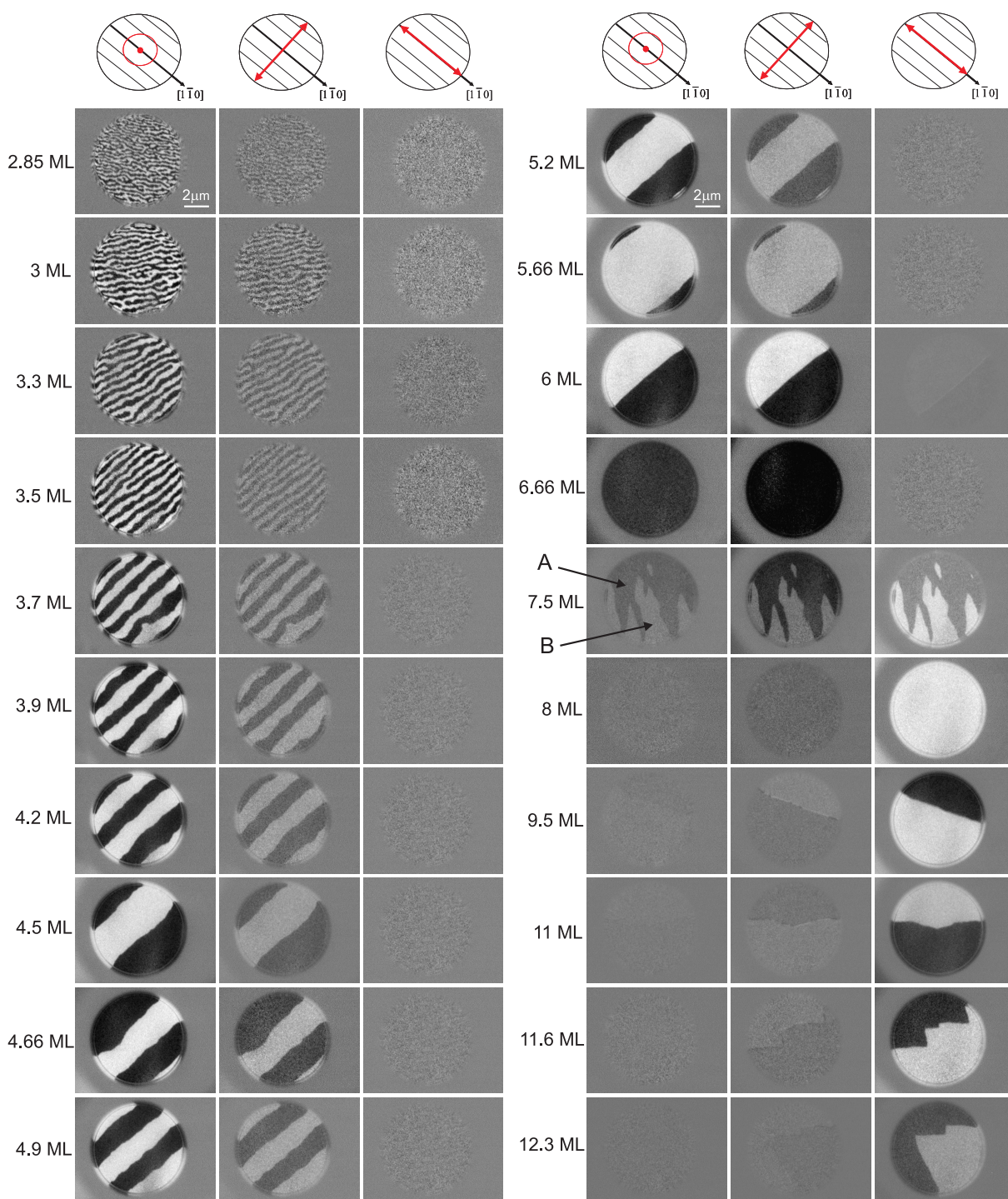
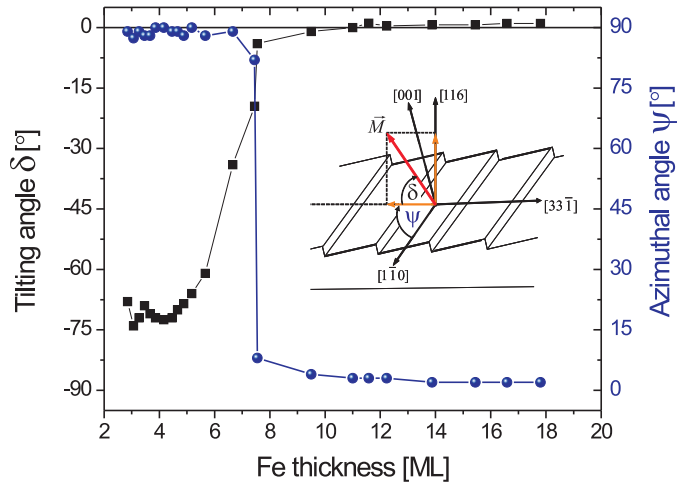


**Figure 5.22:** SPLEEM images with varying thickness of Fe film grown on Ag(116) surface obtained at 130 K. Grey level, with respect to the background corresponding to zero magnetic contrast, represents orientation of magnetization  $\mathbf{M}$  with respect to the polarization  $\mathbf{P}$  of the incident beam (light and dark areas correspond to parallel and anti-parallel orientations of  $\mathbf{M}$  and  $\mathbf{P}$ , respectively). Polarization direction of the illuminating beam is indicated on top of the image columns. The field of view is  $12 \mu\text{m}$  and electron energy is 13.5 eV.

is perceptible, even within the area of a single image (the spread of the thickness within the field of view, from the top to the bottom, is around 0.16 ML). As a consequence, it can be observed that within the single image, there is a gradient of the domain size, which clearly demonstrates the strong dependence of the domain size on Fe film thickness.

**Figure 5.23:** Tilting angle  $\delta$  and azimuthal angle  $\psi$  of magnetization as a function of Fe film thickness evaluated from SPLEEM images within area of a single domain. With decreasing Fe film thickness, magnetization starts to tilt out from the sample plane and discontinuous switch of in-plane magnetization orientation from along the steps towards perpendicular to the steps ( $\psi = 0^\circ \rightarrow \psi = 90^\circ$ ) occurs at 7.5 ML. Tilting angle  $\delta$  of magnetization changes gradually, eventually reaching [001] crystallographic direction, i.e. direction perpendicular to the plane of the atomic terraces.



Up to around 7 ML there is no contrast along the step edges (right column in Fig. 5.22), which means that there is no magnetization component along this direction. There is a weak magnetic contrast perpendicular to the step edges (middle column) and a strong contrast along the sample normal (left column), which means that the magnetization is slightly tilted from the normal to the sample plane keeping its in-plane orientation perpendicular to the steps. The domains form so called stripe phase, which is usually observed for ferromagnetic films with the easy axis perpendicular to the sample plane [185–189].

While the Fe film thickness increases, stripe domains expand and arrange to the alignment with the domain walls oriented perpendicularly to the step edges. Above around 5.2 ML, a continuous increase of the contrast perpendicular to the step edges with the simultaneous decrease of the contrast perpendicular to the sample plane is observed. For 7.5 ML thick Fe film, the domain pattern changes dramatically. A rapid alteration of the magnetization orientation is manifested by domain "splitting". While in part A (see Fig. 5.22) there is still a substantial magnetic contrast along the sample normal (i.e., the magnetization is tilted from the direction perpendicular to the step edges), part B shows negligible magnetic contrast along the sample normal (i.e., the magnetization is oriented almost completely in the sample plane). In addition, approaching the sample plane is associated with an abrupt switching of the in-plane magnetization component to the direction along the step edges.

With further increase of Fe film thickness, magnetic contrast is visible exclusively in the sample plane along the step edges. For 9.5 ML and thicker films, domain wall can be observed from the magnetic contrast perpendicular to the step edges (i.e., when probed perpendicular to the easy axis of magnetization). The interpretation of this contrast is that the domain wall has a *Neél* structure. Moreover, the domains are larger (in comparison to thinner films) and have no preferential orientation with respect to the crystallographic directions of the Fe film.

Using the fact that magnetic contrast in SPLEEM is proportional to the scalar product of the beam polarization and magnetization, more quantitative analysis is possible. By evaluating the magnetic contrast in three orthogonal directions a 3-dimensional orientation of the magnetization vector  $\mathbf{M}$  can be determined. The orientation of the magnetization as a function of Fe film thickness at 130 K is shown in Fig. 5.23. The magnetization is characterized by tilting angle  $\delta$  and azimuthal angle  $\psi$  (as shown in the inset of Fig. 5.23). Initially, starting from the thinnest investigated Fe film, magnetization is tilted out from the sample normal by  $\sim 20^\circ$  with inclination toward perpendicular to the steps ( $\psi = 0^\circ$ ). It means that  $\mathbf{M}$  is oriented nearly along [001] direction, i.e., perpendicular to the terraces plane (the miscut angle between [001] and [116] directions for bare Ag(116) crystal is equal  $13.3^\circ$ ). Up to around 5 ML there are no significant changes in orientation of magnetization. Above 5 ML, the tilting angle starts to decrease while keeping the azimuthal orientation perpendicular to the steps. At 7.5 ML, abrupt change of  $\delta$  and discontinuous switch of in-plane magnetization orientation from perpendicular to the steps toward along



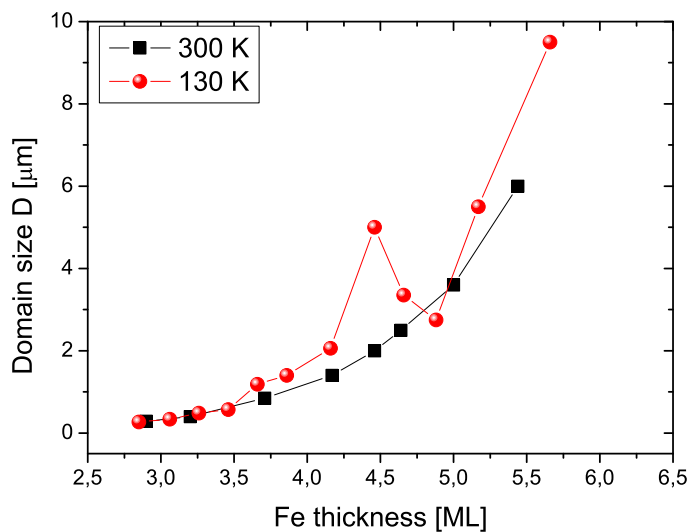


**Figure 5.24:** Domain size  $D$  as a function of thickness of Fe film grown on Ag(116) surface estimated from SPLEEM images obtained at 130 K and 300 K. The size of domains is an averaged value over the area corresponding to the field of view ( $12\mu\text{m}$ ). The error bars are estimated as follows: thickness ( $\pm 0.2\text{ML}$ ), domain size  $D$  ( $\pm 0.3\mu\text{m}$ )

the steps ( $\psi = 90^\circ \rightarrow \psi = 0^\circ$ ) is observed. This rapid alteration of the orientation of magnetization corresponds to the "split" domains shown on Fig. 5.22, where magnetic contrast is changed significantly while passing from part A into part B. With further increase of Fe thickness the orientation of magnetization remains the same, i.e., in-plane along the step edges.

Having well ordered stripe domains, the domain size  $D$  can be estimated by taking the line profile across the domain wall. The thickness dependence of the domain size  $D$  at two different temperatures: 130 K and 300 K is shown in Fig. 5.24. Note that the size of domains shown here is an averaged value over the area corresponding to the field of view ( $12\mu\text{m}$ ). Above  $\sim 5.5\text{ML}$  of Fe, the size of the domains exceeds the field of view (i.e.,  $D > 12\mu\text{m}$ ) and thus, cannot be precisely derived from this set of measurements.

Starting with the thinnest Fe films, the size of the domains  $D$  increases exponentially with the film thickness. At around 4.5 ML, the domains measured at 130 K are nearly three times larger than those measured at 300 K. Interestingly, with further increase of the Fe film thickness, the domains measured at 130 K become similar to those measured at 300 K. Above 5 ML the domain size increases rapidly at both temperatures and eventually, exceeds the field of view ( $D > 12\mu\text{m}$ ). Note that although the values of  $D$  are not derived above  $\sim 6\text{ML}$ , the domain structure was recorded continuously by moving the field of view across the Fe wedge. Therefore, the domain size can be estimated roughly from number of the observed domain walls within certain area. From this estimation, the domain size approach maximal value  $D \sim 70\mu\text{m}$  in the thickness range between 6 ML and 7.5 ML.

The observed local change in the domain size at  $\sim 4.5\text{ML}$  occurs solely at LT and therefore, suggests to be related to QWS contribution to the MA (such contribution can be visible only at LT and only at specific thicknesses). However, there is no anomaly of the tilting angle at this thickness, as could be expected from MOKE measurements at 5 K.

### Effect of sub-monolayer coverage with Au

As can be seen from SPLEEM measurements for uncovered Fe films on Ag(116) surface, the in-plane orientation of magnetization is directly linked to the out-of-plane magnetization component. It is observed that as soon as the magnetization starts to tilt out from the sample plane, a discontinuous in-plane SRT occurs and the magnetization prefers to be oriented perpendicular to the step edges. In order to examine this effect, the domain structure of Fe/Ag(116) was studied as a function of sub-monolayer Au coverage at 130 K. SPLEEM images were recorded for three thicknesses of Fe film: 4.2, 4.25 and 4.5 ML, by closing the shutter of Au e-beam evaporator and probing different part of the Fe wedge. Triplets of SPLEEM images using beam polarization parallel to the surface normal and two orthogonal

polarizations parallel to the film (along the steps and perpendicular to the steps) were recorded. During measurements the electron beam energy and the field of view were kept constant at 13.5 eV and  $12\mu\text{m}$ , respectively.

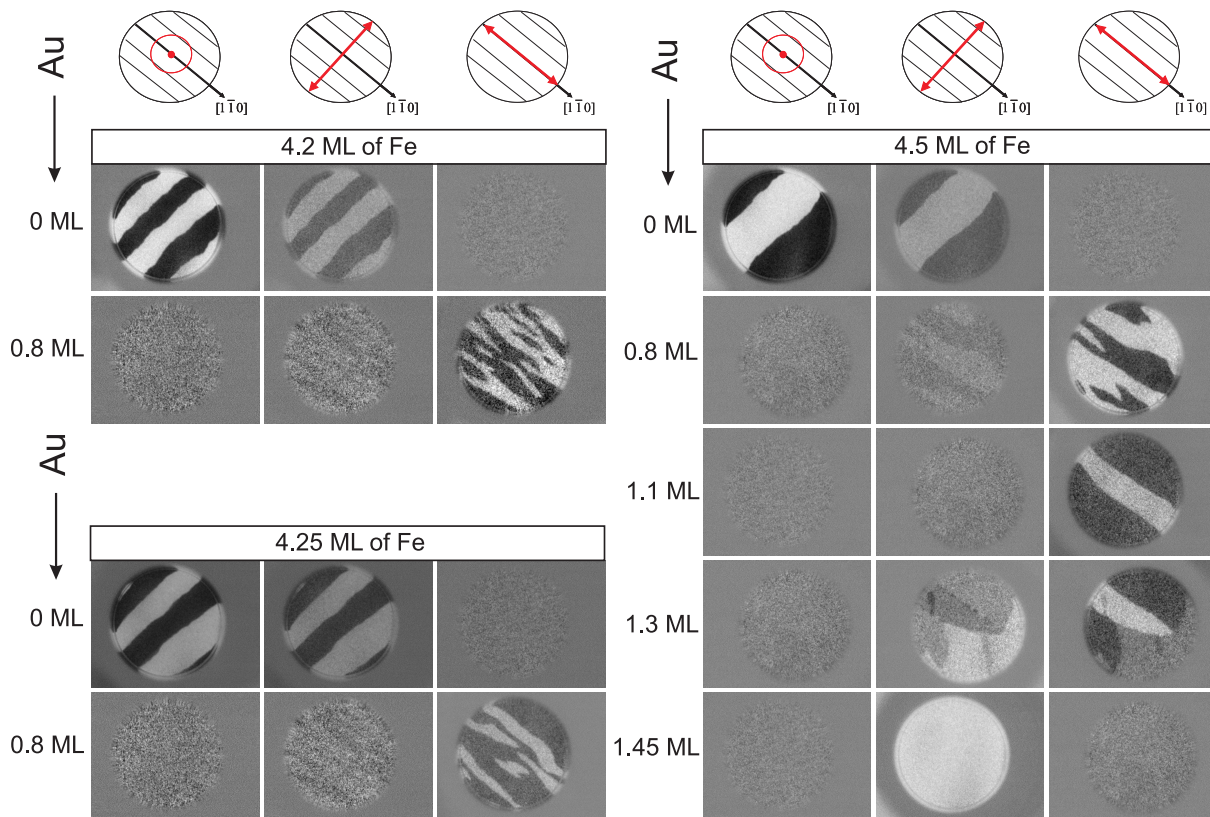


**Figure 5.25:** SPLEEM images with varying thickness of sub-monolayer Au coverage of Fe films grown on Ag(116) surface.  $T = 130\text{ K}$ , the field of view is  $12\mu\text{m}$  and electron energy is 13.5 eV.

The domain pattern and the magnetization direction upon deposition of Au is demonstrated in the sequence of images in Fig. 5.25. As shown before for uncovered sample (0 ML of Au), stripe domains are observed for polarization of the incidence electrons along normal and in-plane perpendicular to the step edges. Already 0.8 ML of Au causes dramatic changes in the domain structure and magnetic contrast is visible solely parallel to the step edges (Fig. 5.25). While for uncovered sample regular stripes are observed, after 0.8 ML of Au domains are less regularly distributed and fuzzy. For all three investigated thicknesses of Fe film, deposition of 0.8 ML of Au suppress completely out-of-plane component of magnetization and the easy axis is oriented along the step edges.

Changes of magnetic contrast upon further deposition of Au are shown for 4.5 ML of Fe (Fig. 5.25). Although domain pattern for 0.8 ML and 1.1 ML thick Au looks similarly (with one stripe distinguished in the middle), the relative contrast between those two domains is reversed (black become white and vice versa). Upon covering with more Au (1.3 ML), magnetic contrast appears in both in-plane directions: parallel and perpendicular to the step edges. State of coexisting phases is observed with adjacent domains oriented parallel and perpendicular to the steps. With further deposition of Au, the magnetization reorients fully toward perpendicular to the step edges direction (1.45 ML of Au) and no contrast along the step edges is visible. Analogous domain pattern (large domains with magnetization oriented perpendicular to the steps) is also observed for 4.2 ML and 4.25 ML thick Fe films covered by 1.45 ML of Au.

The change of the domain structure upon Au deposition confirms that as soon as the magnetization starts to tilt out from the sample plane, a discontinuous in-plane SRT occurs and the magnetization prefers to be oriented perpendicular to the step edges. Interestingly, the change of in-plane magnetization

orientation is also associated with the orientation of the domain walls with respect to the step edges of the vicinal surface. For uncovered Fe film, when the easy axis of magnetization is tilted within vertical plane perpendicular to the step edges, the domain walls are oriented perpendicular to the step edges. In contrast, for Fe film covered by 0.8 ML or 1.1 ML of Au, when the easy axis of magnetization is oriented entirely in the sample plane along the step edges, the domain walls are oriented along the step edges. A more detailed discussion of the multiple SRT upon covering with Au is carried out in Sec. 6.2 in conjunction with MOKE results.

### 5.3.2 Co films on Cu(1113) surface

Similarly as in the case of Fe/Ag(116), SPLEEM images with three orthogonal spin polarizations of the incident electrons were recorded for Co/Cu(1113). As expected from previous reports [38, 39, 57], the easy axis of the magnetization was confirmed to be oriented along the step edges. Large domains (bigger than 18  $\mu\text{m}$ ) with preferential direction of the domain walls along the step edges, were found to be independent of the thickness of Co film within investigated thickness range from 3 to 14 ML at 300 K.

As shown in Sec.5.1.1, the step-induced uniaxial anisotropy of Co film can be significantly modified by coverage with Au. In particular, in the thickness range of Au between 0.5 and 1 ML (Fig. 5.8a), the negative interface contribution from Au compensates the positive interface contribution from UHV/Co. As a result, two in-plane directions, along the step edges and perpendicular to the step edges, become nearly equivalent. Therefore, a small change of MA (e.g., by varying the thickness of the film or temperature) can result in change of the in-plane orientation of the easy axis of magnetization. In particular, in case of oscillatory MA due to QWS, covering of Co/Cu(1113) with a minute amount of Au, allows to observe a change of the orientation of the easy magnetization axis several times with increasing Co film thickness (See Fig. 5.9b). Therefore, in order to image the domain structure of Co in the vicinity of SRT and possibly to observe oscillatory changes of the domain structure, 0.7 ML of Au was deposited at RT on top of Co wedge.

In order to observe the distribution of the domains in the vicinity of the in-plane SRT in more detail, the magnetization was probed along different in-plane directions, starting with polarization perpendicular to the step edges direction ( $\psi = 0^\circ$ ) and changing the axis of polarization with  $45^\circ$  step. The SPLEEM images in the vicinity of in-plane SRT are shown in Fig. 5.26. The polarization direction of the illuminating beam is indicated at the top of the image columns. For 5 ML and 7 ML thick Co film, the brightest/darkest contrast is visible when probing along  $\psi = 0^\circ$  and  $\psi = 180^\circ$ , i.e., perpendicular to the step edges. By rotating the axis of the polarization direction toward along the step edges, magnetic contrast decreases and at  $\psi = 90^\circ$  no contrast is visible, except the domain wall. Interesting changes in the domain structure occurs with further increase of Co film thickness. At 7.6 ML magnetic contrast is still the strongest at  $\psi = 0^\circ$  and  $\psi = 180^\circ$ , however there is an exceptional small region which shows no contrast at those direction. This particular region gives the brightest contrast along the steps. Therefore, state of coexisting phases is observed with domains oriented perpendicular to the steps and domain along the steps. With increasing Co thickness, the fraction of the magnetic contrast along the steps increases and at 8.5 ML magnetization is oriented entirely along the steps. Note that by probing the magnetization perpendicular to the easy axis (see for instance 5 ML of Co probed along  $\psi = 90^\circ$  or 8.5 ML of Co probed along  $\psi = 180^\circ$ ) the domain wall can be observed. The absence of magnetic contrast between adjacent domains confirms that domains are anti-aligned and thereby, separated by a  $180^\circ$  domain wall. The interpretation of this contrast is that the domain wall has a *Neél* structure. Note that the domain wall consists of brighter and darker segments. The fact that different parts of the domain wall shows opposite contrast is consistent with the expectations that *Neél* walls must occur in two chiralities [190]. From the line profile across the domain wall, the domain wall width of about 600 nm is found. A similar value, of about 500 nm was measured for 5.5 ML of Co film grown on Cu(001) [191].

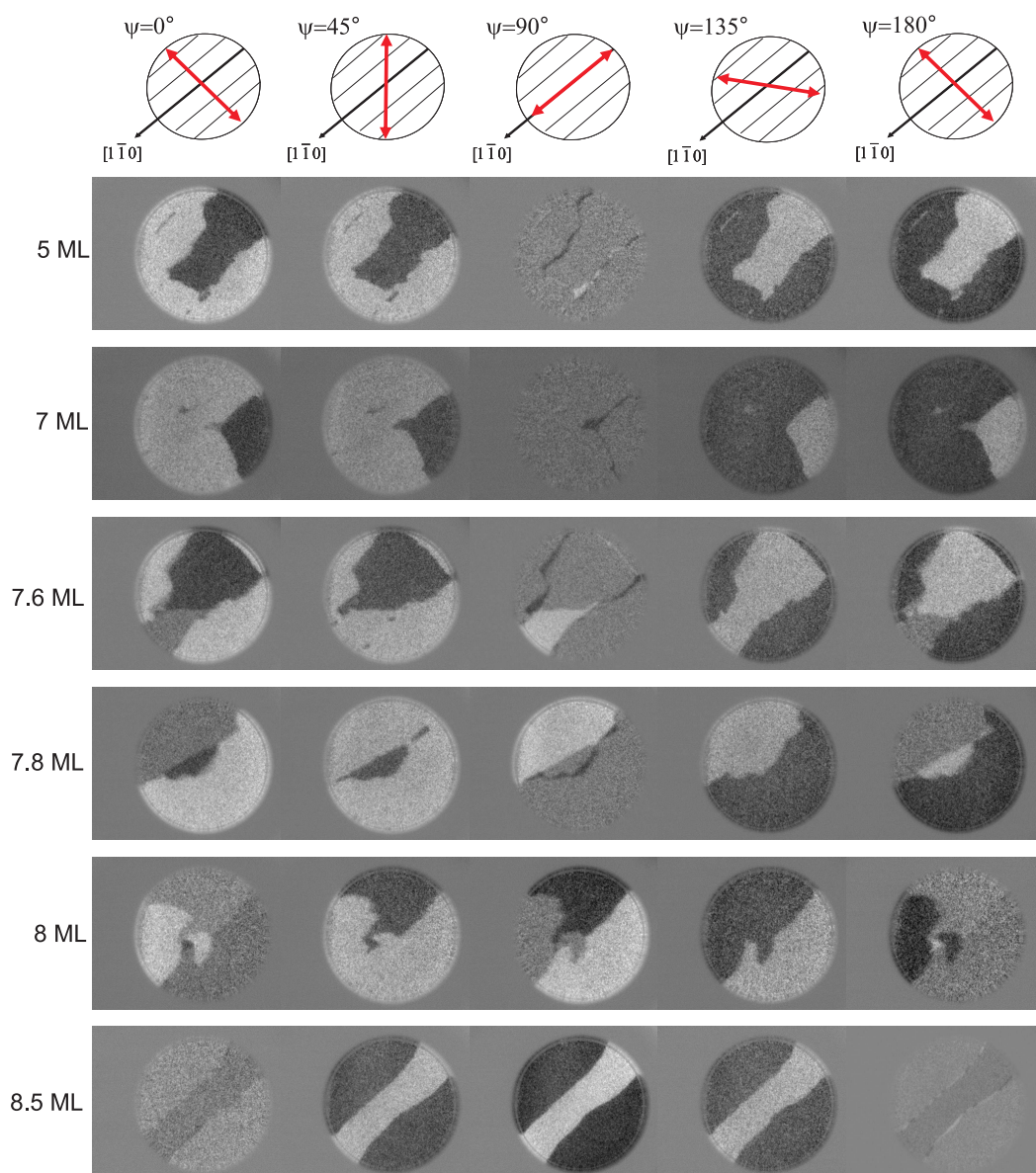


**Figure 5.26:** SPLEEM images with varying thickness of Co film grown on Cu(111)3 surface.  $T = 130$  K, the field of view is  $12 \mu\text{m}$  and electron energy is 8.5 eV.

## 6.1 Necessary conditions for the observation of magnetic anisotropy oscillations

In this chapter the experimental conditions necessary for the observation of magnetic anisotropy (MA) oscillations are described. The results presented in this thesis only constitute a fraction of the effort that was undertaken to observe MA oscillations in a large number of film/substrate combinations. Based on the experience with different systems and different experimental techniques, some facilitative experimental details concerning growth conditions and MOKE measurements, which were successfully applied to observe the oscillatory MA are presented.

### Requirements for QWS formation and their contribution to the magnetic anisotropy

As introduced in Sec. 2.2, QWS may be formed in thin metallic films, when electrons are reflected at the potential barriers created by the interfaces. A decisive requirement for the experimental observation of QWS concerns the quality of the interfaces, that is lateral smoothness and vertical sharpness. To this effect it is necessary to grow the film at an elevated temperature to ensure sufficient mobility of the atoms, promoting layer-by-layer growth and minimizing the chance of defect formation. The temperature, however, has to be limited to avoid intermixing and interdiffusion. Thermal atomic diffusion is indeed suppressed at low temperatures, allowing the film to build up "sharp" interfaces [192]. In order to grow smooth, atomically flat films with well defined interfaces optimum growth conditions have to be determined for the formation and observation of QWS.

In general, almost every film/substrate configuration demands different preparation conditions. Some of the systems presented in this work, such as Fe/Ag(001) or Co/Cu(001), have been extensively studied in the past and optimal growth conditions were used based on available literature. However, many of the systems presented here, have only been studied selectively in the past and optimal preparation conditions had to be experimentally determined by trial and error. In this process, it was found that even small changes in growth and annealing temperatures can have significant impact on the formation of QWS. In the literature, it has been observed for example for Ag/Fe(001) [192, 193] that deposition of Ag films at 100 K and 300 K with equivalent post-annealing temperature results in dramatic changes of the QWS properties. In fact, while deposition at lower temperatures does not indicate any improvement of the surface morphology (when tested with standard techniques like LEED and STM), it however boosts the occurrence of electron confinement and allows to observe atomic-layer resolved QWS, with extremely narrow linewidths [192, 194]. Thus, to optimize the growth conditions of a particular system the it is necessary to study how its affects the QWS and their properties. In this work, such test measurements were performed by determining the oscillatory MA using MOKE.

A strong influence of the deposition temperature on oscillatory magnetic anisotropy was observed, among others, for Fe and Co films deposited on the vicinal surface of Au(001). The Fe/Au(100) system is particularly well suited for creating narrow QWS. The small lattice mismatch (less than 1%) is achieved by 45° rotation of *bcc* Fe with respect to the *fcc* Au. The growth of Fe on Au(100) has been found to proceed layer-by-layer at RT, a Au layer always found on top of the growing Fe surface [88]. This Au overlayer acts as a surfactant by lowering the surface energy of the growing film and thereby preventing island formation. Fe films on Au(001) grown at RT have also been studied by inverse photoemission, where QWS from unoccupied bands were found [195]. However, in this work it was found that Fe films grown at RT on the vicinal surface of Au(001) do not exhibit any oscillatory behavior of the magnetic anisotropy, based on MOKE measurements. Furthermore, deposition at a lower temperature (200 K) or post-annealing lead to the same absence of QWS. These results are surprising in view of the fact that there are many similarities between the Fe/Au(001) and Fe/Ag(001) systems (such as a nearly perfect lattice mismatch resulting in layer-by-layer growth of *bcc* Fe, the formation of a surfactant layer, the existence of an energy gap in the substrate allowing to form QWS inside the Fe film) and oscillations of MA which were clearly observed in Fe/Ag(001). By testing different preparation conditions we found that only the samples grown at an elevated temperature of 400 K and post-annealed at 425 K for 30 min, displayed an oscillatory MA. This is most likely associated with the formation of a Au surfactant layer. Indeed, as mentioned, the growth of Fe at RT results in the segregation of Au atoms on the top layer of the Fe film. However it was shown that this segregation is thickness dependent by Jiang *et al.* [88, 196]. The more Fe atoms are deposited on the surface, the higher is the thermal energy needed to activate segregation or interdiffusion processes. RT deposition of thick Fe films (up to ~ 30 ML in this case) is thereby not sufficient to form a uniform surfactant layer of Au on the top of the Fe film. As a consequence, the film is rougher and can contain some Au atoms across the Fe film. By depositing Fe films at elevated temperature, Au atoms segregate onto the surface, lower the surface energy and improve the surface morphology. Deposition at elevated temperatures therefore results in well defined interfaces, which make electron reflection more efficient and allow to observe the oscillatory MA due to QWS. This also explains why in reference [195] cited earlier, only the two first oscillations of the inverse photoemission intensity were observed for Fe films grown at RT. Above ~ 7 ML, the thermal energy is indeed not sufficient to uniformly segregate the Au atoms, hence the surface roughness increases and eventually, the confinement is gradually suppressed. Note that in the case of our experiment, the oscillations of MA recorded by MOKE persist at least up to 35 ML (see Fig. 5.7).

A similar behavior, concerning the influence of sample preparation conditions on MA oscillations was observed for Co films grown on the vicinal surface of Au(001). Structural studies of Co grown on flat Au(001) have shown that Co layers grow with the epitaxial relationship of *fcc* Au(110) || *bcc* Co(100) [95]. By combining STM, LEED and directional Auger electron spectroscopy it has been shown in reference [92] that growth at RT results in a relatively flat surface and that *bcc* Co films can be stabilized at least up to 10 ML. However, like in case of Fe/Au(001), only Co films grown at elevated temperatures display oscillatory MA. The optimum growth conditions were found for the deposition of Co films at 375 K, post-annealed at 425 K for 30 min. The effect of increased temperature during deposition is similar to the case of Fe films grown on Au(001) surface [93, 95].

The correlation between morphology and magnetic anisotropy and its influence on MA oscillations is particularly evident in the case of  $Fe_{1-x}Co_x$  films grown on the Ag(001) vicinal surface. Since Fe on Ag(001) grows following a well stabilized *bcc* structure, one can expect that Ag(001) is a good candidate for growing *bcc*  $Fe_{1-x}Co_x$  alloys, at least for low concentration of Co. According to previous reports [101, 102],  $Fe_{1-x}Co_x$  films grown at RT on Ag(001) maintain the *bcc* structure in a wide composition range, at least up to  $x = 0.7$  of Co. However, there was no information about the morphology and growth mode of this system [101, 102]. Therefore, STM studies were performed here in order to see how the morphology changes with adding of Co to Fe (see Sec. 3.2). It turns out that there is a significant difference between the growth mode of pure Fe and  $Fe_{1-x}Co_x$  grown on the vicinal surface of Ag(001). The Fe films reproduce the steps of the surface rather well and the width of the terraces, even for 8 ML

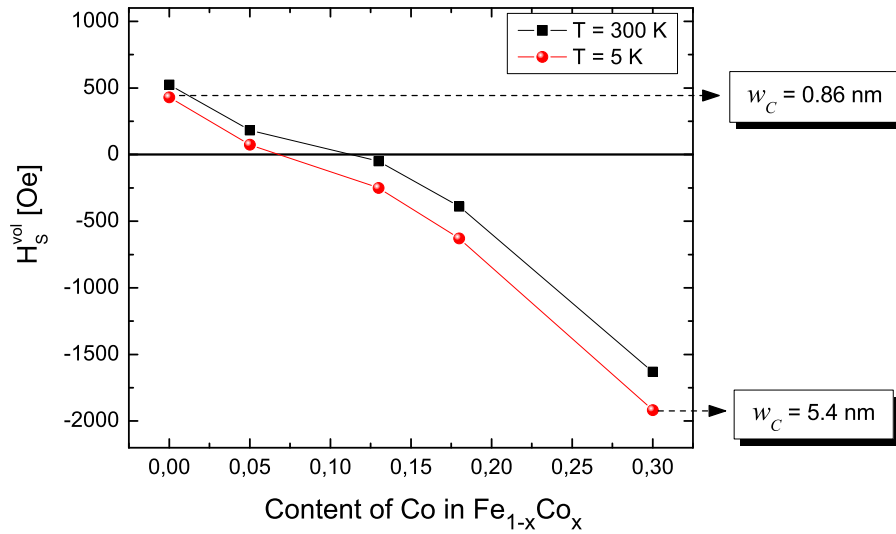


**Figure 6.1:**  $H_s^{vol}$  (the values  $H_s$  approaches in the limit of large film thicknesses) as a function of Co content obtained from MOKE measurements at 300 K and 5 K. The  $w_c$  values correspond to the width of the clusters obtained from STM measurements at 5 K.

thick Fe film, is almost identical to the width of terraces of the Ag(116) surface prior to deposition, i.e.,  $w_c = 0.86 \pm 0.04$  nm. The morphology of the film changes dramatically after codeposition of Co. The  $Fe_{1-x}Co_x$  forms clusters with a slight preferential elongation parallel to the step edges (see Fig. 3.6). The width of these clusters is on average  $w_c = 5.4 \pm 0.4$  nm.

The change in morphology in the presence of Co has a pronounced effect on the MA. We observe that alloying of Fe with Co results in strong in-plane uniaxial magnetic anisotropy, forcing the magnetization to orient itself perpendicularly to the step edges and the shift field  $H_s$  becomes more negative. In order to characterize these changes,  $H_s^{vol}$  values (the values  $H_s$  approaches in the limit of large film thicknesses) are estimated for different compositions of  $Fe_{1-x}Co_x$ . The dependence of  $H_s^{vol}$  as a function of Co content from the MOKE measurements at 300 K and 5 K is shown in Fig. 6.1. It is clearly observed that at both temperatures, the addition of Co to Fe causes  $H_s$  to be more negative. More negative  $H_s$  corresponds to stronger uniaxial anisotropy with the easy axis oriented perpendicularly to the steps. Therefore, by changing the composition of  $Fe_{1-x}Co_x$ , we can tune the in-plane uniaxial anisotropy. Note that already for the lowest investigated Co content ( $x = 0.05$ ), we find that the oscillations of  $H_s$  are almost completely suppressed. While for an Fe film, the oscillation amplitude reaches nearly 550 Oe, in case of  $Fe_{0.95}Co_{0.05}$ , it decreases below 20 Oe. This drastic change of the oscillation amplitude was observed for different growth conditions (several temperatures during deposition and post-annealing procedure were tested for growing  $Fe_{1-x}Co_x$  on Ag(116)). For higher contents of Co, the oscillations of  $H_s$  disappear completely.

Besides changes in morphology, varying composition of  $Fe_{1-x}Co_x$  should also result in changes of the electronic structure of the film. Indeed, it was predicted by Belhadji *et al.* [197, 198] that already  $x = 0.05$  of Co in  $Fe_{1-x}Co_x$  alloy can significantly reduce (even by factor of two) the density of states at the Fermi level of the electronic band with  $\Delta_5$  symmetry. Such changes of the electronic structure at the  $E_F$  can modify the magnetocrystalline anisotropy. In particular, substantial changes of the amplitude of the magnetic anisotropy oscillations due to QWS can be expected (since as it is discussed later in Sec. 6.3.2, the magnetic anisotropy oscillations in *bcc* Fe film are ascribed to QWS with  $\Delta_5$  symmetry).

*FeCo* alloys were also grown on the vicinal surface of Cu(001). In this case, changes in the magnetic anisotropy were studied by gradually adding more Fe to Co. The comparison of the shift field  $H_s$  measured by MOKE at 5 K for pure Co and  $Fe_{0.07}Co_{0.93}$  is shown in Fig. 6.2a. It can be observed that the oscillation amplitude for  $Fe_{0.07}Co_{0.93}$  is roughly twice as small as in pure Co ( $\sim 100$  Oe and  $\sim 200$  Oe,

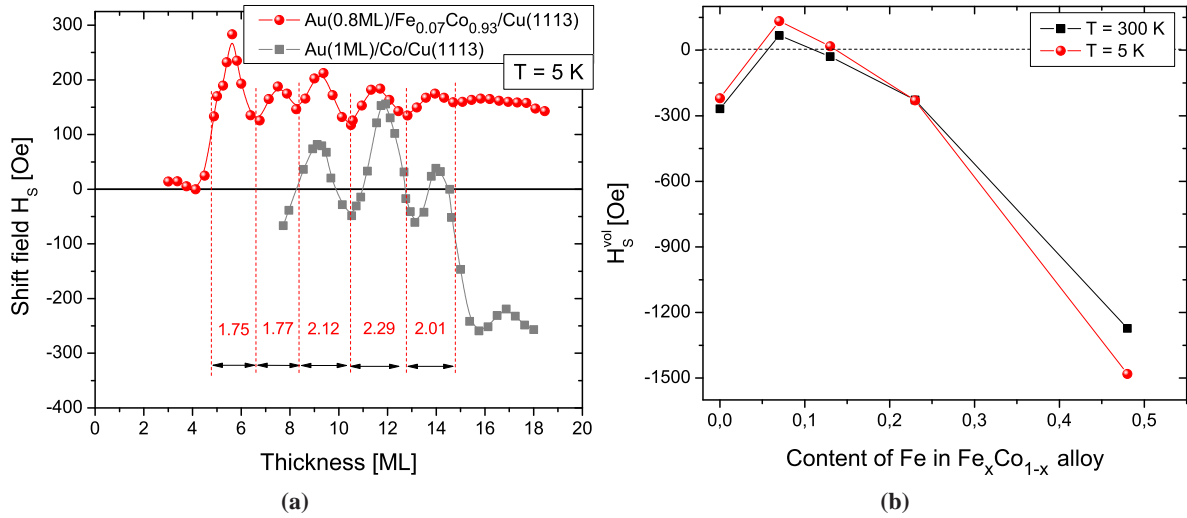


**Figure 6.2:** (a) Shift field  $H_s$  at 5 K for pure Co and  $Fe_{0.07}Co_{0.93}$  as a function of film thickness; (b)  $H_s^{vol}$  (the values  $H_s$  approaches in the limit of large film thicknesses) as a function of Fe content obtained from MOKE measurements at 300 K and 5 K.

respectively). Additionally, the period of oscillations is slightly shorter after adding 0.07 of Fe: it on average equals  $2.0 \pm 0.3$  ML (whereas the period of  $2.3 \pm 0.3$  ML is observed for pure Co). The two  $H_s$  dependencies shown in Fig. 6.2a are slightly shifted vertically due to different amount of Au deposited on top of the samples. Sub-monolayer deposition of Au is used to tune the base value of  $H_s$  closer to  $H_s = 0$  in order to enhance the sensitivity to small variations in  $H_s$  in the MOKE experiment (see Sec. 5.1.1). Deposition of Au however does not affect the volume contribution of  $H_s$ . Thus,  $H_s^{vol}$  values are insensitive to the amount of Au capping and can be compared independently, as in Fig. 6.2b. Further increasing the Fe content, up to  $x = 0.13$ , reduces the amplitude of oscillations to 50 Oe, while it does not change the oscillation period. Eventually, for  $x = 0.23$  and  $x = 0.43$  of Fe, the oscillations disappear completely.

Similarly as in case of  $Fe_{1-x}Co_x$  films grown on the vicinal surface of Ag(001),  $H_s^{vol}$  can be estimated for  $Fe_xCo_{1-x}$  films grown on the vicinal surface of Cu(001) in order to follow overall changes of the in-plane uniaxial magnetic anisotropy. The dependence of  $H_s^{vol}$  as a function of Fe content is shown in Fig. 6.2b. Although generally  $H_s^{vol}$  values become more negative with increasing content of Fe, there is an initial increase in the value of  $H_s^{vol}$  at low Fe concentration. This behavior is associated with the absence of a structural transition. It is known that *fcc* structure of Co on Cu(001) is compressed vertically with respect to Cu. The strain is nearly constant up to 15-16 ML, and then is released via the formation of dislocations. This strain relaxation is accompanied by a rapid drop of  $H_s$  around 15 ML [56] as can be observed in Fig. 6.2a. In the case of  $Fe_xCo_{1-x}$  films however, there is no evidence of such structural transition. This is in agreement with structural studies reported for this system [96, 98, 99] showing that by adding Fe to Co, the value of the vertical interlayer distance increases, which means that the strain is partially relaxed. It is therefore not surprising, that for low concentration of Fe,  $H_s^{vol}$  initially increases (since there is no drop of  $H_s$  associated with a structural transition, the values of  $H_s$  remain positive). Further increase of the Fe content results in vertical expansion of the interlayer distance [99] which is reflected by strong in-plane uniaxial anisotropy perpendicular to the steps ( $H_s$  become more negative) observed in our measurements (Fig. 6.2b).

The structural transitions in Co and  $Fe_xCo_{1-x}$  films on the vicinal surface of Cu(001) have significant consequences on the magnetic anisotropy of these systems. It was shown by M.Cinal *et al.* [21] using calculations of magnetocrystalline anisotropy energy within tight-binding (TB) model for *fcc* Co films on the vicinal surface of Cu(001), that the existence of the structural relaxation has a decisive effect on the oscillatory magnetic anisotropy. By direct comparison between the MA of Co films with the



inclusion of the structural relaxation and without, it was predicted that the MA only oscillates in the latter case. It means that when the *fcc* Co structure is free to relax from the first layers, the MA does not oscillate as a function of Co thickness [21]. This theoretical prediction is observed in our experiment. As can be seen in Fig. 6.2a, the oscillations of  $H_s$  measured by MOKE for pure Co are clearly observed up to the structural transition around 15 ML and are significantly reduced beyond that. The behavior for Co thicknesses before the structural transition thickness (i.e., where the strain is nearly constant) can be compared to the theoretical calculation performed without structural relaxation. On the other hand, after the structural transition thickness, the Co film starts to relax and can be compared to the calculations including structural relaxation. We thus show a first experimental proof of the prediction of M. Cinal in reference [21] concerning the fact that the MA oscillations are essentially only observed in *fcc* Co films which are vertically compressed (not relaxed). This observation can also explain the decreasing oscillation amplitude when adding Fe to Co. As mentioned above, the addition of Fe causes the relaxation of the atomic structure thus, decreasing the MA oscillation amplitude.

### Complex anisotropy and magnetization reversal on stepped surfaces probed by MOKE

The main purpose of growing FM films on vicinal substrates is the ability to measure small anisotropy changes. The detailed evaluation of split hysteresis loops allows to determine both the oscillation period and the oscillation amplitude of the magnetic anisotropy oscillations. As shown in Sec.4.1.3, the split hysteresis loops show additional features, when the easy axis of magnetization is oriented perpendicular to the steps. In this case, the evaluation of the shift field  $H_s$  is more complex and therefore, a detection of the oscillatory magnetic anisotropy can be nontrivial. The understanding of the shape of the split hysteresis loop is thereby very important. Also from the point of view magnetization reversal mechanism itself, explanation of this behavior would be useful for future experiments on vicinal surfaces. In this section, a model explaining such complex hysteresis loops is proposed and discussed together with experimental data.

#### i) Model description

When the easy magnetization axis is oriented perpendicular to the steps, by applying the magnetic field along the steps and decreasing its value below  $H_s$ , the magnetization switches to the easy magnetization axis, i.e., it becomes oriented perpendicular to the steps. In absence of a field component perpendicular to the steps, i.e., when the external magnetic field is applied perfectly along the steps (i.e., at  $\alpha_F = 0$ ) the transition of the magnetization from an orientation along the steps to an orientation perpendicular to the steps can proceed clockwise or counterclockwise. Therefore, at zero field, the magnetization can be oriented perpendicular to the steps in positive or negative direction with equal probability. Consequently, there should be no net magnetization perpendicular to the steps. In a real experiment however, the magnetic field direction can be slightly misalignment with respect to the steps direction ( $\alpha_F \neq 0$ ). Therefore, there is also a field component which is applied perpendicular to the steps. With the magnetic field applied along the steps and decreasing below  $H_s$ , the magnetization switches perpendicular to the steps (i.e., to the easy magnetization axis) into the direction in which the field component perpendicular to the steps is applied.

If the magnetization is probed by laser beam perfectly along the steps (i.e., at  $\alpha_L = 0$ ), it is not sensitive to the magnetization perpendicular to the steps and zero Kerr signal is detected in remanence in this case. In the experiment, the linearly polarized laser light is usually not oriented perfectly along the steps ( $\alpha_L \neq 0$ ). Therefore, both the magnetization component along the steps and the magnetization component perpendicular to the steps can be probed.

In a real experiment, the direction of the applied magnetic field ( $\alpha_F$ ) and the direction defined by the plane of incoming and outgoing laser beam ( $\alpha_L$ ) are not necessarily the same. In this case, with no field or at low field applied along the steps ( $H < H_s$ ), there will be net magnetization perpendicular to the steps. As a consequence, a low field hysteresis loop corresponding to the magnetization component perpendicular

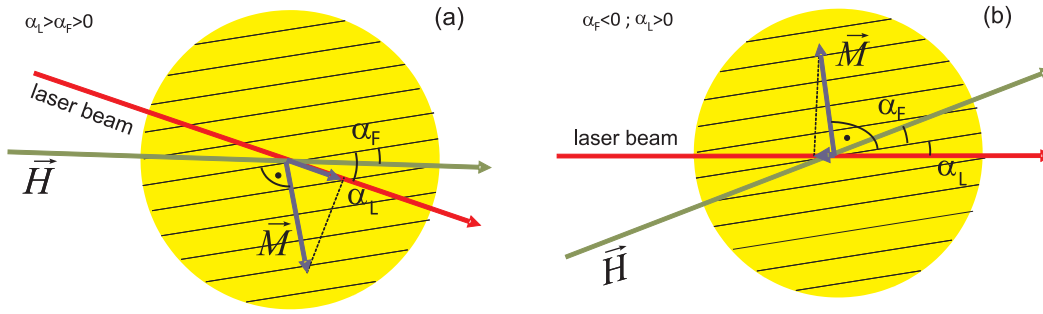


**Figure 6.3:** Schematic diagrams showing how the laser beam and magnetic field are oriented with respect to the steps for: (a) both  $\alpha_L$  and  $\alpha_F$  positive (or both negative) and (b)  $\alpha_L$  and  $\alpha_F$  of opposite sign. Note that the projection of the magnetization oriented: (a) along the laser beam direction and (b) opposite to the laser beam direction, results in normal and reversed low field hysteresis loop, respectively.

to the steps can be measured. Moreover, the Kerr signal can be either positive or negative depending on whether it is probed in the same or the opposite direction of the projection of the magnetization perpendicular to the steps on the laser beam direction. Therefore, such low field hysteresis loop can be normal (i.e., corresponding to a positive Kerr signal at positive fields) or reversed (i.e., corresponding to a negative Kerr signal at positive fields) depending on the sample orientation.

When the laser beam orientation  $\alpha_L$  and the field orientation  $\alpha_F$  are both positive or both negative, the projection of the magnetization perpendicular to the steps on the laser beam direction is always oriented in the same direction in which the magnetization is probed (Fig. 6.3(a)). It follows that in this case the low field hysteresis loops should be normal (i.e., not reversed). The situation is different, when  $\alpha_L$  and  $\alpha_F$  are of opposite sign. The projection of the magnetization perpendicular to the steps on the laser beam is now always oriented oppositely to the direction in which the magnetization is probed (Fig. 6.3(b)). Therefore, reversed low field hysteresis loops are expected to be measured in this case.

As shown in Sec. 4.1.3, when the magnetization is oriented perpendicular to the steps, is tilted out of the sample plane and in consequence, there is a polar contribution to the Kerr signal in longitudinal geometry. Therefore, when one considering the projection of the magnetization perpendicular to the steps, also the polar contribution associated with this projection has to be taken into account. In order to describe the Kerr signal contribution quantitatively, the longitudinal  $\Delta\phi_L$  and polar  $\phi_P$  Kerr signals will be considered below separately.

The intensity of the low field contribution to the longitudinal Kerr signal  $\Delta\phi_L$  obviously depends on the field and the laser beam orientation with respect to the sample (since it comes from the projection of the magnetization on the laser beam direction. See Fig. 6.3). From simple geometrical considerations it is expected to increase as the sine of the misalignment between the direction of the laser-beam and the step direction. Approaching  $\alpha_L = \pm 90^\circ$  (i.e., probing the magnetization along the easy magnetization axis), the low field contribution reaches saturation, and rectangular hysteresis loops are measured. By considering a small misalignment between the magnetic field and the laser-beam direction with respect to the steps in the longitudinal MOKE experiment, we can identify three different regimes of the low field contribution to the longitudinal Kerr signal  $\Delta\phi_L$ . For positive  $\alpha_F$  and  $\alpha_L$ , the low field hysteresis loops are normal,  $\Delta\phi_L$  is positive and increases from zero to saturation as  $\Delta\phi_L = +\phi_L^s \sin(|\alpha_L|)$ , where  $\phi_L^s$  is the saturation value of the longitudinal Kerr signal. For  $\alpha_L$  and  $\alpha_F$  of opposite signs, the low field hysteresis loops are reversed,  $\Delta\phi_L$  is negative and decreases from zero to a finite negative value at  $\alpha_F \rightarrow 0$ , as  $\Delta\phi_L = -\phi_L^s \sin(|\alpha_L|)$ . For negative  $\alpha_F$  and  $\alpha_L$ , the low field hysteresis loops are normal and  $\Delta\phi_L$  increases from a finite positive value to saturation as  $\Delta\phi_L = +\phi_L^s \sin(|\alpha_L|)$ . Note that the abrupt change from finite negative to finite positive  $\Delta\phi_L$  happens because the field direction crosses the step direction, i.e.,  $\alpha_F$  changes sign.

Following the discussion above, when probing the magnetization along the steps, the polar Kerr

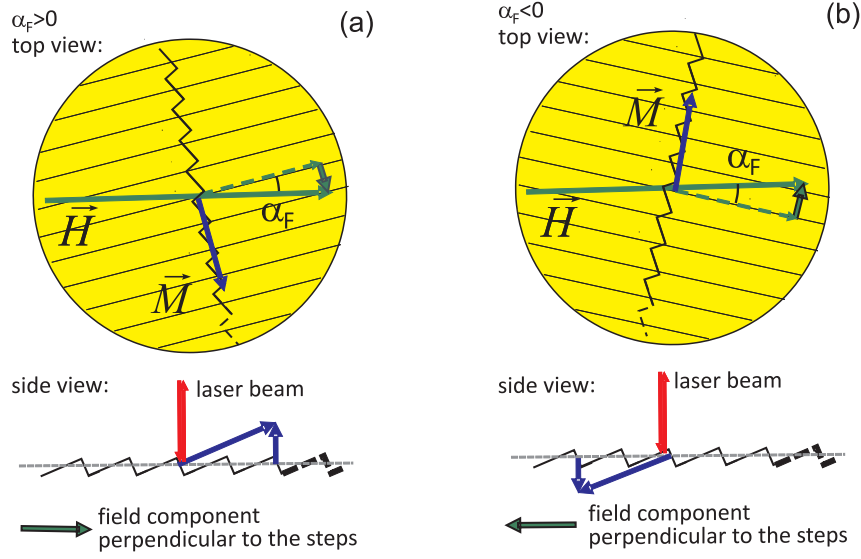


**Figure 6.4:** Schematic diagrams of the magnetization configuration for  $H < H_s$  and (a)  $\alpha_F > 0$ , (b)  $\alpha_F < 0$ . Note that the normal component of the magnetization, indicated by the small blue arrow in the bottom diagrams, is pointing up (a) and down (b), respectively.

signal  $\phi_P$  should contribute only at low field (because only then the magnetization is oriented perpendicular to the steps). Switching of the magnetization perpendicular to the steps switches also its normal component and thereby, the polar Kerr effect gives an additional contribution of size  $\phi_P$  to the low field hysteresis loops.

As long as the magnetization is oriented perpendicular to the steps the normal component of the magnetization is independent of  $\alpha_F$ . However, as illustrated schematically in Fig. 6.4, the out-of-plane component of the magnetization changes polarity abruptly at  $\alpha_F = 0$ . Note that the actual polarity depends on the step geometry and can be reversed by changing the sample orientation by  $180^\circ$ . Since the incidence angle of the laser beam with respect to the surface normal is fixed by the experimental geometry, also  $\phi_P$  will be constant apart from changing its sign at  $\alpha_F = 0$ . For simplicity, in the following discussion, it is assumed that  $\phi_P$  is positive for positive  $\alpha_F$  and negative for negative  $\alpha_F$ .

Eventually, the contributions of the longitudinal  $\Delta\phi_L$  and the polar Kerr signal  $\phi_P$  can be combined to  $\Delta\phi = \Delta\phi_L + \phi_P$ . Depends on the relative orientation of the laser beam  $\alpha_L$  and the external magnetic field  $\alpha_F$  direction with respect to the steps direction (i.e.,  $\alpha_L = 0$  and  $\alpha_F = 0$ ) it can be written in general form:

$$\Delta\phi = \begin{cases} -|\phi_P| + \phi_L^s \sin(|\alpha_L|), & \alpha_L < 0, \alpha_F < 0 \\ -|\phi_P| - \phi_L^s \sin(|\alpha_L|), & \alpha_L > 0, \alpha_F < 0 \text{ (or } \alpha_L < 0, \alpha_F > 0) \\ +|\phi_P| + \phi_L^s \sin(|\alpha_L|), & \alpha_L > 0, \alpha_F > 0 \end{cases} \quad (6.1.1)$$

## ii) MOKE results in view of the model

The model described above can be verified when applied to the experimental data for FM film on vicinal surface which posses the easy magnetization axis perpendicular to the steps. As an example, experimental results from MOKE measurements on Fe films grown on Au(1113) surface are used here. In order to verify the model in detail, hysteresis loops were probed upon increasing misalignment of the magnetic field with respect to the steps direction. The sample was rotated clockwise (toward  $\alpha^+$ ) and counterclockwise (toward  $\alpha^-$ ) with respect to the orientation along which magnetic field is assumed to be oriented along the steps. In Fig. 6.5 representative hysteresis loops are shown for 15 ML thick Fe film grown on Au(1113) at different sample orientations: (i)  $\alpha > \alpha_b$ , (ii)  $\alpha_c < \alpha < \alpha_b$  and (iii)  $\alpha < \alpha_c$ ,

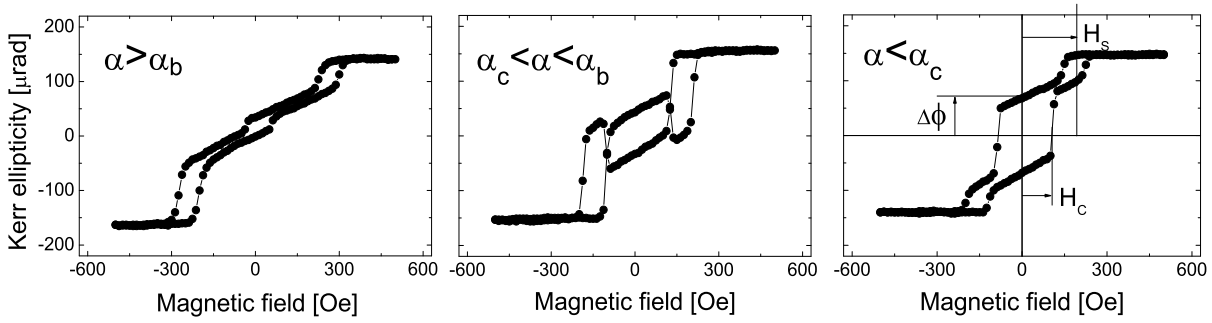


**Figure 6.5:** Hysteresis loops measured for 15 ML of Fe on Au(1113) at varying sample orientation  $\alpha$  :  $\alpha > \alpha_b$ ,  $\alpha_c < \alpha < \alpha_b$  and  $\alpha < \alpha_c$ . Here,  $\alpha_b$  corresponds to the sample orientation at which the low field component vanishes and  $\alpha_c$  to the orientation where the low field component abruptly changes its polarity.  $\Delta\phi$  and  $H_c$  denote remanence and coercivity of the low field hysteresis loop, respectively.  $H_s$  denotes shift field.

where  $\alpha_c$  and  $\alpha_b$  are chosen arbitrary as the angles at which the measured loops experience characteristic changes.

The hysteresis loops measured at  $\alpha > \alpha_b$  show double-step behavior with a non-zero Kerr signal in remanence which gives rise to an additional hysteresis loop at low magnetic field. The positive contribution to the total Kerr signal at low field decreases with decreasing  $\alpha$  for  $\alpha > \alpha_b$  and vanishes for  $\alpha = \alpha_b$ .

The hysteresis loops measured at  $\alpha_c < \alpha < \alpha_b$  show also double-step behavior (see Fig. 6.5). The signal in remanence is also not zero and again gives rise to an additional hysteresis loop at low magnetic field. As shown already in Sec. 4.1.3, the shape of such hysteresis loop is explained as superposition of split loop and reversed loop (as shown schematically in Fig. 4.4).

The hysteresis loops measured at  $\alpha < \alpha_c$  again show double-step behavior. At low field a normal (not reversed) hysteresis loop is observed, similarly as in the case of the loops measured at  $\alpha > \alpha_b$  but with higher signal at remanence. The positive contribution to the total Kerr signal at low field increases with decreasing  $\alpha$ .

In order to get more insight into the transition of the low hysteresis loop (from reversed into normal one), an additional measurements were performed in very close vicinity of  $\alpha_c$ . Interestingly, it was not possible to measure hysteresis loop with zero Kerr signal in remanence at  $\alpha_c$ . Instead, one can get two different loops for  $\alpha_c \pm \Delta\alpha$ , where  $\Delta\alpha = 0.5^\circ$  (Fig. 6.6). Although the low field component in both loops has similar intensity, for one loop the low field component is normal (for negative  $\Delta\alpha$ ), for the second one it is reversed (for positive  $\Delta\alpha$ ).

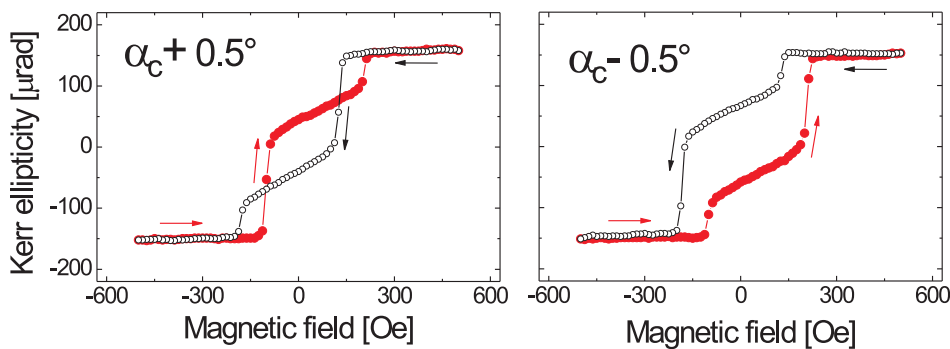


**Figure 6.6:** Hysteresis loops measured for 15 ML of Fe grown on Au(1113) at  $\alpha_c \pm 0.5^\circ$ .

The measurements performed after rotation of the sample by  $180^\circ$  show exactly the same saturation signal and features at low field as in case loops shown in Fig. 6.5 and Fig. 6.6.

Similar measurements (i.e., angular dependence in the vicinity of the orientation along which magnetic field is assumed to be oriented along the steps) were performed for 58 ML thick Fe film grown on Au(1113) (Fig. 6.7). It is observed that the hysteresis loops experience changes with increasing thickness of the Fe film. In particular, the aforementioned complex shape of the hysteresis loops is not visible any more for the 58 ML thick Fe films. This is because  $H_s$  decreases with increasing thickness of Fe, whereas the coercivity of the low field hysteresis loop remains more or less the same. Nevertheless, for 58 ML thick Fe film all the parameters of the hysteresis loops depend on the orientation  $\alpha$  in the same way as described for 15 ML of Fe.

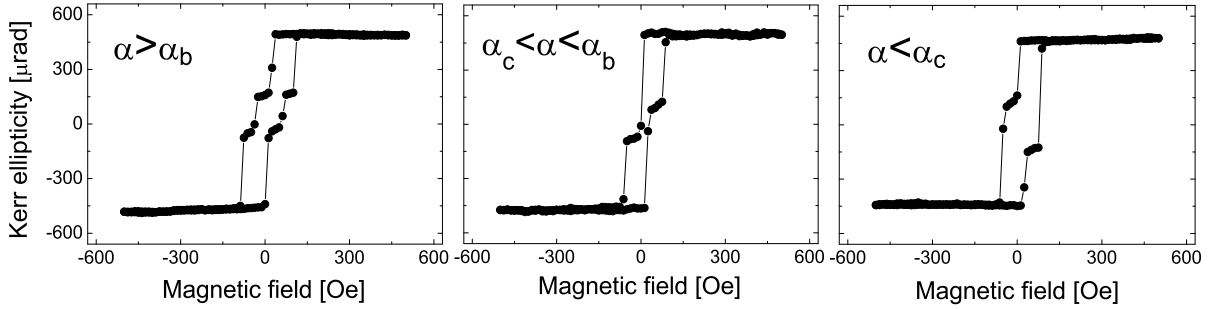
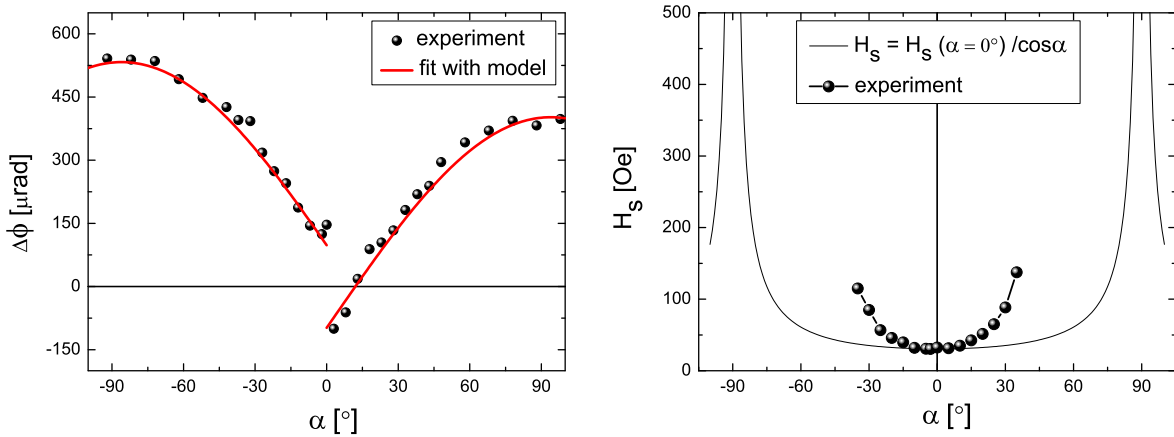


**Figure 6.7:** Hysteresis loops measured for 58 ML of Fe on Au(1113) at varying sample orientation  $\alpha$ : (i)  $\alpha > \alpha_b$ , (ii)  $\alpha_c < \alpha < \alpha_b$  and (iii)  $\alpha < \alpha_c$ . The hysteresis were measured at the same orientations  $\alpha$  as the ones for 15 ML of Fe shown in Fig. 6.5

As shown in equation 6.1.1, in order to interpret experimental results correctly, a possible polar signal  $\phi_P$  and longitudinal signal contribution  $\Delta\phi_L$  have to be known. The contribution of the polar Kerr signal can be determined quantitatively from the dependence 4.1.6 (see also Fig. 4.2). The saturation of the longitudinal Kerr signal  $\phi_L^s$  is simply saturation value for the hysteresis loop measured along the steps (polar Kerr signal contributes only at low fields and therefore, the saturation value originates exclusively from longitudinal Kerr signal).

In our model, two important parameters determining orientation of the magnetic field and laser beam direction were used,  $\alpha_F$  and  $\alpha_L$ , respectively (Eq. 6.1.1). At  $\alpha_F = 0$ , both the longitudinal and the polar Kerr signal at low field change abruptly in polarity. Hence, the characteristic orientation  $\alpha_c$ , observed in measured hysteresis loops (Fig. 6.6), can be identified as  $\alpha_F = 0$  (i.e., as the sample orientation where the magnetic field is perfectly oriented along the steps). At  $\alpha_L = 0$ , the magnetization is probed perfectly along the step edges. Thus, in such case, no longitudinal Kerr signal at low field should be detected. However, a non-zero signal can be detected due to the polar signal at low fields. The characteristic orientation  $\alpha_b$  corresponds to the situation when the longitudinal and polar contributions at low fields compensate each other and is not equivalent to  $\alpha_L = 0$  (i.e.,  $\alpha_b$  does not correspond to the sample orientation in which the laser-beam is aligned perfectly parallel to the steps).

The total Kerr signal at zero field ( $\Delta\phi$ ) is plotted as a function of the sample orientation  $\alpha$  (Fig. 6.8a). The difference in signal between the maximum values is due to the polar Kerr signal which contribute to the  $\Delta\phi$  with opposite polarity at  $\alpha = +90^\circ$  and  $\alpha = -90^\circ$ , while longitudinal signal does not change. The difference in  $\Delta\phi$  however is bigger at  $\alpha = 0$ , because both: polar and longitudinal Kerr signal, change in polarity. The orientation  $\alpha = 0$  corresponds to the magnetic field oriented perfectly along the steps, i.e., to  $\alpha_F = 0$  (i.e., the characteristic orientation  $\alpha_c$  in the experiment). However, since the laser beam direction ( $\alpha_L$ ) and the magnetic field direction are not necessarily the same, it is not expected that  $\alpha = 0$  corresponds also to  $\alpha_L = 0$ . Thus, Eq.6.1.1 has to be rewritten in the form:



(a) Contribution to the Kerr signal from magnetization oriented perpendicular to the steps at zero field versus  $\alpha$  for 58 ML of Fe on Au(1113).  $\alpha = 0$  refers to the situation where the magnetic field is applied perfectly along the steps.

(b) Magnetic field which has to be applied to switch the magnetization of 58 ML of Fe on Au(1113) from perpendicular to along the steps direction (i.e., pseudo- $H_s$ ) versus  $\alpha$ .

**Figure 6.8:** LMOKE measurements of the Kerr signal at zero field ( $\Delta\phi$ ) and the shift field  $H_s$  performed at 300 K.

$$\Delta\phi = \begin{cases} -|\phi_P| + \phi_L^s \sin(|\alpha - \beta|), & \alpha > \beta \\ -|\phi_P| - \phi_L^s \sin(|\alpha - \beta|), & \beta > \alpha > 0 \\ +|\phi_P| + \phi_L^s \sin(|\alpha - \beta|), & \alpha < 0 \end{cases} \quad (6.1.2)$$

Here  $\beta$  corresponds to the difference between the magnetic field and the laser beam direction ( $\beta = \alpha_L - \alpha_F$ ). As described earlier,  $|\phi_P|$  and  $\phi_L^s$  can be determined from individual hysteresis loops. This yields a value of  $|\phi_P| = 70 \mu\text{rad}$  and  $\phi_L^s = 470 \mu\text{rad}$ . Therefore,  $\beta$  is the only undetermined variable in the Eq.6.1.2. As a result, the three equations (Eq.6.1.2) can be combined to describe the expected behavior of the low field Kerr signal  $\Delta\phi$  as a function of  $\alpha$ , in the whole angular range. Thus,  $\beta$  can be used as a fitting parameter to fit Eq.6.1.2 to experimental data shown in Fig. 6.8a. The best fit was found for  $\beta = 3^\circ$ . Thus, the misalignment between the laser beam direction and magnetic field direction is  $\alpha_L - \alpha_F = 3^\circ$ . The positive angle  $\alpha \approx 10^\circ$  at which  $\Delta\phi$  changes polarity corresponds to the characteristic orientation  $\alpha_b$  observed in measured hysteresis loops (Fig. 6.5 and Fig. 6.7) and is associated with the situation, when the negative polar Kerr signal is compensated by the positive longitudinal signal.

As mentioned in the beginning of this section, the correct evaluation of the shift field  $H_s$  is very important in case of studies of FM grown on vicinal surfaces. Besides of changes associated with the variation of the Kerr signal at low field, also the shift field  $H_s$  is modified upon rotation of the sample (as shown in hysteresis loops in Fig. 6.5 and Fig. 6.7).  $H_s$  apparently increases with increasing misalignment between the magnetic field direction and the step edges direction  $|\alpha|$ . The reason is that a larger total magnetic field needs to be applied with increasing misalignment, to keep the value of the magnetic field along the steps sufficient to switch the magnetization. However, the measured shift field  $H_s$  (i.e., pseudo- $H_s$ ) depends on  $|\alpha|$  in a more complicated manner than one would expect from simple geometrical considerations. This is due to the fact that the magnetic field is applied both along and perpendicular to the steps. While the field component along the steps forces the magnetization to switch to the intermediate magnetization axis, the component perpendicular to the steps stabilizes its orientation along the easy magnetization axis. Hence, the dependence of pseudo- $H_s$  upon rotation of the sample is much stronger than expected from a simple  $H_s / \cos(|\alpha|)$  dependence (see Fig. 6.8b). The dependence of  $H_s$  on  $\alpha$  is symmetric around  $\alpha = 0$ , which is another confirmation that  $\alpha_c$  corresponds to the orientation at which the magnetic field is oriented exactly along the steps.

The observed split hysteresis loops with low field features are not specific to Fe films grown on

## SECTION 6.1

Au(1113) and were observed for many different film/substrate combinations. Generally, the low field features can be only observed in case, when the easy magnetization axis is oriented perpendicular to the steps and the external magnetic field is applied along the steps. In contrast, if the easy magnetization axis is oriented along the steps (and thereby the external magnetic field is applied perpendicular to the steps), then only the "outer" split loops will be influenced by the polar Kerr signal. The reason is that only these parts of the hysteresis loops reflect the magnetization oriented perpendicular to the steps. In this case, the polar signal has no influence on the total Kerr signal at small fields. Thus, much simpler split hysteresis loops with nearly no low field component are measured.

## 6.2 Spin reorientation transition in films grown on vicinal surfaces

The evaluation of the tilting angle  $\delta$  as a function of film thickness gives the opportunity to follow precisely, step-by-step, the orientation of the magnetization in the vicinity of a spin reorientation transition (SRT). As shown for *bcc* Fe films on Ag(116) probed by MOKE (Sec. 5.1.1) and SPLEEM (Sec. 5.3.1), the SRT possesses peculiar properties, not observed in films grown on flat surfaces. In particular it is observed that the in-plane orientation of magnetization is directly linked to the out-of-plane magnetization component. In this chapter, the results of the experiments concerning SRT are discussed together with a phenomenological model [199].

### Phenomenological model

The dependence of the measured tilting angle  $\delta$  on the film thickness can be interpreted using a phenomenological model which describes the magnetic anisotropy of a ferromagnetic film deposited on a stepped substrate. The energy of the film depends on the direction of the magnetization  $\mathbf{M}$  according to:

$$\begin{aligned} E(\theta, \psi) &= K_d \cos^2 \theta + K_s \sin^2 \theta' - K_u \sin^2 \theta' \sin^2 \psi - \frac{1}{2} K_{sp} \sin 2\theta' \cos \psi + E_{\text{bulk}}(\theta', \psi) \\ &\equiv E_d + \delta E + E_{\text{bulk}} \equiv E_d + E_{\text{MCA}} \end{aligned} \quad (6.2.1)$$

where  $\theta$  is the polar angle measured from the normal to the macroscopic film surface and the azimuthal angle  $\psi$  is measured with respect to the direction perpendicular to the steps (as defined in Fig. 4.6). To simplify this notation,  $\theta'$  is introduced as the polar angle measured with respect to the normal to the terrace plane direction, i.e., with respect to the [001] crystallographic direction. Thus, for an orientation of  $\mathbf{M}$  perpendicular to the steps  $\theta' = \theta + \omega$  (where  $\omega$  denotes the vicinal angle), while for an orientation parallel to the steps  $\theta' = \theta$ . The shape anisotropy is defined according to Eq. 2.1.5. All energies are defined per surface unit or per surface atom. The magnetocrystalline anisotropy (MCA) energy  $E_{\text{MCA}}$  consists of the second-order energy correction  $\delta E$  (Eq. 2.1.3) and the fourth-order contribution

$$E_{\text{bulk}} = \frac{1}{4} K_b \sin^2 2\theta' + \frac{1}{4} K_b \sin^4 \theta' \sin^2 2\psi \quad (6.2.2)$$

corresponding to bulk MCA. The second-order correction to MCA energy for a FM film on a vicinal surface can be expressed by three anisotropy constants:

$$K_s = E_{\text{MCA}}(001) - E_{\text{MCA}}(100) = E_{\text{MCA}}(\theta'=\pi/2, \psi=0) - E_{\text{MCA}}(\theta'=0, \psi=0) \quad (6.2.3)$$

$$K_u = E_{\text{MCA}}(100) - E_{\text{MCA}}(010) = E_{\text{MCA}}(\theta'=\pi/2, \psi=0) - E_{\text{MCA}}(\theta'=\pi/2, \psi=\pi/2) \quad (6.2.4)$$

$$K_{sp} = E_{\text{MCA}}(10\bar{1}) - E_{\text{MCA}}(101) = E_{\text{MCA}}(\theta'=\pi/4, \psi=0) - E_{\text{MCA}}(\theta'=-\pi/4, \psi=0) \quad (6.2.5)$$

where  $E_{\text{MCA}}(hkl)$  is the magnetocrystalline anisotropy energy for different orientations ( $hkl$ ) of the magnetization. Note that the anisotropy constants  $K_u$  and  $K_{sp}$  [40, 42] arise from the existence of steps and vanish for flat films with cubic crystal structure.

As shown by MOKE and SPLEEM measurements for Fe films grown on Ag(116) surface, the magnetization can be tilted from the macroscopic film surface when lies in the vertical plane perpendicular to the steps. The optimal value of the tilting angle  $\delta = \pi/2 - \theta_{\text{min}} = \pi/2 - \theta'_{\text{min}} + \omega$  is obtained by minimizing the energy for magnetization lying perpendicular to the steps:

$$E_{\perp}(\theta') = E(\theta' \psi=0) = K_d \cos^2 \theta + K_s \sin^2 \theta' - \frac{1}{2} K_{sp} \sin 2\theta' + \frac{1}{4} K_b \sin^2 2\theta' \quad (6.2.6)$$

The optimal angle  $\theta' = \theta'_{\text{min}}$  can be found from the condition for a local extremum of  $E_{\perp}(\theta')$ :



SECTION 6.2

$$\partial E_{\perp}(\theta')/\partial \theta' = -K_d \sin 2\theta + K_s \sin 2\theta' - K_{sp} \cos 2\theta' + \frac{1}{2}K_b \sin 4\theta' = 0 \quad (6.2.7)$$

Thus, the optimal angle  $\theta'_{\min}$  depends on  $K_s$ ,  $K_{sp}$ ,  $K_b$ , and  $K_d$  but not on  $K_u$  (since the orientation of the magnetization is limited to the vertical plane perpendicular to the steps). The bulk anisotropy  $K_b$  is much smaller than  $K_s$  and  $K_d$  and can be neglected. Eventually, the solution for  $\theta' = \theta'_{\min}$  can be expressed as follows:

$$\tan 2\theta' = \tan 2\omega \frac{K_d \cos 2\omega - K_{sp}/\tan(2\omega)}{K_d \cos 2\omega - K_s} \quad (6.2.8)$$

or equivalently, in terms of the tilting angle  $\delta$ :

$$\tan 2\delta = \tan 2\omega \frac{K_{sp}/\tan(2\omega) - K_s}{K_d/\cos 2\omega - K_s - K_{sp} \tan 2\omega} \quad (6.2.9)$$

Since the Eq. (6.2.9) is the condition for a local energy extremum, it does not define the optimal tilting angle  $\delta$  uniquely. Nevertheless, it can be shown that the optimal  $\delta$  which corresponds to the minimum of the energy  $E_{\perp}(\theta)$  can be chosen uniquely in the following way:

$$\text{if } K_s > K_d \cos 2\omega \quad \text{then} \quad -135^\circ + \omega < \delta < -45^\circ + \omega \quad (6.2.10)$$

$$\text{if } K_s < K_d \cos 2\omega \quad \text{then} \quad -45^\circ + \omega < \delta < 45^\circ + \omega \quad (6.2.11)$$

The formula for the optimal  $\delta$  allows to predict the dependency of  $\delta$  depends on  $K_d$ ,  $K_s$  and  $K_{sp}$ . In particular, it can be shown that the sign of  $\delta$  depends on the value of  $K_{sp}$  with respect to  $K_s$ . For positive  $K_s$  and positive  $K_d$

(i)  $\delta$  is positive if  $(K_{sp}/\tan 2\omega) > K_s$

(ii)  $\delta$  is negative if  $(K_{sp}/\tan 2\omega) < K_s$

Note that inclusion of  $K_{sp}$  is crucial for proper reproduction of the experimentally observed values of the tilting angle. In particular, if  $K_{sp} = 0$ , the magnetization of a FM film on a vicinal surface cannot reach the orientation

(i) perpendicular to the film surface ( $\delta = \pm 90^\circ$ )

(ii) perpendicular to the terrace plane ( $\delta = 90^\circ + \omega, -90^\circ + \omega$ )

(iii) parallel to the film surface ( $\delta = 0$ ), while being within the plane perpendicular to the steps

Furthermore, the positive sign of the tilting angle in the interval  $0 < \delta \leq 90^\circ + \omega$  (or the equivalent range  $-180^\circ < \delta \leq -90^\circ + \omega$ ) is not possible for  $K_{sp} = 0$  and  $K_s > 0$ . Such conclusion can be deduced directly by noting that the shape anisotropy energy  $K_d \sin^2 \delta$  has the same value for  $\delta$  and  $-\delta$  while  $K_s \cos^2(\delta - \omega)$  is larger for  $0 < \delta < (90^\circ + \omega)$  than for the corresponding negative  $\delta$  (if  $K_s > 0$ ). This means that the anisotropy energy  $E_{\perp}(\delta)$  (with  $K_{sp} = 0$ ,  $K_b = 0$ ) is smaller for negative  $\delta$ . Since the discussed orientations forbidden for  $K_{sp} = 0$  are observed experimentally,  $K_{sp} \neq 0$  needs to be included in the MCA energy of a FM film on vicinal surface.

Based on equation 6.2.9, any given tilting angle can be achieved by a suitable choice of  $K_s$ ,  $K_{sp}$  and  $K_d$ . Therefore, by using the tilting angle values of magnetization from the MOKE experiment on Fe/Ag(116),  $K_s$  and  $K_{sp}$  anisotropy constants can be found. The dependence of the tilting angle  $\delta$  as a function of Fe film thickness obtained from MOKE measurements at 300 K and the corresponding fit are shown in Fig. 6.9.

In the case of an uncovered Fe film, the best fit was found for:

$$K_s = 0.9 - 0.0079 \cdot (N_0 - N)^2 \quad \text{with } N \leq N_0, \quad K_s = 0.9 \quad \text{with } N > N_0 \quad (\text{where } N_0 = 10 \text{ ML}),$$

$$K_{sp}/\tan(2\omega) = K_s - 0.07$$

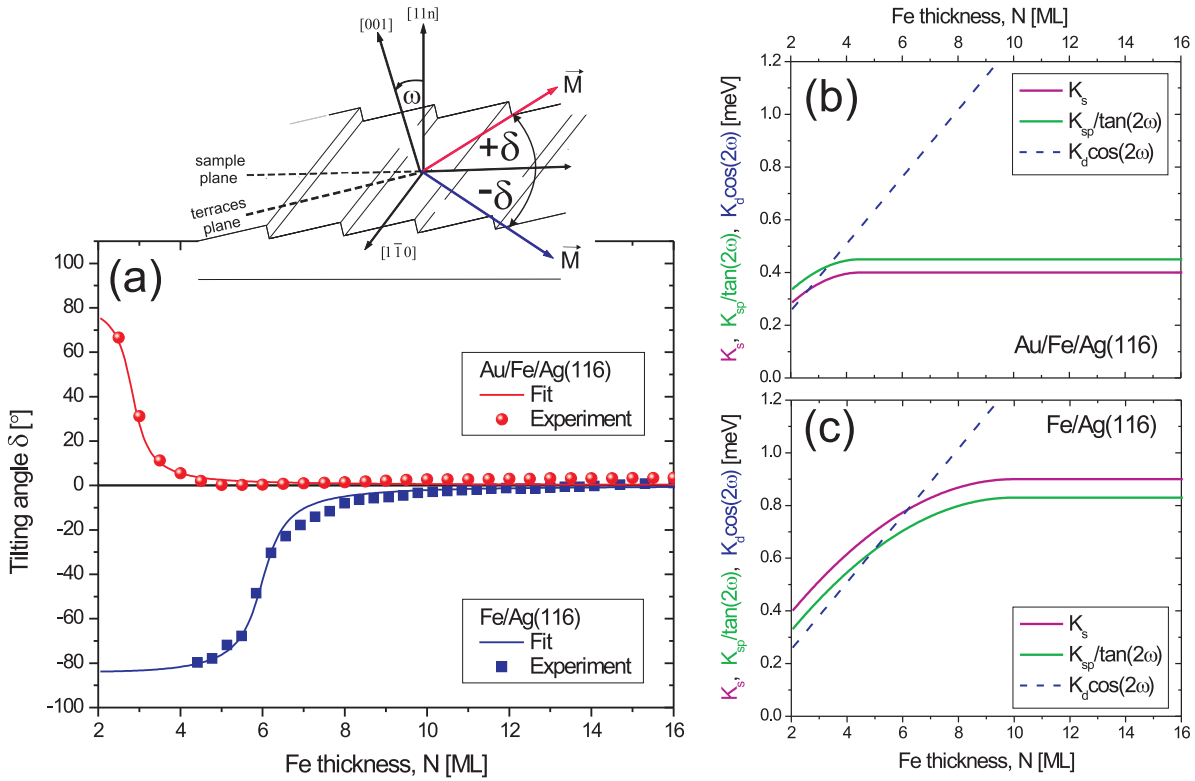


**Figure 6.9:** The dependence of the tilting angle of the magnetization  $\delta$  as a function of Fe film thickness obtained from a MOKE experiment at 300 K (points) and from the theoretical fit (lines), for uncovered and Au-covered Fe films on Ag(116) vicinal surface. The corresponding anisotropy constants used in the fit are shown in (b) and (c), for Au-covered and uncovered Fe film, respectively.

In the case of Au-covered Fe film the best fit was found for:

$$K_s = 0.4 - 0.0019 \cdot (N_0 - N)^2 \text{ with } N \leq N_0, \quad K_s = 0.4 \text{ with } N > N_0 \quad (\text{where } N_0 = 4.5 \text{ ML}),$$

$$K_{sp}/\tan(2\omega) = K_s + 0.05$$

In both cases, the shape anisotropy is assumed to be  $K_d = 0.142 \cdot N$ , while  $N$  denotes number of monolayers ML and  $\omega$  is the vicinal angle which in this case equals  $13.3^\circ$ .

The obtained from the fit values of uniaxial perpendicular anisotropy  $K_s$  are in agreement with previous studies [162, 200]. Namely, it was observed that by deposition of Au on top of uncovered *bcc* Fe films on flat Ag(001),  $K_s$  decreased from  $0.96 \text{ mJ/m}^2$  (for Fe(001)/UHV interface) down to  $0.4\text{--}0.47 \text{ mJ/m}^2$  (for Fe(001)/Au interface) [162, 200]. This is the reason why the SRT from in-plane to out-of-plane orientation of the magnetization is shifted down to  $\sim 3$  ML for Au-covered Fe film in comparison to the uncovered Fe film, in which the SRT occurs at  $\sim 6$  ML (see Fig. 6.9(a)). However, there is another important consequence of the reduced perpendicular anisotropy upon deposition of Au, that has not been considered so far in the literature. As can be seen in Fig. 6.9(a), the tilting angle  $\delta$  in the vicinity of SRT is of the opposite sign for Au-covered and uncovered Fe films. Depending whether  $K_s$  is larger (Fig. 6.9(c)) or smaller (Fig. 6.9(b)) than  $K_{sp}/\tan 2\omega$ , the tilting angle  $\delta$  becomes negative or positive, respectively. A deposition of Au cover layer reduces the value of  $K_s$  and in consequence, the sign of the tilting angle changes. Note that a different sign of  $\delta$  means that the rotation of the magnetization from in-plane to out-of-plane orientation proceeds differently for uncovered and Au-covered films (see inset in Fig. 6.9(a)). Therefore, through the appropriate choice of the Fe layer and Au layer thicknesses, any desirable orientation of the magnetization (within the vertical plane perpendicular to the steps) can be obtained.

Another interesting observation is that below some critical Fe film thickness  $N_0$  ( $N_0 = 10$  ML for

uncovered and  $N_0 = 4.5$  ML for Au-covered film),  $K_s$  and  $K_{sp}$  decrease with decreasing Fe film thickness. Reduced uniaxial perpendicular anisotropy  $K_s$  for very thin Fe films grown on Ag(001) was also observed by Heinrich *et al.* [201] and Hicken *et al.* [202]. The decrease of  $K_s$  with decreasing Fe film thickness was studied in detail by Schaller *et al.* [81] and it was found that the decrease of  $K_s$  is associated with thickness dependent roughness of the Fe film. Note that the roughness can also induce dipolar surface anisotropy [203]. Therefore, as suggested in [81], the effect of roughness on magnetic anisotropy results in change of both the perpendicular anisotropy and the dipolar surface anisotropy. Since the dipolar surface anisotropy is not considered in our model, we cannot separate both effects and the observed change of  $K_s$  is an effective change, composed of the two contributions.

So far in this section, our discussion was limited to changes of MA associated with the tilting angle  $\delta$  of the magnetization, i.e., when the magnetization lies within a vertical plane perpendicular to the steps. However, as observed in our experiments, the out-of-plane magnetization component is directly linked to the in-plane orientation of magnetization. In particular, it is evident from SPLEEM results that as soon as the magnetization starts to tilt from the sample plane, a discontinuous in-plane SRT occurs and the magnetization prefers to orient itself perpendicular to the step edges (see Fig. 5.22). This is because the energy when the magnetization is within the plane perpendicular to the steps  $E_{\perp}(\theta' = 0) = K_d \cos^2 \omega$  (Eq. 6.2.6) is smaller than energy when the magnetization is parallel to the steps  $E_{\parallel} = E(\theta' = \pi/2, \psi = \pi/2) = K_s - K_u$ . A further decrease of the energy  $E_{\perp}(\theta')$ , with respect to  $E_{\parallel}$ , can be achieved by choosing an optimal angle  $\theta'_{\min}$  since  $E_{\perp}(\theta' = \theta'_{\min}) < E_{\perp}(\theta' = 0)$ . With decreasing Fe film thickness and approaching the SRT, the easy axis of magnetization cannot be parallel to the steps since  $K_s - K_u > K_d$ . Contrary to the gradual variation of the tilting angle of the magnetization (second-order SRT), the azimuthal angle (describing the in-plane orientation of magnetization) changes discontinuously (first-order SRT). Such peculiar SRT was also observed before for Ni films grown on the vicinal surface of Cu(001) [204, 205] and seems to be a common characteristic of the SRT in FM films grown vicinal surfaces.

The orientation of the magnetization in the vicinity of the SRT was also obtained from XMCD measurements in remanence (Sec. 5.2.2). The XMCD results confirm that below the SRT thickness (i.e., below 7.5 ML) the magnetization is tilted exclusively within the plane perpendicular to the steps (Table 5.1). Note however that the orientation of the magnetization obtained by XMCD is averaged over a finite area of the sample and cannot resolve the mechanism of the abrupt in-plane SRT at 7.5 ML. Consequently, the azimuthal orientation of the magnetization can adopt intermediate values of  $\psi$ , i.e., with the magnetization oriented between the steps and perpendicular to them. Based on this, it is possible to conclude that the in-plane SRT is continuous [205], which is misleading. From the domain structure it is clearly evident that there are only two possible magnetization orientations in the sample plane: perpendicular to or along the steps. Intermediate orientations are not observed. This result highlights the advantage of using SPLEEM over other methods that only probe the average orientation of the magnetization.

Such a discontinuity of the in-plane SRT was also observed in Co/Cu(1113) (see Fig. 5.26). In this case, the change of the easy axis of the magnetization with increasing Co thickness is however governed by a different mechanism. As shown in Fig. 5.8, covering Co films with a sub-monolayer of Au modifies the interface contribution to the step-induced anisotropy. By deposition of  $\sim 0.7$  ML of Au, the negative interface contribution from Au compensates the positive interface contribution from the UHV/Co interface and the two in-plane directions, along the steps and perpendicular to the steps, become nearly equivalent. Therefore, the in-plane SRT in this case spreads out over a wider range of Co thicknesses and is less abrupt than in Fe/Ag(116).

The fact that the SRT from the out-of-plane to the in-plane orientation of the magnetization for Fe/Ag(116) is related to a continuous change of the tilting angle  $\delta$  is confirmed by SPLEEM measurements. In particular, the values of the tilting angle  $\delta$  obtained by SPLEEM for *as grown* Fe films are

nearly identical to those obtained from MOKE measurements. Furthermore, by looking at the domain structure of Fe/Ag(116) it is clearly evident that the change of  $\delta$  results from the continuous rotation of magnetic domains (see Fig. 5.22). In agreement with MOKE measurements and the phenomenological model presented earlier, the domains rotate within the vertical plane perpendicular to the steps. The rotation of the magnetization perpendicular to the step direction is also supported by the existence of Bloch-type domain walls. Since the magnetization in this case is canted exclusively perpendicular to the step direction, it is natural that the preferred orientation of the Bloch walls also is perpendicular to the steps. Interestingly, the presence of Bloch domain walls is only observed in the case of tilted magnetization. Above 8 ML of Fe, i.e., when the easy magnetization axis is oriented in the sample plane parallel to the step edges, *Neél* walls are observed. In the case of *Neél* walls, the in-plane magnetization is perpendicular to the wall. Thus, *Neél* walls can be distinguished when looking at the magnetic contrast probed perpendicular to the easy magnetization axis (see e.g. for 9.5 ML of Fe in Fig. 5.22).

The SRT from an out-of-plane to an in-plane magnetization orientation should also be reflected in changes of the domain size  $D$ . Indeed, the size of domains in a FM film with the easy magnetization axis perpendicular to its plane is determined by the competition between domain wall energy  $\sigma_w = 4\sqrt{A \cdot K_{eff}}$  and magnetostatic energy  $E_d$ , where  $A$  is the exchange constant and  $K_{eff}$  is the effective perpendicular anisotropy constant [185–188, 206, 207]. With approaching a SRT from an out-of-plane to an in-plane orientation of magnetization (i.e., with decreasing of  $K_{eff}$ ), the domain size is predicted to decay exponentially. This is due to the fact that as the effective perpendicular anisotropy energy decreases, it becomes comparable to the magnetostatic energy which eventually dominates. The minimization of the film energy then leads to the formation of domain walls [185–187]. This was confirmed experimentally for instance in the case of Co/Au(111) [189, 208, 209] and Fe/Cu(001) [210]. The decrease of the domain size when approaching a SRT was also observed in the case of Fe/Ag(001), however, only in a very narrow thickness range (between 3.3 ML and 3.8 ML of Fe) [211].

A different behavior of the domain size is observed in the case of our experiments on Fe films grown on Ag(116). As shown in Fig. 5.24, with increasing Fe film thickness and approaching a SRT from an out-of-plane to an in-plane magnetization orientation, the domain size increases exponentially, i.e., just opposite as predicted by theory. Note however, that theoretical calculations in references [185–188, 206, 207] are valid for FM films grown on atomically flat surfaces, while in our experiment, Fe films are grown on the Ag(116) vicinal surface. The main difference, concerning the SRT, between films deposited on flat and vicinal surfaces is that in the latter case the magnetization is tilted. As a consequence, the effective perpendicular anisotropy constant  $K_{eff}$ , which determines the size of the domains is most likely different in both cases. In general, one can expect that additional magnetic anisotropy constants associated with the presence of vicinal surfaces, like  $K_{sp}$  and/or  $K_u$ , have to be included in  $K_{eff}$  in order to describe the observed domain sizes. Additionally, in the presence of a tilted magnetization, the magnetostatic energy is also different, and can modify the domain size dependence in the vicinity of the SRT. The quantitative analysis of the domain size dependence observed in our experiment demands deeper theoretical investigation.

## 6.3 Oscillatory magnetic anisotropy

### 6.3.1 Magnetic anisotropy oscillations due to $d$ -QWS in Co films

The following chapter concerns the detailed discussion of the magnetic anisotropy oscillations which were observed experimentally in  $fcc$  and  $bcc$  Co films grown on Cu(1113) and Au(1113) surface, respectively. The main interest is paid to  $fcc$  Co films, since only for this system, the oscillatory behavior of the magnetic anisotropy energy MAE was predicted by theoretical calculations [19–21]. This allows a direct comparison to experiments and detailed discussion of the mechanism and properties of the magnetic anisotropy oscillations due to QWS.

#### $fcc$ Co films on Cu(1113)

The first report on the oscillatory behavior of the MAE in  $fcc$  Co films on Cu(001) substrate was made by Szunyogh *et al.* [20]. Using the fully relativistic spin-polarized version of the screened Korringa-Rostoker method, they clearly demonstrated that the magnetocrystalline anisotropy energy oscillates as a function of Co film thickness with a period of 2 ML [20]. The reason for the oscillatory behavior of the MAE was not fully understood at that time.

Independently, Cinal [19] performed calculations of the MAE on the same system by using a tight-binding (TB) model with and without  $sp$ - $d$  hybridization included. By careful analysis of the electronic structure with increasing number of Co atomic layers he has shown that oscillations of MAE in Co films on Cu(001) are a superposition of two oscillatory contributions: the dominating one coming from the neighborhood of the  $\bar{\Gamma}$  point with a period of 2.12 ML (2.33 ML without  $sp$ - $d$  hybridization included) and the other originating in the region around the  $\bar{M}$  point with a larger period of 5.15 ML (3.32 ML without  $sp$ - $d$  hybridization included), but of significantly smaller amplitude. Both oscillatory contributions are attributed to QWS formed in the Co layer. Later, such oscillatory behavior of MAE was also predicted by theory for Co films on vicinal Cu(001), where the uniaxial magnetocrystalline anisotropy was found to oscillate with a period close to 2 ML, as well [21].

The MOKE measurements of the shift field  $H_s$  and Kerr ellipticity  $\phi^H$  presented in Sec. 5.1.1 confirm the presence of the oscillatory MAE in  $fcc$  Co films. In order to compare our experimental results with theory, the dependence of  $H_s$  on Co thickness is plotted together with MAE calculated by Szunyogh *et al.* [20] (see Fig. 6.10). The  $H_s$  oscillates with a period of  $2.3 \pm 0.3$  ML, which is very close to the period of 2 ML [20] and 2.12 ML (2.33 ML without  $sp$ - $d$  hybridization included) [19], obtained theoretically.

There are three different regimes of oscillations visible in both experiment and theory: (a) for  $N < 6$ , with a pronounced maximum at 3 ML and 5.5 ML; (b)  $6 < N < 9$ , with no clear maxima; and (c)  $N > 9$ , with three distinct maxima at about 9, 12, and 14 ML. The agreement between theory and experiment is almost perfect in this case, except for a large MAE calculated for 2 ML, but not observed experimentally. This is most likely due to the growth of Co on Cu(001), which is initially not layer-by-layer as is assumed in the theoretical calculations [20]. The lack of clear oscillations in regime (b) is associated with the discrete thickness sampling [19]. Since the period of oscillations is not exactly equal to a multiple of the interlayer distance ( $N \cdot ML$ ), it produces a phase shifts of the reflected electron wavefunctions and in consequence, additional long period (*beat*) of the MAE oscillations [19]. This *beat* can significantly reduce or enhance the oscillations amplitude, when destructive or instructive interference occur, respectively. This explains why in the regime (b), the oscillations are hardly observed (Fig. 6.10).

As mentioned in Sec. 2.3, the MAE oscillation amplitude is expected to decrease with increasing temperature. A significant contribution to the MCA energy occurs when two states  $|n\sigma\mathbf{k}_{||}\rangle$  and  $|n'\sigma'\mathbf{k}_{||}\rangle$  have their energies close to each other and they lie on two sides of the Fermi level  $E_f$ , within a few  $k_B T$  from it. In particular, this can take place when the pair of states are close to  $E_f$  at  $\bar{\Gamma}$  (i.e., at  $k_{||} = (k_x, k_y) = 0$ ), where they are degenerated (Fig. 2.2). Such favorable alignment of the QWS pairs is found only for particular thicknesses (and only for those thicknesses QWS contribute to the MAE).

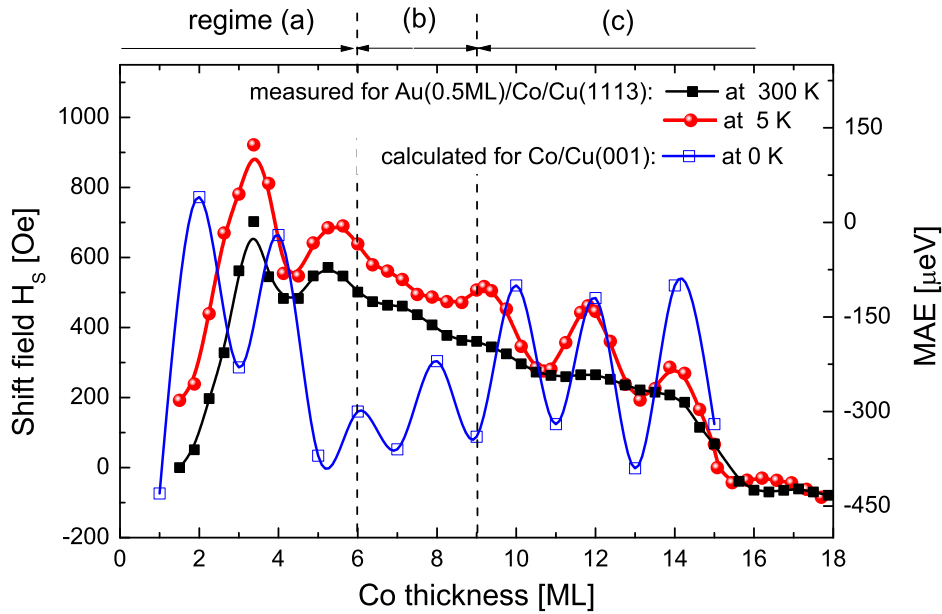


**Figure 6.10:** Shift field  $H_s$  measured at 300 K and 5 K vs Co thickness for Co/Cu(1113) covered with 0.5 ML of Au. Experimental data are compared to the magnetic anisotropy energy MAE calculated for Co/Cu(001) by Szunyogh *et al.* [20]

At those particular thicknesses at which QWS contribution to MAE is significant, the dependence on temperature can be expected [19]. As shown in Fig. 5.9b, the shift field  $H_s$  at 9.3, 11.9, 14 and 16.6 ML depends strongly on temperature, whereas for 10.6, 13, and 15.6 ML,  $H_s$  changes only a little with temperature. This is also visible in Fig. 6.10 (compare  $H_s$  dependence at 300 K and 5 K). Calculations [19, 21] predict strong dependence on temperature almost for exactly the same thickness of Co, mainly for 9, 11, 13, and 15 ML. The amplitude of the anisotropy oscillations is significantly reduced at RT and vanish completely at 365 K. This means that for thicknesses at which QWS contribute to the MAE, the spread of the Fermi function becomes comparable to the energy difference between the two states of each QWS pair contributing to the MAE.

The calculated oscillation amplitude of the MAE for Co films on Cu(001) is of the order of  $\sim 250 \mu\text{eV}$  per surface atom at 0 K [20] and  $\sim 150 \mu\text{eV}$  per surface atom at RT [19]. Very similar result of  $\sim 140 \mu\text{eV}$  per step atom was obtained for Co films on vicinal Cu(001) system at RT [21]. In our experiment, the step-induced uniaxial anisotropy is measured, which is only locally (i.e., at the steps) introduced to the Co film [21, 27], and thus our results should be considered per step atom. Accordingly, the change of the anisotropy energy corresponding to the experimentally observed  $H_s$  oscillation amplitude of maximally  $\sim 300$  Oe is estimated to be  $\sim 230 \mu\text{eV}$ . Considering that the experiments were performed at 5 K, this is in very good agreement with theory.

From the comparison with theory it is clearly evident that experimentally observed oscillations of the magnetic anisotropy are governed by QWS formed inside of Co films. The theoretical calculations using the parametrical TB model [19] has an advantage that, due to its high numerical efficiency, one can diagonalize the full film Hamiltonian and through appropriate analysis of MAE, identify individual quantum states responsible for the MAE oscillations. It was found that the oscillations originate mostly from minority-spin  $\Delta_5$  band, doubly degenerated at  $\bar{\Gamma}$  point. This band crosses the Fermi level  $E_F$  at  $k_{env} = 0.472 k_{BZ}$  with inclusion of the  $sp-d$  hybridization and at  $k_{env} = 0.43 k_{BZ}$  in the  $d$ -band only. These two values of  $k_{env}$  correspond to the periods  $L^{spd} = 2.12$  ML and  $L^d = 2.33$  ML, respectively. I.e., exactly the same periods which are observed for oscillatory  $H_s$ . Note that although  $L^{spd}$  value is closer to the one obtained by *ab-initio* like calculations, i.e., 2 ML [20], the period  $L^d$  is almost exactly the same as in case of our experiment, i.e.,  $2.3 \pm 0.3$  ML. After all, the hybridization between  $sp$  and  $d$  electrons does

not affect significantly the oscillation period and amplitude of the MAE coming from the neighborhood of  $\bar{\Gamma}$  point [19].

The situation is different in case of minority band around the  $\bar{M}$  point. Inclusion of the *sp-d* hybridization results in significant change of the electronic band, so that the positions of the crossing points with the Fermi level are modified. The corresponding periods are  $L^d = 3.32$  ML and  $L^{spd} = 5.15$  ML, respectively. Additionally, including the hybridization of the *sp-d* electrons results in a substantial decrease of the amplitude of the MAE oscillations. The total oscillation amplitude of MAE results from a superposition of two contributions originating from the neighborhoods of the  $\bar{\Gamma}$  and  $\bar{M}$  points. By considering two scenarios, with and without *sp-d* hybridization included, it was shown that only in case of hybridized bands the total MCA energy oscillates with the clear period close to 2 ML with dominating contribution from the neighborhood of the  $\bar{\Gamma}$  point [19].

Having established the mechanism of the MAE oscillations it can be expected that they will decay with increasing Co film thickness. When the film becomes thicker the energies of the QWS pairs existing near the  $\bar{\Gamma}$  point become closer to each other and therefore, more than one pair can contribute to the MAE for a given thickness. As a consequence, the amplitude of the MA oscillations becomes smaller. The amplitude of the MCA oscillations is predicted to monotonically decrease with increasing thickness of Co film above  $\sim 18$  ML [19]. In this way, clear oscillations persist at least up to  $\sim 20$  ML. However, different behavior is observed in the experiment. A discontinuous decrease of the oscillation amplitude is observed only after characteristic rapid drop of the shift field  $H_s$  at  $\sim 15$  ML (see Fig. 6.10 or Fig. 5.9b), resulting from the strain relaxation of Co lattice [56]. As a consequence, after hardly visible maximum of  $H_s$  at 16.6 ML, the oscillatory behavior vanishes completely. This discrepancy is associated with the lattice relaxation, which is not taken into account in theoretical calculations. In both aforementioned theoretical reports [19, 20], the structure of Co is assumed to be *fcc*, with interlayer distances corresponding to Cu lattice spacing. This is a good approximation, but only in the Co film thickness regime below  $\sim 15$  ML, i.e., before the lattice strain starts to relax. Most likely, the change of the electronic structure of Co film due to the strain relaxation is not favorable for the formation such QWS pairs, which can result in oscillatory MCA. The influence of the structural relaxation on the amplitude of MAE oscillations was also observed by theory for *fcc* Co films grown on vicinal surface of Cu(001) [21]. In case of Co film for which the strain relaxation was omitted in the calculations, MAE oscillates with a period close to 2 ML (i.e., exactly as in the case of Co film on a flat surface of Cu(001)). On the other hand, once the strain relaxation was included, the oscillatory behavior of MAE was not observed anymore. This theoretical prediction coincides with our experimental observation, i.e., lack of MAE oscillations for Co film thicknesses above the structural transition. It is also another confirmation, that MAE oscillations due to QWS are very sensitive to any change of the electronic structure.

### ***bcc* Co films on Au(1113) surface**

It is well known that crystal structure and symmetry play a significant role in determining the electronic band structure. Therefore, by changing the structure symmetry of Co film from *fcc* to *bcc*, one can expect also changes in magnetocrystalline anisotropy. Indeed, this is what is observed from MOKE measurements for *bcc* Co films grown on Au(1113) surface (Sec. 5.1.1). First of all, the step-induced uniaxial anisotropy is very strong in this case. The easy magnetization axis is oriented perpendicular to the steps (i.e.,  $H_s$  is negative). Such high magnitude of  $H_s$  results in difficulty in accurate determination of the amplitude and period of the oscillations. Note that such difficulty in case of *fcc* Co film grown on Cu(1113) was overcome by depositing a minute amounts of Au, which due to negative interface contribution to the step-induced anisotropy, significantly reduced the magnitude of  $H_s$  and brought it close to  $H_s = 0$  over a wide thickness range (sec.5.1.1). However, in case of *bcc* Co films grown on Au(1113), in order to reduce the magnitude of  $H_s$ , a capping layer introducing positive interface contribution to the step-induced uniaxial anisotropy is needed, which was found difficult to be realized experimentally. Instead, square hysteresis loops with the magnetic field applied perpendicular to the steps were mea-

sured carefully, with small  $\Delta H$  steps, in order to determine coercivity  $H_c$  as precisely as only possible. The coercivity is strongly related to the magnetization reversal process and the properties of the domain structure [167, 212]. Different reversal processes, like nucleation, coherent and incoherent rotations and domain wall motion, depend on shape anisotropy, magnetocrystalline anisotropy, exchange stiffness, temperature and film thickness. Since the precise relation between coercivity and magnetic anisotropy is not known in this case, no quantitative information about the anisotropy changes can be obtained. However, since there is a certain proportionality between the coercivity  $H_c$  and magnetic anisotropy (both, for perpendicular and in-plane magnetization easy axis [168, 213]), some qualitative informations can be extracted from the measurement of  $H_c$ . A dependence of  $H_c$  on magnetic anisotropy is also visible from MOKE measurements at 5 K (Sec. 5.1.1). The fact that minima of the shift field  $H_s$  (which is a measure of the in-plane uniaxial magnetic anisotropy) coincide with maxima of the coercivity  $H_c$  at exactly the same thicknesses of Co film, indicates that oscillatory behavior of the coercivity  $H_c$  originates from periodic changes of the magnetic anisotropy.

The oscillation period of the coercivity  $H_c$  obtained for *bcc* Co film is equal  $L_{Co} = 4.1 \pm 0.3$  ML, i.e., nearly double in comparison to the oscillation period of the shift field  $H_s$  and Kerr ellipticity observed in the case of *fcc* Co film. As shown in Sec. 2.3, the oscillation period  $L$  is determined by the wave vector  $k_{env}$  of the electron waves and can be used to identify the electronic states which contribute to the MAE. In order to do that, the knowledge of the electronic structure of *bcc* Co is obligatory. There are several reports concerning the band structure of *bcc* Co.

First calculations were triggered by successfully synthesized *bcc* Co on GaAs(110) [214] and performed under the assumption that the *bcc* structure is not strained [215, 216]. More recent papers have shown however, that the true metastable phase is a body-centered tetragonal (*bct*) phase [85, 217]. First-principles band-structure calculations including the tetragonal distortion of Co film grown on Fe(001) surface combined with photoemission studies were performed by Duo *et al.* [85]. Based on the electronic structure calculated there [85] it can be found that the minority-spin  $\Delta_5$  band cross  $E_F$  at  $k_{env} = 0.24 \pm 0.05 k_{BZ}$ . This corresponds to the period of  $L_{Co} = 4.2 \pm 0.3$  ML, i.e., almost exactly the same as the period of oscillatory  $H_c$  observed experimentally. Note that there is no *d*-band of another symmetry in the neighborhood of the minority-spin  $\Delta_5$  which cross  $E_F$ . Therefore, the selection of the minority-spin  $\Delta_5$  band is unique. The majority-spin  $\Delta_5$  is far below the Fermi level and is automatically excluded, since only the bands in close vicinity of  $E_F$  can contribute to MCA energy. A clear signature of the minority-spin  $\Delta_5$  at the  $E_F$  was confirmed very recently by spin-resolved photoemission and *ab-initio* calculations [218].

The MAE oscillations in case of *fcc* Co and *bcc* Co are related to the quantization of the same electronic band, the minority-spin  $\Delta_5$ . The period of oscillations is different in both cases because the bands cross  $E_F$  at different points of Brillouin zone (the  $\Delta_5$  band is shifted down in energy in *bcc* Co film with respect to the  $\Delta_5$  band in *fcc* Co). Note that the  $\Delta_5$  was found to be responsible for oscillatory magnetic anisotropy also in the case of Pd/Co system [73]. The uniqueness of the  $\Delta_5$  band comes from the fact that its degenerated at the  $\bar{\Gamma}$  point. Therefore, the QWS of these band form intrinsic pair of states which have energies very close to each other for  $k_{||}$  around the  $\bar{\Gamma}$  point and contribute strongly to MAE when  $E_F$  lies in between the energies of the QWS pair states [19, 73].

The oscillatory behavior of  $H_s$  and  $\delta$  as a function of thickness of Co films is also observed when they are grown on Fe/Ag(116) system. The oscillation period in this case is equal  $L_{Co} = 2.6 \pm 0.3$  ML, i.e., very similar as in the case of *fcc* Co films on Cu(1113). This indicates that Co films grown on Fe/Ag(116) are stabilized rather in *fcc* structure than in *bcc* structure. This is because in case of the *bcc* Co structure, longer oscillation period is expected,  $\sim 4$  ML, as observed for Co films grown on Au(1113). According to literature, Co films on *bcc* Fe(001) grow in *bct* structure with the interlayer distance contracted by  $\sim 8\%$  [83–85]. On the other hand, when Co films are grown on *fcc* Ag(001), *fcc* structure of Co is formed [219–221]. One possible explanation of our result is that Co films on Fe/Ag(001) grow more like on Ag(001) (i.e., in *fcc*) rather than like on Fe(001) (i.e., in *bcc*). It can be justified since for thin Fe films



on Ag(001) (5.5 ML and 13 ML of Fe in this case), the in-plane lattice constant is still slightly different in comparison to bulk Fe(001). Moreover, the large difference (of the order of 29%) in the lattice constant in the film normal direction between *bcc* Fe(001) and *fcc* Ag(001) may influence the growth mode of Co on top of Fe films grown on the vicinal surface of Ag(001). Our experiment on Co/Fe/Ag(001) shows therefore that the period of the magnetic anisotropy oscillations can be also used as a verification of the electronic structure or the crystal order (since the oscillation period is directly correlated with the wavevector of the confined electronic band).

### 6.3.2 Magnetic anisotropy oscillations due to *d*-QWS in Fe films

There are a few theoretical reports concerning the MAE calculations as a function of Fe film thickness on Ag(001) [222] and Au(001) [223, 224]. In fact, in all those theoretical studies a sort of oscillatory behavior of the MAE was found. However, the reason of the MAE oscillations was not understood at that time. This is partially due to computational limitations: in order to determine the period of the oscillations, the MAE has to be calculated in relatively wide range of Fe thickness. Also, in [222] and [223], the *fcc* structure of Fe with the lattice constant of Ag(001) and Au(001), respectively was assumed, in order to simplify the system. This however results in substantially different vertical interlayer distance of Fe atoms and can change the MAE dramatically [224].

The role of QWS on MAE oscillations of *bcc* Fe was considered by *Guo* [224]. From *ab-initio* calculations for  $Fe(N)/Au_5$  superlattice he found the oscillations of MAE with a period of  $\sim 9$  ML. Thus, different than in our experiment, where  $L = 5.35 \pm 0.3$  ML for Fe/Ag(116) and  $L = 6.1 \pm 0.3$  ML for Fe/Au(1113). The oscillatory behavior of MAE calculated by *Guo* was ascribed to QWS from  $\Delta_5$  minority-spin state. However, by looking at the bulk electronic structure of *bcc* Fe [225–227], it can be observed that  $\Delta_5$  minority-spin state cross the Fermi level at around  $0.5 k_{BZ}$ . Thus, according to Eq. 2.2.3,  $\Delta_5$  minority-spin state should result in QWS with a period of  $\sim 2$  ML, i.e., matching neither to the observed in our experiments nor predicted by *Guo* [224].

As seen from MOKE measurements (Sec. 5.1), *bcc* Fe films grown on vicinal Ag(116) and Au(1113) surfaces show the oscillatory behavior of the the shift field  $H_s$  and the tilting angle  $\delta$  as a function of Fe film thickness at 5 K. The period of oscillations  $L$  is very similar in both cases and on average equals  $5.35 \pm 0.3$  ML and  $6.1 \pm 0.3$  ML, respectively. Essentially, there are two electronic bands in *bcc* Fe which could possibly result in period of 5 - 6 ML. The minority state  $\Delta_2'$  which cross  $E_F$  at  $k_{env} = \sim 0.2 k_{BZ}$  (corresponding to  $L = 5$  ML) and the majority state  $\Delta_5$  which cross  $E_F$  at  $k_{env} = \sim 0.165 k_{BZ}$  (corresponding to  $L = 6$  ML) [225, 227]. Moreover, both of these electronic states can form QWS in Fe film grown on Ag(001), due to lack of electronic states with the same symmetry in Ag. Therefore, based only on the information about the period of the MA oscillations obtained from MOKE measurements, it cannot be distinguished, whether majority  $\Delta_5$  or minority  $\Delta_2'$  state is responsible for MA oscillations.

The most direct method to measure occupied QWS is photoemission spectroscopy (PES). Since photoemission intensity is roughly proportional to the density of states, the formation of QWS manifests itself as peaks in the photoemission spectrum [60]. The PES measurements on Fe films grown on Ag(001) were performed by *Li et al.* [228]. It was shown that indeed, QWS with a period of  $\sim 5.6$  ML are present in the Fe film. The symmetry of the electronic band forming QWS and its spin character has not been however uniquely specified. In order to elucidate the origin and properties of QWS in Fe films, the PES measurements were performed on this system very recently, thanks to cooperation with A. Winkelmann and coworkers at the MPI Halle [229]. The PES spectra were recorded in normal emission with two polarizations of the incident light, *s* and *p*, i.e., with the electric field vector perpendicular and parallel to the optical plane, respectively. Note that *s* polarization corresponds to the electric field vector parallel to the surface, while for *p* polarization there are two components of the electric field vector, perpendicular to the surface and parallel to the surface, since the incident light is always oriented under some angle with respect to the surface ( $48^\circ$  from the surface for this experimental setup). The use of two polarizations is very useful, since it allows to specify the symmetry of the electronic band forming

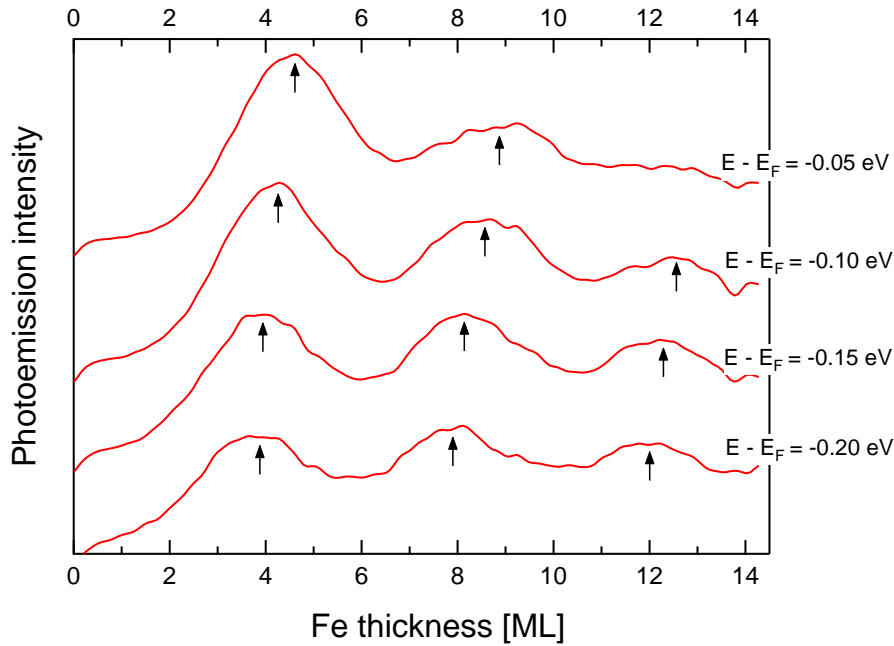


**Figure 6.11:** Photoemission intensity as a function of thickness of Fe film grown on Ag(001) for chosen energies below the  $E_F$ . The positions of the intensity peaks are indicated by arrows. The photoemission spectra were obtained at normal emission at  $T=160$  K for  $s$ -polarized incident light with energy  $h\nu = 6$  eV [229].

QWS. According to the dipole selection rules for the emission along (001) direction in  $bcc$  structure, the transitions are limited to only two initial states,  $\Delta_1$  and  $\Delta_5$  depending whether the electric field vector is perpendicular or parallel to the surface, respectively [230, 231]. Thus, for  $s$  polarization, only the transitions from  $\Delta_5$  initial states are explored, whereas both types of transition, from  $\Delta_5$  and  $\Delta_1$  may occur for  $p$  polarization [230, 231].

The photoemission intensity as a function of Fe thickness for  $s$  polarization is shown in Fig. 6.11. The oscillations of the PES intensity confirm the existence of QWS in the vicinity of the Fermi level of Fe. Since the QWS can be observed for  $s$  polarization, it is clearly evident that they originate from the band with  $\Delta_5$  symmetry. Consistently with expectations based on the dipole selection rules, similar oscillations of the PES intensity are also observed for  $p$  polarization.

At first glance, the oscillation period of the photoemission intensity is  $\sim 4$  ML (see line intensity for  $E - E_F = -0.20$  eV in Fig. 6.11). However, due to dispersion of QWS, that is the dependence of their energies on the Fe film thickness, the period of oscillation is energy and thickness dependent. Note that this dispersion is smaller than in case of typical QWS formed from  $sp$  bands. Moreover, QWS diminish rapidly with increasing Fe film thickness. This is due to the fact that  $d$  wave functions are much more localized, in comparison to  $sp$  one [232]. From the intensity peaks at different energies as indicated by arrows in Fig. 6.11, one can notice that the positions of the peaks move slightly toward thicker Fe film with approaching the  $E_F$ . Eventually, the intensity peaks at  $E - E_F = -0.05$  eV (i.e., just below the  $E_F$ ) appear respectively at  $\sim 4.5$  ML,  $\sim 8.5$  ML and  $\sim 13$  ML. Hence, the period of oscillations slightly increases with increasing Fe thickness ( $L = \sim 4$  ML and  $L = \sim 4.5$  ML, respectively).

Note that the electronic structure of thin Fe film grown on Ag(001) can be slightly different than Fe bulk and therefore, results in a different period of oscillations of the photoemission intensity in comparison to the estimated from the electronic structure of bulk Fe. With increasing Fe thickness, the electronic structure of Fe film grown on Ag(001) should converge to the electronic structure of the bulk Fe. Since the oscillation period of the photoemission intensity slightly increases with increasing Fe thickness, it confirms that observed QWS originate from  $\Delta_5$  majority states (because the oscillation period increases and therefore approaches the expected period for  $\Delta_5$  majority state, i.e.,  $L = \sim 6$  ML). A verification

of the spin character of the observed QWS from  $\Delta_5$  should be possible with future spin-polarized PES measurements.

The question is whether the QWS observed by PES are indeed the QWS which are responsible for the oscillatory MA? Prior to answering this question and comparison of the PES results with MOKE and XMCD results, a better understanding of the oscillatory MA is necessary. As shown in Sec. 5.1, the oscillations of MA as seen by MOKE, are reflected in two observables, shift field  $H_s$  and tilting angle  $\delta$ . Both quantities, measured for uncovered, Au-covered and Co-covered Fe films are summarized in Fig. 6.12. As explained in Sec. 2.3, a contribution to MA due to QWS should occur mainly at LT and at specific thicknesses, at which QWS are very close to  $E_F$ . By looking at the thickness dependencies of  $\delta$  (left column in Fig. 6.12) such contributions to MA can be observed at  $\sim 8$  ML and  $\sim 13$  ML (since at these thicknesses,  $\delta$  changes the most in comparison to its value at RT). Moreover, in all three samples, QWS contribute to MA exactly at the same thicknesses of Fe and always changes  $\delta$  toward more negative values. This clearly indicates that independently of the coverage material of the Fe film, the oscillatory part of the tilting angle remains the same (i.e., originates from the quantization of the same electronic states). By covering with Au or Co however, the perpendicular magnetic anisotropy of the Fe film is modified in compare to uncovered film. As a consequence, a *base* dependence of the tilting angle  $\delta$  is different (e.g., sign of  $\delta$  is changed).

In particular, in case of Fe film covered with Co, the perpendicular magnetic anisotropy is reduced so significantly, that SRT is completely suppressed. This allows to measure oscillatory changes of  $\delta$  down to 2 ML, which is not possible in the case of uncovered and Au-covered Fe films. The reason is that the oscillatory dependence of  $\delta$  is strongly perturbed below  $\sim 7$  ML and  $\sim 5$  ML, respectively, due to approaching SRT.

An oscillatory behavior as a function of Fe thickness is also visible from  $H_s$  (right column in Fig. 6.12). In particular, a large maximum of  $H_s$  can be observed at  $\sim 13$  ML for all three samples, i.e., exactly at the same thickness at which  $\delta$  becomes more negative. Therefore, based on the estimated periodicity of the oscillatory changes of  $\delta$  one could expect that with decreasing Fe thickness the next maximum of  $H_s$  should occur at  $\sim 8$  ML. Instead, the oscillation period of  $H_s$  seems to be shortened and the maximum of  $H_s$  is observed at  $\sim 9$  ML. The shortening of the oscillation period of  $H_s$  is caused by the perpendicular anisotropy contributing more to the total anisotropy of the system upon decreasing the thickness of the Fe film (in the vicinity of SRT). As shown in Sec. 6.2, as soon as the magnetization starts to tilt out from the sample plane, it prefers to be oriented perpendicular to the step edges (what corresponds to negative values of  $H_s$ ). Therefore, for uncovered and Au-covered Fe films, where the tilting angle increases its absolute value to around  $20^\circ$  at  $\sim 8$  ML, the magnetization is forced to be oriented perpendicular to the step edges. This results in maximum of  $H_s$  at  $\sim 9$  ML, which does not originate from the QWS contribution to the magnetic anisotropy only.

In contrast, in the case of Fe film covered with Co, changes of the tilting angle are small (of the order of a few degrees) and the effect of tilted magnetization on value of  $H_s$  should be negligible. This is exactly what is observed in our experiment. The maximum of  $H_s$ , which was observed at  $\sim 9$  ML for uncovered and Au-covered Fe film is now slightly shifted to lower thickness of Fe, i.e., to  $\sim 8.5$  ML. Additionally, due to the lack of SRT, the oscillations of  $H_s$  can be measured for thinner Fe films than for the uncovered and Au-covered Fe/Ag(116) samples. As a consequence, for Fe film covered with Co, four maxima of  $H_s$  are distinguished at  $\sim 4.5$  ML,  $\sim 8.5$  ML,  $\sim 13$  ML and  $\sim 18$  ML of Fe. Note that these maxima occur exactly at the same thicknesses at which maxima in the photoemission intensity are observed (compare Fig. 6.11 and Fig. 6.12). This clearly indicates that the oscillatory dependence of  $H_s$  is govern by the same QWS, which are observed by PES. It also confirms, that the oscillation period in both: PES intensity and  $H_s$  increases with increasing Fe thickness. This is why, for thicker Fe films (above 15 ML), the oscillation period of  $H_s$  has been found to be equal  $5.7 \pm 0.3$  ML [22, 27, 161]. Such tiny changes of the periodicity can be due to the relaxation of Fe lattice [233]. Differently, the shortening of the oscillation period with decreasing Fe thickness is not so clearly observed in case of the tilting angle  $\delta$ . Therefore, the question arises: do oscillations of  $\delta$  and  $H_s$  originate from the same electronic

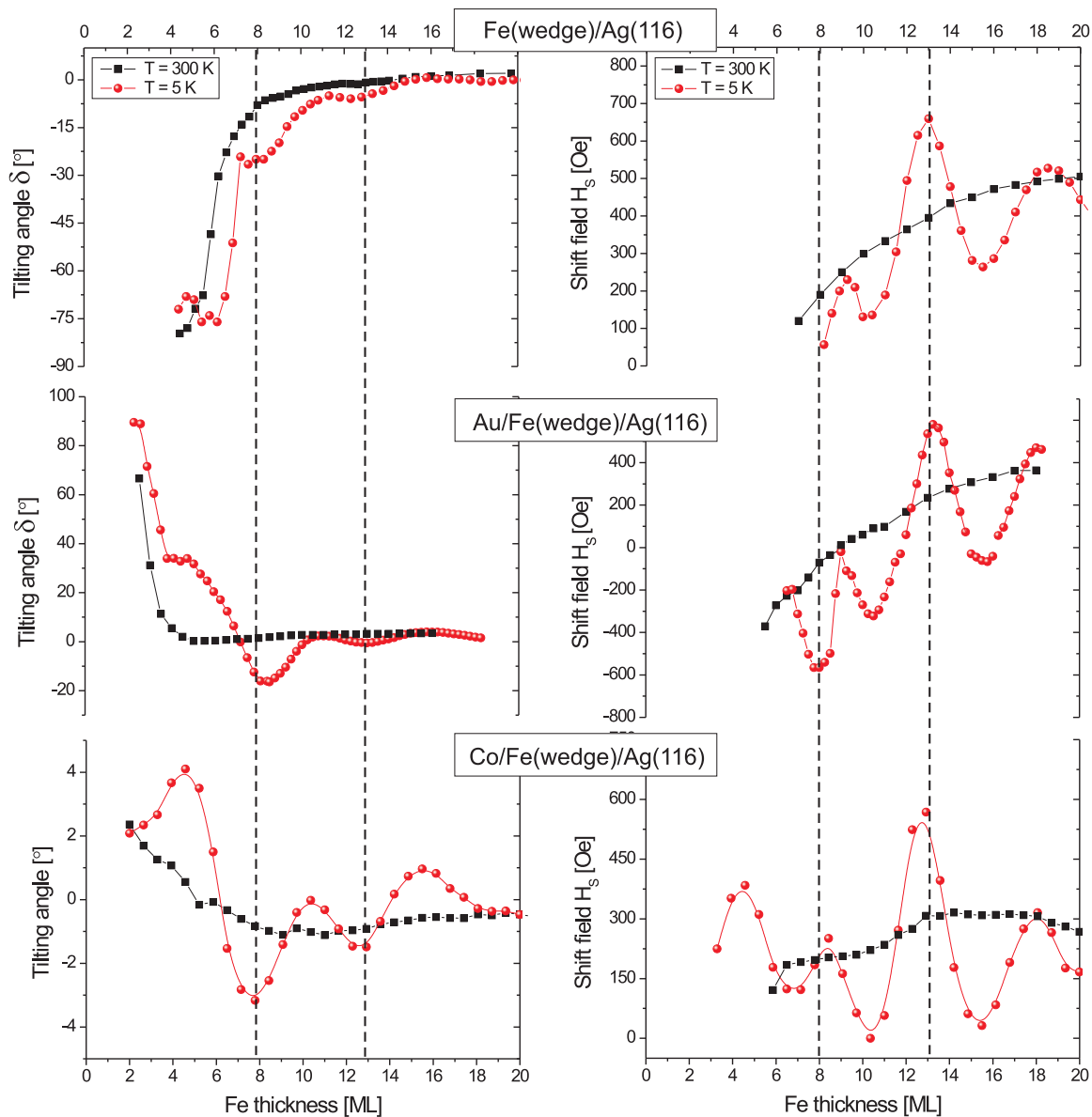


**Figure 6.12:** Tilting angle  $\delta$  and shift field  $H_s$  as a function of Fe thickness for uncovered, Au-covered and Co-covered Fe film grown on Ag(116) vicinal surface. The dependencies were obtained by LMOKE measurements at 300 K and 5 K.

states?

Principally speaking, the tilting angle of the magnetization results from the competition between magnetocrystalline and shape anisotropy. From the MOKE measurements performed along the step edges (Fig. 5.4), Kerr signal changes linearly with Fe thickness indicating that the magnetization and the optical constants do not oscillate with the Fe thickness. This confirms, that magnetocrystalline anisotropy is the only reason for the oscillations of  $\delta$ . As mentioned in Sec. 6.2, magnetization can be tilted only within vertical plane perpendicular to the step edges. Therefore, a change of  $\delta$  arises from change of the MCA energy  $E_{MCA}(001) - E_{MCA}(100)$ , i.e., the difference in the MCA energy between perpendicular to the terraces plane and in the terraces plane perpendicular to the step edges, respectively (see Eq. 6.2.3). Note, however, that  $\delta$  can change either due to change of  $E_{MCA}(001)$  or  $E_{MCA}(100)$ . E.g., the increase of the absolute magnitude of  $\delta$  can be caused either by increase of  $E_{MCA}(001)$  or alternatively, by decrease of  $E_{MCA}(100)$ .

As can be seen in Fig. 6.12, for thicker Fe films (above  $\sim 10$  ML), the maxima of the absolute magnitude of  $\delta$  coincides with the maxima of  $H_s$ . Such coincidence in the oscillations of  $H_s$  and  $\delta$  can be understood as follows. For positive  $H_s$  (i.e., the easy axis of magnetization parallel to the step edges), the increase of  $H_s$  corresponds to the larger magnetic field which has to be applied perpendicular to the step edges in order to switch the magnetization. In other words, larger  $H_s$  means that the axis perpendicular to the steps is "harder" (i.e., the energy  $E_{\text{MCA}}(100)$  is smaller). If the axis perpendicular to the steps is "harder", also  $\delta$  should increase, because the direction perpendicular to the steps become less favorable. Nevertheless, for Fe films covered with Co (i.e., in the case where there is no SRT and oscillatory  $\delta$  and  $H_s$  can be measured down to 2 ML) such correlations between  $\delta$  and  $H_s$  does not exist below  $\sim 8$  ML. This is most likely due to the fact that with decreasing Fe thickness, the MCA energy perpendicular to the terraces plane  $E_{\text{MCA}}(001)$  changes as well, and in consequence, the dependence of  $\delta$  is not solely govern by changes of the MCA energy in the terraces plane perpendicular to the step edges  $E_{\text{MCA}}(100)$ . This can results in different period of oscillations for  $\delta$  with respect to  $H_s$ , which is however artificially produced and originate from the superimposed changes of  $E_{\text{MCA}}(001)$ .

The discussion above, concerning the correlation of the oscillatory behavior of  $H_s$  and  $\delta$  was carried out with the assumption that the axis perpendicular to the step edges becomes "harder" at specific thicknesses of Fe (i.e.,  $E_{\text{MCA}}(100)$  becomes smaller). Note however that  $H_s$  is a measure of the uniaxial in-plane anisotropy (i.e., the energy difference between two in-plane magnetization orientations) and therefore, larger  $H_s$  could be also equivalently explained by the situation when the axis parallel to the step edges becomes "easier" (i.e.,  $E_{\text{MCA}}(010)$  becomes larger).

In order to verify, whether oscillatory changes of  $\delta$  and  $H_s$  are caused by changes of  $E_{\text{MCA}}(100)$ , the information about  $E_{\text{MCA}}$  for each particular crystallographic direction can be obtained from XMCD measurements. As shown in Fig. 5.20a, the oscillatory behavior of the orbital moment is observed mostly along one specific direction: in the sample plane perpendicular to the step edges. Note that a sort of oscillatory behavior can be also observed for  $m_{orb}$  along the step edges, however with much smaller amplitude and only below  $\sim 10$  ML of Fe. In a first approximation, the in-plane orbital magnetic moment is determined by the out-of-plane  $d$ -orbitals of  $d_{xz}$  and  $d_{yz}$  symmetry [137]. These two orbitals form the electronic bands with the  $\Delta_5$  symmetry [234]. Therefore, the periodic changes of the in-plane orbital moment obtained from XMCD should be correlated with the periodic changes of the  $\Delta_5$  electronic band, i.e., the electronic band which shows oscillatory photoemission intensity as a function of Fe thickness (Fig. 6.11). This is a direct experimental prove, that the quantization of  $d_{xz}$ ,  $d_{yz}$  orbitals leads to the quantization of the in-plane orbital magnetic moment and in consequence, to oscillatory MAE as a function of Fe thickness.

In order to compare oscillatory behavior of  $m_{orb}$  with MOKE measurements, it is more suitable to follow changes of the anisotropy of the orbital moment  $\Delta m_{orb}$  rather than of  $m_{orb}$  itself. The dependence of the anisotropy of the in-plane orbital moment  $\Delta m_{orb}$  (i.e., the difference between  $m_{orb}$  along the step edges and  $m_{orb}$  perpendicular to the step edges) on Fe thickness is shown in Fig. 6.13. Three maxima in the anisotropy of the orbital moment can be distinguished at  $\sim 5$  ML,  $\sim 8.5$  ML and  $\sim 12.5$  ML, i.e., at the same thicknesses of Fe (within the experimental error  $\pm 0.3$  ML), at which maxima of  $H_s$  and maxima of PES intensity are observed. This indicates that changes of the  $m_{orb}$  as a function of Fe thickness are due to QWS and that they result in oscillatory behavior of the shift field  $H_s$  and the tilting angle  $\delta$ . Note that similarly as in the case of  $H_s$  at 5 K, the maximum of  $\Delta m_{orb}$  at  $\sim 8.5$  ML is of much smaller amplitude than the maximum at  $\sim 12.5$  ML. As discussed before, this can be due to the influence of the tilted magnetization on the in-plane orientation of the magnetization. Interestingly, the maximum of  $\Delta m_{orb}$  at  $\sim 8.5$  ML originates from increased  $m_{orb}$  parallel to the step edges, i.e., differently than in the case of the maxima at  $\sim 5$  ML and  $\sim 12.5$  ML, that originate from the decreased  $m_{orb}$  perpendicular to the step edges.

In the case of Fe films on vicinal surfaces, the symmetry is broken by regular mono-atomic steps and as a consequence, the MA is more complex in comparison to Fe films on atomically flat surfaces. For a ferromagnetic film showing four-fold symmetry, like Fe films on atomically flat Ag(001), the  $d_{xz}$  and

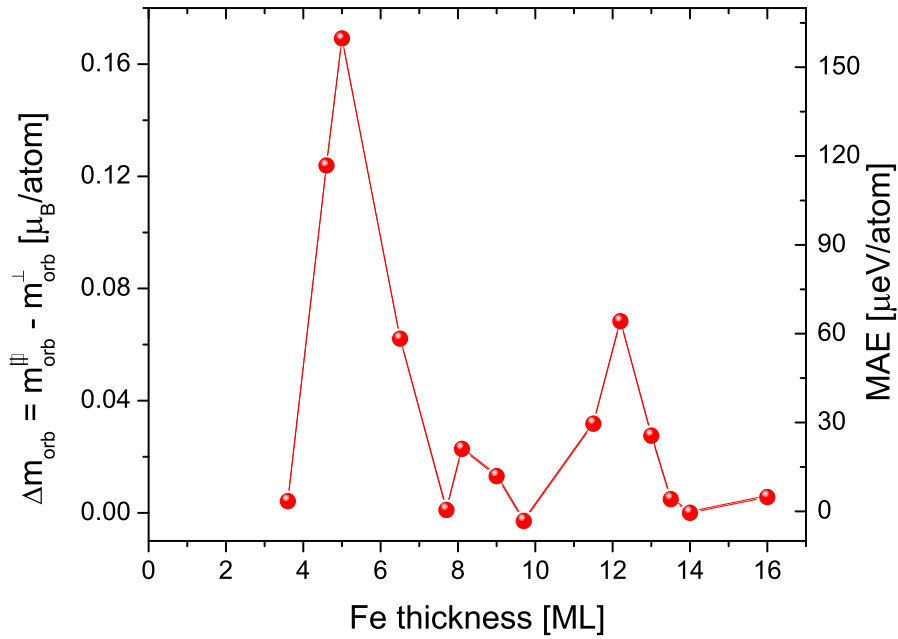


**Figure 6.13:** The in-plane anisotropy of the orbital moment  $\Delta m_{orb} = m_{orb}^{\parallel} - m_{orb}^{\perp}$  as a function of thickness of Fe film grown on Ag(116) obtained from XMCD measurements at 5 K in saturation. The corresponding changes of the magnetocrystalline anisotropy energy were calculated according to  $\text{MAE} = -\alpha \frac{\xi}{4\mu_B} \Delta m_{orb}$ , where  $\alpha = 0.07$  and  $\xi = -54$  meV (see text for details).

$d_{yz}$  orbitals are degenerated\*. Consequently, it results in the same values of the in-plane orbital moment along the corresponding two directions. This is why there are two equivalent in-plane easy axes in such ferromagnetic film. Differently, for a ferromagnetic film with two-fold symmetry, like Fe films grown on vicinal Ag(116) surface, degeneracy of the  $d_{xz}$  and  $d_{yz}$  orbitals is lifted due to anisotropy of the crystal field [235]. In other words, the orbitals elongated in the direction perpendicular to the steps have different charge distribution in comparison to the orbitals elongated in the direction parallel the steps. This is why the in-plane directions parallel to the steps and perpendicular to the steps are not equivalent and the uniaxial step-induced anisotropy is present in such system. Since the  $d_{xz}$  and  $d_{yz}$  orbitals are split in energy, it is not surprising that the oscillatory behavior of the orbital magnetic moment in our experiment is found to be different when probed parallel to the step edges and perpendicular to the step edges. Our results show that the orbitals within vertical plane along the steps (which are responsible for the orbital magnetic moment perpendicular to the steps), result in oscillatory MA due to QWS. In contrast, the orbitals within vertical plane perpendicular to the steps (which are responsible for the orbital magnetic moment parallel to the steps) are shifted in energy in such a way, that cannot contribute significantly to the MAE due to their quantization.

Considering the symmetry of our vicinal surface one can also expect the formation of the QWS with the in-plane wavevector  $\mathbf{k}$  perpendicular to the steps (since the steps are separated from each other only by 3 interatomic distances). Therefore, orbitals within vertical plane perpendicular to the steps can be confined and in consequence, have different energy than orbitals within vertical plane parallel to the steps. Note that such "in-plane" QWS should not change their energy with increasing Fe thickness if the terraces at the surface of growing film reflect the terraces of the substrate and their width remains constant.

It should be noted that the first maximum of  $\Delta m_{orb}$  at  $\sim 5$  ML is much larger than other maxima because originates not only from QWS contribution to MAE but also reflects a change of the MAE due

\*Note that this degeneracy can be lifted by spin-orbit interaction [71].

to the SRT from in-plane to out-of-plane orientation of magnetization with decreasing film thickness. As shown in Fig. 4.6, due to broken symmetry of the system, the measurements of the XAS spectra in  $\theta$  and  $-\theta$  geometry can result in different values of the orbital magnetic moment, when the easy axis of magnetization is tilted out of the sample plane. In particular, with approaching the SRT, the easy axis of magnetization rotates toward [116] crystallographic direction within the vertical plane perpendicular to the steps (as shown in Sec. 5.3.1). This means, that in the thickness range between 3 ML and 6 ML, the easy axis of magnetization is nearly perpendicularly oriented to the incident x-ray vector, when measured with the incidence angle  $\theta$ . As a consequence, the values of  $m_{orb}$  in this thickness range are reduced. The observation of the sharp minimum at  $\sim 5$  ML in the  $m_{orb}$  value perpendicular to the steps (Fig. 5.20 (a)), i.e., at the thickness at which first QWS in PES experiment is observed, indicates a strong change of the  $m_{orb}$  due to QWS contribution to MAE. Interestingly, at the same thickness of Fe, a rapid change of the domain size was observed by SPLEEM measurements (Fig. 5.24). Since the size of domains depends on the MAE, it might be another indication of the QWS contribution to the MAE. Especially, that such a rapid change of the size of domain is observed exclusively at lower temperature.

As shown by Bruno [11], the anisotropy of the orbital magnetic moment is proportional to the MAE. Therefore, obtained dependence of  $\Delta m_{orb}$  can be recalculated to MAE according to Eq. 2.1.4. As mentioned in Sec. 2.1.1, the formula derived by Bruno [11] has to be corrected by including the majority band contribution to MAE and the presence of spin-flip terms [34]. These two corrections can be taken into account by including the numeric correction  $\alpha$  for Fe [235, 236] into Eq. 2.1.4. Eventually, the MAE can be calculated as follows:  $MAE = -\alpha \frac{\xi}{4\mu_B} \Delta m_{orb}$ , where  $\alpha = 0.07$  and  $\xi = -54$  meV is the *spin-orbit coupling constant* [235, 236]. The calculated values of the MAE are indicated on the right side of the plot in Fig. 6.13.

Summarizing, by combination of the PES, MOKE and XMCD studies, the symmetry and spin character of the electronic band responsible for the oscillatory MAE for *bcc* Fe has been determined. The oscillatory behavior of MAE with increasing Fe thickness is a direct consequence of the quantization of the  $\Delta_5$  majority-spin band. Since  $\Delta_5$  electronic band is represented by  $d_{xz}$ ,  $d_{yz}$  out-of-plane orbitals, the periodic contributions to the MAE due to QWS are governed by the in-plane orbital magnetic moment. Due to broken symmetry of vicinal surface, the periodic changes of the orbital magnetic moment are clearly visible only along one in-plane direction, perpendicular to the step edge. The resultant changes of the magnetic anisotropy modulate shift field  $H_s$  and tilting angle  $\delta$  of magnetization as a function of Fe thickness. The oscillation period, both for QWS itself and MAE, increases with increasing Fe thickness and on average is equal  $5.35 \pm 0.3ML$  (where the average is performed within the Fe thickness range from  $\sim 3ML$  to  $\sim 18ML$ ). Note that the oscillatory  $H_s$  and  $\delta$  on thickness was also found for Fe films on Au(1113) (see Sec. 5.1). The oscillation period in this case is slightly larger ( $\sim 6.1ML$  on average) and similarly as in the case of Fe/Ag(116), increases with increasing film thickness. Slightly different period of the oscillations for Fe/Ag(116) and Fe/Au(1113) is most likely due to the tiny difference in the lattice mismatch of Fe with respect to the substrate (0.8% and 0.6% for Ag(001) and Au(001), respectively).

### 6.3.3 Magnetic anisotropy oscillations due to *sp*-resonant states in Cu films

As mentioned in Sec. 2.3, the oscillatory MAE can be caused not only by QWS formed in FM layer, but also by QWS formed in NM layer, adjacent to FM layer. Although the resultant period of MA oscillations is related to the electronic structure similarly in both cases (Eq. 2.2.3), the mechanism concerning periodic changes of MA due to QWS is different. The results presented in Sec. 5.1.2 show that at LT, the shift field  $H_s$  oscillates as a function of Cu thickness overlayer grown on Co/Cu(1113) and Fe/Ag(116) with a period of  $5.8 \pm 0.3$  ML and  $6 \pm 0.3$  ML, respectively. Identical periods were observed by photoemission and inverse photoemission experiments carried out for Cu films on Co(001) and Fe(001) [63, 75, 76]. Moreover, the maxima of the photoemission intensity at the Fermi level were detected for the same thicknesses of Cu [63, 75, 76] as the maxima of  $H_s$  in our experiment. This suggests that QWS formed in Cu are responsible for the oscillatory MA of the ferromagnetic film (Fe or Co) underneath. In this section, based on experimental observations shown in Sec. 5.1.2 and recent theoretical calculations [25], the mechanism of oscillatory MAE due in Cu/Co and Cu/Fe bilayers is discussed.

The calculations of MAE for Cu/Co bilayer system using a realistic tight-binding model show that the oscillations of MA with an increasing Cu thickness are a consequence of the resonant effect between *sp*-QWS in Cu and *d*-bands in Co. The *d*-bands in Co are split into minority and majority states in such way, that their hybridization with *sp*-QWS from Cu occurs only in minority-spin channel [172]. This results only in partial confinement of *sp* minority states and so called resonant states are formed [171, 172, 237]. The resultant states spanning over the whole Cu/Co bilayer are localized mainly in Co, but also have significant components in Cu. Within the Cu film, the probability amplitude of these states, depends on the distance from the Cu surface in an oscillatory way [172].

The phase of such resonant *sp* states localized in the Cu part of the bilayer is different at the Cu/Co interface for different Cu thicknesses while being almost fixed (independent of Cu thickness) at the Cu/UHV interface. As a result, the amplitude of these *sp* states at the Cu/Co interface oscillates as the Cu thickness increases. This modifies the *sp-d* hybridization across this interface between *sp*-state component localized in Cu (which is minor), and *d*-state in Co (dominating one). As a consequence, oscillatory changes of the energies of the hybridized Co *d* states with increasing Cu thickness are observed (see Fig. 6.14(b)). Such changes in electronic structure in the vicinity of the Fermi result in period modulation of MAE as a function of Cu thickness as shown in Fig. 6.14(a). The MAE was calculated by applying perturbation theory (see Sec. 2.1.1) for Cu on Co(001) flat surface as a energy difference with the magnetization pointing two orthogonal directions (i.e., perpendicular to the sample plane and in the sample plane).

In view of the second order perturbation theory, each pair of the occupied and unoccupied states of the energies close to the Fermi level can contribute to MAE. Therefore, occupied (unoccupied) states shown in Fig. 6.14(b) can contribute to the anisotropy energy if coupled to any other unoccupied (occupied) electronic state of the energy close to  $E_F$ . The energy distance between the coupled states decreases when the energy of the resonant state approaches  $E_F$ . After crossing  $E_F$ , the resonant state becomes unoccupied, but can still couple to the other, occupied state. With increasing Cu thickness, the resonant state shifts to higher energies. Eventually, the energy distance between both coupled states increases and there is no contribution to MAE. In this way, the maximum contribution to MAE occurs for the thicknesses of Cu, at which resonant states cross  $E_F$  (i.e., at which the energy distance between the coupled states is the smallest). This mechanism can be observed in Fig. 6.14: for the energies of the resonant states close to the Fermi level the MAE values are the largest (since MAE is negative, enhanced anisotropy corresponds to minima). A similar mechanism of the magnetic anisotropy oscillations with increasing Cu thickness should also be valid for Cu/Fe bilayers. The only difference is that in this case, *sp* state in Cu hybridize mostly with majority-spin *d*-band in Fe [238].

The period  $L_{Cu}$  of MAE oscillations is identical to the period with which resonant *sp* state (coupled with *d* state) cross  $E_F$ . Therefore,  $L_{Cu}$  can be derived from the equation 2.2.3. The *sp* resonant state originate from the bulk Cu band with  $\Delta_1$  symmetry close to the *X* point in the 3-dimensional Brillouin



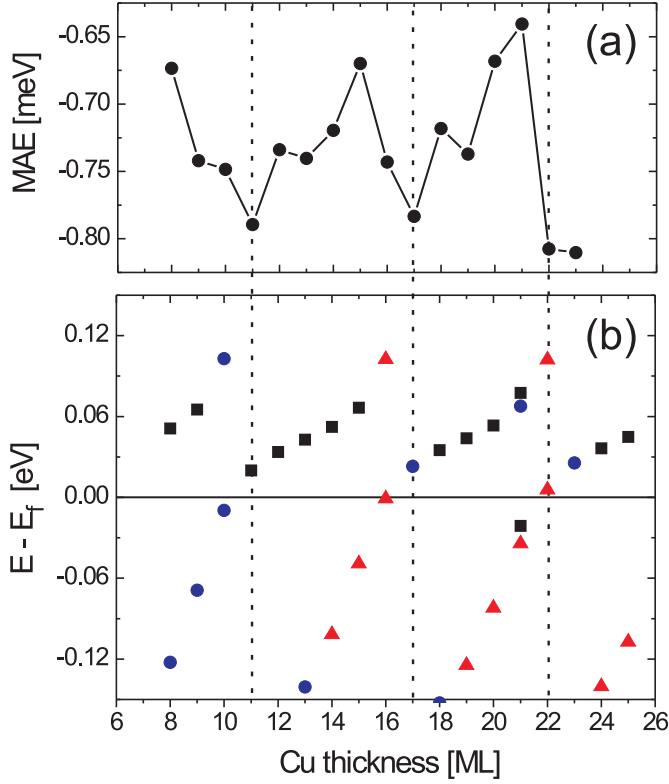


**Figure 6.14:** The results of tight-binding calculations at  $T = 30$  K for Cu/Co(11 ML) bilayer: (a) magnetic anisotropy energy MAE; (b) energies of minority-spin states at the  $\mathbf{k}_{\parallel}=(0.13,0)\pi/a$  point, which are localized in Co layer with the probability  $x > 0.65$  and in Cu with the probability:  $0.03 < y < 0.1$  (square/black),  $0.1 < y < 0.2$  (circle/blue),  $0.2 < y < 0.35$  (triangle/red) where  $x + y = 1$  [25]

zone and cross  $E_F$  at  $k_{env} = 0.173 k_{BZ}$  [76]. It corresponds to the period of oscillations  $L_{Cu} = 5.8$  ML, i.e., the same as the oscillations of  $H_s$  observed in the experiment.

The oscillatory contribution to MA is expected only if the  $d$ -QWS in Co is distant from  $E_F$  by less than the magnitude of its energy changes due the varying Cu thickness. Since such energy range is found to be minor, the oscillations arise in small regions in the 2-dimensional Brillouin zone near the  $\mathbf{k}_{\parallel}$  points at which QWS in Co cross  $E_F$ . This explains why the oscillatory contribution to MAE can disappear even with a small increase in temperature (i.e., if thermal fluctuations become comparable with the energy changes due to QWS in Cu). This is why the oscillations of  $H_s$  are not visible in the experiment performed at RT (see Sec. 5.1.2).

In Cu films on Co(001) surface there exist also other QWS, with shorter periodicity of  $\sim 2.6$  ML, observed around the *neck* of the Fermi surface [74, 239–241]. These states however are more effectively reflected at the interfaces, i.e., do not hybridize with Co bands. Lack of MA oscillations with this periodicity is therefore not surprising and confirms that the resonant effect between  $sp$  states from Cu and  $d$  states from Co is crucial for modulation of magnetic anisotropy. Note that effect of hybridization of  $sp$  states in Cu has also significant impact on strength of the interlayer exchange coupling (IEC) [239]. In contrast to MA oscillations, the dominating contribution to the IEC comes from the vicinity of the *neck* (i.e., with the shorter period), while the long period ( $\sim 5.8$  ML) coming from the vicinity of the *belly* is negligible. This is because only  $sp$  states from the vicinity of the *neck* Fermi surface form "true" QWS (not resonant states).

The oscillations of  $H_s$  as a function Cu thickness were experimentally observed before [23, 24], however by measurements only down to 170 K and solely for Cu grown on Co/Cu(001) vicinal surface [23, 24]. According to theory, the MA oscillations supposed to be the strongest at lower temperatures both, due to QWS formed inside nonmagnetic layer and modulating the MA through the interface with ferromagnetic layer [73], and due to QWS formed in the ferromagnetic layer [19]. This is why, previously measured MA oscillations as a function of Cu film thickness at 170 K posses significantly smaller amplitude [23, 24], in comparison to the oscillations obtained in our experiment carried out at 5 K.

The fact that hybridization of the electronic states plays an important role in the case of oscillatory magnetic anisotropy of Cu/Fe and Cu/Co bilayers can also be helpful in understanding of other such NM/FM systems, where oscillations due to QWS are expected. In particular, in the case of Au overlayers grown on Fe/Ag(116), where no indication for the oscillatory MA is observed (Sec. 5.1.2). The lack of MA oscillations in the case of Au/Fe bilayer is most likely related to presence of "true" QWS (not resonant states) [13, 174–177]. As a consequence, QWS from Au layer cannot hybridize with *d* electrons from Fe layer and therefore, periodic contribution to MA as a function of Au thickness cannot be observed.

## Conclusion

In this thesis, we investigated the magnetic anisotropy in ferromagnetic thin films as well as in nonmagnetic/ferromagnetic bilayers grown on vicinal surfaces. In particular, we demonstrated that the confinement of  $d$ -electrons in ferromagnetic films leads to magnetic anisotropy oscillations as a function of film thickness. We identified the symmetry and spin character of the electronic bands responsible for the oscillations and have shown the influence of temperature on the amplitude of the oscillations.

The period of the magnetic anisotropy oscillations is related to the electronic structure and is determined by the wavevector of the corresponding quantum well states (QWS) at the Fermi level. The fact that different oscillation periods are observed in different systems, confirms the correlation between QWS and oscillatory magnetic anisotropy. The obtained oscillation periods and corresponding confined electronic bands are summarized in Table 7.1. We conclude that oscillations of the magnetic anisotropy as a function of thickness of ferromagnetic Co and Fe films are a direct consequence of the quantization of the  $\Delta_5$  electronic band. The  $\Delta_5$  band consists of  $d_{xz}$ ,  $d_{yz}$  out-of-plane orbitals and its contributions to the magnetic anisotropy energy with increasing film thickness manifest in changes of the in-plane orbital magnetic moment. Due to the broken symmetry of the vicinal surface, periodic changes of the orbital magnetic moment are clearly visible in our experiments only along one in-plane direction, perpendicular to the step edges. We have shown that even minute differences in the lattice mismatch between the film and the substrate, such as found between  $bcc$  Fe films grown on Ag(116) and Au(113) or between  $fcc$  Co films grown on Cu(113) and Fe/Ag(116), can modify already the electronic structure and as a consequence, the period of the magnetic anisotropy oscillations. The results are summarized in Table 7.1, which shows the different oscillation periods in films grown of different substrates.

System	$bcc$ Fe film grown on		$fcc$ Co film grown on		$bcc$ Co film grown on
	Ag(116)	Au(113)	Cu(113)	Fe/Ag(116)	Au(113)
Oscillation period	$5.35 \pm 0.3$	$6.1 \pm 0.3$	$2.3 \pm 0.3$	$2.6 \pm 0.3$	$4.1 \pm 0.3$
Confined electronic band	$\Delta_5$ majority-spin		$\Delta_5$ minority-spin		$\Delta_5$ minority-spin

**Table 7.1:** Measured oscillation periods and the electronic bands leading to the formation of QWS, which contribute periodically to the magnetic anisotropy with increasing film thickness.

The oscillatory magnetic anisotropy due to QWS in ferromagnetic films has been theoretically investigated in  $fcc$  Co films [19–21]. Our results on such Co films are in excellent agreement with the theoretical predictions. Besides confirming the oscillation period, we have equally confirmed that a strong temperature dependence is only observed at those thicknesses for which QWS significantly contribute to magnetic anisotropy.

Based on the results from FeCo alloys we have shown that the formation of magnetic anisotropy oscillations is very sensitive to the film morphology and to the structural relaxation of the film. In particular, for  $fcc$  FeCo alloys grown on the Cu(113) surface, the decrease of the oscillation amplitude

with increasing Fe content is ascribed to changes in the interlayer vertical distance. We also demonstrated that the mixing of Fe with Co leads to strong in-plane uniaxial anisotropy with the easy magnetization oriented perpendicular to the step edges.

This work also sheds light on the effect of QWS in a nonmagnetic overlayer on the magnetic anisotropy of the underlying ferromagnetic film. Experimentally, an effect had so far only been reported for Cu films grown on the vicinal surface of Co/Cu(001) [23, 24]. In references [23, 24] it was observed that the oscillatory magnetic anisotropy consists of two periods, of 2.4 and 5.4 ML, which correspond to two extreme points of the Cu Fermi surface, namely, the "neck" and the "belly". Our results on the same system demonstrated however that only oscillations with a single period of  $5.8 \pm 0.3$  ML are visible. In addition, we observed anisotropy oscillations with nearly exactly the same period, namely of  $6.0 \pm 0.3$  ML, for Cu overlayers grown on Fe/Ag(116). Our observations are confirmed by recent theoretical calculations presented in this thesis [25]. These calculations found that the oscillations of the magnetic anisotropy energy with increasing Cu thickness are a consequence of the hybridization between resonant *sp* states in Cu and *d* states in Co. Although QWS with a periodicity of around 2.4 ML indeed exist in Cu films [74, 239], they do not hybridize with *d* states in Co and as a consequence, do not influence the magnetic anisotropy. The absence of hybridization of the electronic states could be also concluded to be responsible for the lack of magnetic anisotropy oscillations in our experiment on Au film grown on Fe/Ag(116).

Besides demonstrating the presence of oscillatory magnetic anisotropy due to QWS, the results presented in this thesis provide new insight into spin reorientation transition (SRT) phenomena. While previous studies of SRT in thin films grown on vicinal surfaces have mostly concentrated on parameters such as thickness and temperature required to obtain a magnetization perpendicular to the film plane, little or no attention was paid to the interplay between perpendicular and in-plane magnetic anisotropies. We showed here that for Fe films grown on Ag(116) this interplay significantly affects the orientation of the easy magnetization axis and the domain structure. It is observed that as soon as the magnetization starts to tilt away from the sample plane, it is exclusively oriented perpendicular to the step edges. This implies that the change of the easy magnetization axis from in-plane to out-of-plane is accompanied by the switching of the in-plane magnetization component into the direction perpendicular to the step edges. In addition, our domain structure studies demonstrated that the change of the magnetization orientation from in-plane to out-of-plane proceeds via a continuous rotation of stripe domains. Moreover, the direction of the magnetization rotation is well defined and can be tuned by altering the relative strength of the uniaxial perpendicular anisotropy  $K_s$  and the step anisotropy  $K_{sp}$ . For instance, through the deposition of an Au capping layer, we showed that the uniaxial perpendicular anisotropy  $K_s$  is reduced and the direction of the magnetization rotation can be reversed. In contrast to the rotation of the magnetization from in-plane to out-of-plane, the in-plane orientation of the magnetization changes discontinuously via a state of coexisting phases with only two possible magnetization orientations: perpendicular to or along the step edges. A phenomenological model discussed in the thesis describing the magnetic anisotropy of ferromagnetic films on vicinal surfaces, successfully predicts the orientation of the magnetization observed in our experiments and can equally be applied to other systems.

The results presented in this work open the possibility of further experimental and theoretical investigations in the field of oscillatory magnetic anisotropy and QWS arising from *d*-bands in ferromagnetic films. It is particularly interesting for example to investigate the effect of electric fields on the oscillatory magnetic anisotropy. Since electric fields affect magnetic anisotropy by altering the density of states at the Fermi level [242], one can also expect external electric fields to influence QWS from *d*-bands and thereby oscillatory magnetic anisotropy. The control of the magnetization by means of electric fields is considered attractive because of its simplicity, low power consumption and coherent behavior. Very recently it was shown that it is possible to coherently switch the magnetization using voltage pulses [6]. As shown in reference [6], a key requirement for achieving voltage-induced magnetization reversal is

## CHAPTER 7

the use of system with tilted magnetization. In this work we have shown that any desirable value of the tilting angle of the magnetization can be achieved by the appropriate choice of the film thickness or of the nonmagnetic capping layer. Such systems could therefore be essential for future investigations of voltage-induced magnetization switching.



## Bibliography

- [1] GRÜNBERG, P, R. SCHREIBER, Y. PANG, M. B. BRODSKY and H. SOWERS: *Layered Magnetic Structures: Evidence for Antiferromagnetic Coupling of Fe Layers across Cr Interlayers*. Phys. Rev. Lett., 57(19):2442–2445, November 1986.
- [2] BAIBICH, M. N., J. M. BROTO, A. FERT, F. NGUYEN VAN DAU, F. PETROFF, P. ETIENNE, G. CREUZET, A. FRIEDERICH and J. CHAZELAS: *Giant Magnetoresistance of (001)Fe/(001)Cr Magnetic Superlattices*. Phys. Rev. Lett., 61(21):2472–2475, November 1988.
- [3] PARKIN, STUART S. P., CHRISTIAN KAISER, ALEX PANCHULA, PHILIP M. RICE, BRIAN HUGHES, MAHESH SAMANT and SEE-HUN YANG: *Giant tunnelling magnetoresistance at room temperature with MgO (100) tunnel barriers*. Nat Mater, 3(12):862–867, December 2004.
- [4] WOLF, S. A., D. D. AWSCHALOM, R. A. BUHRMAN, J. M. DAUGHTON, S. VON MOLNAR, M. L. ROUKES, A. Y. CHTCHELKANOVA and D. M. TREGER: *Spintronics: A Spin-Based Electronics Vision for the Future*. Science, 294(5546):1488–1495, 2001.
- [5] WANG, WEI-GANG, MINGEN LI, STEPHEN HAGEMAN and C. L. CHIEN: *Electric-field-assisted switching in magnetic tunnel junctions*. Nat Mater, 11(1):64–68, January 2012.
- [6] SHIOTA, YOICHI, TAKAYUKI NOZAKI, FREDERIC BONELL, SHINICHI MURAKAMI, TERUYA SHINJO and YOSHISHIGE SUZUKI: *Induction of coherent magnetization switching in a few atomic layers of FeCo using voltage pulses*. Nat Mater, 11(1):39–43, January 2012.
- [7] BURKERT, TILL, LARS NORDSTRÖM, OLLE ERIKSSON and OLLE HEINONEN: *Giant Magnetic Anisotropy in Tetragonal FeCo Alloys*. Phys. Rev. Lett., 93(2):027203–, July 2004.
- [8] WINKELMANN, AIMO, MAREK PRZYBYLSKI, FENG LUO, YISHENG SHI and JOCHEN BARTHEL: *Perpendicular Magnetic Anisotropy Induced by Tetragonal Distortion of FeCo Alloy Films Grown on Pd(001)*. Phys. Rev. Lett., 96(25):257205–, June 2006.
- [9] DAALDEROP, G. H. O., P. J. KELLY and F. J. A. DEN BROEDER: *Prediction and confirmation of perpendicular magnetic anisotropy in Co/Ni multilayers*. Phys. Rev. Lett., 68(5):682–685, February 1992.
- [10] YILDIZ, F., F. LUO, C. TIEG, R. M. ABRUDAN, X. L. FU, A. WINKELMANN, M. PRZYBYLSKI and J. KIRSCHNER: *Strongly Enhanced Orbital Moment by Reduced Lattice Symmetry and Varying Composition of Fe<sub>1-x</sub>Co<sub>x</sub> Alloy Films*. Phys. Rev. Lett., 100(3):037205–, January 2008.
- [11] BRUNO, P.: *Theory of interlayer magnetic coupling*. Phys. Rev. B, 52(1):411–439, July 1995.
- [12] ÖZER, MUSTAFA M., YU JIA, ZHENYU ZHANG, JAMES R. THOMPSON and HANNO H. WEITERING: *Tuning the Quantum Stability and Superconductivity of Ultrathin Metal Alloys*. Science, 316(5831):1594–1597, 2007.
- [13] SUZUKI, Y., T. KATAYAMA, P. BRUNO, S. YUASA and E. TAMURA: *Oscillatory Magneto-Optical Effect in a Au (001) Film Deposited on Fe: Experimental Confirmation of a Spin-Polarized Quantum Size Effect*. Phys. Rev. Lett., 80(23):5200–5203, June 1998.
- [14] LI, YAN, WEI HAN, A. G. SWARTZ, K. PI, J. J. I. WONG, S. MACK, D. D. AWSCHALOM and R. K. KAWAKAMI: *Oscillatory Spin Polarization and Magneto-Optical Kerr Effect in Fe<sub>3</sub>O<sub>4</sub> Thin Films on GaAs(001)*. Phys. Rev. Lett., 105(16):167203–, October 2010.

- [15] UPTON, M. H., C. M. WEI, M. Y. CHOU, T. MILLER and T.-C. CHIANG: *Thermal Stability and Electronic Structure of Atomically Uniform Pb Films on Si(111)*. Phys. Rev. Lett., 93(2):026802–, July 2004.
- [16] NOZAKI, T., N. TEZUKA and K. INOMATA: *Quantum Oscillation of the Tunneling Conductance in Fully Epitaxial Double Barrier Magnetic Tunnel Junctions*. Phys. Rev. Lett., 96(2):027208–, January 2006.
- [17] ABALLE, L., A. BARINOV, A. LOCATELLI, S. HEUN and M. KISKINOVA: *Tuning Surface Reactivity via Electron Quantum Confinement*. Phys. Rev. Lett., 93(19):196103–, November 2004.
- [18] FU, YING-SHUANG, SHUAI-HUA JI, XI CHEN, XU-CUN MA, RUI WU, CHEN-CHEN WANG, WEN-HUI DUAN, XIAO-HUI QIU, BO SUN, PING ZHANG, JIN-FENG JIA and QI-KUN XUE: *Manipulating the Kondo Resonance through Quantum Size Effects*. Phys. Rev. Lett., 99(25):256601–, December 2007.
- [19] CINAL, M: *Origin of magnetocrystalline anisotropy oscillations in (001) face-centred-cubic Co thin films and effect of sp-d hybridization*. Journal of Physics: Condensed Matter, 15(2):29, 2003.
- [20] SZUNYOGH, L., B. UJFALUSSY, C. BLAAS, U. PUSTOGOWA, C. SOMMERS and P. WEINBERGER: *Oscillatory behavior of the magnetic anisotropy energy in Cu(100)/Co<sub>n</sub> multilayer systems*. Phys. Rev. B, 56(21):14036–14044, December 1997.
- [21] CINAL, M. and A. UMERSKI: *Magnetic anisotropy of vicinal (001) fcc Co films: Role of crystal splitting and structure relaxation in the step-decoration effect*. Phys. Rev. B, 73(18):184423–, May 2006.
- [22] LI, J., M. PRZYBYLSKI, F. YILDIZ, X. D. MA and Y. Z. WU: *Oscillatory Magnetic Anisotropy Originating from Quantum Well States in Fe Films*. Phys. Rev. Lett., 102(20):207206–, May 2009.
- [23] WÜRSCH, CH., C. STAMM, S. EGGER, D. PESCIA, W. BALTENSBERGER and J. S. HELMAN: *Quantum oscillations in a confined electron gas*. Nature, 389(6654):937–939, October 1997.
- [24] WEBER, W., A. BISCHOF, R. ALLENSPACH, CH. WÜRSCH, C. H. BACK and D. PESCIA: *Oscillatory Magnetic Anisotropy and Quantum Well States in Cu/Co/Cu(100) Films*. Phys. Rev. Lett., 76(18):3424–3427, April 1996.
- [25] MANNA, S., P. L. GASTELOIS, M. DĄBROWSKI, P. KUSWIK, M. CINAL, M. PRZYBYLSKI and J. KIRSCHNER: *Effect of quantum well states in Cu overlayer on magnetic anisotropy of Fe and Co films revisited*. Phys. Rev. B, 87(13):134401–, April 2013.
- [26] BRUNO, PATRICK: *Tight-binding approach to the orbital magnetic moment and magnetocrystalline anisotropy of transition-metal monolayers*. Phys. Rev. B, 39(1):865–, January 1989.
- [27] BAUER, U. and M. PRZYBYLSKI: *Large amplitude oscillation of magnetic anisotropy engineered by substrate step density*. Phys. Rev. B, 81(13):134428–, April 2010.
- [28] BAUER, E, T DUDEN and R ZDYB: *Spin-polarized low energy electron microscopy of ferromagnetic thin films*. Journal of Physics D: Applied Physics, 35(19):2327–, 2002.
- [29] VLECK, J. H. VAN: *On the Anisotropy of Cubic Ferromagnetic Crystals*. Phys. Rev., 52(11):1178–1198, December 1937.
- [30] DIRAC, P. A. M.: *The Quantum Theory of the Electron*. Proc. R. Soc. Lond. A, 117:610–624, 1928.
- [31] SCHIFF, LEONARD I.: *Quantum mechanics*. New York, McGraw-Hill, 1968.
- [32] STÖHR, J. and H. SIEGMANN: *Magnetism From Fundamentals to Nanoscale Dynamics*. Springer Berlin Heidelberg, 2006.
- [33] CINAL, M. and D. M. EDWARDS: *Magnetocrystalline anisotropy in Co/Pd structures*. Phys. Rev. B, 55(6):3636–3648, February 1997.
- [34] LAAN, GERRIT VAN DER: *Microscopic origin of magnetocrystalline anisotropy in transition metal thin films*. Journal of Physics: Condensed Matter, 10(14):3239–, 1998.
- [35] BLAND, J. ANTHONY C. and BRETISLAV HEINRICH: *Ultrathin Magnetic Structures I. An Introduction to the Electronic, Magnetic and Structural Properties*. Springer Berlin Heidelberg, 1994.
- [36] GRADMANN, U., J. KORECKI and G. WALLER: *In-plane magnetic surface anisotropies in Fe(110)*. Applied Physics A, 39(2):101–108, 1986.



- [37] CHUANG, D. S., C. A. BALLENTINE and R. C. O'HANDLEY: *Surface and step magnetic anisotropy*. Phys. Rev. B, 49(21):15084–15095, June 1994.
- [38] BERGER, A., U. LINKE and H. P. OEPEN: *Symmetry-induced uniaxial anisotropy in ultrathin epitaxial cobalt films grown on Cu(1 1 13)*. Phys. Rev. Lett., 68(6):839–842, February 1992.
- [39] WEBER, W., C. BACK, A. BISCHOF, D. PESCIA and R. ALLENSPACH: *Magnetic switching in cobalt films by adsorption of copper*. Nature, 374(6525):788–790, April 1995.
- [40] KAWAKAMI, R. K., ERNESTO J. ESCORCIA-APARICIO and Z. Q. QIU: *Symmetry-Induced Magnetic Anisotropy in Fe Films Grown on Stepped Ag(001)*. Phys. Rev. Lett., 77(12):2570–2573, September 1996.
- [41] WULFHEKEL, W., S. KNAPPMANN and H. P. OEPEN: *Magnetic anisotropy of Co on Cu(1 1 17)*. J. Appl. Phys., 79(2):988–992, January 1996.
- [42] WU, Y. Z., C. WON and Z. Q. QIU: *Magnetic uniaxial anisotropy of Fe films grown on vicinal Ag(001)*. Phys. Rev. B, 65(18):184419–, April 2002.
- [43] BISIO, F., R. MORONI, F. BUATIER DE MONGEOT, M. CANEPA and L. MATTERA: *Isolating the Step Contribution to the Uniaxial Magnetic Anisotropy in Nanostructured Fe/Ag(001) Films*. Phys. Rev. Lett., 96(5):057204–, February 2006.
- [44] WEBER, W., C. H. BACK, A. BISCHOF, CH. WÜRSCH and R. ALLENSPACH: *Morphology-Induced Oscillations of the Magnetic Anisotropy in Ultrathin Co Films*. Phys. Rev. Lett., 76(11):1940–1943, March 1996.
- [45] HYMAN, R. A., A. ZANGWILL and M. D. STILES: *Magnetic reversal on vicinal surfaces*. Phys. Rev. B, 58(14):9276–9286, October 1998.
- [46] OEPEN, H. P., Y. T. MILLEV, H. F. DING, S. PÜTTER and J. KIRSCHNER: *Field-driven reorientation in ultrathin ferromagnetic films with uniaxial anisotropy*. Phys. Rev. B, 61(14):9506–9512, April 2000.
- [47] WU, Y. Z., C. WON, H. W. ZHAO and Z. Q. QIU: *Surface magneto-optic Kerr effect study of Co thin films grown on double curved Cu(001)*. Phys. Rev. B, 67(9):094409–, March 2003.
- [48] LI, J., M. PRZYBYLSKI, Y. HE and Y. Z. WU: *Experimental observation of quantum oscillations of perpendicular anisotropy in Fe films on Ag(1,1,10)*. Phys. Rev. B, 82(21):214406–, December 2010.
- [49] COYLE, S. T. and M. R. SCHEINFELD: *Magnetic ordering in Co films on stepped Cu(100) surfaces*. J. Appl. Phys., 83(11):7040–7042, June 1998.
- [50] DÜRR, H. A., G. VAN DER LAAN, J. VOGEL, G. PANACCIONE, N. B. BROOKES, E. DUDZIK and R. MCGRATH: *Enhanced orbital magnetism at the nanostructured Co/Cu(1 1 13) surface*. Phys. Rev. B, 58(18):R11853–R11856, November 1998.
- [51] PIETZSCH, O., A. KUBETZKA, M. BODE and R. WIESENDANGER: *Real-Space Observation of Dipolar Antiferromagnetism in Magnetic Nanowires by Spin-Polarized Scanning Tunneling Spectroscopy*. Phys. Rev. Lett., 84(22):5212–5215, May 2000.
- [52] RICKART, M, S O DEMOKRITOV and B HILLEBRANDS: *Non-monotonic step-induced magnetic anisotropy of Fe films prepared on vicinal Au(001) surfaces with different step orientations*. Journal of Physics: Condensed Matter, 14(39):8947–, 2002.
- [53] ROUGEMAILLE, N. and A. K. SCHMID: *Self-organization and magnetic domain microstructure of Fe nanowire arrays*. J. Appl. Phys., 99(8):08S502–3, April 2006.
- [54] STUPAKIEWICZ, A., A. KIRILYUK, A. FLEURENCE, R. GIENIUSZ, T. MAROUTIAN, P. BEAUVILLAIN, A. MAZIEWSKI and TH. RASING: *Interface magnetic and optical anisotropy of ultrathin Co films grown on a vicinal Si substrate*. Phys. Rev. B, 80(9):094423–, September 2009.
- [55] BORUKHIN, SHIRLY, CECILE SAGUY, MARIA KOIFMAN and BOAZ POKROY: *Self-Ordered Vicinal-Surface-Like Nanosteps at the Thin Metal-Film/Substrate Interface*. J. Phys. Chem. C, 116(22):12149–12155, May 2012.
- [56] WEBER, W., A. BISCHOF, R. ALLENSPACH, C. H. BACK, J. FASSBENDER, U. MAY, B. SCHIRMER, R. M. JUNGBLUT, G. GÜNTHERODT and B. HILLEBRANDS: *Structural relaxation and magnetic anisotropy in Co/Cu(001) films*. Phys. Rev. B, 54(6):4075–4079, August 1996.

- [57] BAUER, U., M. DĄBROWSKI, M. PRZYBYLSKI and J. KIRSCHNER: *Experimental confirmation of quantum oscillations of magnetic anisotropy in Co/Cu(001)*. Phys. Rev. B, 84(14):144433–, October 2011.
- [58] SMITH, N. V.: *Phase analysis of image states and surface states associated with nearly-free-electron band gaps*. Phys. Rev. B, 32(6):3549–3555, September 1985.
- [59] SMITH, N. V., N. B. BROOKES, Y. CHANG and P. D. JOHNSON: *Quantum-well and tight-binding analyses of spin-polarized photoemission from Ag/Fe(001) overlayers*. Phys. Rev. B, 49(1):332–338, January 1994.
- [60] QIU, Z Q and N V SMITH: *Quantum well states and oscillatory magnetic interlayer coupling*. Journal of Physics: Condensed Matter, 14(8):R169–, 2002.
- [61] LINDGREN, S. A and L. WALLDÈN: *Electron-Energy-Band Determination by Photoemission from Overlayer States*. Phys. Rev. Lett., 61(25):2894–2897, December 1988.
- [62] HAMAWI, A, S-A LINDGREN and L WALLDÈN: *Quantum Size Effects in Thin Metal Overlayers*. Physica Scripta, 1991(T39):339–, 1991.
- [63] ORTEGA, J. E., F. J. HIMPSEL, G. J. MANKEY and R. F. WILLIS: *Quantum-well states and magnetic coupling between ferromagnets through a noble-metal layer*. Phys. Rev. B, 47(3):1540–1552, January 1993.
- [64] T.-C, CHIANG: *Photoemission studies of quantum well states in thin films*. Surface Science Reports, 39(7-8):181–235, September 2000.
- [65] MILUN, M, P PERVAN and D P WOODRUFF: *Quantum well structures in thin metal films: simple model physics in reality?* Reports on Progress in Physics, 65(2):99–, 2002.
- [66] JOHNSON, P. D. and S. L. HULBERT: *Inverse photoemission*. Rev. Sci. Instrum., 61(9):2277–2288, September 1990.
- [67] CHIANG, CHENG-TIEN, AIMO WINKELMANN, PING YU, JÜRGEN KIRSCHNER and JÜRGEN HENK: *Spin-orbit coupling in unoccupied quantum well states: Experiment and theory for Co/Cu(001)*. Phys. Rev. B, 81(11):115130–, March 2010.
- [68] ZDYB, R. and E. BAUER: *Spin-Resolved Unoccupied Electronic Band Structure from Quantum Size Oscillations in the Reflectivity of Slow Electrons from Ultrathin Ferromagnetic Crystals*. Phys. Rev. Lett., 88(16):166403–, April 2002.
- [69] CROMMIE, M. F., C. P. LUTZ and D. M. EIGLER: *Confinement of Electrons to Quantum Corrals on a Metal Surface*. Science, 262(5131):218–220, 1993.
- [70] OKA, H., P. A. IGNATIEV, S. WEDEKIND, G. RODARY, L. NIEBERGALL, V. S. STEPANYUK, D. SANDER and J. KIRSCHNER: *Spin-Dependent Quantum Interference Within a Single Magnetic Nanostructure*. Science, 327(5967):843–846, 2010.
- [71] LESSARD, A., T. H. MOOS and W. HÜBNER: *Magnetocrystalline anisotropy energy of transition-metal thin films: A nonperturbative theory*. Phys. Rev. B, 56(5):2594–2604, August 1997.
- [72] CINAL, M. and D. M. EDWARDS: *Quantum-well states and magnetocrystalline anisotropy in Co/Pd structures*. Phys. Rev. B, 57(1):100–103, January 1998.
- [73] CINAL, M: *Analysis of magnetocrystalline anisotropy oscillations in Co/Pd thin films*. Journal of Physics: Condensed Matter, 13(5):901–, 2001.
- [74] SEGOVIA, P., E. G. MICHEL and J. E. ORTEGA: *Quantum Well States and Short Period Oscillations of the Density of States at the Fermi Level in Cu Films Grown on fcc Co(100)*. Phys. Rev. Lett., 77(16):3455–3458, October 1996.
- [75] ORTEGA, J. E. and F. J. HIMPSEL: *Quantum well states as mediators of magnetic coupling in superlattices*. Phys. Rev. Lett., 69(5):844–847, August 1992.
- [76] ORTEGA, J. E., F. J. HIMPSEL, G. J. MANKEY and R. F. WILLIS: *Quantum well states and magnetic coupling between noble metals and ferromagnets (invited)*. J. Appl. Phys., 73(10):5771–5775, May 1993.
- [77] KIRSCHNER, J., H. ENGELHARD and D. HARTUNG: *An evaporation source for ion beam assisted deposition in ultrahigh vacuum*. Rev. Sci. Instrum., 73(11):3853–3860, November 2002.

- [78] JONKER, B.T. and G.A. PRINZ: *Comment on "the growth of Fe overlayers on Ag(100)" by G.C. Smith, H.A. Padmore and C. Norris*. Surface Science Letters, 172(3):L568–L570, July 1986.
- [79] STAMPANONI, M., A. VATERLAUS, M. AESCHLIMANN and F. MEIER: *Magnetism of Epitaxial bcc Iron on Ag(001) Observed by Spin-Polarized Photoemission*. Phys. Rev. Lett., 59(21):2483–2485, November 1987.
- [80] QIU, Z. Q., J. PEARSON and S. D. BADER: *Asymmetry of the spin reorientation transition in ultrathin Fe films and wedges grown on Ag(100)*. Phys. Rev. Lett., 70(7):1006–1009, February 1993.
- [81] SCHALLER, D. M., D. E. BÜRGLER, C. M. SCHMIDT, F. MEISINGER and H.-J. GÜNTHERODT: *Spin reorientations induced by morphology changes in Fe/Ag(001)*. Phys. Rev. B, 59(22):14516–14519, June 1999.
- [82] BÜRGLER, D. E., C. M. SCHMIDT, D. M. SCHALLER, F. MEISINGER, R. HOFER and H.-J. GÜNTHERODT: *Optimized epitaxial growth of Fe on Ag(001)*. Phys. Rev. B, 56(7):4149–4158, August 1997.
- [83] LI, HONG and B. P. TONNER: *Direct experimental identification of the structure of ultrathin films of bcc iron and metastable bcc and fcc cobalt*. Phys. Rev. B, 40(15):10241–10248, November 1989.
- [84] KIM, S. K., C. PETERSEN, F. JONA and P. M. MARCUS: *Ultrathin films of cobalt on Fe001 and the effect of oxygen*. Phys. Rev. B, 54(3):2184–2190, July 1996.
- [85] DUO, L., R. BERTACCO, G. ISELLA, F. CICCACCI and M. RICHTER: *Electronic and magnetic properties of the Co/Fe(001) interface and the role of oxygen*. Phys. Rev. B, 61(22):15294–15301, June 2000.
- [86] KELLAR, S. A., Y. CHEN, W. R. A. HUFF, E. J. MOLER, Z. HUSSAIN and D. A. SHIRLEY: *Surface structure determination of Au(1 ML)/Fe(15 ML)/Au(100) using angle-resolved photoemission extended fine structure*. Phys. Rev. B, 57(3):1890–1895, January 1998.
- [87] WILGOCKA-SLEZAK, D., K. FREINDL, A. KOZIOL, K. MATLAK, M. RAMS, N. SPIRIDIS, M. SLEZAK, T. SLEZAK, M. ZAJAC and J. KORECKI: *Thickness-driven polar spin reorientation transition in ultrathin Fe/Au(001) films*. Phys. Rev. B, 81(6):064421–, February 2010.
- [88] OPITZ, R, S LÖBUS, A THISSEN and R COURTHS: *An angle-scanned photoelectron diffraction (XPD) study of the growth and structure of ultrathin Fe films on Au(001)*. Surface Science, 370:293–310, January 1997.
- [89] BLUM, V., CH. RATH, S. MÜLLER, L. HAMMER, K. HEINZ, J. M. GARCIAA, J. E. ORTEGA, J. E. PRIETO, O. S. HERNAN, J. M. GALLEGRO, A. L. VAZQUEZ DE PARGA and R. MIRANDA: *Fe thin-film growth on Au(100): A self-surfactant effect and its limitations*. Phys. Rev. B, 59(24):15966–15974, June 1999.
- [90] SCHMID, A.K. and J. KIRSCHNER: *In situ observation of epitaxial growth of Co thin films on Cu(100)*. Ultramicroscopy, 42-44, Part 1(0):483–489, July 1992.
- [91] KATAYAMA, T., W. GEERTS, Y. SUZUKI, D. FUJITANI and N. OKUZAWA: *Oscillation of magneto-optical Kerr effect in Co ultra-thin films*. Journal of Magnetism and Magnetic Materials, 156:171–172, April 1996.
- [92] SPIRIDIS, N., T. SLEZAK, M. ZAJAC and J. KORECKI: *Ultrathin epitaxial bcc-Co films stabilized on Au(001)-hex*. Surface Science, 566-568(0):272–277, September 2004.
- [93] KAWAGOE, T., T. MIYAMACHI, M. SOMETA, T. KUDO and S. SUGA: *Embedded Co nanostructures on Au(001) substrate studied by scanning tunneling microscopy*. Surface Science, 602(3):L15–L19, February 2008.
- [94] KAWAGOE, TAKESHI, MASAOKI GESHI, TOSHIO MIYAMACHI and SHIGEMASA SUGA: *Spin-Polarized Surface States of Metastable Body-Centered Cubic Co(001)*. Applied Physics Express, 2(4):043001, 2009.
- [95] KAWAGOE, TAKESHI, TOSHIO MIYAMACHI and SHIGEMASA SUGA: *Growth and Surface Structure of Thin Co Films on Au(001) Studied by Scanning Tunneling Microscopy*. Jpn. J. Appl. Phys., 51:025602–, 2012.
- [96] ZHARNIKOV, M., A. DITTSCHAR, W. KUCH, K. MEINEL, C.M. SCHNEIDER and J. KIRSCHNER: *Epitaxial fcc Fe-Co alloy films on Cu(001)*. Thin Solid Films, 275:262–265, April 1996.

- [97] ZHARNIKOV, M., A. DITTSCHAR, W. KUCH, C.M. SCHNEIDER and J. KIRSCHNER: *Spin-resolved photoemission and band-mapping in epitaxial fcc FeCo alloys on Cu(100)*. Journal of Magnetism and Magnetic Materials, 165:250–253, January 1997.
- [98] DITTSCHAR, A., M. ZHARNIKOV, W. KUCH, M.-T. LIN, C. M. SCHNEIDER and J. KIRSCHNER: *Composition-driven spin-reorientation transition in ferromagnetic alloy films*. Phys. Rev. B, 57(6):R3209–R3212, February 1998.
- [99] DITTSCHAR, A, W KUCH, M ZHARNIKOV and C.M SCHNEIDER: *Interrelation of morphology, structure, and magnetism in  $Fe_xCo_{1-x}/Cu(100)$  epitaxial alloy films*. Journal of Magnetism and Magnetic Materials, 212(3):307–322, April 2000.
- [100] SCHUMANN, F. O. and J. G. TOBIN: *Magnetic properties of Fe-based alloys*. J. Appl. Phys., 87(9):5460–5462, May 2000.
- [101] SCHELLENBERG, R., E. KISKER, M. FAUST, A. FANELSA and F. U. HILLEBRECHT: *Structure and local magnetic moments of epitaxial  $Fe(100)_{100-x}Co_x$  alloy films determined by photoelectron diffraction and magnetic linear dichroism*. Phys. Rev. B, 58(1):81–84, July 1998.
- [102] KISKER, E., A. FAUST, R. SCHELLENBERG, A. FANELSA and F. U. HILLEBRECHT: *Epitaxial  $Fe[sub 100 - x]Co[sub x]/Ag(001)$  alloy films: Structure and element-specific magnetic moments from magnetic linear dichroism*. J. Appl. Phys., 83(11):7094–7096, June 1998.
- [103] HEINRICH, B., Z. CELINSKI, J. F. COCHRAN, W. B. MUIR, J. RUDD, Q. M. ZHONG, A. S. ARROTT, K. MYRTLE and J. KIRSCHNER: *Ferromagnetic and antiferromagnetic exchange coupling in bcc epitaxial ultrathin  $Fe(001)/Cu(001)Fe(001)$  trilayers*. Phys. Rev. Lett., 64(6):673–676, February 1990.
- [104] PAYNE, A. P., B. M. LAIRSON, S. BRENNAN, B. J. DANIELS, N. M. RENSING and B. M. CLEMENS: *Epitaxial strain and the growth of  $Cu(001)$  on  $Fe(001)$* . Phys. Rev. B, 47(23):16064–16067, June 1993.
- [105] WU, Y. Z., A. K. SCHMID and Z. Q. QIU: *Spin-Dependent Quantum Interference from Epitaxial  $MgO$  Thin Films on  $Fe(001)$* . Phys. Rev. Lett., 97(21):217205–, November 2006.
- [106] ALLMERS, T. and M. DONATH: *Controlling Cu diffusion in Co films grown on  $Cu(001)$* . Surface Science, 605(21â??22):1875–1880, November 2011.
- [107] ELLIS, W.P. and R.L. SCHWOBEL: *LEED from surface steps on  $UO_2$  single crystals*. Surface Science, 11(1):82–98, July 1968.
- [108] HENZLER, M.: *LEED-investigation of step arrays on cleaved germanium (111) surfaces*. Surface Science, 19(1):159–171, January 1970.
- [109] HENZLER, M.: *LEED studies of surface imperfections*. Applications of Surface Science, 11â??12(0):450–469, July 1982.
- [110] BINNIG, G., H. ROHRER, CH. GERBER and E. WEIBEL: *Surface Studies by Scanning Tunneling Microscopy*. Phys. Rev. Lett., 49(1):57–61, July 1982.
- [111] BECKER, T., H. HÖVEL, M. TSCHUDY and B. REIHL: *Applications with a new low-temperature UHV STM at 5 K*. Applied Physics A, 66(1):S27–S30, 1998.
- [112] GIESEN, MARGRET, F. SCHMITZ and H. IBACH: *The growth of cobalt films on vicinal copper surfaces*. Surface Science, 336(3):269–279, August 1995.
- [113] MIDOIR, ANNE CHAUMIN, HELENE MAGNAN, FABRICE SCHEURER, HERVE BULOUE, LUC BARBIER, PATRICK LE FEVRE and DOMINIQUE CHANDESIRIS: *Magnetism, structure and morphology of thin cobalt films deposited on  $Cu(115)$* . Surface Science, 532-535(0):70–75, June 2003.
- [114] CHAUMIN MIDOIR, A., H. MAGNAN, L. BARBIER, P. LE FEVRE and D. CHANDESIRIS: *Structure and morphology of thin cobalt films deposited on vicinal surface  $Cu(1,1,11)$* . Applied Surface Science, 188:115–121, March 2002.
- [115] BADER, S.D., E.R. MOOG and P. GRÜNBERG: *Magnetic hysteresis of epitaxially-deposited iron in the monolayer range: A Kerr effect experiment in surface magnetism*. Journal of Magnetism and Magnetic Materials, 53(4):L295–L298, January 1986.

- [116] MOOG, E. R., C. LIU, S. D. BADER and J. ZAK: *Thickness and polarization dependence of the magneto-optic signal from ultrathin ferromagnetic films*. Phys. Rev. B, 39(10):6949–6956, April 1989.
- [117] MOOG, E. R., J. ZAK, M. L. HUBERMAN and S. D. BADER: *Magneto-optic rotation and ellipticity of ultrathin ferromagnetic films*. Phys. Rev. B, 39(13):9496–9499, May 1989.
- [118] BENNETT, W. R., W. SCHWARZACHER and JR. EGELHOFF, W. F.: *Concurrent enhancement of Kerr rotation and antiferromagnetic coupling in epitaxial Fe/Cu/Fe structures*. Phys. Rev. Lett., 65(25):3169–3172, December 1990.
- [119] ZAK, J., E.R. MOOG, C. LIU and S.D. BADER: *Universal approach to magneto-optics*. Journal of Magnetism and Magnetic Materials, 89:107–123, September 1990.
- [120] BADER, S.D.: *SMOKE*. Journal of Magnetism and Magnetic Materials, 100:440–454, November 1991.
- [121] ARGYRES, PETROS N.: *Theory of the Faraday and Kerr Effects in Ferromagnetics*. Phys. Rev., 97(2):334–345, January 1955.
- [122] KONDORSKY, E. I. and A. V. VEDIAEV: *The Electron-Phonon Scattering Contribution to the Anomalous Magneto-optical Effects in Ferromagnetic Metals*. J. Appl. Phys., 39(2):559–561, February 1968.
- [123] NÝVLT, M.: *PhD dissertation*. PhD thesis.
- [124] BALLENTINE, C.A., R.L. FINK, J. ARAYA-POCHET and J.L. ERSKINE: *Exploring magnetic properties of ultrathin epitaxial magnetic structures using magneto-optical techniques*. 49(5):459–466–, 1989.
- [125] YOKOYAMA, TOSHIHIKO, TAKESHI NAKAGAWA and YASUMASA TAKAGI: *Magnetic circular dichroism for surface and thin film magnetism: Measurement techniques and surface chemical applications*. International Reviews in Physical Chemistry, 27(3):449–505, July 2008.
- [126] DING, H.F, S PÜTTER, H.P OEPEN and J KIRSCHNER: *Experimental method for separating longitudinal and polar Kerr signals*. Journal of Magnetism and Magnetic Materials, 212(1-2):5–11, March 2000.
- [127] QIU, Z. Q. and S. D. BADER: *Surface magneto-optic Kerr effect*. Rev. Sci. Instrum., 71(3):1243–1255, March 2000.
- [128] MIKUSZEIT, N., S. PÜTTER and H.P. OEPEN: *Thickness dependent magnetization canting in Co on Cu (1,1,13)*. Journal of Magnetism and Magnetic Materials, 268(3):340–347, January 2004.
- [129] SCHULZ, L. G.: *The Optical Constants of Silver, Gold, Copper, and Aluminum. I. The Absorption Coefficient  $k$* . J. Opt. Soc. Am., 44(5):357–362, May 1954.
- [130] SCHULZ, L. G. and F. R. TANGHERLINI: *Optical Constants of Silver, Gold, Copper, and Aluminum. II. The Index of Refraction  $n$* . J. Opt. Soc. Am., 44(5):362–367, May 1954.
- [131] JOHNSON, P. B. and R. W. CHRISTY: *Optical Constants of the Noble Metals*. Phys. Rev. B, 6(12):4370–4379, December 1972.
- [132] JOHNSON, P. B. and R. W. CHRISTY: *Optical constants of transition metals: Ti, V, Cr, Mn, Fe, Co, Ni, and Pd*. Phys. Rev. B, 9(12):5056–5070, June 1974.
- [133] ZAK, J., E. R. MOOG, C. LIU and S. D. BADER: *Magneto-optics of multilayers with arbitrary magnetization directions*. Phys. Rev. B, 43(8):6423–6429, March 1991.
- [134] SCHÜTZ, G., W. WAGNER, W. WILHELM, P. KIENLE, R. ZELLER, R. FRAHM and G. MATERLIK: *Absorption of circularly polarized x rays in iron*. Phys. Rev. Lett., 58(7):737–740, February 1987.
- [135] THOLE, B. T., P. CARRA, F. SETTE and G. VAN DER LAAN: *X-ray circular dichroism as a probe of orbital magnetization*. Phys. Rev. Lett., 68(12):1943–1946, March 1992.
- [136] CARRA, PAOLO, B. T. THOLE, MASSIMO ALTARELLI and XINDONG WANG: *X-ray circular dichroism and local magnetic fields*. Phys. Rev. Lett., 70(5):694–697, February 1993.
- [137] STÖHR, J. and H. KÖNIG: *Determination of Spin- and Orbital-Moment Anisotropies in Transition Metals by Angle-Dependent X-Ray Magnetic Circular Dichroism*. Phys. Rev. Lett., 75(20):3748–3751, November 1995.

- [138] GEJO, T, Y TAKATA, T HATSUI, M NAGASONO, H OJI, N KOSUGI and E SHIGEMASA: *Angle-resolved photoion spectroscopy of NO<sub>2</sub> and SO<sub>2</sub>*. Chemical Physics, 289(1):15–29, April 2003.
- [139] KOIDE, T., T. SHIDARA and H. FUKUTANI: *Bakable superconducting magnet for magnetic circular dichroism and magnetic-imaging photoemission-spectromicroscopy studies*. Rev. Sci. Instrum., 63(1):1462–1465, January 1992.
- [140] NAKAGAWA, TAKESHI, YASUMASA TAKAGI, YOSHIHIRO MATSUMOTO and TOSHIHIKO YOKOYAMA: *Enhancements of Spin and Orbital Magnetic Moments of Submonolayer Co on Cu(001) Studied by X-ray Magnetic Circular Dichroism Using Superconducting Magnet and Liquid He Cryostat*. Jpn. J. Appl. Phys., 47(4):2132–, 2008.
- [141] NAKAJIMA, REIKO, J. STÖHR and Y. U. IDZERDA: *Electron-yield saturation effects in L-edge x-ray magnetic circular dichroism spectra of Fe, Co, and Ni*. Phys. Rev. B, 59(9):6421–6429, March 1999.
- [142] CHEN, C. T., Y. U. IDZERDA, H.-J. LIN, N. V. SMITH, G. MEIGS, E. CHABAN, G. H. HO, E. PELLEGRIN and F. SETTE: *Experimental Confirmation of the X-Ray Magnetic Circular Dichroism Sum Rules for Iron and Cobalt*. Phys. Rev. Lett., 75(1):152–, July 1995.
- [143] GAMBARDELLA, P., S. RUSPONI, M. VERONESE, S. S. DHESI, C. GRAZIOLI, A. DALLMEYER, I. CABRIA, R. ZELLER, P. H. DEDERICHS, K. KERN, C. CARBONE and H. BRUNE: *Giant Magnetic Anisotropy of Single Cobalt Atoms and Nanoparticles*. Science, 300(5622):1130–1133, 2003.
- [144] BAUER, E: *Low energy electron microscopy*. Reports on Progress in Physics, 57(9):895–, 1994.
- [145] ROUGEMAILLEA, N. and A. K. SCHMID: *Magnetic imaging with spin-polarized low-energy electron microscopy*. The European Physical Journal - Applied Physics, 50:20101, 2010.
- [146] GRZELAKOWSKI, K., T. DUDEN, E. BAUER, H. POPPA and S. CHIANG: *A new surface microscope for magnetic imaging*. Magnetism, IEEE Transactions on, 30(6):4500–4502, 1994.
- [147] GRZELAKOWSKI, K. and E. BAUER: *A flange-on type low energy electron microscope*. Rev. Sci. Instrum., 67(3):742–747, March 1996.
- [148] BAUER, E., T. DUDEN, H. PINKVOS, H. POPPA and K. WURM: *LEEM studies of the microstructure and magnetic domain structure of ultrathin films*. Journal of Magnetism and Magnetic Materials, 156:1–6, April 1996.
- [149] MAXSON, J.B., N. PERKINS, D.E. SAVAGE, A.R. WOLL, L. ZHANG, T.F. KUECH and M.G. LAGALLY: *Novel dark-field imaging of GaN 0001 surfaces with low-energy electron microscopy*. Surface Science, 464:217–222, October 2000.
- [150] FIGUERA, J. DE LA, J.M. PUERTA, J.I. CERDA, F. EL GABALY and K.F. MCCARTY: *Determining the structure of Ru(0001) from low-energy electron diffraction of a single terrace*. Surface Science, 600(9):L105–L109, May 2006.
- [151] ALTMAN, M S: *Trends in low energy electron microscopy*. Journal of Physics: Condensed Matter, 22(8):084017–, 2010.
- [152] TELIEPS, W. and E. BAUER: *The  $(7 \times 7) \leftrightarrow (1 \times 1)$  phase transition on Si(111)*. Surface Science, 162:163–168, October 1985.
- [153] TELIEPS, W.: *Surface imaging with LEEM*. 44(1):55–61–, 1987.
- [154] MUNDSCHAU, M., E. BAUER and W. SWIECH: *Defects on the surface of Mo011 observed by low-energy electron microscopy*. Philosophical Magazine A, 59(2):217–226, February 1989.
- [155] FU, C. L., A. J. FREEMAN and T. OGUCHI: *Prediction of Strongly Enhanced Two-Dimensional Ferromagnetic Moments on Metallic Overlayers, Interfaces, and Superlattices*. Phys. Rev. Lett., 54(25):2700–2703, June 1985.
- [156] RICHTER, ROY, J. G. GAY and JOHN R. SMITH: *Spin Separation in a Metal Overlayer*. Phys. Rev. Lett., 54(25):2704–2707, June 1985.
- [157] WOOTEN, C. L., J. CHEN, G. A. MULHOLLAN, J. L. ERSKINE and J. T. MARKERT: *Direct observation of enhanced magnetic moments in Fe/Ag(100)*. Phys. Rev. B, 49(14):10023–10026, April 1994.

- [158] JAL, EMMANUELLE, MACIEJ DĄBROWSKI, JEAN-MARC TONNERRE, MAREK PRZYBYLSKI, STEPHANE GRENIER, NICOLAS JAOUEN and JÜRGEN KIRSCHNER: *Magnetization profile across Au-covered bcc Fe films grown on a vicinal surface of Ag(001) as seen by x-ray resonant magnetic reflectivity*. Phys. Rev. B, 87(22):224418–, June 2013.
- [159] LI, CHUN, A. J. FREEMAN, H. J. F. JANSEN and C. L. FU: *Magnetic anisotropy in low-dimensional ferromagnetic systems: Fe monolayers on Ag(001), Au(001), and Pd(001) substrates*. Phys. Rev. B, 42(9):5433–5442, September 1990.
- [160] HEINRICH, B., K. B. URQUHART, A. S. ARROTT, J. F. COCHRAN, K. MYRTLE and S. T. PURCELL: *Ferromagnetic-resonance study of ultrathin bcc Fe(100) films grown epitaxially on fcc Ag(100) substrates*. Phys. Rev. Lett., 59(15):1756–1759, October 1987.
- [161] PRZYBYLSKI, M., M. DĄBROWSKI, U. BAUER, M. CINAL and J. KIRSCHNER: *Oscillatory magnetic anisotropy due to quantum well states in thin ferromagnetic films (invited)*. J. Appl. Phys., 111:07C102–6, April 2012.
- [162] HEINRICH, B., Z. CELINSKI, J. F. COCHRAN, A. S. ARROTT and K. MYRTLE: *Magnetic anisotropies in single and multilayered structures (invited)*. J. Appl. Phys., 70(10):5769–5774, November 1991.
- [163] LIU, C. and S. D. BADER: *Perpendicular surface magnetic anisotropy in ultrathin epitaxial Fe films*. J. Vac. Sci. Technol. A, 8(3):2727–2731, May 1990.
- [164] REICHL, I., A. VERNES, P. WEINBERGER, L. SZUNYOGH and C. SOMMERS: *Reorientation transition in  $Fe_n/Au(100)$* . Phys. Rev. B, 71(21):214416–, June 2005.
- [165] YUASA, SHINJI, AKIO FUKUSHIMA, HITOSHI KUBOTA, YOSHISHIGE SUZUKI and KOJI ANDO: *Giant tunneling magnetoresistance up to 410magnetic tunnel junctions with bcc Co(001) electrodes*. Appl. Phys. Lett., 89(4):042505–3, July 2006.
- [166] GIVORD, D., F. ROSSIGNOL, M. and W. TAYLOR, D.: *Coercivity mechanisms in hard magnetic materials*. J. Phys. IV France, 02(C3):C3–95–C3–104, 1992.
- [167] RIBAS, R, B DIENY, B BARBARA and A LABRATA: *The magnetization process and coercivity in random anisotropy systems*. Journal of Physics: Condensed Matter, 7(17):3301–, 1995.
- [168] HERZER, G., W. FERNENGEL and E. ADLER: *On the theory of nucleation fields in uniaxial ferromagnets*. Journal of Magnetism and Magnetic Materials, 58:48–54, 1986.
- [169] KLÄSGES, R., D. SCHMITZ, C. CARBONE, W. EBERHARDT, P. LANG, R. ZELLER and P. H. DEDERICHS: *Short-period oscillations in photoemission from Cu films on Co(100)*. Phys. Rev. B, 57(2):R696–R699, January 1998.
- [170] JOLY, L., L. TATI-BISMATHS and W. WEBER: *Quantum-Size-Induced Oscillations of the Electron-Spin Motion in Cu Films on Co(001)*. Phys. Rev. Lett., 97(18):187404–, November 2006.
- [171] ROTENBERG, ELI, Y. Z. WU, J. M. AN, M. A. VAN HOVE, A. CANNING, L. W. WANG and Z. Q. QIU: *Non-free-electron momentum- and thickness-dependent evolution of quantum well states in the Cu/Co/Cu(001) system*. Phys. Rev. B, 73(7):075426–, February 2006.
- [172] NORDSTRÖM, L., P. LANG, R. ZELLER and P. H. DEDERICHS: *Ab Initio Calculation of Quantum Well States in Cu/Co (100)*. EPL (Europhysics Letters), 29(5):395–, 1995.
- [173] VAZ, C. A. F. and J. A. C. BLAND: *Dependence of the coercive field on the Cu overlayer thickness in thin Co/Cu(001) and Ni/Cu(001) fcc epitaxial films*. J. Appl. Phys., 89(11):7374–7376, June 2001.
- [174] GEERTS, WIM, Y. SUZUKI, T. KATAYAMA, K. TANAKA, K. ANDO and S. YOSHIDA: *Thickness-dependent oscillation of the magneto-optical properties of Au-sandwiched (001) Fe films*. Phys. Rev. B, 50(17):12581–12586, November 1994.
- [175] BRUNO, P., Y. SUZUKI and C. CHAPPERT: *Magneto-optical Kerr effect in a paramagnetic overlayer on a ferromagnetic substrate: A spin-polarized quantum size effect*. Phys. Rev. B, 53(14):9214–9220, April 1996.
- [176] KOERKAMP, M. GROOT, A. KIRILYUK, W. DE JONG, TH. RASING, J. FERRE, J. P. JAMET, P. MEYER and R. MEGY: *Nonlinear magneto-optical Kerr effect study of quantum-well states in a Au overlayer on a Co(0001) thin film*. J. Appl. Phys., 79(8):5632–5634, April 1996.

- [177] JOLY, L., L. TATI BISMATHS, F. SCHEURER and W. WEBER: *Quantum-well state induced oscillations of the electron-spin motion in Au films on Co(001)*. Phys. Rev. B, 76(10):104415–, September 2007.
- [178] MA, XIAO-DONG, TAKESHI NAKAGAWA and TOSHIHIKO YOKOYAMA: *Effect of surface chemisorption on the spin reorientation transition in magnetic ultrathin Fe film on Ag(001)*. Surface Science, 600(19):4605–4612, October 2006.
- [179] HAHN, A., C. ANDERSSON, J. HUNTER DUNN, B. SANYAL, O. KARIS and D. ARVANITIS: *Structure and magnetism of ultrathin epitaxial Fe on Ag(100)*. Phys. Rev. B, 73(13):134423–, April 2006.
- [180] FREEMAN, A.J.: *Electronic structure and magnetism of surfaces and interfaces*. Journal of Magnetism and Magnetic Materials, 35:31–36, March 1983.
- [181] OHNISHI, S., A. J. FREEMAN and M. WEINERT: *Surface magnetism of Fe(001)*. Phys. Rev. B, 28(12):6741–6748, December 1983.
- [182] IZQUIERDO, J., A. VEGA, L. C. BALBAS, DANIEL SANCHEZ-PORTAL, JAVIER JUNQUERA, EMILIO ARTACHO, JOSE M. SOLER and PABLO ORDEJON: *Systematic ab initio study of the electronic and magnetic properties of different pure and mixed iron systems*. Phys. Rev. B, 61(20):13639–13646, May 2000.
- [183] SCHERZ, A., H. WENDE, P. POULOPOULOS, J. LINDNER, K. BABERSCHKE, P. BLOMQUIST, R. WÄPLING, F. WILHELM and N. B. BROOKES: *Induced V and reduced Fe moments at the interface of Fe/V(001) superlattices*. Phys. Rev. B, 64(18):180407–, October 2001.
- [184] QIU, Z. Q., J. PEARSON and S. D. BADER: *Two-dimensional Ising transition of epitaxial Fe films grown on Ag(100)*. Phys. Rev. B, 49(13):8797–8801, April 1994.
- [185] KASHUBA, A. and V. L. POKROVSKY: *Stripe domain structures in a thin ferromagnetic film*. Phys. Rev. Lett., 70(20):3155–3158, May 1993.
- [186] KASHUBA, A. B. and V. L. POKROVSKY: *Stripe domain structures in a thin ferromagnetic film*. Phys. Rev. B, 48(14):10335–10344, October 1993.
- [187] YAFET, Y. and E. M. GYORGY: *Ferromagnetic strip domains in an atomic monolayer*. Phys. Rev. B, 38(13):9145–9151, November 1988.
- [188] KAPLAN, B.: *Domain morphology in ultrathin ferromagnetic films with perpendicular magnetization*. Journal of Magnetism and Magnetic Materials, 298(2):135–138, March 2006.
- [189] OEPEN, H. P., M. SPECKMANN, Y. MILLEV and J. KIRSCHNER: *Unified approach to thickness-driven magnetic reorientation transitions*. Phys. Rev. B, 55(5):2752–2755, February 1997.
- [190] RAMCHAL, R., A. K. SCHMID, M. FARLE and H. POPPA: *Magnetic domains and domain-wall structure in Ni/Cu(001) films imaged by spin-polarized low-energy electron microscopy*. Phys. Rev. B, 68(5):054418–, August 2003.
- [191] BERGER, A. and H. P. OEPEN: *Magnetic domain walls in ultrathin fcc cobalt films*. Phys. Rev. B, 45(21):12596–12599, June 1992.
- [192] PAGGEL, J. J., T. MILLER and T.-C. CHIANG: *Quasiparticle Lifetime in Macroscopically Uniform Ag/Fe(100) Quantum Wells*. Phys. Rev. Lett., 81(25):5632–5635, December 1998.
- [193] CHIANG, T.-C: *Photoemission studies of quantum well states in thin films*. Surface Science Reports, 39:181–235, September 2000.
- [194] PAGGEL, J. J., T. MILLER and T.-C. CHIANG: *Quantum-Well States as Fabry-Parot Modes in a Thin-Film Electron Interferometer*. Science, 283(5408):1709–1711, 1999.
- [195] HIMPSEL, F. J.: *Fe on Au(100): Quantum-well states down to a monolayer*. Phys. Rev. B, 44(11):5966–5969, September 1991.
- [196] JIANG, Q., Y.-L. HE and G.-C. WANG: *Thermal stability and intermixing of ultrathin Fe films on a Au(001) surface*. Surface Science, 295:197–212, September 1993.
- [197] BELHADJI, B. and L. CALMELS: *Modification of the  $\Delta_1$  and  $\Delta_5$  electron states induced by alloying effects in Fe-based alloys for magnetic tunnel junctions*. J. Appl. Phys., 107(9):09C713–3, May 2010.



- [198] BELHADJI, B. and L. CALMELS: *Bulk electron states with  $\Delta$  symmetry in disordered Fe-based alloys for magnetic tunnel junctions*. Phys. Rev. B, 83(9):092401–, March 2011.
- [199] CINAL, M., M. DĄBROWSKI, M. PRZYBYLSKI and J. KIRSCHNER: *to be published*. unpublished, 2014.
- [200] JOHNSON, M T, P J H BLOEMEN, F J A DEN BROEDER and J J DE VRIES: *Magnetic anisotropy in metallic multilayers*. Reports on Progress in Physics, 59(11):1409–, 1996.
- [201] HEINRICH, B., K. B. URQUHART, J. R. DUTCHER, S. T. PURCELL, J. F. COCHRAN, A. S. ARROTT, D. A. STEIGERWALD and W. F. EGELHOFF, JR.: *Large surface anisotropies in ultrathin films of bcc and fcc Fe(001) (invited)*. J. Appl. Phys., 63(8):3863–3868, April 1988.
- [202] HICKEN, R. J., S. J. GRAY, A. ERCOLE, C. DABOO, D. J. FREELAND, E. GU, E. AHMAD and J. A. C. BLAND: *Magnetic anisotropy in ultrathin epitaxial Fe/Ag(100) films with overlayers*. Phys. Rev. B, 55(9):5898–5907, March 1997.
- [203] BRUNO, PATRICK: *Dipolar magnetic surface anisotropy in ferromagnetic thin films with interfacial roughness*. J. Appl. Phys., 64(6):3153–3156, September 1988.
- [204] KLEIN, C., R. RAMCHAL, M. FARLE and A. K. SCHMID: *Direct imaging of spin-reorientation transitions in ultrathin Ni films by spin-polarized low-energy electron microscopy*. Surf. Interface Anal., 38(12-13):1550–1553, 2006.
- [205] DHESI, S. S., H. A. DÜRR and G. VAN DER LAAN: *Canted spin structures in Ni films on stepped Cu(001)*. Phys. Rev. B, 59(13):8408–8411, April 1999.
- [206] KAPLAN, B. and G.A. GEHRING: *The domain structure in ultrathin magnetic films*. Journal of Magnetism and Magnetic Materials, 128:111–116, November 1993.
- [207] KAPLAN, B.: *Ferromagnetic stripe domains in ultrathin films*. Journal of Magnetism and Magnetic Materials, 288(0):178–182, March 2005.
- [208] SPECKMANN, M., H. P. OEPEN and H. IBACH: *Magnetic Domain Structures in Ultrathin Co/Au(111): On the Influence of Film Morphology*. Phys. Rev. Lett., 75(10):2035–2038, September 1995.
- [209] OEPEN, H. P., Y. T. MILLEV and J. KIRSCHNER: *The reorientation transition in Co/Au(111)*. J. Appl. Phys., 81(8):5044–5046, April 1997.
- [210] MAN, K.L, M.S ALTMAN and H POPPA: *Spin polarized low energy electron microscopy investigations of magnetic transitions in Fe/Cu(100)*. Surface Science, 480(3):163–172, June 2001.
- [211] HOFFMANN, R, D.E BÜRGLER, P.J.A VAN SCHENDEL, H.J HUG, S MARTIN and H.-J GÜNTHERODT: *Perpendicular magnetic domains of a thin Ag/Fe/Ag film observed by magnetic force microscopy at room temperature*. Journal of Magnetism and Magnetic Materials, 250(0):32–38, September 2002.
- [212] EDMUND, C STONER: *Ferromagnetism: magnetization curves*. Reports on Progress in Physics, 13(1):83–, 1950.
- [213] HU, XIAO: *Magnetization reversal and coercive force in ultrathin films with perpendicular surface anisotropy: Micromagnetic theory*. Phys. Rev. B, 55(13):8382–8389, April 1997.
- [214] PRINZ, G. A.: *Stabilization of bcc Co via Epitaxial Growth on GaAs*. Phys. Rev. Lett., 54(10):1051–1054, March 1985.
- [215] BAGAYOKO, D., A. ZIEGLER and J. CALLAWAY: *Band structure of bcc cobalt*. Phys. Rev. B, 27(12):7046–7049, June 1983.
- [216] LEE, J.I., C.L. FU and A.J. FREEMAN: *Electronic structure and magnetism of metastable bcc Co(001)*. Journal of Magnetism and Magnetic Materials, 62(1):93–100, November 1986.
- [217] TONG, LIU-NIU, CAI-LIAN DENG, FRANK MATTHES, MARTINA MÜLLER, CLAUS M. SCHNEIDER and CHAN-GYU LEE: *Influence of MgO overlayers on the electronic states of bcc Co(001) thin films grown on bcc Fe(001)/GaAs(001)*. Phys. Rev. B, 73(21):214401–, June 2006.
- [218] BONELL, F., T. HAUET, S. ANDRIEU, F. BERTRAN, P. LE FEVRE, L. CALMELS, A. TEJEDA, F. MONTAIGNE, B. WAROT-FONROSE, B. BELHADJI, A. NICOLAOU and A. TALEB-IBRAHIMI: *Spin-Polarized Electron Tunneling in bcc FeCo/MgO/FeCo(001) Magnetic Tunnel Junctions*. Phys. Rev. Lett., 108(17):176602–, April 2012.

- [219] BLAND, J. A. C., A. D. JOHNSON, C. NORRIS and H. J. LAUTER: *Absolute value of the magnetic moment per atom in Ag/Fe/Ag(001) and Ag/Co/Ag(001) epitaxial sandwich structures*. J. Appl. Phys., 67(9):5397–5399, May 1990.
- [220] BLAND, J A C, C DABOO, G A GEHRING, B KAPLAN, A J R IVES, R J HICKEN and A D JOHNSON: *Magnetization of ultrathin ferromagnetic films at finite temperatures*. Journal of Physics: Condensed Matter, 7(32):6467–, 1995.
- [221] DEGROOTE, B., J. DEKOSTER and G. LANGOUCHE: *Step decoration and surface alloying: growth of cobalt on Ag(100) as a function of deposition temperature*. Surface Science, 452:172–178, May 2000.
- [222] SOMMERS, C., J. ZABLOUDIL, C. UIBERACKER, P. WEINBERGER and L. SZUNYOGH: *Multiple reorientation transition of the magnetization of free surfaces of Fe on Ag(100)*. Phys. Rev. B, 58(9):5539–5543, September 1998.
- [223] SZUNYOGH, L., B. UJFALUSSY and P. WEINBERGER: *Magnetic anisotropy of iron multilayers on Au(001): First-principles calculations in terms of the fully relativistic spin-polarized screened KKR method*. Phys. Rev. B, 51(15):9552–9559, April 1995.
- [224] GUO, G Y: *Magnetocrystalline anisotropy oscillations predicted in Fe/Au(001) superlattices*. Journal of Physics: Condensed Matter, 11(22):4329–, 1999.
- [225] CALLAWAY, J. and C. S. WANG: *Energy bands in ferromagnetic iron*. Phys. Rev. B, 16(5):2095–2105, September 1977.
- [226] FRITSCHÉ, L, J NOFFKE and H ECKARDT: *A relativistic treatment of interacting spin-aligned electron systems: application to ferromagnetic iron, nickel and palladium metal*. Journal of Physics F: Metal Physics, 17(4):943–, 1987.
- [227] SCHÄFER, J., M. HOINKIS, ELI ROTENBERG, P. BLAHA and R. CLAESSEN: *Fermi surface and electron correlation effects of ferromagnetic iron*. Phys. Rev. B, 72(15):155115–, October 2005.
- [228] LI, J., G. CHEN, Y. Z. WU, E. ROTENBERG and M. PRZYBYLSKI: *Quantum Well States and Oscillatory Magnetic Anisotropy in Ultrathin Fe Films*. Magnetism, IEEE Transactions on, 47(6):1603–1609, 2011.
- [229] WINKELMANN, A., M. PAZGAN, T. PEXIOTO, M. DĄBROWSKI, M. PRZYBYLSKI and J KIRSCHNER. *to be published*, 2013.
- [230] EBERHARDT, W. and F. J. HIMPSEL: *Dipole selection rules for optical transitions in the fcc and bcc lattices*. Phys. Rev. B, 21(12):5572–5576, June 1980.
- [231] SCHNEIDER, C. M. and J. KIRSCHNER: *Spin- and angle-resolved photoelectron spectroscopy from solid surfaces with circularly polarized light*. Critical Reviews in Solid State and Materials Sciences, 20(3):179–283, January 1995.
- [232] LUH, D.-A., J. J. PAGGEL, T. MILLER and T.-C. CHIANG: *d-Band Quantum Well States*. Phys. Rev. Lett., 84(15):3410–3413, April 2000.
- [233] HAHLIN, A., C. ANDERSSON, J. HUNTER DUNN, O. KARIS and D. ARVANITIS: *Structure and magnetism on in situ ultrathin epitaxial films: XMCD and EXAFS on Fe/Ag(100)*. Surface Science, 532-535(0):76–81, June 2003.
- [234] EL-BATANOUNY, M. and F. WOOTEN: *Symmetry and Condensed Matter Physics. A Computational Approach*. 2008.
- [235] JAFFRES, H., D. BERTRAND, A.R. FERT, J. VOGEL, A. FONTAINE, N. B. BROOKES, A. SCHUHL and F. NGUYEN VAN DAU: *In-plane magnetic anisotropy of stepped epitaxial Fe(001) thin films probed by x-ray magnetic circular dichroism*. Phys. Rev. B, 63(17):174411–, April 2001.
- [236] ANISIMOV, A. N., M. FARLE, P. POULOPOULOS, W. PLATOW, K. BABERSCHKE, P. ISBERG, R. WÖPLING, A. M. N. NIKLASSON and O. ERIKSSON: *Orbital Magnetism and Magnetic Anisotropy Probed with Ferromagnetic Resonance*. Phys. Rev. Lett., 82(11):2390–2393, March 1999.
- [237] SEGOVIA, P., A. MASCARAQUE, E.G. MICHEL, A. NÄRMANN and J.E. ORTEGA: *Resonant quantum well states in thin copper films on fcc-Co(100)*. Surface Science, 433-435(0):425–429, August 1999.

- [238] NIKLASSON, A M N, LARS NORDSTRÖM, S MIRBT, B JOHANSSON and H L SKRIVER: *Magnetic interlayer coupling and interaction between interface states in a quantum-well system*. Journal of Physics: Condensed Matter, 11(4):975–, 1999.
- [239] MATHON, J., MURIELLE VILLERET, R. B. MUNIZ, J. D’ALBUQUERQUE E CASTRO and D. M. EDWARDS: *Quantum Well Theory of the Exchange Coupling in Co/Cu/Co(001)*. Phys. Rev. Lett., 74(18):3696–3699, May 1995.
- [240] HUANG, D-J., P. D. JOHNSON and X. SHI: *Quantum-well states and the short period of oscillation in Cu/Co(001) multilayers*. Phys. Rev. B, 54(23):17123–17127, December 1996.
- [241] CURTI, F. G., A. DANESE and R. A. BARTYNSKI: *Experimental and Model Theoretical Dispersions of Unoccupied Metallic Quantum Well States in the Cu/fccCo/Cu(100) System*. Phys. Rev. Lett., 80(10):2213–2216, March 1998.
- [242] WEISHEIT, MARTIN, SEBASTIAN FÄHLER, ALAIN MARTY, YVES SOUCHE, CHRISTIANE POINSIGNON and DOMINIQUE GIVORD: *Electric Field-Induced Modification of Magnetism in Thin-Film Ferromagnets*. Science, 315(5810):349–351, 2007.



## Publications

TEKIELAK, M., M. DĄBROWSKI, M. KISIELEWSKI, A. MAZIEWSKI and V. ZABLITSKII: *Magnetic states and magnetization reversal in magnetostatically coupled multilayers with low perpendicular anisotropy*. J. Appl. Phys., 107(8):083911–9, April 2010.

BAUER, U., M. DĄBROWSKI, M. PRZYBYLSKI and J. KIRSCHNER: *Complex anisotropy and magnetization reversal on stepped surfaces probed by the magneto-optical Kerr effect*. Journal of Magnetism and Magnetic Materials, 323(11):1501–1508, June 2011.

BAUER, U., M. DĄBROWSKI, M. PRZYBYLSKI and J. KIRSCHNER: *Experimental confirmation of quantum oscillations of magnetic anisotropy in Co/Cu(001)*. Phys. Rev. B, 84(14):144433–, October 2011.

PRZYBYLSKI, M., M. DĄBROWSKI, U. BAUER, M. CINAL and J. KIRSCHNER: *Oscillatory magnetic anisotropy due to quantum well states in thin ferromagnetic films (invited)*. J. Appl. Phys., 111:07C102–6, April 2012.

MANNA, S., P. L. GASTELOIS, M. DĄBROWSKI, P. KUSWIK, M. CINAL, M. PRZYBYLSKI and J. KIRSCHNER: *Effect of quantum well states in Cu overlayer on magnetic anisotropy of Fe and Co films revisited*. Phys. Rev. B, 87(13):134401–, April 2013.

JAL, E. , M. DĄBROWSKI, J. M. TONNERRE, M. PRZYBYLSKI, S. GRENIER, N. JAOUEN and J. KIRSCHNER: *Magnetization profile across Au-covered bcc Fe films grown on a vicinal surface of Ag(001) as seen by x-ray resonant magnetic reflectivity*. Phys. Rev. B, 87(22):224418–, June 2013.



## Acknowledgments

I would like to thank my supervisor Prof. Jürgen Kirschner for his continuous support, guidance and numerous suggestions. His deep interest in physics has been stimulating me to work harder and learn more.

I am very grateful to Prof. Marek Przybylski. He cared about my studies in every detail and offered enormous help in many aspects. It was a great pleasure to work with him.

I wish to acknowledge Prof. Toshihiko Yokoyama, Dr. Aimo Winkelmann, Dr. Jean-Marc Tonnerre, Dr. Andreas Schmid, Dr. Sebastian Gliga and Dr. Marek Cinal, who read the manuscript and always offered nice and efficient suggestions. Without their help, this thesis could not go to this stage.

Many thanks to Dr. Sujit Manna for his help in the experiments and the STM images. The friendly period we had together is really unforgettable.

I also would like to thank Dr. Jochen Barthel, Mrs. Heike Menge and Mr. Wolfgang Greie for their kind support.

I am grateful to my friends and colleagues: Pawel Buczek, Rantej Bali, Uwe Bauer, Mariusz Pazgan, Thiago Pexioto, Pedro Lana Gastelois, Piotr Kuswik, Agnieszka Stepniak, Masaki Takada, Takeshi Nakagawa, Tzu-Hung Chuang, Emmanuelle Jal, Cheng-Tien Chiang, Fikret Yildiz, Hirofumi Oka, Daniele Preziosi and Matthias Schmidt.

Last but not least I would like to express my gratitude to my family and my fiancée Marta, for their continuous support and love throughout all the years of my Ph.D. studies.





## **Erklärung an Eides statt**

Hiermit erkläre ich, dass ich die vorliegende Dissertation

*"Effect of quantum well states on the magnetic anisotropy of ferromagnetic films"*

selbständig und ohne fremde Hilfe verfasst und keine anderen als die von mir angegebenen Quellen und Hilfsmittel benutzt habe. Die den benutzten Werken wörtlich oder inhaltlich entnommenen Stellen sind als solche kenntlich gemacht habe. Weiterhin erkläre ich, dass ich bisher keine vergeblichen Promotionsversuche unternommen habe.

Halle, den 27.08.2013

Maciej Dąbrowski



## Curriculum vitae

Name Maciej Krzysztof Dąbrowski  
Date of Birth March 8, 1984  
Place of Birth Białystok, Poland  
Nationality Polish  
E-mail mdabrows@mpi-halle.mpg.de

---

### EDUCATION

1999 - 2004 Secondary Electrical School in Białystok, Poland  
Specialty: electronic technician

2004 - 2009 Studies in the Faculty of Physics University of Białystok, Poland  
Master thesis subject:  
*Magnetization processes and magnetic domain structures in multilayered systems Co/Au*  
Supervisor - Prof. Dr. Andrzej Maziewski

Since 2009 Max Planck Institute of Microstructure Physics, Halle  
PhD thesis subject:  
*Effect of quantum well states on the magnetic anisotropy of ferromagnetic films*  
Supervisor - Prof. Dr. Jürgen Kirschner

---

Halle, den 27.08.2013

Maciej Dąbrowski